Carbon Capture Science & Technology 16 (2025) 100421

Contents lists available at ScienceDirect

Carbon Capture Science & Technology

journal homepage: www.elsevier.com/locate/ccst

Review

Biochar production, activation, and applications: A comprehensive technical review

Lisa Mingzhe Sun[a], Sean R. McIntyre[a], Paul Iacomi[a], Katie Everden[a], Paul T. Williams[b,*], Shuang Zong[c,d], Xinying Liu[c,*], Xiefei Zhu[e], Yanke Yang[e], Shuangjun Li[f], Gang Wu[g], Fei Huang[h], Lina Liu[h], Xiangzhou Yuan[g], Huiyan Zhang[g,*], Junjie Zhang[i], Haiping Yang[i,*], Wei Chen[k], Hongman Sun[j], Yang Cao[k], Dongdong Feng[l], Zhenyu Cheng[l], Xiong Zhang[m], Daxin Liang[n], Shengkai Liu[n], Xiaoxiao Zhang[o], Xiaohong Zhu[p], Ye Shui Zhang[q,*], Yongliang Yan[r,*], Jianrui Zha[s], Yuanting Qiao[t], Salman Masoudi Soltani[u,*], Ning Zhang[v], Shouliang Yi[w], Chunfei Wu[x,*]

[a] *Surface Measurement Systems Ltd., Alperton, London HA0 4PE, UK*
[b] *School of Chemical and Process Engineering, University of Leeds, Leeds LS2 9JT, UK*
[c] *Institute for Catalysis and Energy Solutions, University of South Africa, Private Bag X6, FL, Roodepoort 1709, South Africa*
[d] *Hebei Chemical & Pharmaceutical College, No. 88 Fangxing Road, Shijiazhuang, Hebei Province, China*
[e] *Sun Yat-sen University, School of Advanced Energy, Shenzhen Campus of Sun Yat-sen University, No.66, Gongchang Road Guangming District, Shenzhen, Guangdong 518107, China*
[f] *Department of Chemical and Biological Engineering, Korea University, 145 Anam-ro, Seongbuk-gu, Seoul 02841, Republic of Korea*
[g] *Ministry of Education of Key Laboratory of Energy Thermal Conversion and Control, School of Energy and Environment, Southeast University, Nanjing 210096, China*
[h] *Ministry of Education Key Laboratory of Pollution Processes and Environmental Criteria, College of Environmental Science and Engineering, Nankai University, Tianjin 300350, China*
[i] *State Key Laboratory of Coal Combustion, Huazhong University of Science and Technology, Wuhan 430074, China*
[j] *State Key Laboratory of Heavy Oil Processing, College of Chemistry and Chemical Engineering, China University of Petroleum, Qingdao, 266580, China*
[k] *College of Engineering, Nanjing Agricultural University, No. 40 Dianjiangtai Road, Nanjing, Jiangsu Province 210031, China*
[l] *School of Energy Science and Engineering, Harbin Institute of Technology, Harbin 150001, China*
[m] *State Key Laboratory of Coal Combustion, School of Energy and Power Engineering, Huazhong University of Science and Technology, Wuhan 430074, China*
[n] *College of Materials Science and Engineering, Northeast Forestry University, No. 26 Hexing Road, Harbin 150040, China*
[o] *Department of Civil and Environmental Engineering, The Hong Kong Polytechnic University, Hung Hom, Kowloon, Hong Kong, China*
[p] *Key Laboratory of Urban Security and Disaster Engineering of Ministry of Education, Beijing University of Technology, Beijing, China*
[q] *School of Engineering, University of Aberdeen, Aberdeen AB24 3UE, UK*
[r] *School of Engineering, Newcastle University, Newcastle Upon Tyne NE1 7RU, United Kingdom*
[s] *Key Laboratory of Process Optimisation and Intelligent Decision-making of Ministry of Education, Hefei University of Technology, Hefei 210096, China*
[t] *Department of Chemical Engineering, Faculty of Engineering, Swansea University, Swansea SA1 8EN, United Kingdom*
[u] *Department of Chemical Engineering, Brunel University of London, Uxbridge UB8 3PH, UK*
[v] *Department of Earth and Environmental Engineering, Columbia University, NY 10027, United States*
[w] *Department of Civil and Environmental Engineering, University of Pittsburgh, 3700 O'Hara St., Pittsburgh, PA 15261, USA*
[x] *School of Chemistry and Chemical Engineering, Queen's University Belfast, Belfast BT7 1NN, UK*

ARTICLE INFO

Keywords:
Biochar production
Biochar characterisation
Carbon neutrality
Environmental remediation, Soil amendments
Pollutant removal
Techno-economic analysis

ABSTRACT

Our planet has been facing critical challenges since the late 20th century, including climate change, resource shortages, environmental degradation and pollution, demanding urgent and sustainable solutions. Biochar, a carbon-rich material produced via biomass pyrolysis, has gained attention for its great potentials in environmental remediation, pollutant removals, carbon neutrality, soil amendment, building materials, and etc. The performance of biochar in these applications is closely linked to its physicochemical properties, which are influenced by the feedstock and the preparation/activation methods. This paper reviews a wide range of biochar produced from various feedstocks, and the associated performance in different applications. Advanced character-

* Corresponding authors.
E-mail addresses: p.t.williams@leeds.ac.uk (P.T. Williams), liux@unisa.ac.za (X. Liu), hyzhang@seu.edu.cn (H. Zhang), yanghaiping@hust.edu.cn (H. Yang), yeshui.zhang@abdn.ac.uk (Y.S. Zhang), yongliang.yan@ncl.ac.uk (Y. Yan), Salman.MasoudiSoltani@brunel.ac.uk (S.M. Soltani), c.wu@qub.ac.uk (C. Wu).

https://doi.org/10.1016/j.ccst.2025.100421
Received 22 December 2024; Received in revised form 4 April 2025; Accepted 5 April 2025

isations are discussed to unveil the fundamental mechanisms and provide insights for further improvement and optimization. The techno-economic analysis evaluates the feasibility, challenges, and opportunities for scaling up and adopting biochar in potential applications. By focusing on biochar's multifunctionality and sustainability, this paper provides a reference for future research on developing biochar as a green technology with environmental and economic benefits.

1. Introduction

Climate change has been one of the major challenges for the past few decades, affecting ecosystems worldwide. Global temperature reached a historic high level in 2024, for the first time exceeding the 1.5°C limit set by the Paris Agreement (CopernicusClimateChangeService, 2024). The rise in temperature is closely linked to CO_2 emissions from anthropogenic activities, such as fossil fuel combustion and cement production (Sun et al., 2019). The emission of CO_2 is estimated to be 41.6 billion tonnes in 2024, 1 billion tonnes higher than in 2023, indicating an increasing trend (WMO, 2024). This rise is primarily due to the over-dependence on fossil fuels. The negative consequences of the global warming have been observed globally, such as hurricanes, droughts, extreme weathers, and etc., resulting in approximately two million deaths and $4 trillion in economic losses over the past 50 years (UnitedNations, 2023).

In addition to global warming, other environmental challenges such as air and water pollution, soil degradation, and deforestation have also posed significant threats to both human and ecosystems. Estimated by World Health Organization (WHO), air pollution leads to 7 million deaths every year, with 3.8 million and 4.2 million attributed to indoor and outdoor air pollution, respectively (CleanAir, 2024). Meanwhile, due to climate change and water pollution, freshwater availability per person has decreased by 20 % over the past two decades, leaving 2.3 billion people facing water stress (Mishra, 2023). Due to agricultural expansion and climate change, deforestation has emerged as another major concern. According to the 2024 Forest Declaration Assessment, global forest loss approached approximately 6.37 million hectares in 2023, 45 % more than the target set in the Glasgow Leaders' Declaration, which was signed by over 140 countries committing to terminate deforestation by 2030 (ForestDeclarationAssessmentPartners, 2024).

Biochar, a carbon-rich material derived from biomass pyrolysis, has gained increasing attention as a promising sustainable solution to address the environmental and resource challenges. As a carbon sequestration tool, biochar can retain up to 70 % of the carbon in biomass from being released as CO_2, removing up to 2.62 Gt of CO_2 per year globally, rendering it a key technology for achieving net-zero emissions targets (Werner et al., 2022). As a soil additive, biochar significantly improves the yields of plants by neutralizing soil acidity, enhancing nutrient and water retention, and improving soil aeration (Tran et al., 2023). Moreover, the high porosity makes biochar an effective material for environmental remediation, such as water treatment and air purification, through adsorption and catalytic processes (Cha et al., 2016; Wang, Tianqi et al., 2021; Yadav et al., 2023). In addition, biochar is increasingly utilized in building materials to enhance thermal insulation, improve structural strength, and contribute to carbon sequestration (Senadheera et al., 2023). These wide-ranging applications highlight the potential of biochar to address environmental, agricultural, and energy challenges sustainably.

Biochar has been extensively studied in the past decades. However, significant gaps remain regarding its production, activation, and applications. While fundamental research primarily focuses on material properties, characterization techniques, and novel modifications, real-world implementation prioritizes efficiency, stability, and scalability. However, these aspects are not contradictory. A better understanding of fundamental research provides the basis for optimizing large-scale applications. Bridging this gap requires translating laboratory findings into practical solutions by identifying key performance metrics, optimizing production processes for industrial feasibility, and integrating biochar into existing environmental and agricultural systems. A comprehensive review connects research innovations with real-world challenges is crucial for advancing biochar toward large-scale deployment. This review therefore, aims to bridge the gap between fundamental research and practical applications by systematically analysing biochar production from various feedstocks, exploring its applications in different fields, and discussing advanced characterization techniques to unravel its fundamental mechanisms. Additionally, a techno-economic assessment is provided to evaluate the feasibility, challenges, and prospects of biochar adoption. By addressing these critical aspects, this review not only consolidates existing knowledge but also highlights key research priorities to advance biochar science and its practical applications in achieving global sustainability goals.

2. Biochar and biomass characterization techniques

Due to the variations in biochar feedstock which can affect the morphology and chemistry of the biochar product, the physical and chemical characterization of biochar is essential when considering any potential environmental applications. By examining the biochar structure, surface area, and porosity, we can infer for example effectiveness in soil enhancement and carbon sequestration to specific properties. Biochar chemical characterization, including elemental analysis and spectroscopy, reveals elemental content and potential contaminants, as well as specific functionality that may attribute to biochar efficacy. Ultimately, a comprehensive understanding of the biochar chemical and physical properties helps optimize production processes and tailor the biochar product for specific uses, and aids in the development of synthesis routes to achieve the best biochar products. A summary of chemical and physical characterization techniques, as well as characterization techniques to evaluate environmental stability and contamination, is detailed below.

2.1. Chemical properties

2.1.1. pH of biochar

The pH of biochar generally ranges from 7.1 to 10.5, meaning they are generally alkaline (Inyang et al., 2010; Lehmann et al., 2011). Other reports in the literature state that the pH actually ranges from 3.1 to 12.0 (Lehmann et al., 2006), although biochar is accepted as more commonly being basic. It is the presence of organic matter and nutrients in biochar that leads to its alkaline nature, and subsequently, the addition of biochar to soil increases the soil pH, as well as influencing other properties, such as electrical conductivity and cation-exchange capacity (Jyoti et al., 2019). The alkaline constituents and minerals in biochar include ash containing nitrogen, phosphorus, potassium, and other trace elements, which provide great agronomic benefits to the soil. The amended soil generally becomes less acidic if biochar with a higher pH is added to the soil. The pH of the biochar depends on the feedstock used and the production conditions, including the duration and temperature of production (Jyoti et al., 2019). Generally, biochar derived from wood has a pH of around 2, which is lower than biochar produced from other sources under similar pyrolysis conditions (Tag, A. et al., 2016). The reason for non-wood biochar having higher basicity is due to the presence of salts from carbonates and chlorides of potassium and calcium in the ash (Montes-Morán et al., 2004). Other reports have correlated biochar pH with the contents of cellulose, hemicellulose, or

lignin (Ma, Z. et al., 2019), as well as oxygen functionalities, such as those in the carboxylate (COO^-) and oxide (O^-) groups (Yuan et al., 2011). Many other studies have also correlated oxygen-rich functional groups to higher biochar pH, particularly from functional groups such as γ-pyrone-type, chromene, diketone, or quinine groups (Yuan et al., 2011).

With an increase in pH, soil fertility and quality increase accordingly, which in turn, increases moisture retention capabilities, which further attracts microbes and fungi. This improves cation exchange and preserves the nutrients in the soil. The reduction in soil acidity caused by the increasing pH from the addition of biochar is sometimes referred to as the limiting effect, which helps nutrient and fertilizer retention (Lehmann et al., 2006).

Various studies have been completed on producing biochar with differing pH. A study investigated how using different biochar sources while keeping the production temperature (300°C) the same produced biochar with different resulting pHs (Yuan et al., 2011). When corn straw was used, the resulting biochar demonstrated a pH of 9.4. For peanuts, the resulting biochar was pH 8.6, and when soybean was used, the resulting biochar was pH 7.7. In contrast, biochar produced from canola straw proved to be acidic, with a pH of approximately 6.5. El-Gamal et al. showed that sugarcane biochar had a pH of 8.6, whilst rice husk biochar had a pH of 8.9, possibly owing to the sugarcane biochar having a lower ash content than the rice husk (El-Gamal et al., 2017). It is thought that the increase in pH values in biochar can be due to the decomposition of organic matrix and the concentration of non-pyrolyzed inorganic elements (García-Jaramillo et al., 2015). Researchers also examine incubation experiments, taking five types of alkaline soils and one type of biochar with a slightly lower pH than the soils used (Liu et al., 2012). Incubation was completed for 4 and 11 months, with a control soil and biochar-amended soils containing 4, 8 and 16 g of biochar/kg of soil. These samples were then tested, and it was revealed that the addition of alkaline biochar did not increase the soil pH. In fact, it displayed a decreasing trend, particularly magnified with higher biochar application rates (Liu et al., 2012). Biochar can be derived from sewage sludge feedstocks, whereby this feedstock also results in biochar with increased pH due to an increase in ash content (Hossain et al., 2011). pH of biochar is also affected by temperature, where biochar produced at high temperatures (>400°C) generally has a greater pH than those produced at temperatures <400°C (Balwant Singh, 2017). There are recommended procedures for measuring the pH of biochar, as small changes can result in different pH values being recorded. It was found previously that soil pH measurements in CaCl and KCl solutions gave lower pH values than those measured with deionized water (Thomas 1996). The ratio of solid to solution, shaking time, and position of the pH electrode in relation to the suspension can also result in different pH values being measured and recorded. It is now recommended to use a pH meter with glass-calomel electrodes, deionized water, reciprocating shakers, and standard buffers of pH 4, 7 and 10.

2.1.2. Functional groups of biochar

Understanding the surface chemistry of biochar is extremely important, owing to this being where many biological and chemical reactions take place. A biochar surface is categorized as either aliphatic or aromatic, and then more specific functional groups can be determined. It is also known that free radicals exist on biochar surfaces (Xiao et al., 2018). The type and concentration of surface functional groups have been shown to have a key role in the adsorption capacity and in the removal mechanisms of adsorbates (Tomczyk, A. et al., 2020). It has been shown that an increase in aromaticity combined with an increase in pyrolysis temperature can enhance resistance to microbial decomposition (Xie et al., 2016).

Alongside aliphatic and aromatic groups, other functional groups on a biochar surface may include hydroxyl, carboxyl, carbonyl, ether, epoxy, acyl, ester, amido, sulfonic and azyl. These different functional groups have been typically analysed using methods such as solid-state ^{13}C NMR, FT-IR, X-ray photoelectron spectroscopy, C-1 s near-edge X-ray absorption fine structure spectroscopy and more. Precise characterisation for analysis of all functional groups in biochar materials can still prove challenging. Therefore, most biochar analyses focus more specifically on the most abundant functionalities, particularly surface phenolic -OH, carboxyl, carbonyl, and ester groups. Some research has focused on combining techniques to quantify functional groups more accurately. For example, one method proposed to combine FT-IR with a modified acid/base consuming model to quantitatively identify chemical states, pKa, and contents of surface functional groups.

More specifically, when heating temperatures between 350–650°C are used, chemical bonds in the biomass are broken and rearranged, forming new functional groups such as carboxyl, lactone, lactol, quinine, chromene, anhydride, phenol, ether, pyrone, pyridine, pyridone and pyrrole (Mia et al., 2017). With biochar produced at 600–700°C, the biochar is highly hydrophobic in nature and has well-organized C layers. The contents of H and O are lower due to dehydration and deoxygenation of biomass (Uchimiya et al., 2011). Biochar produced at 300–400°C shows more organic character due to the aliphatic and cellulose type structures (Glaser et al., 2002; Novak et al., 2009).

Certain compounds and by-products are produced during pyrolysis of biochar, which add to the presence of some functional groups. For example, when cellulose undergoes pyrolysis, levoglucosan is formed, alongside levoglucosenone, furfural, 2,3-butanedione and 5-methylfurfural as by-products. These all result in the production of oxygen functional groups (Tomczyk, A. et al., 2020).

Biochar is also known to have surface free radicals, where one report noted abundant and persistent free radicals particularly in biochar derived from corn stalks, rice, and wheat straws, and was detected by electron paramagnetic resonance (EPR) (Liao et al., 2014). EPR can be used to monitor radical generations and transitions during pyrolysis.

2.1.3. Elemental composition and elemental distribution of biochar

Biochar is a carbon-rich, porous, high surface-area material produced from the pyrolysis of different biomasses. Biochar is made up of elements such as carbon, hydrogen, sulphur, oxygen, and nitrogen, and it additionally contains minerals from the ash fraction. Due to the organic matter and nutrients, using biochar to improve soil quality can increase the amount of organic carbon, total nitrogen and available phosphorus in the soil, improving soil quality and crop production (Jyoti et al., 2019). Following the pyrolysis process, alkali salts, including Na and K, and salts of alkaline elements, including Ca and Mg, generally increase the pH of biochar (Singh et al., 2010). Different pyrolysis conditions and different raw materials used will produce biochar with different nutrient levels (Chan et al., 2007). Typically, cellulose, hemicellulose, and lignin polymers are the main biopolymers found in biomass for biochar production (Sullivan and Ball, 2012). These components can come from sources such as tree bark, wood chips, leaves, crop residues, manure, sewage and paper sludge (Jyoti et al., 2019).

Carbon is the major element found in biochar and combines with other elements to develop some key functional groups found on the surface of the material. Inorganic carbon is also responsible for contributing to the generally alkaline nature of biochar. Carbon in biochar is also responsible for carbon sequestration, for example, in soil amendment applications (Xiao et al., 2018). Silicon also exists in biochar in several forms (including polymeric and crystalline forms), is a nutrient element, protects the organic phase, and can co-precipitate with heavy metals. Hydrogen is also crucial in biochar for the formation of hydrogen bonds, as an aromaticity index for biochar (when a H/C ratio is provided) and is also involved in association and dissociation mechanisms. Similarly to carbon, oxygen is important in biochar for forming different functional groups, and an O/C ratio can be presented as an index of the ageing degree for biochar. Oxygen is also involved in complexation with different metal ions. Nitrogen, another key element in biochar studies, is another nutrient element that adds to the soil improvement properties of biochar. It also improves the thermal stability of biochar and provides

active sites for reaction and modification. Phosphorus is another important nutrient element for soil improvement, but it is also a precipitator of heavy metals. Sulfur is also a nutrient element and solid acid catalyst and is important for increasing the solubility of carbon materials. Iron can exist in biochar as several different compounds, zero-valent iron, or in other metal complexes. It can increase the sorption ability of anions, is involved in graphitizing during pyrolysis, provides magnetism, and is involved in catalysis for organic pollutant degradation. Similarly, magnesium forms various compounds and metal complexes and is responsible for increasing anion sorption. It is also involved in CO_2 capture and is a nutrient element. The metal complexes and compounds of manganese also increase capacity and heavy metal sorption, whilst the compounds and metal complexes of nickel are involved in catalysing the production of syngas during biochar gasification. Other elements can be found within biochar; however, the above are the most significant.

Typically, elemental analyses are performed on biochar to gain information on elemental composition. For example, when an initial biochar feedstock of sewage sludge is used, which is high in ash, the concentration of Si has been found to range between 19–58 %, the concentration of Ca has been found to range between 5.1–7.4 %, and the concentration of P has been found to range between 3.4–4.9 % (Zielińska et al., 2015). Faecal and sewage sludge derived biochar generally have a lower total carbon concentration compared to cellulose derived biochar, due to the high ash content in the original feedstock (Nicholas et al., 2022). Carbon contents for faecal sludge biochar have been reported as ranging from 27.4–34.9 % (Gold et al., 2018), 17.2–34.1 % (Krueger et al., 2020), 6.5–11.1 % (Koetlisi and Muchaonyerwa, 2017) and 19.5 % (Woldetsadik et al., 2017).

Scanning Electron Microscopy (SEM) in combination with Energy Dispersive X-ray (EDX) analysis is a commonly used technique to illustrate the porous biochar structures as well as identify the presence of certain elements. SEM shows porous biochar structures that have a resemblance to the cellular structure of the original feedstocks used (Fuertes et al., 2010). SEM images can show high ash contents, whereas EDX can then provide numerical confirmation of elements. Typical EDX for biochar reveals high wt. % of carbon and oxygen, with smaller quantities of elements such as Ca, S, Si, K, Al, Mg, P, and Na. One investigation examined the differences in elemental composition of the biochar based on the different feedstocks used. Apple tree branch, oak tree, rice husk and rice straw were examined, and the percentage compositions for C, H, N and O were recorded (Jindo et al., 2014). H/C and O/C ratios are also useful indicators of biochar properties and are often reported. It was found that the percentages of C and H were significantly higher for biochar produced at temperatures of 400°C, 500°C, 600°C, 700°C and 800°C for the biochar derived from the apple tree branch and oak tree, compared to rice husk and rice straw. Another observed trend was that as the temperature was increased, a larger loss of H and O was observed compared to C. With increasing temperature, the H/C and O/C ratios steadily decrease as a result of the loss of easily degradable carbon compounds. A lower C/O ratio at higher temperatures is also indicative of a structural arrangement of aromatic rings that form very stable crystal graphite-like structures.

Thermal analysis is another insightful method to examine the composition of biochar materials, where in this reported investigation, the thermal degradation profile showed weight loss proportionally increasing with the increasing pyrolysis temperature. In this particular study, the clear difference between wood versus non-wood feedstocks and the resulting weight losses were shown. The biochar produced from apple tree branch and oak tree biomass feedstocks resulted in 90 % weight loss, whilst the rice husk and rice straw resulted in 40–50 % loss of the total weight, reflecting the higher mineral content in the rice materials compared to wood.

Biochar elemental composition has been found to depend on the method of analysis used, whereby key conclusions are that the classical elemental analysis rather than the spectroscopic method is better for determining nitrogen, as EDX spectroscopy is insensitive to nitrogen detection (Nzediegwu et al., 2021). Research has shown that ultimate analysis, energy dispersive X-ray spectroscopy and X-ray photoelectron spectroscopy are widely used for composition determination of materials such as biochar; however, the models that describe the relationship in elemental composition between ultimate and spectroscopic methods are limited.

The classical method for elemental composition determination of biochar is ultimate analysis, which involves combusting samples at >900°C in an elemental analyser. C, H, N and S concentrations are then estimated from the combusted gases that are released during sample combustion (these include CO_2, N_2O, and more). Elemental oxygen is then estimated from the difference. In contrast, techniques such as EDX and XPS have advantages over the classical method as they can simultaneously measure other properties of biochar, such as morphology and binding states, which can be advantageous. The disadvantages surrounding elemental composition determination are how effectively different spectroscopic methods can be linked and how effective their models are.

A further technique that may be used to characterise the composition of biochar is Electron Paramagnetic Resonance (EPR) which can provide detailed information about the local environment of paramagnetic centers in biochar, such as the nature of the ligands and includes the symmetry and geometry of metal complexes formed within biochar (Prosser and Walsby, 2017). These complexes can influence the biochar effectiveness in applications like soil conditioning and pollutant remediation. EPR, often used in conjunction with other, aforementioned, techniques like Fourier Transform Infrared (FTIR) or Raman spectroscopy, helps in identifying functional groups on the biochar surface (Gao et al., 2025). These functional groups are important for interactions with metal ions and other pollutants. In a study by Matos et al., EPR was used in the characterization of biochar from guava waste (pulp and seeds) to determine the nature of the Cu^{2+} complexes within the material as a result of different preparation conditions (Matos et al., 2019).

2.1.4. Surface energy of biochar

The surface energy, a measure of the free energy of a material's surface, of biochar is another parameter of interest to researchers, where contact angle is typically used to reflect the wettability of biochar surfaces. This is of interest since the contact angle often reflects how different biochar will affect soil water retention, transport and aggregation of particles in the environment, and sorption of environmental pollutants (Yang et al., 2020). The surface energy of a solid can be estimated by measuring the contact angle using solvents of differing polarity. The surface energy is then calculated from the contact angle in combination with Young's equation, although other variations and theories have been used, often leading to slight differences in reported surface energy values. Two methods of obtaining the contact angle of biochar exist: the sessile drop method, which is more commonly used to measure static contact angles, and the Washburn method. The sessile drop method involves colloidal biochar being attached to a double-sided adhesive tape that is attached to a glass microscope slide or using an ultrafiltration membrane to make a flat film.

For most contact angles recorded of biochar, the angles are larger than 90°, which infers that the biochar is generally hydrophobic. Other observed trends include that when biochar ages in soil, the contact angle generally decreases, and the biochar surface becomes more hydrophilic, possibly due to the oxidation of surface functional groups. This oxidation can lead to the formation of carboxyl groups, increasing the surface hydrophilicity and propensity to create surface charge. The recorded contact angle for biochar is affected by several parameters, including the pyrolysis process and conditions, feedstock used, and particle shape and size. Biochar has also been explored as a low-cost adsorbent for aqueous heavy metal removal, owing to the fact that the porous structure of biochar results in increased specific surface energy and provides extra effective sites for the adsorption of heavy metals(Qiu et al., 2021).

2.2. Physical properties

2.2.1. Phase analysis of biochar

Biochar can typically refer to sections as organic and inorganic phases. Depending on sorption mechanisms, it can also be distinguished into an organic-partitioning and a surface adsorption phase. Also, regarding their solubility, biochar can be categorized as a dissolved and undissolved phase. If carbon stability is referred to, it can be further classified into a labile phase and a stable phase. There are conditions whereby the different phases increase or decrease. For example, when the pyrolysis temperature is increased, and the biochar is dehydrated, the organic components are disrupted, and there is also successive aromatization, the aliphatic labile portion and dissolved-phase fraction would decrease, whilst the aromatic stable portion and the undissolved-phase would increase (Xiao et al., 2018). Over time, other chemical phases and states have been proposed. One is a transition phase with preserved crystalline character of the precursors, another is an amorphous phase with cracked molecules and aromatic polycondensations, another is a composite phase with poorly ordered graphene stacks, and a final phase is a turbostratic phase with disordered graphitic crystallites.

X-ray diffraction (XRD) is a common technique that has been used to confirm mineral components in biochar. Example mineral phases that have been commonly found in biochar include quartz, sylvite, calcite, calcium sulphate, and albite, which form during pyrolysis due to reactions between CO_2, alkaline earth metals and alkaline oxyhydroxides (Nicholas et al., 2022). Differences in mineral composition and phases can occur due to contamination. X-ray diffraction is also useful in comparing amorphous and crystalline regions, whereby crystalline regions are comprised of very ordered atom arrangements, whilst amorphous regions arise from disordered atom arrangements.

2.2.2. Surface area of biochar

The specific surface area (SSA) of biochar is a key factor that determines its ability to interact with other phases and/or chemical species. It is a critical parameter for any applications that hinges on fluid-solid interactions: gas/vapour separation, capture and storage (Dissanayake et al., 2020; Luo et al., 2022), environmental contaminant remediation (Dai et al., 2019; Qiu et al., 2022), catalysis (Fatnassi et al., 2022; Lyu et al., 2020) and supercapacitors (Luo et al., 2022; Song et al., 2019), or microbial growth (Liao et al., 2021; Ren et al., 2020). Surface area is often highly correlated with porosity, as discussed in the next section.

It is generally understood that the increase in pyrolysis temperature and residence time increases the total surface area of the product biochar material (Jiang et al., 2019) as hemicellulose, cellulose and lignin decompose in the 200–500°C range. Above a certain threshold (around 800–1000°C), a collapse of the structure and a reduction of surface area and porosity is expected (Sørmo et al., 2021). Engineered biochar can start with SSAs below 1 $m^2\ g^{-1}$ and increase to an average range of 8 to 132 $m^2\ g^{-1}$ (Leng et al.), with SSAs over 500 $m^2\ g^{-1}$ attainable with certain feedstocks and pyrolysis conditions, with an overview shown in Fig. 2.1 (Leng et al., 2021). Subsequent activation and surface treatments can dramatically increase the surface area to above 1000 $m^2\ g^{-1}$ (Liu, D. et al., 2016). Different biochar utilization avenues have varying surface area demands, although most applications benefit from a moderate SSA of a few 100 $m^2\ g^{-1}$. More in-depth works covering biochar engineering and measurement of surface area and porosity are found in previous literature (Ahmed et al., 2016; Sizmur, Tom et al., 2017; Weber, K. and Quicker, P., 2018).

SSA is typically measured using gas physisorption techniques (Thommes et al., 2015) as recommended by IUPAC. The procedure relies on determining the number of gas molecules required to completely cover the material's surface in a complete layer, or monolayer. Using an average value for the cross-sectional area of each adsorbed molecule, the SSA can be determined. Experimentally, this consists in recording a sorption isotherm of a gas or vapour adsorbent, then applying an appropriate model to obtain the sorption mechanism and uptake of a single layer, like the commonly used multilayer Brunauer-Emmett-Teller (BET) model or, more rarely the monolayer Langmuir model.

For performing the experiment, it is best practice to select a molecular adsorbent gas which minimizes any specific interaction with surface sites. The surface is first cleaned by applying a vacuum and heating. Then, an isotherm, the amount adsorbed on the surface as a function of pressure at a constant temperature, can be measured in a temperature / partial pressure range where the surface monolayer is formed. Commonly recommended adsorbent gases are nitrogen at 77 K (as adapted from the ASTM D6556–10 carbon black method) and argon at 87 K (Thommes et al., 2015), with argon being preferred as a spherical, inert molecule.

Measuring the surface area is known to be particularly challenging to apply when the surface is part of micropore walls, pores which

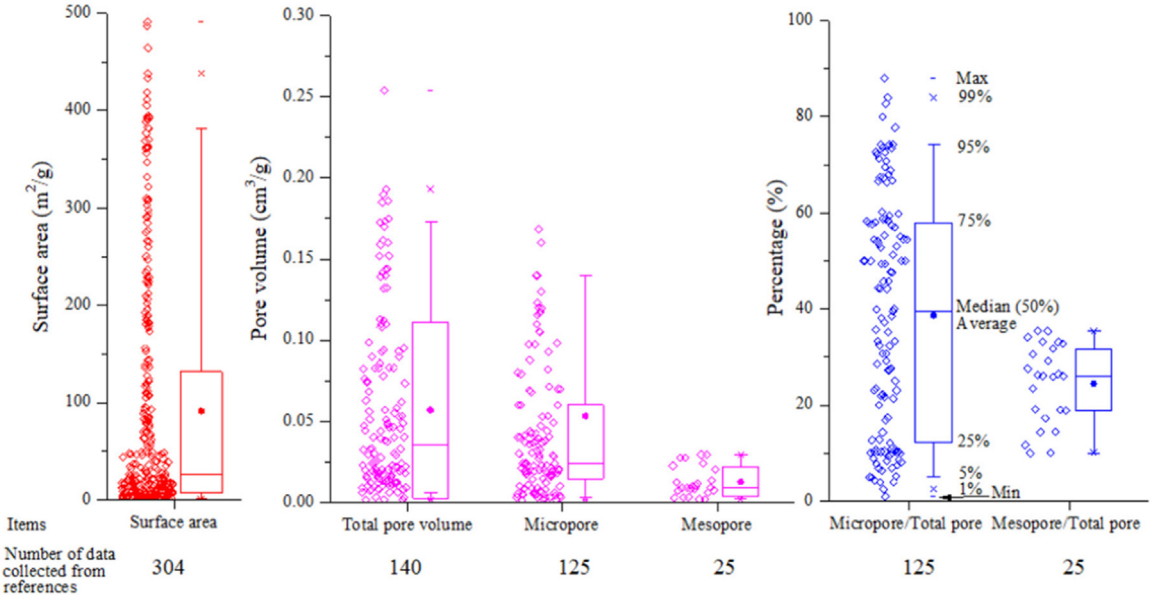

Fig. 2.1. A comprehensive overview of biochar surface area and micro-/meso-porosity from published literature. Adapted from (Leng et al., 2021).

form a significant percentage of biochar porosity (Leng et al., 2021; Rouquerol et al., 2007; Thommes et al., 2015). From a technical standpoint, surface area derived from physisorption in micropores does not have physical significance, as the adsorbent molecule does not form a single layer and rather fills the pore completely. Nevertheless, micropore SSA can be useful as a material fingerprint. Smaller molecules that can access ultramicropores below 0.5 nm, such as CO_2 at 273 K have been used for surface area determination (Kim et al., 2016; Sigmund et al., 2017) in biochar. Adsorption at higher temperatures also can overcome any diffusional limitations of sorption. Carbon dioxide's strong quadrupolar moment generally means that it has the potential to interact with surface functionalities, invalidating the BET model. For biochar with low surface areas, krypton sorption at 77 K (Thommes et al., 2015) and hydrocarbon sorption at ambient temperatures (Ribeiro Carrott et al., 2001) may be useful. The latter also has the advantage of minimizing thermal shock and pore contraction effects associated with rapid cooling to cryogenic temperatures.

Within the concept of specific surface area, we also include the active surface area (ASA). The ASA is a fraction of the total biochar SSA relevant to the end application. For example, this could be the SSA covered by catalytic (Lee et al., 2017) active sites, reactive functional groups or simply the fraction of sorption sites accessible for the target molecule or ions (Chi et al., 2021). Very rarely is the active surface area synonymous with the specific surface area, though they can often be intimately correlated. Depending on the relevant ASA, it may be evaluated using chemisorption techniques such as thermal programmed desorption, sorption-resorption experiments, or surface area determinations (Arenillas et al., 2002) with target or analogue molecules (Sato et al., 2022). A general conclusion is that active or accessible surface area may be a better metric than SSA as it more closely represents the end requirements.

2.2.3. Porosity of biochar

Porosity relates to the volume of voids within biochar (pore volume - PV) and their sizes (pore size distribution – PSD). As commonly defined (Thommes et al., 2015), porosity spans a wide range of length scales from microporous (< 2 nm) to mesoporous (between 2 to around 50 nm) to macroporous (between 50 nm to a couple of microns). Void volume above macropores generally consists of large capillaries or interparticle porosity and is often associated with large structural features and packing of biochar.

Biochar has been shown to display a hierarchical pore structure covering the whole porosity range – from ultramicropores in closely packed graphitic sheets (Keiluweit et al., 2010), mesopores formed though escape of volatiles during pyrolysis and macropores from residual feedstock structural features. Microporosity tends to develop exponentially at higher pyrolysis temperatures (Tan et al., 2018) and disproportionally contributes to the overall pore volume of biochar (Leng et al., 2021), as exemplified in Fig. 2.2. We similarly direct the reader to other more specific reviews from existing literature (Brewer et al., 2014; Leng et al., 2021; Luo et al., 2022; Weber, K. and Quicker, P., 2018).

Total biochar PV similarly affects biochar properties such as the surface area, and indeed, the two properties are related (Weber, K. and Quicker, P., 2018). More broadly, PV, PSD and tortuosity influence the transport properties of fluids, ions and microbes through biochar. When using biochar as an additive to concrete, the exchange of water from biochar pores with the cement matrix affects moisture regulation and the resulting curing time (Senadheera et al., 2023). Here, the porosity of biochar, particularly in the macropore region, affects the ultimate strength, breathability and moisture retention of the bulk material (Senadheera et al., 2023). The porosity of biochar used for soil amendment (Brewer et al., 2014) affects not only the transport of water, oxygen and nutrients but also the migration of microorganisms through the pore network.

A literature review by Leng et al. (Leng et al., 2021) identified the common distribution of biochar micro/mesoporosity to around 0.016–

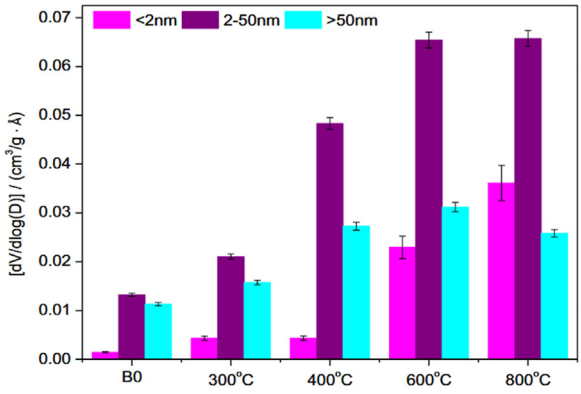

Fig. 2.2. Evolution of different pore volumes as a function of biochar preparation temperature. Biochar feedstock is rice wheat straw, with the evaluation of porosity performed by nitrogen physisorption. Bio adapted from (Tan et al., 2018).

0.083 $cm^3\ g^{-1}$, with upper values close to 0.25 $cm^3\ g^{-1}$. Again, further processing, like alkaline activation, can increase porosity in the range of conventional microporous carbons (Liu, D. et al., 2016). Interestingly, microporosity appears to be the dominant contribution to biochar porosity, as observed in Fig. 2.3. No information was available for the contributions of microporosity and large voids.

As the hierarchical porosity of biochar spans a wide range of length scales, no single method can give a complete characterization of PV and PSD, with some applicable methods showcased in Fig. 2.. It is, therefore, crucial to specify the methodology used during characterization. Mercury intrusion porosimetry and gas sorption are the most common methods used to assess the porosity of biochar, as they are widely applicable, mostly sample independent, generally accessible, and can characterize porosity in an extensive range of scales (Denoyel et al., 2004; Schlumberger and Thommes, 2021). The methods have different applicability ranges and some overlap, with gas sorption typically able to measure pores from small nanopores (0.5–1 nm) up to the high mesopore range (50–100 nm), while mercury intrusion porosimetry is applicable in the mid mesopore (20–40 nm) to the high macropore range.

In sorption methods, isotherms of a relevant adsorbent such as nitrogen or argon (Thommes et al., 2015) are collected over a full range of pressure up to its vapour pressure. In most cases, the increase of adsorbent gas uptake as pressure increases corresponds to a sequential filling of pores of different sizes. The isotherms are then processed with PSD models that relate a pore's characteristic size to its filling pressure. The models use various theory levels, like the Dubinin potential model for micropores (e.g. Horvath-Kawazoe), Kelvin's capillary condensation model for mesopores (e.g. Barett-Joyner-Halenda or Dollimore-Hill), or kernel fitting applicable to the full pore range (collections of isotherms obtained through DFT/NLDFT/QSDFT/GCMC etc). The models make significant assumptions about the shape and accessibility of the pores and often have limited applicability ranges in temperature, adsorbent gas and even surface functionalization, so a judicious choice must be made.

Mercury intrusion is a method to determine biochar porosity that relies on the low surface wettability of liquid mercury on most surfaces (Schlumberger and Thommes, 2021). In an experiment, liquid mercury is forced at high pressure into the biochar pores through hydrostatic pressure. A capillary filling model then relates increasing fluid pressure to intrusion within pores of a progressively smaller size. Similarly to gas sorption, a characteristic pore geometry must be assumed for the calculation. Another important factor is that high hydrostatic pressure may damage or crush the fine biochar structures. It is therefore important to perform multiple cycles of intrusion/extrusion to evaluate any structural attrition due to the method and evaluate any retention of mercury inside the porous structure.

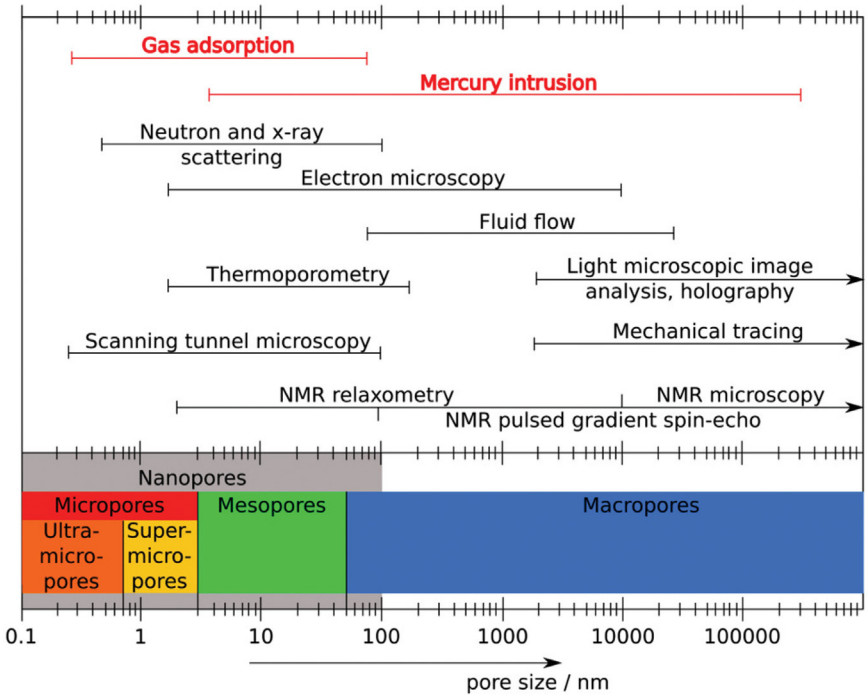

Fig. 2.3. Characterization of porosity at various length scales. Reproduced from [ref (Schlumberger and Thommes, 2021)] originally from (Klobes and Munro, 2006).

Macroporosity can also be observed and quantified through imaging techniques like SEM and TEM (Hassan, M. et al., 2020). These methods directly observe the sample's structure to ascertain the size and shape of the exterior pore openings. To accurately determine the extent of porosity from microscopic techniques, enough representative images should be acquired and processed to obtain an accurate evaluation. Other methods like positron annihilation lifetime spectroscopy (PALS(Sato et al., 2022)), small angle X-ray and neutron scattering (SAXS/(Liu, Y. et al., 2021)SANS), time-domain nuclear magnetic resonance (TD-NMR(Wong et al., 2019)), are advanced options which can yield a wealth of information on porosity, though uncommonly available.

2.2.4. *Density of biochar*

The density of biochar is a physical property closely related to porosity. It determines its specific volume, a crucial parameter that, in practice, is related to the space utilization in biochar-based applications, from equipment sizing to the cost of transport.

Due to the porous and finely divided nature of biochar, we can divide its density into several different components (Fig. 2.4). The skeletal or true density corresponds to the density of the solid carbon matrix backbone, excluding any micro-, meso- or macroporosity. Then, the particle or envelope density sets the delimiting boundary at the surface of individual biochar particles, meaning it includes intraparticle porosity, but excludes any inter-particle voids. Finally, the bulk or packing density corresponds to the density of a bed of material. In practical terms, the lower the density, the lighter the biochar becomes. The limit of 1 g cm^{-3} is particularly important as any material with a lower density will float on water (as measured by non-wettable density), which plays a role in its transport in the environment (Brewer et al., 2014). For other considerations, bulk density is the most relevant design parameter as it pertains to practical storage and sizing considerations.

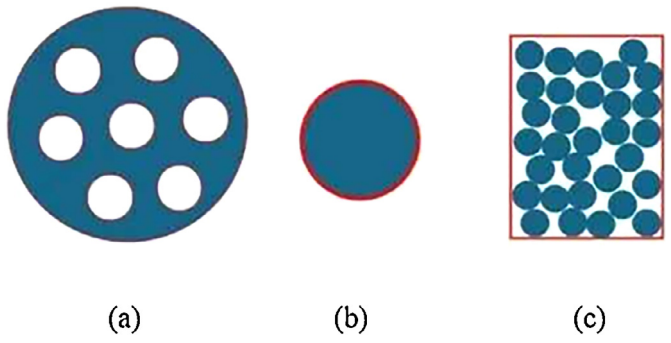

Fig. 2.4. Definition of skeletal (a), particle (b) and bulk density (c).

As the total porosity of biochar increases, the bulk and envelope densities necessarily decrease (Weber, K. and Quicker, P., 2018) – a higher percentage of void volume leads to a lower proportion of solids per unit volume. Therefore, the opposite trends are observed for density for PV with respect to pyrolysis temperature, heating rate, subsequent activation, etc. Somewhat counterintuitively, biochar skeletal density often has an opposite trend (Brewer et al., 2014; Weber, K. and Quicker, P., 2018). This can be explained as the solid matrix of biochar condenses throughout volatilization and forms higher-density aromatic components similar to graphite (Lehmann and Joseph, 2015).

Skeletal density is usually measured using gas pycnometry. The technique consists of expanding a pressurized gas from a reference volume to a sample volume containing a known quantity of biochar, both volumes previously calibrated while empty. After expansion, the volume of the sample is determined through the difference between the sample volumes as newly calculated and previously known, and density can be calculated based on the measured sample mass. The gas is generally prescribed as helium, which closely approaches ideality and avoids adsorption on the sample's surface. The biochar's surface should be clean of adsorbed gases and humidity. Indeed, the gas pycnometric method is similar to volumetric sorption set-ups used to determine BET surface area and micro/meso porosity. As these devices often include a helium expansion as part of the measurement, using a sample cell with pre-calibrated volume allows the determination of a reasonably accurate sample density.

Bulk density can be measured using simple graduated cylinders or other calibrated volumes that are significantly larger than the biochar grains (Schmidt et al., 2013). It can vary depending on the biochar's packing efficiency and therefore, should be

evaluated a sufficient number of times to obtain a reproducible determination.

Envelope density can be one of the most challenging properties as it must be measured using adsorbents that are large enough not to enter the porosity but small enough to completely fill all interparticle voids. Pycnometry using fine solid granules with a well-defined particle size distribution in the micrometer range (Brewer et al., 2014). A good coverage of the granules on the biochar flakes in the instrument should be achieved to attain the best accuracy.

Fluid immersion pycnometer is another common technology used for determining particle density, but this method is discouraged for porous materials like biochar. This is due to the unknown surface wetting and pore filling characteristics of the fluid in the porous network of the biochar – meaning it is unclear whether the density measured is a skeletal or envelope density.

2.2.5. Morphology of biochar

The morphology of biochar is commonly understood as its microstructure, particle shape, and other structural surface features. In biochar application, surface morphology is known to influence its biocompatibility with microbes and bacteria when used for soil amendment (Gul et al., 2015) and its surface compatibility with various support structures/matrices like electrodes (Song et al., 2019), concretes (Gupta and Kua, 2019) or resins (Bartoli et al., 2019).

Common observations on biochar morphology demonstrate that it is often closely derived from and similar to the morphology of its parent feedstock (Hassan, M. et al.). Plant cell features are still recognizable for wood, straw, and other similar materials. Increasing temperature leads to microstructure evolution through graphitization, closer packing, and vesicle formation from gas volatilization. Fig. 2.5 shows scanning electron microscope images of pinewood biomass and the derived biochar produced at pyrolysis temperatures of 300 and 700°C.

Due to its intricacy, the determination of biochar morphology is often difficult to interpret conclusively. It can be observed directly using microscopy or microimaging techniques such as scanning electron microscopy (SEM) and transmission electron microscopy (TEM). This technique allows for visualizing the biochar's surface textures and identifying any structural features that may impact its functional properties (Ahmad et al., 2012; Liu et al., 2010). An evaluation of the fractal characteristics and roughness of the surface can also be obtained through scattering techniques, such as SAXS (Rechberger et al., 2017).

The state of the biochar backbone microstructure is a similar indication of biochar morphology. With increasing pyrolysis temperatures, the graphitization of biochar carbon will rearrange the amorphous and disordered chains towards ordered, increasingly aromatic turbostratic and graphitic structures. The evolution of well-ordered sheets can be followed though diffractive methods, most commonly X-rays (XRD). The observation of well-defined peaks in XRD patterns signifies the presence of ordered matter, and their intensity, positions, and width can be related to the degree of graphitic crystallinity, sheet-to-sheet distance and particle size, respectively (Amin et al., 2016).

2.2.6. Particle size of biochar

Particle size affects the biochar's interaction with any matrix it is embedded in, such as soil or concrete. It generally dominates the flowability of the grains during production. Moreover, mass transport through a porous material like biochar is often dominated by the particle's size. The decrease in average particle size also impacts specific surface area through a change in the surface to volume ratio, as well as some porosity and bulk density through the particle packing characteristics (He et al., 2018). The optimization of biochar particle size is also imperative to mitigate some of the harmful environmental and cytotoxic effects (Xiang et al., 2021) associated with nanoparticulates, such as air quality.

Particle size is significantly affected by the pellet/grain sizes of the original feedstock. This original particle size distribution is modified through shrinkage and expansion, as well as mechanical attrition during the pyrolysis process and subsequent grinding (Lehmann and Joseph, 2015). These changes depend heavily on the process conditions and starting material, but a few general observations are possible. While microporosity increases, the bulk grains tend to shrink as the carbon matrix rearranges. Harsher pyrolysis conditions, especially faster heating rates, tend to break apart the grains and reduce the average size (Mendonça et al., 2017; Weber, K. and Quicker, P., 2018).

Sieve analysis, image analysis or diffractive/scattering methods are employed to quantify the particle size distribution. For larger particle sizes between 0.5 mm and above 50 mm, sieving using sieves of progressive mesh sizes is a straightforward recommended method (Initiative, 2015). The IBI standard suggests a sequence of standard sieves that can be used in this range, as well as a range-percentage-per-weight reporting method. Image analysis uses snapshots obtained from either optical or electron microscopy, obtaining a size distribution by directly observing the size of individual particles and building a statistical population. It has the added advantage of giving information about the particles' shape and is usually applicable from the micron to the mm range.

Finally, the particle distribution of submicron biochar dust can be measured using scattering techniques, like static or dynamic light scattering (SLS and DLS). SLS has an accuracy range from nm to mm. A refractive index for the material must be known for accurate size determination (Kim, K.H. et al., 2012; Pituello et al., 2018). Traditionally, SLS required a stable particle suspension, though recent advances have made possible measurements in a fluidized bed. DLS measures distributions of biochar particles in suspension from nanoparticle to a few micron ranges (Fang et al., 2020). It requires a stable suspension of particles for measurement. It should be noted that particle size methods may not necessarily provide shape analysis and rather give a critical size – e.g. preferred orientation when using sieves, hydrodynamic diameter for DLS, spherical approximation for SLS, etc.

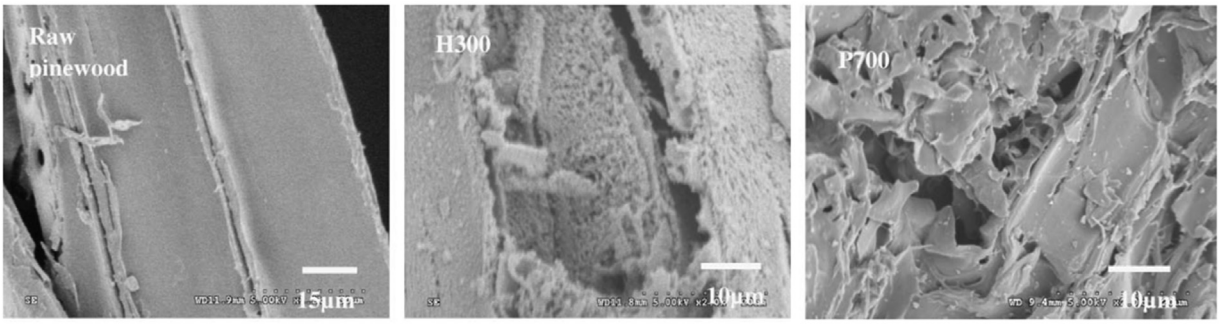

Fig. 2.5. Evolution of pinewood-derived biochar at different pyrolysis temperatures (left) parent material (center) pyrolyzed at 300°C (right) pyrolyzed at 700°C. Adapted from (Liu et al., 2010).

2.2.7. Thermal conductivity and heat capacity of biochar

Thermal conductivity is indicative of a material's ability to transfer heat, while heat capacity is a measure of the energy exchange required to change it. In biochar applications, thermal conductivity is immediately relevant to its use in building materials as it changes the overall insulation ability and thermal retention potential (Legan et al., 2022) – with a low thermal conductivity and high heat capacity desirable. Less obviously, the two properties are important in biochar's use as a sorbent and catalytic material. Heat management of a sorbent material ensures its temperature is optimal throughout the process by allowing excess heat to be removed or heating to be applied. Heating cycles are often used to regenerate the original material by removing adsorbed components. In these cases, the inverse is true – a high thermal conductivity and low heat capacity is desirable.

Both properties can vary widely, generally as a function of biochar's porosity and implicitly its density. It is noted that the thermal properties are significantly impacted by any fluid or solid filling the biochar's pores. The higher the porosity, the more the bulk thermal properties are a function of the pore content rather than the matrix itself. Generally, increasing porosity lowers the thermal conductivity due to the proportion of empty space relative to the solid skeleton. The thermal conductivity of raw feedstocks is in the order of 0.2–0.45 W m^{-1} K^{-1}, decreasing to below 0.1 W m^{-1} K^{-1} as the porosity increases (Gupta and Kua, 2019; Hekimoğlu et al., 2021). Thermal conductivity is a property that can also vary with the direction of heat transfer, i.e., it can show anisotropicity. The anisotropic behaviour is more pronounced if the heterogenous feedstock structure of the biochar grains is maintained (Weber, K. and Quicker, P., 2018). It was shown that by increasing pyrolysis temperature and thereby homogenizing the biochar structure, the anisotropy in thermal conductivity is reduced. Heat capacity is reported on a weight basis, and it is therefore not impacted by density and more a function of the biochar's composition (Dupont et al., 2014), like the proportion of non-volatilized light solids, ash, and graphitized carbon. Measured values for heat capacity range in the order of 1000–1300 J $kg^{-1}K^{-1}$ (Weber, K. and Quicker, P., 2018), which are comparable to other graphitized carbon structures.

Thermal conductivity is measured using steady state or time-domain techniques such as the hot disk or transient plane source (TPS) method (Orlova et al., 2016). These evaluate the thermal response and heat dissipation properties of individual biochar grains to a steady or short heat pulse. Correct set-up of the experimental method is crucial as the measurement is often prone to errors due to challenges in interface conditions, anisotropy, homogeneity, etc. (Palacios et al., 2019).

Heat capacity is commonly evaluated in a differential scanning calorimeter (DSC) or in an adiabatic calorimeter. Thermal analysis methods measure the temperature and heat flow to a sample. By heating in a relevant temperature range, the heat capacity C_p can be determined at each temperature as the heat flow required to change the biochar's temperature. Both methods have been successfully used (Weber, K. and Quicker, P., 2018), though selecting the method which affords a larger sample can improve accuracy.

2.3. Environmental stability and contamination

2.3.1. Environmental contamination by biochar

Naturally, the product stream of biochar via the pyrolysis of variable biomass feedstocks introduces possible risks in the absence of necessary oversight. Since the feedstocks of biochar are variable, from manure biochar (MBs) to those produced from plant biomass biochar (BBs), municipal solid waste biochar (MSWBs), and coal refuse biochar (CRBs), there are variations in the chemical and physical properties. Although biochar is primarily composed of carbon, amongst other elements such as calcium, magnesium, hydrogen, and nitrogen, some feedstocks can introduce toxic heavy metals such as Cd, Ni, Pb, and Cr. Feedstocks that are most likely to contain heavy metals are MBs, MSWBs, and CRBs, with heavy metals accumulating in the ash fractions during pyrolysis. Heavy metals are suspected to arise from the presence of inorganic salts and hydroxides, which are converted into thermally stable substances as the pyrolysis temperature increases. The heavy metal concentration is also enriched via the decomposition of organics during the pyrolysis procedure. Due to the high surface area of wood-derived biochar, a consequence of its high lignin content, wood-derived biochar often contains heavier metals, but lower concentrations of metals overall compared to biochar prepared from other feedstocks (Murtaza et al., 2022).

As such, the heavy metal content of biochar must be tested before they are introduced to the environment, in applications such as fertilizer, to prevent heavy metals from leeching into the environment. A number of ecological risk indicators (ERIs) can be used to describe the impact of biochar on the environment; these ERIs are detailed in Table 2.1.

In general, a GAI is measured between 0 and 5, with 0 being unpolluted and 5 being extremely polluted. Likewise, PERI values follow a similar trend: 30>PERI – PERI>120, representing low risk – very high risk.

A study by Kujaska (Kujawska, 2023) observed the heavy metal contents of biochar produced from Biomass (BB), municipal waste (MSWB), compost (BP), and coal refuse (CRB). Heavy metals were first extracted with water, and samples were then placed in a microwave digester. The heavy metal contents, Cr, Ni, Cu, Zn, Pb, As, and Cd, were determined using ICP-MS. The metal contents of the CRB were found to be significantly higher than all other biochar samples tested. The distribution of heavy metals in relation to metal concentration followed the sequence Pb>Cr>Ni>Cu>Zn>As>Cd for BB; Zn>Cr>Cu>Pb>Cd>As for BP; Zn>Cr>Cu>Pb>Ni>Cd>As for CRB; and Zn>Cr>Ni>Cu>Pb>Cd>As for MSWB. Overall, the heavy metal contents were found to be below the threshold levels for environmental contamination. PERI values were seen to be low to moderate (50–100) for all biochars except CRB, which had a high PERI above 250.

Wang et al. (Wang, A. et al., 2021) studied the heavy metal contents of biochar produced from manure species, chicken manure (CMB), and water-washed swine manure (WSMB), at different pyrolysis temperatures. Samples were pyrolyzed at 200, 350, 500, 650, and 800°C, with heavy metal analysis undertaken using a CHNOS Elemental analyzer. Metals under investigation included Zn, Ni, Mn, Cr, As, and Cd. The concentrations of heavy metals in CMB and WSMB followed decreasing trends of Mn>Zn>Cu>Cr>Ni>As>Cd and Zn>Mn>Cu>Ni>Cr>As>Cd, respectively. The concentration of Zn and Cu were found to be an order of magnitude higher in WSMB than CMB and over the threshold value for environmental contamination, with WSMB Mn concentrations also showing almost double that of CMB at 184.40 mg kg^{-1} and 326.29 mg kg^{-1}, respectively. The study concluded that increasing the pyrolysis temperature of the biochar for both CMB and WSMB decreased the leaching rates of all metals within the biochar. At higher temperatures of pyrolysis, it was suggested that higher ash concentrations inhibit the diffusion of heavy metals out of the biochar structure, leading to lower leaching rates. For both CMB and WSMB, the PERI was seen to decrease with increasing pyrolysis temperature from around 45 to below 30.

Oleszczuk et al. (Oleszczuk et al., 2013) also studied the heavy metal contents of four biochars from plant biomass, along with the presence of polymeric aromatic hydrocarbons (PAHs). The presence of these PAHs is assumed to arise from the pyrolysis temperature and the biochar feedstock, with most PAHs forming via demethylation and dihydroxylation of lignin and cellulose species at high temperatures (>700°C), therefore mitigating the environmental benefit of the possible reduction in heavy metal leaching with higher pyrolysis temperatures. The study applied biological tests (bioassays) to study the phytotoxic effect of both heavy metals and PAHs on seed germination and microbial growth. Heavy metals were analyzed using ICP-MS post-microwave digestion, and PAHs were analyzed using HPLC. The metal content of the biochar was found to be distinctly tied to the feedstocks, with biochar from silver grass showing the highest metal content, with Pb content being at similar concentrations across all biochar samples; significant differences were observed in Cr (0 – 18 mg/kg) and Zn (30 – 102 mg/kg). Despite the high

Table 2.1
A summary of ecological risk indicators related to the use of biochar, the equations, and their description.

Ecological risk indicator	Equation	Description
Geo-accumulation index, GAI	$GAI = \log_2 \frac{c_n}{1.5B_n}$	A value denoting the accumulation of heavy metals in the environment, where c_n is the measured content of heavy metals in plant and other matter, and B_n is the background value of heavy metals.
Pollution Coefficient, c_f^i	$c_f^i = \frac{c_D^i}{c_R^i}$	A value that defines the likelihood of heavy metal pollution, where $C_D{}^i$ is the heavy metal content in the sample, and $C_R{}^i$ is the background heavy metal content.
Ecological risk, E_r^i	$E_r^i = T_r^i \times c_f^i$	A value that defines ecological risk, where $T_r{}^i$ is the toxicity factor of heavy metals
Potential Ecological Risk Index, PERI	$PERI = \sum_{i=1}^{n} E_r^i$	PERI is the potential ecological risk index of the overall contamination risk of the biochar from multiple heavy metals.

metal content, the concentrations were found to be lower than EU regulated standards. Similarly, the PAH concentrations depended heavily on the feedstock between 1 – 28.3 mg/kg, with biochar from silver grass displaying the highest PAH concentration. Looking at the ecotoxicological effects, some biochar was seen to inhibit root growth. However, some biochar was seen to increase root growth. Biochar from wicker was observed to increase root growth by 12–14 %, with a similar root stimulation found when introducing coconut biochar. Biochar derived from silver grass and wheat straw displayed significant root growth inhibition above 5 % soil dosage. Overall, the study raised concerns about PAH levels, causing a potential risk to biological life.

A similar study by Buss et al. (Buss et al., 2015) also looked at the organic compounds found in biochar and the potential toxic effects. Particular interest was placed on the contamination of biochar by re-condensed pyrolysis liquids, which contain large concentrations of volatile organic compounds (VOCs). Softwood pellets were first pyrolyzed at 550 C, and then the pyrolysis liquids and gases were reintroduced to the biochar to produce the contaminated samples. The concentrations of organic species in the pristine and contaminated samples were measured using GC–MS, UV–Vis, and mass spectrometry. Similar to the results reported by Oleszczuk et al., the phytotoxic potential was investigated using seed germination. As expected, pristine biochar displayed little toxicity, whereas contaminated biochar contained high VOC content and caused adverse effects on seed growth. In contaminated biochar, PAHs were found to be above the soil toxicity level at >27 ug/g. It was suggested that the more mobile VOCs posed a greater risk than the PAHs and that VOC content should be checked for biochar quality control.

In a separate study, Buss et al. (Buss et al., 2016) suggested methods by which biochar may be synthesized with minimal PAH contamination. The study involved 46 biochar samples from varied feedstocks, produced under highly controlled pyrolysis conditions, monitoring temperature (350 – 750°C), residence time (10 – 40 min), and carrier gas flows (0 – 0.67 L min^{-1}). For PAH analysis, biochar was ground, followed by Soxhlet toluene extraction; extracted PAHs were then analyzed using GC–MS. PAH concentrations were found to vary widely between samples from 1.2 – 1000 mg kg^{-1}, with 46 % of biochar found to be higher than the Index of Biological Integrity (IBI) threshold of 20 mg kg^{-1}. Analysis of temperature on the PAH formation revealed little change between 350 – 650°C but increases in PAH concentration at a temperature of 750°C with the magnitude dependent on the feedstock. Carrier gas flow rate used during biomass pyrolysis was also found to have a significant impact on PAH mitigation, with higher flow rates (0.67 L min^{-1}) decreasing the biochar PAH contamination irrespective of temperature or residence time. As shown in previous studies, the PAH concentration was also strongly dependent on the feedstock, with large differences found between wood and straw-derived biochar, with woody biochar producing fewer PAHs. Conclusions were drawn around proper pyrolysis reactor design and higher carrier gas flow rates to minimize PAH formation, with temperature effects playing a less important role.

(Qiu et al., 2015) also investigated the effect of feedstock and pyrolysis temperatures on the PAH and metal contents of biochar samples. Biochar were pyrolyzed from both plant residues and animal waste at 300, 400, and 600°C. Extracted metals were analysed using ICP-MS, and PAHs were analysed using Accelerated Solvent Extraction and then GC–MS. Conclusions were drawn that the feedstock of the biochar plays a significant role in the metal contents, whereas temperature has a small effect. In contrast, PAHs were found to be affected by the pyrolysis temperature, with biochar pyrolyzed at 450°C containing higher PAH concentrations than those pyrolyzed at 300 and 650°C, as well as being affected by the feedstock. It was suggested that biochar should be synthesized at lower temperatures to be more cost-effective or at higher temperatures to reduce environmental impact.

Lyu et al. (Lyu, Honghong et al., 2016) looked at the direct role of pyrolysis temperature on the toxicity of biochar arising from PAH formation, along with polychlorinated dioxins and furans (PCDD/PCDF). Biochar was produced from sawdust at temperatures between 200 – 700°C. Soxhlet extraction was performed using dichloromethane or toluene for PAHs and PCDD/PCDF, respectively, and subsequent analysis was performed by HPLC–MS. Toxicity studies were undertaken by adding the extracted PAHs to H4IIE-luc cell line assays and Mictrotox bacteria bioassays. The concentration of PAHs was said to have achieved a maximum at 400°C (0.86 mg kg^{-1}), falling moderately at higher temperatures to 0.59 mg kg^{-1}. The study attributed this PAH concentration decrease to a decrease in 5–6-ring PAHs found in biochar pyrolyzed above temperatures of 400°C. In general, biochar pyrolyzed at lower temperatures (<400°C) was found to be much more toxic, with EC50 values (effective concentration 50 %) more than seven times lower than biochar pyrolyzed at 700°C. This conclusion is contradictory to previous studies and reinforces the point raised by Buss et al. (2016) that the pyrolysis temperature alone is not a significant contributor to toxicity, but rather feedstock, the pyrolysis reactor, and pyrolysis experiment design as a whole are much more important.

Finally, the effects of ageing and the deployment environment were studied by Zhang et al. (Zhang, Y. et al., 2022) on biochar produced from pine needles. The environmental pH and organic content (HA and SDBS) were controlled, along with the suspension (ageing) time. The toxicity was measured using algae cultivation, cell growth inhibition, and free-radical detection (EPR). The toxicity of pristine and aged biochar decreased with increasing pH by up to 40 %, and it was theorized that a lower pH adjusts the redox active moieties on the surface of the biochar, which affects metal leaching. As the pH increases, the net positive charge on the biochar surface decreases due to the deprotonation of carboxylic acid and hydroxyl groups. The addition of humic acid (HA) was also seen to decrease the toxicity of pristine biochar but increase the toxicity of aged biochar by between 20–40 %. The same effect was observed for the addition of sodium dodecyl benzene sulfonate (SDBS). It was concluded that the toxicity of biochar arises mainly from the adhesion of biochar on the cell surface and the oxidative damage caused by adhered biochar. Fig. 2.6 summarises the impact of contaminated biomass on the environment.

2.3.2. Stability of biochar

Since the toxicity of biochar is somewhat dependent on the stability, an examination of the biochar stability in the deployed environment is required. Biochar is characterized by its aromatic carbon structures, organized into amorphous and crystalline phases. As such, the stability of biochar arises predominately from the stability of these carbon struc-

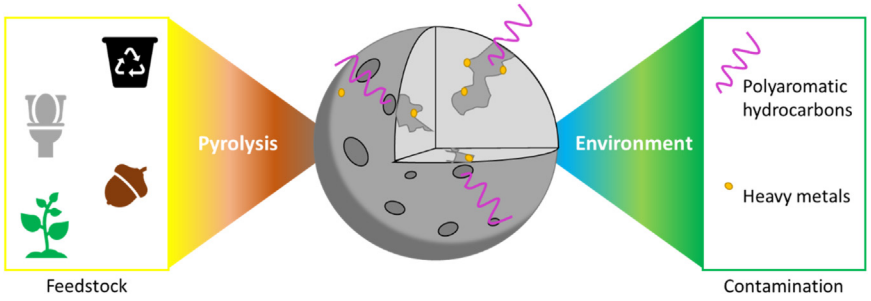

Fig. 2.6. Feedstock conversion into biochar, followed by environmental contamination.

Table 2.2
The effect of biomass feedstock on the post-pyrolaysation content.

Biomass	Volatile matter (VM)	Fixed carbon (FC)	Ash	N	C	O	H/C	T_{max}
Bark	81.8±0.3	15±1	2.8±0.8	0.25	45	46	1.5	400
Corn	71.2±0.6	17±1	11.7±0.7	1	40	43	1.6	355
Litter	62±5	1±8	38±10	2.1	23	35	1.5	350
Manure	76±6	1±4	24±6	4.1	34	31	1.7	340

tures, and the degree of aromaticity provides an indication of biochar stability. Non-aromatic, functionalized moieties such as C – O and C – N functional groups on the biochar surface provide points in the biochar structure with relatively high reactivity (Chen, D. et al., 2016b), which can lead to structure degradation.

The oxidative stability can be measured by thermal oxidative degradation (temperature-programmed oxidation, TPO) using thermogravimetric analysis (TGA) or differential scanning calorimetry (DSC). In a typical TPO, the sample is heated in an atmosphere containing oxygen, with the mass loss curve used to assess the relative stability of biochar from various feedstocks. The volatile matter (VM) that leaves the biochar upon heating is typically assessed using analytical methods such as GC–MS (Kaal et al., 2012). The peak temperature (the highest temperature of the pyrolysis method) during material heating is seen to be the most reliable parameter to characterize material oxidative stability.

A study was undertaken by Conti et al. (Conti et al., 2016) on a set of 22 biochar from various feedstocks, pyrolyzed under various conditions, to assess the effect of feedstock and biomass pyrolysis conditions on oxidative stability. The stability of biochar was analyzed using Py-GC–MS at 900°C for 100 s using He as a carrier gas.

The largest differences between samples arose in fixed carbon content (FC) between corn stalk biochar and mushroom litter biochar, between corn stalk ash content and bark ash content, and between mushroom litter volatile matter and bark volatile matter. It was asserted that a trend was seen between H/C content and T_{max}. Materials with H/C content between 1.6 and 1.8 tended to have lower T_{max} values and materials with H/C content lower than 1.5 tended to have higher T_{max} temperatures. This trend was also observed using corn stalk biochar pyrolyzed at increasing temperatures between 400 – 650°C over various times, which changed the H/C ratio and subsequent T_{max} (Table 2.2). A study by McBeath et al. (McBeath et al., 2015) is suggested for those who are interested in an in-depth study of feedstock and pyrolysis conditions on the physical properties of biochar. The conclusions drawn in this study are consistent with those discussed above.

The changes in biochar composition and stability due to the feedstock were also investigated by Choudhary et al. (Choudhary et al., 2019), who looked at sugarcane, rice husk, and farmyard manure-derived biochar at 350°C. The elemental composition was obtained by titration (N), the ammonium heptamolybdate-ammonium vanadate method (P), a flame photometer (K), and atomic absorption spectroscopy (heavy metals and micronutrients). Biochar produced from farmyard manure (FM) was seen to have a higher fixed carbon % and lower volatile matter and ash contents than the other two feedstocks. In all cases, the heavy metal content was negligible, and though sugarcane (SF) derived biochar had a high nutrient (mineral) content, the content was not too dissimilar to that of the other feedstocks. FM biochar was seen to produce biochar of smaller particle size, with rice husk biochar producing the largest samples; a similar trend was observed with surface area. Given the variation in feedstock and biochar properties, it is difficult to draw conclusions directly on which feedstocks produce more stable biochar, as such properties as particle size and aromatic content can also be manipulated in the pyrolysis stage. Regardless, in this work, it was concluded that SF biochar displayed higher thermal stability (thermogravimetric analysis) than SF and RH biochar.

Other factors introduced during the pyrolysis process can influence the stability of biochar. A study by Manya et al. (Manyà et al., 2014) also looked at the effect of pyrolysis pressure and particle size, in addition to peak temperature on theoretical particle stability. Biochar was produced from crushed vine shoots, which were then sieved to obtain three feedstock particle sizes between 0.98 - 3.01 cm. These vine shoot particles were then pyrolyzed at pressures between 0.1 and 1.1 MPa and peak temperatures between 400 – 600°C. The biochar produced from larger particles tended to contain higher percentages of aromatic content and lower O/C ratios. A similar trend was also seen with peak temperature. The effects of pressure on the fixed carbon content and O/C ratio were seen to be statistically insignificant. Since no actual stability tests were performed, it is somewhat difficult to draw complete conclusions. However, given previous studies, it does look like a higher particle size and peak temperatures do reduce the presence of oxidizable functional groups in biochar.

In a laboratory, these oxidative pathways can be accelerated via chemical methods using oxidation agents such as potassium dichromate used by Knicker et al. (Knicker et al., 2007). The consumption of dichromate was measured spectrophotometrically, with the mass of oxidized carbon calculated using the mass balance equation (Eq. 2.1):

$$2K_2Cr_2O_7+3C+8H_2SO_4=2K_2SO_4+2Cr_2(SO_4)_3+3CO_2+8H_2O \quad \text{(Eq. (2.1))}$$

The carbon loss calculated from potassium dichromate oxidization was seen to be related to the ratio of oxygen/carbon, again indicating that oxygen-containing functional groups provide points for degradation in the structure. Another method of accelerating oxidation is via the use of potassium permanganate, as performed by Calvelo Pereira et al. (Calvelo Pereira et al., 2011), which also found correlations between oxidization and H/C and O/C molar ratios; however, oxidized fractions were observed to be consistently lower than those found for dichromate.

Further, a study by Naisse et al. (Naisse et al., 2013) looked at two techniques for assessing biochar stability: acid hydrolysis and dichromate. Tests were applied to biochar with different elemental compositions (induced by differing feedstocks), and it was found that the dichromate test was better for observing trends between H/C ratio and stability than the acid hydrolysis test. From the stability tests, it appears that gasification chars (those chars obtained at higher temperatures >1000°C in the presence of an oxidizing agent) were more stable under oxidation conditions compared to those obtained from hydrothermal carbonation. However, it is likely that the gasification chars have already had moieties unstable under oxidization conditions removed during the synthesis procedure. For a full review of biochar accelerated aging methods, this review suggested reading the review led by Leng et al. (2021) which covers a range of biochar stability assessment methods.

Yang et al. (Yang, Y. et al., 2018) studied the correlation between mineral content and biochar stability (oxidation resistance). Biochar was produced from two feedstocks, rice straw (RI) and swine manure (SW), at temperatures between 250 and 600°C. Portions of the biochar were de-ashed using an acid solution and centrifugation. Likewise, some of the biochar samples were iron-doped using a $FeCl_3$ solution. Biochar samples were characterized using elemental analysis (C, H, N, and O), XPS (surface), XRD (Fe), EDS (sub-surface), and NMR (C^{13}). The stability of biochar was performed using both thermal (TGA <900°C) and chemical (dichromate) oxidation. The H/C and O/C ratios were again observed to decrease with pyrolysis temperature, with the C^{13} indicating an increase in aromaticity, which further points to increasing stability. From the XRD studies, the SW biochar was found to contain crystal mineral phases, which were absent in RI biochar, indicating an influence of feedstock on mineral content. After $FeCl_3$ treatment, Fe was detected throughout the biochar sample using SEM-EDS between 2.9–13.9 %. The presence of this Fe content was observed to influence the biochar stability, with mixed results based on the chemical oxidant used and the conditions.

In order to characterize the structure of wood chars, Cao et al. (Cao et al., 2012) employed solid-state C^{13} NMR. The idea behind the research stems from the fact that a higher pyrolysis temperature seems to increase biochar stability, and as such, this work looked at the structures of biochar pyrolyzed between 300–700°C. As expected, complementary EDS showed the usual trend of H/C and O/C ratios decreasing with increasing pyrolysis temperature. However, the NMR revealed much more about the changing structure of the wood biochar. At a pyrolysis temperature of 300°C, the biochar structure was majorly composed of lignocellulosic moieties, carbohydrates containing many CH and CO groups. At 400°C, the frequency of protonated aromatic carbons decreased, becoming non-protonated, and the number of C—O groups decreased. Above 400°C, these non-protonated aromatic structures were seen to cluster together up to 27 rings observed at 700°C, which will aid oxidative stability.

In a critical review of biochar environments on stability and sorption, Lian and Xing (2017) reached many of the same conclusions as those discussed in this chapter. The pyrolysis temperature or heat treatment temperature (HTT) was seen as the main factor for increasing stability by lowering the H/C and O/C ratio. The review also looked at the microbial decomposition of biochar, the most likely degradation pathway, and it is suggested that readers review this section if such discussions are of interest. In summary, biochar was seen to have two degradation stages, which occur at different rates: one fast stage degrades the volatile fractions in the biochar, and a slow stage degrades the aromatic rings.

3. Biochar production

Biochar refers to the solid product that results from the pyrolysis of biomass. Pyrolysis is a thermochemical process that converts organic materials under oxygen-deprived conditions at high temperatures, and yields gaseous and liquid by-products (Bridgwater, 1994). Due to its stable molecular structure, characterized by strongly bonded carbon atoms, biochar can persist in the environment for thousands of years (Edeh et al., 2020). Biochar has a low density, high stability, and strong adsorption capacity (Lyu, H et al., 2016). Coupled with its excellent physical and chemical properties, it can be employed in various industries, as illustrated in Fig. 3.1 (Deena et al., 2022; Ruan et al., 2019), including energy (Bhatia et al., 2021; Senthil et al., 2021) and air and water treatment applications (Kang et al., 2022; Wang, C. et al., 2021). It is particularly useful in mitigating climate change and improving soil health (Ciampi et al., 2023; Hou et al., 2023).

Biomass is transformed into biochar by means of various thermochemical processes, such as slow pyrolysis in an inert atmosphere, combustion in an oxygen-lean air or environments, hydrothermal carbonization (HTC), and gasification. Table 3.1 summarizes the conventional parameters and characteristics of various production processes. The most common approach is slow pyrolysis (Qambrani et al., 2017), which typically yields 35 % biochar (dry biomass weight). The process operates at a moderate temperature (400–650°C) and requires a longer vapour residence time (10–20 s). Fast pyrolysis is commonly employed to produce bio-oil and syngas (Cheah et al., 2016). It is effective with most fluidised bed reactors due to the high temperatures employed, the rapid fragmentation, ease of control, and product collection (Yaashikaa, P. et al., 2020). Flash pyrolysis is a variant of fast pyrolysis, characterized by a short residence time, a high temperature, and a high heating rate (Ighalo et al., 2022). Microwave pyrolysis requires fewer process parameters and occurs at a higher heating rate, with rapid quenching conditions, which minimizes secondary reactions occurring (Foong et al., 2020). Vacuum pyrolysis involves the thermal degradation of biomass in a vacuum or low oxygen environment. Despite similar heating conditions and rates to that used with slow pyrolysis, the final products differ significantly (Tahir et al., 2020). Solar pyrolysis is an environmentally friendly process that operates without an external heating source such as electricity or fossil fuel. However, it requires expensive and complex solar reactors (Zeng et al., 2017). Each pyrolysis method has advantages and limitations, which means that careful consideration of the process variables and operating conditions is required in order to achieve the desired product yield and quality. HTC typically involves hydrothermal carbonization of biomass at a temperature of 150–250°C under high pressure, which results in biochar with a high energy density. With the flash pyrolysis process, rapid vaporisation occurs at elevated pressure (1–2 MPa), with biomass being converted into gas and a solid energy form (Cha et al., 2016). Gasification uses thermochemical processes to transform carbon-containing materials into syngas, including CO, CO_2, CH_4, and H_2, with the reaction temperature playing a key role in syngas formation (Sakhiya et al., 2020). Generally, different heating processes and parameters (e.g. heating temperature and residence time) result in biochar with varying properties, which determines its suitability for various applications. The production of biochar is not a simple carbonization process; rather, it is a complex process that is influenced by various factors. The chapter explores the technology used for biochar production, including factors such as selection of the feedstock, reactor design, control of pyrolysis temperature, and the impact of various additives. Variations in the feedstock used result in differences in the structure and performance of biochar, which affects its suitability for use in various application domains. Factors such as pyrolysis temperature, pressure, reactor design, additives and dopants introduce additional variables to the production process, and this determines the applications in which biochar can be used. Through an in-depth examination of these influencing factors, the critical elements of biochar production have been identified and are discussed in depth, in an attempt to unravel the entire mechanism involved in biochar production. We studied the scientific principles that underlie the production technology, and unveil the range of biochar properties, which lays a solid foundation for extensive applications in the fields of energy, materials, and chemical engineering.

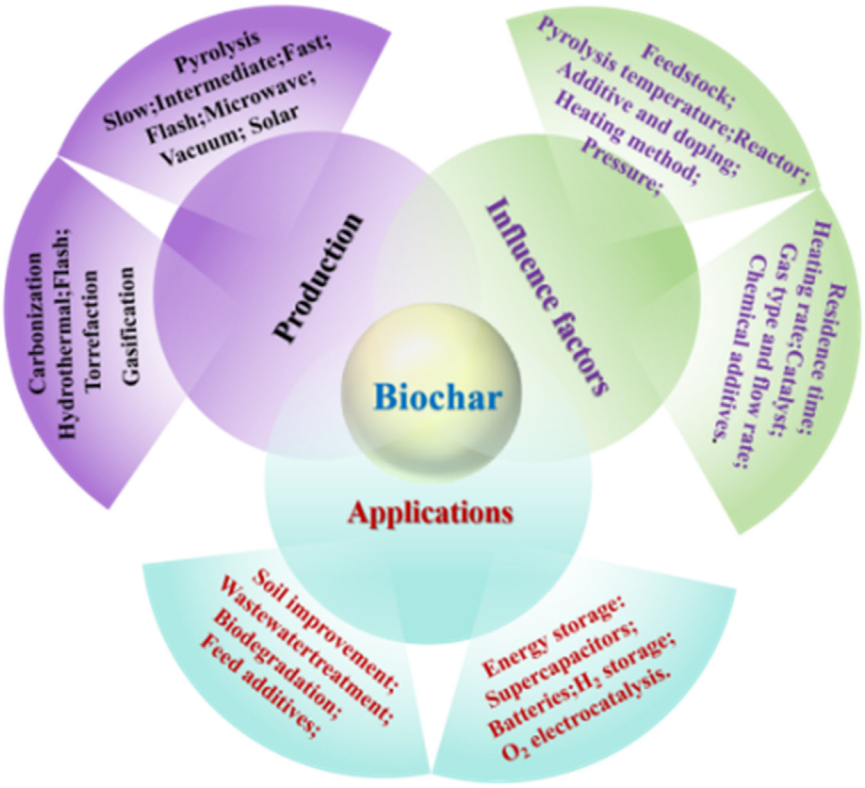

Fig. 3.1. Common biochar production methods, influencing factors, and applications.

3.1. Effect of feedstock

The type, nature, and source of the feedstock have a strong influence on the properties of the biochar (Uday et al., 2022). Biomass can be categorised into five groups, based on the natural or anthropogenic source, i.e. (Vassilev et al., 2012): herbaceous species (such as straw, husks, seeds, etc.); woody waste (including tree parts, wood, sawdust, etc.); industrial waste (such as waste sludge, solid waste, etc.); aquatic plants like algae (including microalgae and macroalgae); and human and animal waste (including municipal solid waste such as pig manure). Biochar produced from different feedstocks exhibits distinct properties. For example, biochar from wood residues has a microporous structure, high specific surface area (SSA), low ash content, low moisture content, and high stability. Biochar from agricultural feedstocks contains more hydroxyl and carboxyl functional groups, which results in a higher yield but lower lignin content, and hence lower stability (Tomczyk, A. et al., 2020). Agricultural feedstocks like rice straw, rice husk, and peanut shells yield biochar with a higher yield (Pandey et al., 2020). Biochar derived from fertiliser/sludge exhibits a high pH, increased ash content, and low stability, due to the presence of unstable carbon structures (Xu et al., 2018). A comparative study done on biochar produced from various types of animal manure at 300°C reports biochar yields ranging from 39.18 % to 80.96 %. Buffalo and chicken manure exhibit the lowest yields (39.18 % and 48.89 %, respectively), while the highest yields are observed in alpaca and cow manure (73.10 % and 80.96 %, respectively) (Hossain et al., 2021). More recently, commercial grade biomass combustion bottom ash generated at a local biomass thermal power plant in the UK (i.e. Drax power plant), was effectively valorised to directly extract unburnt carbonaceous residue (char) from the bottom ash. The char was then activated and surface modified to enhance porosity and surface functional groups. The process demonstrated a viable pathway to produce functional activated porous carbon suitable for CO_2 adsorption (Gorbounov et al., 2024; Gorbounov et al., 2025).

The properties of biochar relate primarily to surface morphology (SSA and pore volume), stability (carbon content, H/C ratio, O/C ratio, pH), productivity (elemental content of N, P, Mn, K, conductivity, CEC, and active sites (functional groups). A thorough analysis of the impact of different feedstocks on the properties of biochar provides significant guidance regarding its possible applications. When applying a specific pyrolysis temperature and duration, variations in the biochar properties are mainly attributed to differences in the feedstock (Janus et al., 2015; Windeatt et al., 2014). Different feedstocks exhibit distinct characteristics depending on their chemical composition, including carbon content, lignin, cellulose, and nutrient levels. (See Table 3.2.) Biochar produced from different feedstock types can develop different properties under the same pyrolysis temperature conditions (Weber, K. and Quicker, P.J.F., 2018). When using the same pyrolysis temperature (below 700°C): biochar produced from walnut shells had a pH of 7.2, SSA of 222 m^2/g, and a carbon content of 91.2 %; while biochar produced from poultry manure had a pH of 10.3, SSA of 9 m^2/g, and a carbon content of 44.0 % (Yu, O-Y et al., 2017).

3.1.1. Effect on the surface morphology of biochar

The composition of feedstock plays a key role in determining the SSA and pore structure of biochar. Table 3.2 provides details of the analysis of biochar produced from different types of feedstocks, showing the variations in SSA and pore structure. Alkali and alkaline earth metals in the feedstock can act as self-activating agents for pore development during the pyrolysis process. A study on lotus stems and leaves revealed that biochar produced from lotus stems had a higher SSA (1610 m^2/g) than biochar produced from lotus leaves (1039 m^2/g). This was primarily attributed to differences in the metal ion content, particularly potassium (Zhang, Y. et al., 2017). Cho et al. (Cho et al., 2019) synthesized a novel biochar composite by means of pyrolysis of redwood and lignin, which had a higher SSA and pore volume than the pyrolysis product of lignin. This was attributed to the reducing effect of lignin decomposition products on iron oxide. One study indicates that biochar

Table 3.1
Summary of biochar production processes.

Method	Feedstock	Condition (T^1, P^2, HR^3 and RT^4)	Product			Characteristics	Ref
			Biochar yield (%)	Bio-oil yield (%)	Syngas yield (%)		
Slow pyrolysis	Wood and algal biomass; Agricultural and urban waste	T: 300–600 °C; HR: 5–7 °C/min; RT: 30–180 min.	35	30	35	High carbon content; Good stability; Biomass particle diameter > 5 mm.	(Gabhane et al., 2020; Kaur et al., 2018)
Intermediate pyrolysis	Fruit and vegetable waste; Some woody biomass	T: 400–650 °C; HR: 60–600 °C/min; RT: 10–20 s;	20	50	30	Controlled chemical reaction process; Biomass particle size 1–5 mm.	(Bridgwater and bioenergy, 2012)
Fast pyrolysis	Woody biomass, Energy crops and energy plants	T: 500–1000 °C; HR: 300 °C/s; RT: 0.5–10 s.	12	75	13	Smaller pore sizes; Higher SSA; Biomass particle size < 1 mm;	(Dhyani and Bhaskar, 2018); (Yaashikaa, P. et al., 2020)
Flash pyrolysis	High cellulose content biomass; Certain crop residues	T: 900–1200 °C; HR: 1000 °C/s; RT: < 0.5 s.	10–30	30–70	5–15	Need optimization of process parameters, handling of pyrolysis vapours and gases, and ensuring consistent biochar properties; Biomass particle size < 0.5 mm;	(Al-Rumaihi et al., 2022); (Park, H.C. et al., 2019)
Microwave pyrolysis	Apple wood, mango peel, and peanut shells	T: 450–825 °C; Microwave frequency: 2450 MHz; Microwave power: 790–2250 W.	79–97	2–3	3	High quality bio-oil, biochar.	(Foong et al., 2020; Zhang, H. et al., 2022)
Vacuum pyrolysis	Date palm tree waste	P: 50–200 KPa; T: 450–600 °C; HR: 300 °C/min.	40–60	20–40	10–20	It can reduce the secondary decomposition reactions and prevent further cracking and re-condensation reactions.	(Tahir et al., 2020)
Solar pyrolysis	Wood, straw, wood chips, agricultural residue, and food waste	T: 150–2000 °C; HR: 5–450 °C/s.	10–60	20–70	1–10	Environmentally-friendly; does not require external heating sources; requires a costly, complex solar reactor.	(Parthasarathy et al., 2022; Zeng et al., 2017)
Hydrothermal carbonization	Rotten apple, grape pomace, and apple juice pomace	T: 220–240 °C; P: 2–20 MPa.	50–80	5–20	2–5	High carbon yield	(Amalina et al., 2022; Zhang et al., 2018)
Flash carbonization		P: 1–2 MPa.	40–60	20–40	10–20	High-temperature, short-duration process; High energy consumption; Complex equipment.	(Cha et al., 2016)
Gasification	Waste wood and wood residues; Woody biomass	T: 700–1500 °C.	5	10	85	High energy consumption and equipment cost.	(Sakhiya et al., 2020; Yao et al., 2018)
Torrefaction Carbonization	Fruit shell, hardwood, straw and agricultural residues	T: 200–300 °C; RT: 30 min.	80	0	20	Absence of oxygen and slow heating rate.	(Hassan, Masud et al., 2020; Tumuluru et al., 2011)

Notes: 1: Temperature; 2: Pressure; 3: Heating Rate; 4. Residence Time.

produced from macroalgae has a larger porous structure than biochar produced from microalgae, as macroalgae have a higher carbohydrate content than microalgae (Lee et al., 2020).

The morphological structure of feedstock is closely related to the development of pores in biochar and plays a decisive role in determining the shape of the pores. Because of the original biomass cells, both sugarcane bagasse-based biochar and durian sawdust-based biochar exhibit a distinct tubular pore structure (Jin et al., 2016). The particle morphology of the feedstock influences the pore structure of biochar. For example, biochar particles from microalgae are compact and irregular, with fewer pores (Mubarik et al., 2016), while sludge-derived biochar has a rough particle structure and a relatively developed pore structure,

Table 3.2
Factors related to biochar preparation and their physicochemical properties.

Biomass	Temp.[1] (°C)	SSA[2] (m^2/g)	Pore size (nm)	Element analysis (%)	pH	CEC[3] (cmol/kg)	EC[4] (dS/m)	Functional groups	Ref
Wheat straw	350	—	—	C=57.54; H=4.37 O=25.27; N=1.29	7.56	56.34	1.27	—	(Aon et al., 2023)
Rice (Oryza sativa husk)	400	—	—	C=37.2; N=1.3 H=1.2; O=12.4	6.7	—	0.7	—	(Kameyama et al., 2016)
Walnut shell	900	227.1	—	C=55.3; N=0.47 H=0.89; O=1.6 P=0.64; K=9.32	9.7	33.4	—	C=O; C=C	(Mukome et al., 2013)
Wheat straw	450	184	11.3	C=65.2; N=0.9 H=2.3; O=31.5	—	—	—	C-C; C-H	(Mohanty et al., 2013)
Sugarcane bagasse	500	155.41	2.535	C=60.1; H=0.68 N=0.688; S=0.058 O=23.59; Si=0.563	7.19	86.96	—	-CO-; -OH -C-OH	(Mansee et al., 2023)
Pine sawdust	650	1.43	5–550	C=66.35; O=8.27	7.3	—	—	-OH; $-CH_3$; $-CH_2$; CO-H	(Wang et al., 2023)
Sawdust	280	7.4265	1.66	C=48.23; O=28.15 S=23.62	—	—	—	C-O-H; -COOH C=C	(Hassaan et al., 2023)
Cardboard	650	1.74	—	C=49.54; H=1.37 N=0.08; S=3.23	7.41	—	—	—	(Zuhara et al., 2023)
Fish scale	600	1131.29	1.98	C=65.95; O=3.41 N=0.17	5.0	—	—	C=O; O-H C-S; C=S; C-N	(Chen et al., 2023)
Tobacco stem	400	32.78	—	—	—	—	—	C=C; C-H; C-N	(Cui et al., 2022)
Sewage sludge	700	97	—	C=29.6; H=1.24 N=1.13; Ca=21 Mg=5.3; Fe=23	—	—	—	—	(Krahn et al., 2023)
Sludge	700	67.45	—	C=7.09; H=0.48 N=0.52; S=0.32 O=10.59; Al=7.23 Fe=6.33; Ca=2.24 Mg=0.92; K=0.91 Ti=0.43; Zn=0.39	8.57	—	—	—	(Zhang, Xiufang et al., 2022)
Seaweed	800	183.49	3.40	C=69.85; O=27.75	7.58	—	—	C=C; C-C/C-C C-O/C-O-C	(Al Masud et al., 2023)
Waste tobacco stems	600	2.74	16.16	C=60.53; H=1.64 N=2.12; S=0.46 O=35.26	—	—	—	H-H; C=O(C-O); C-H	(Ma et al., 2023)

Note: 1: Pyrolysis temperature; 2: Specific surface area; 3: Cation exchange capacity; 4: Electrical conductivity.

as a result of its complex composition and relatively high ash content (Soni and Karmee, 2020). The lignin content in crops is generally positively correlated to the SSA and pore structure of biochar (Leng et al.; Leng et al., 2021). A study done by Rodriguez et al. (Rodriguez et al., 2020) suggests that wood-based feedstock typically results in biochar with the maximum SSA. The size of the feedstock particles also affects the physical properties of biochar - rather than the elemental properties - and controls the rate of heat and mass transfer during the process. For example, when the particle size of feedstock decreases from 1 mm to 0.053 mm, the SSA of biochar increases from 5.2 to 51.1 m^2/g, while the porosity of biochar decreases slightly as the particle size decreases from 1 mm to 0.053 mm (Sangani et al., 2020).

3.1.2. Effect on the stability of biochar

Carbon content is a crucial parameter in biochar, ranging from 3 % to 95 %, depending on the type of material used (Ok et al., 2015). A higher C and O content in the feedstock is reported to result in a higher biochar yield and net heating value (Leng and Huang, 2018). For example, it was shown that after pyrolysis, the C content of straw ranges between 40 % and 50 %, while that of shell-based biochar is between 70 % and 90 %. The C content in pig manure biochar is between 40 % and 60 % (Sarfaraz et al., 2020). The effect of high-temperature pyrolysis on the carbon content of biochar varies with the type of feedstock used. For example, the increase in C content at a high pyrolysis temperature (> 500°C) is more significant in woody biochar than in corn straw biochar and almond grass biochar. This suggests that, with the same energy expenditure, woody biochar can yield a higher C content than corn straw and almond grass (Zielińska et al., 2015). Li et al. (Li, L. et al., 2023) systematically reviewed the impact of pyrolysis temperature (175–950°C) on biochar properties (C content, H/C ratio, N content, pH, SSA, ash content, and pore volume) when using different feedstocks (corn straw, willow, and wood). The results indicate that woody biochar consistently exhibits a higher carbon content and a larger SSA, regardless of the pyrolysis temperature used, and a lower N and ash content. The H/C molar ratio in biochar serves as an indicator of its carbonization degree, stability, and aromaticity (Chen, J. et al., 2021). Carbon materials are generally hydrophobic owing to the presence of non-polar carbon-carbon bonds, although this can change depending on the existing surface functional groups and those introduced upon surface modification (Gorbounov et al., 2024). The O/C molar ratio, however, can indicate the degree of hydrophilicity of biochar, which varies with different feedstocks. The reduction in the H/C and O/C ratios in biochar corresponds to high aromaticity and low polarity, which signifies robust resistance against microbial decomposition (Liew et al., 2022). The pH of biochar is highly dependent on the type of feedstock used, with biochar produced from different materials exhibiting distinct pH values (Ahmad et al., 2014; Rondon et al., 2007). However, biochar can be prepared from feedstock with almost any pH value in the range of 4 to 12. Many factors are influenced by pH, including CEC, ash content, nutrient availability, and more (Ding et al., 2016). Ji et al. (Ji et al., 2022) reported that the pH of woody biochar is lower than that of crop residues and organic waste.

3.1.3. Effect on biochar productivity

Biochar productivity encompasses parameters such as ash content, the concentration of elements like N, P, Mn, and K, electrical conductivity, and CEC. Some studies indicate that feedstock that is rich in lignin (such as wood) tends to produce biochar with a higher carbon concen-

tration and lower ash content, whereas those rich in cellulose (such as agricultural residue) often yield biochar with a lower C content and a higher ash content (Adeniyi et al., 2021; Zhang, H. et al., 2017). The N content of biochar is a key factor in terms of its use as fertilizer. A high concentration of large-molecule amino acids and proteins in feedstock results in a higher N content in biochar. Among the crop residues, woody biomass and organic waste crop residues typically have a higher N content than woody biomass, but a lower content than organic waste (Pariyar et al., 2020). The P content in biochar depends on the type of feedstock used, with the highest to lowest distribution of the P content being as follows: bio-solid waste > animal waste > green waste > crop residues (Glaser and Lehr, 2019). Different feedstock types exhibit a distinct chemical composition (content of elements such as C, H, O, N), which influences the C content and crystallinity of biochar, which affects electrical conductivity.

Choudhary et al. (Choudhary et al., 2019) investigated the stability and compositional changes of biochar derived from various agricultural residues, including sugarcane filter cake (SF), farmyard manure (FM) and rice husk (RH). These feedstocks underwent pyrolysis at 350°C, and yielded biochar with diverse physicochemical properties, with FM displaying relatively higher electrical conductivity. Furthermore, the electrical conductivity of biochar is strongly affected by the method used to process the feedstock. Mittal et al. (Mittal et al., 2023) reported that plasma-treated biochar prepared in a few minutes (electrical conductivity: 58,914.695 μS/cm) exhibited higher conductivity than biochar obtained by drum kiln processing (electrical conductivity: 3.17534 μS/cm). CEC represents the number of exchangeable cations (e.g. Ca^{2+}, Mg^{2+}, K+, Na^{+}, NH_4^{+}), while biochar's CEC depends on the type of feedstock used. In 2020, Rodriguez et al. (Rodriguez et al., 2020) noted that biochar derived from crop residues, herbaceous plants, and animal manure/sludge exhibited a higher CEC. When using an operating temperature of 500°C, biochar produced from pig manure (32.7 cmol/kg) had a lower CEC content than biochar produced from chicken manure (81.4 cmol/kg) (Cely et al., 2015). However, biochar produced from paper mill waste (9.0–18.0 cmol/kg) (Van Zwieten et al., 2010) exhibited significantly lower CEC content than biochar produced from sugarcane residue (122.0 cmol/kg). These differences are the result of biomass with a high ash content generating biochar with a higher CEC (Tag, A.T. et al., 2016; Yang et al., 2015). It has also been reported that reducing the particle size from 0.25 mm to 0.053 mm increases the biochar's CEC and anion exchange capacity (AEC) (Liao and Thomas, 2019; Sangani et al., 2020).

3.1.4. Effect on biochar active sites

The surface functional groups in biochar symbolise its active sites. Table 3.2 summarises the distinct functional groups in biochar obtained from different types of feedstocks. An abundance of minerals (such as K, Ca, Na, and Mg) in biochar contributes to the formation of surface functional groups, which leads to a higher CEC value (Liao and Thomas, 2019). Gezahegn et al. (Gezahegn et al., 2019) conducted pyrolysis on 19 types of Canadian temperate wood feedstock, using temperatures ranging from 300 to 700°C. The study revealed that the composition of functional groups varied with the type of feedstock used, particularly at pyrolysis temperatures < 500°C. Biochar derived from coniferous trees had a higher concentration of carboxyl and lactate functional groups than biochar from angiosperms.

3.1.5. Summary

The carbonisation mechanism of different biomass types, such as lignin, hemicellulose and cellulose, influences the final properties of biochar. Even with the same biomass type, biochar's microstructure is substantially affected by the specific pyrolysis process used. For example, variations in microstructure due to pyrolysis methods affect biochar's adsorption capacity and mass transfer properties, thereby influencing its application in energy storage and environmental management. In-depth research into the selection of biomass types, the application of pyrolysis techniques, and related influencing factors not only advances our comprehensive understanding of biochar formation mechanisms and property control pathways but also significantly supports the resolution of environmental and energy-related challenges.

3.2. Influence of pyrolysis temperature

Research indicates that the initial step of the pyrolysis process for biomass waste is pre-pyrolysis, specifically, the cracking phase. The subsequent step occurs in a temperature range of approximately 400–500°C and involves the decomposition of biomass components and the formation of oxygen-rich functional groups (Fawzy et al., 2021); (Wang, Q. et al., 2020). The pyrolysis temperature predominantly influences the molecular structure (Singh et al., 2020) and physicochemical properties, such as the SSA, functional groups, pore structure, and element composition (Tag, A.T. et al., 2016). Even when using the same feedstock, the pyrolysis temperature has a significant impact on the resulting biochar. For example, at 350°C, the SSA of walnut shell biochar is 1.01 m^2/g, whereas at 700°C, its physicochemical properties are markedly different (Yu, O. Y. et al., 2017). The literature indicates that a higher pyrolysis temperature increases pH, SSA, volatile matter and carbon fraction but decreases the quantity of surface functional groups and CEC (Tomczyk, M.M. et al., 2020). The relationship between pyrolysis temperature and the properties of biochar is summarised in Table 3.3. The effect of these properties must be carefully regulated by adjusting the temperature applied during pyrolysis. This, however, also results in the release of volatile organic compounds, especially at elevated temperatures (Sun et al., 2014). Therefore, selecting an appropriate pyrolysis temperature involves ensuring a delicate balance between chemical and surface properties, with the commonly accepted optimal range for producing desired biomass char materials being 500–800°C (Wang et al., 2013).

In this section, choosing the temperature to be used during pyrolysis and related matters are discussed thoroughly, including differences in biochar properties when using different temperatures, e.g. surface structure (pore structure, SSA), pH, chemical composition and CEC. A comparative analysis of the experimental results was conducted to better understand the crucial role temperature plays during pyrolysis in adjusting the properties of biochar.

3.2.1. Impact on biochar yield

The biochar yield generally decreases with an increase in the temperature during pyrolysis (Table 3.3), due to enhanced primary decomposition of organic matter in crop residue. Additionally, secondary decomposition processes, such as carbonization and detachment of biochar residue, can contribute to a reduction in biochar yield. In a study, a decrease in biochar yield with an increase in temperature during pyrolysis of straw and corn straw pellets was noted (Yang, C. et al., 2021). Du et al. (Du et al., 2019) reported a similar trend in the temperature range of 350–750°C when they investigated the effect of pyrolysis temperature on the biochar yielded from comfrey, i.e. the biochar yield gradually decreased as the temperature increased. When producing biochar from coconut biomass, temperature emerged as a key operational parameter noticeably affecting biochar yield, characteristics, and stability profoundly (Ighalo, Joshua O. et al., 2022). Arán et al. (Arán et al., 2023) investigated the differences in the properties of biochar derived from poultry litter (PL), maize straw, the macrophyte Juncus imbricatus, and phytoremediation waste after pyrolysis at a temperature of 300 and 600°C. The results indicate that biochar yield decreased with an increase in temperature, which may be directly correlated with the inorganic components in the raw materials. The biochar yield from poultry litter is significantly higher than biochar derived from plant biomass at both pyrolysis temperatures. This may be due to the relatively lower

Table 3.3
Properties of biochar produced from different commonly used types of biomass.

Biomass	Temp[1] (°C)	SSA[2] (m^2/g)	PV[3] (m^3/g)	pH	CEC[4] (cmol/kg)	EC[5] (dS/m)	CC[6] (%)	Ash (%)	BY[7] (%)	ElC[8] (%)	Ref
Pine sawdust	400	83.9	0.012	6.35	27.5	2.44	—	22	55	C=0.517; H=0.0497; O=0.338; Ca=0.23; K=0.069.	(Laghari et al., 2016)
	700	65.2	0.016	9.08	24.9	0.76	—	68	16.7	C=0.736; H=0.0296; O=0.129; Ca=0.468; K=0.119.	
Oak bark	400	—	—	—	—	—	—	11.19	—	C=57.47; H=3.48; N=0.54; Ca=0.023; K=0.00023; Mg=0.0008; P=0.0046; S=0.0006.	(Saletnik et al., 2022)
	450	—	—	—	—	—	—	12.88	—	C=60.96; H=3.05; N=0.54; Ca=0.024; K=0.00026. Mg=0.0014; P=0.0048; S=0.0005.	
	500	—	—	—	—	—	—	12.96	—	C=60.99; H=3.07; N=0.53; Ca=0.025; K=0.00025; Mg=0.0016; P=0.0051; S=0.0005.	
Rice straw	350	2.9	0.024	9.94	—	—	—	—	41.9	C=48.71; H=3.55; N=0.91; S=0.0.26.	(Yang, C. et al., 2021)
	650	14.33	0.1	11.15	—	—	—	—	8.76	C=39.75; H=1.73; N=0.71; S=0.36.	
Symphytum officinale L	350	11.54	0.021	10.05	—	13.02		42.92	—	C=41.08; H=2.73; 1.87; S=0.68; O=10.72.	(Du et al., 2019)
	550	34.48	0.090	10.38	—	13.57		47.83	—	C=38.47; H=1.48; N=1.73; S=0.7; O=9.79.	
	750	273.8	0.243	13.57	—	15.66		55.78	—	C=33.56; H=0.93; N=1.52; S=0.73; O=7.48.	
Sewage sludge	300	5.11	—	6.43	—	—	—	83.25	91.05	C=7.53; H=0.78; N=1.31; O=7.13.	(Zhang, Xin et al., 2022)
	500	15.23	—	6.96	—	—	—	87.93	85.72	C=5.63; H=0.48; N=0.76; O=5.20.	
	700	13.57	—	10.50	—	—	—	91.93	81.23	C=3.96; H=0.29; N=0.46; O=3.36.	
Animal dung	800	—	—	—	—	—	—	34	53.1	C=27.78; H=3.98; N=1.67; O=20.3.	(Zhou et al., 2020)
Dairy cattle manure	600	225	0.076	8.3	114	2.2	15	23	49.1	C=35.2; H=3.1; N=2.2; O=33.3; S=0.7.	(Atienza-Martínez et al., 2020)
Magnetic cattle manure	200	4.71	0.023	—	—	-OH; -CH2; -CH3; C=O; C-H; C-O; H-Ar;			—	C=61.16; N=3.41; O=33.39.	(Zhu et al., 2020)
	400	18.52	0.064	—	—	-OH; C=O; C-H; C-O; H-Ar;			—	C=33; N=2.84; O=45.8.	
	600	188.56	0.18	—	—	-OH; C=O; C-H; C-O; H-Ar;			—	C=21.29; N=1.96; O=49.4.	
Manure	550	14.033	0.042	10.43	—	4.123	—	—	41.64	C=28.46; N=1.58; H=0.88; S=0.48.	(Stylianou et al., 2020)
Biosolids		3.98	0.022	9.77	—	0.745	—	—	18.6	C=39.57; N=5.67; H=1.17; S=0.38.	
Spend coffee grounds		1.53	0.008	9.42	—	2.723	—	—	21.23	C=87.38; N=4.28; H=2.36; S=0.25.	
Swine manure	600	—	—	—	—	—	32.85	57.63	—	C=33.03; N=1.85; H=0.62; S=0.38; O=6.49.	(Zhou et al., 2019)
Dairy cattle manure		—	—	—	—	—	41.95	48.95	—	C=44.64; N=1.97; H=0.98; S=0.54; O=2.91.	
Beef cattle manure		—	—	—	—	—	36.77	52.8	—	C=41.53; N=1.69; H=0.89; S=0.40; O=2.69.	
Broiler litter		—	—	—	—	—	33.50	56.94	—	C=37.47; N=3.17; H=0.91; S=1.18; O=3.08.	
Layer chicken litter		—	—	—	—	—	23.74	60.54	—	C=33.81; N=1.91; H=0.71; S=0.70; O=2.33.	

(*continued on next page*)

Table 3.3 (*continued*)

Biomass	Temp[1] (°C)	SSA[2] (m^2/g)	PV[3] (m^3/g)	pH	CEC[4] (cmol/kg)	EC[5] (dS/m)	CC[6] (%)	Ash (%)	BY[7] (%)	ElC[8] (%)	Ref
Hornbeam wood chips	575	—	—	—	—	—	14.16	0.36	—	C=48.86; N=0.10; H=6.15; S=0.03; O=44.86.	(Ercan et al., 2023)
Swine Manure	450	16.15	0.0178	7.8	—	2.4	11.9	48.9	53	C=27.6; N=1.9; H=1.5; O=17.9; S=0.2.	(Wang, K. et al., 2020)
Switchgrass	700	22.9	—	10.1	309.6	240	31.4	4.4	—	P=0.2; Ca=0.8; K=0.4; Mg=0.3; Na=0.03; S=0.04.	(Antonangelo et al., 2019)
Poultry litter		9.278	—	10.2	235.9	9150	27.75	45.9	—	P=4; Ca=5; K=8; Mg=2; Na=3; S=1.	
Eucalyptus wood	450	—	—	5.3	—	123.3	—	0.60	42.76	C=74.96; N=1.25; H=3.76; O=19.41; K=0.182; Ca=0.085; P=0.016; Fe=0.001.	(Chaves Fernandes et al., 2020)
	550	—	—	6.7	—	97.4	—	0.74	38.00	C=79.25; N=1.49; H=1.00; O=18.01; K=0.140; Ca=0.104; P=0.016; Fe=0.003.	
	650	410.48	—	9.7	—	134.3	—	0.63	34.69	C=87.06; N=0; H=1.60; O=10.70; K=0.164; Ca=0.115; P=0.023; Fe=0.006.	
	750	402.51	—	9.8	—	164.6	—	0.84	34.27	C=87.74; N=1.06; H=0.87; O=9.47; K=0.210; Ca=0.130; P=0.017; Fe=0.006.	
	850	362.90	—	9.1	—	161.6	—	0.82	32.44	C=88.01; N=1.27; H=0.89; O=8.99; K=0.210; Ca=0.104; P=0.025; Fe=0.004.	
	950	224.43	—	9.2	—	273.1	—	1.06	33.47	C=86.90; N=1.34; H=0.90; O=10.57; K=0.286; Ca=0.176; P=0.031; Fe=0.004.	

Note: 1: Pyrolysis temperature; 2: Specific surface area; 3: Pore volume; 4: Cation exchange capacity; 5: Electrical conductivity; 6: Carbon content; 7: Biochar yield; 8: Elementary composition.

volatile matter content and higher ash content. This finding aligns with the finding of Wei et al. (Wei et al., 2019), who concluded that biochar derived from plant sources has a lower yield than biochar from animal waste. Careful selection of appropriate pyrolysis conditions, especially the combination of temperature and raw material type, is crucial to ensuring the appropriate quality of biochar for use in specific application domains.

3.2.1.1. Impact on carbon content (CC) and ash fraction of biochar. Biochar comprises primarily carbon, which constitutes approximately 50–90 % of its weight. One of the most important parameters in biochar production is the carbon content (CC), which is affected by the temperature of the pyrolysis process and the raw materials used. Carbonisation occurs at temperatures exceeding 600°C, which eliminates nearly all remaining non-carbon atoms and enhances the carbon concentration in biochar (Lehmann et al., 2006). A meta-analysis done by Zielinska et al. (Zielińska et al., 2015) reported that the average CC in woody biochar is notably higher (74.99 %) than in corn straw biochar (62.93 %) and reed biochar (60.98 %). These differences can be attributed to variations in the cellulose, hemicellulose, and lignin content of the three raw materials. Reported studies indicate that the CC of pyrolyzed straw is 40–50 %, for shell biochar, it is 70–90 %, and for pig manure it is 40–60 % (Schmidt, 2023); (Gondek and Mierzwa-Hersztek, 2016; Sarfaraz et al., 2020). Domingues et al. (Domingues et al., 2017) reported a decrease in CC with increasing temperature for biochar derived from chicken manure. Jung et al. (Jung et al., 2017) observed a similar trend in their study. However, the CC is also highly dependent on the type of biomass. One study reported that an increase in pyrolysis temperature, resulted in the ash fraction, with the CC of cellulose-derived biochar also increasing. A higher CC indicates that biochar still carries a certain amount of original organic plant residue, such as cellulose (El-Bassi et al., 2021; Laghari et al., 2021). The ash content of biochar generally increases with an increase in temperature, and this escalation is attributed to the gradual concentration of inorganic components and the combustion residue of organic matter (Jin et al., 2016). Rafiq et al. (Rafiq et al., 2016) reported that an increase in pyrolysis temperature leads to an increase in ash content of 5.7 %-18.7 %. Furthermore, Domingues et al. reported that the increase in Mg, Ca, K, and P in biochar produced at a high pyrolysis temperature is due to the increase in ash content, ranging from 4.0 % to 33.1 %. After carbonization, the mineral residues that form the ash persist in the biochar (Domingues et al., 2017).

3.2.1.2. Influence on the surface structure of biochar. The surface features of biochar are primarily determined by its SSA and pore structure. In a study, it was reported that an increase in pyrolysis temperature resulted in an accelerated decomposition of organic compounds, which, in turn, increased the release of volatile substances. Consequently, this led to the creation of larger pores, significantly altering the porosity and SSA of biochar (Sizirici et al., 2021). However, at extremely high temperatures, this effect may plateau or decrease because excessive heat can cause pore collapse or excessive carbonization, leading to a reduction in SSA. Generally, biochar produced at high-temperature pyrolysis has a higher SSA than biochar produced at low-temperature pyrolysis. This increase is particularly pronounced in wood materials that contain lignin and cellulose, primarily due to the augmentation of micropore volume induced by the release of volatile compounds (Hue, 2020). For willow biochar, the pore volume surpasses that of straw biochar and wood biochar, regardless of the pyrolysis temperature (Brewer et al., 2014). Ferraro et al. (Ferraro et al., 2021) revealed a notable effect, particularly at 550°C,

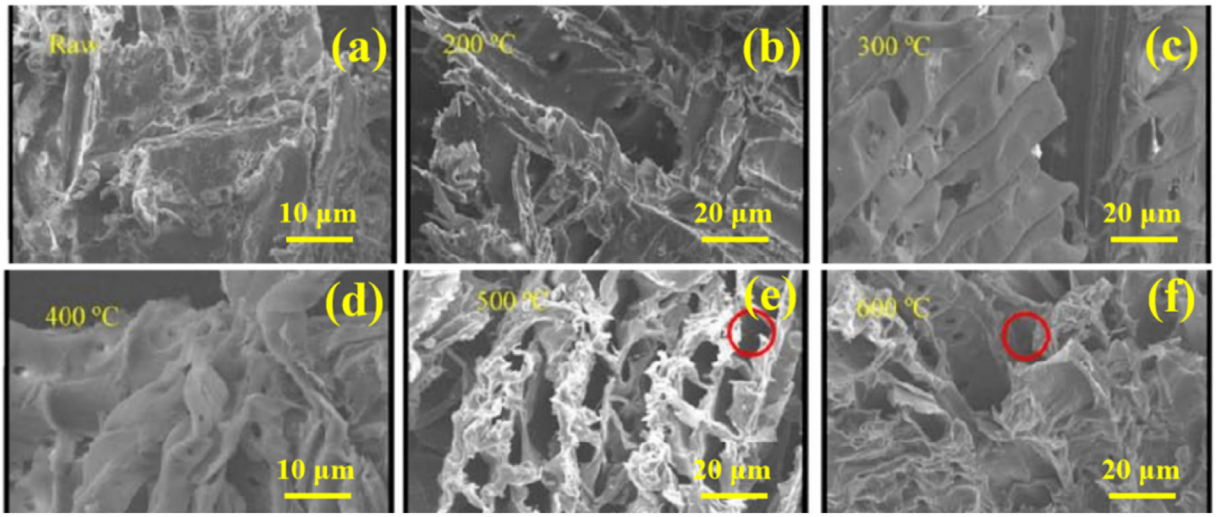

Fig. 3.2. Scanning electron microscopy (SEM) micrographs of biochar derived from sawdust biomass at different temperatures: a) raw condition; b) 200°C; c) 300°C; d) 400°C; e) 500°C; f) 600°C (Liu, Y. et al., 2016).

with a maximum SSA of 504 m^2/g for pine biochar. The impact of temperature on pore structure was also verified in the research conducted by Liu et al. (Liu, Y. et al., 2016). Their study on biochar derived from pyrolyzing sawdust at temperatures ranging from 200 to 600°C showed that no pores were visible at 200°C. However, at 300 and 400°C, several pore structures became visible. At 500°C, partial skeletal structures appeared, which researchers speculated originated from the decomposition of cellulose and hemicellulose. At 600°C, a honeycomb-like pore structure emerged from the decomposition of wood cellulose (Fig. 3.2).

3.2.1.3. Effect on the pH and electrical conductivity (EC) of biochar. The pH of biochar is positively correlated with the generation of carbonates and the concentration of inorganic alkalis (Li, L. et al., 2021). As the pyrolysis temperature increases, the content of carbonates and alkaline cations rises, which elevates the pH. This phenomenon is attributed to the increase in ash content during the pyrolysis process, the emergence of basic functional groups, and the disappearance of acidic functional groups, which provides additional support for the pH increase (Adewuyi et al., 2021; de Souza et al., 2021; Liao et al., 2020; Tomczyk, M.M. et al., 2020). Additionally, at a high temperature, the salts that separate from the organic matter contribute to the higher pH (Luo, D. et al., 2021). Even with the same raw material, using different pyrolysis temperatures results in distinct pH values. Singh et al. (Singhal et al., 2021) concluded that biochar prepared at a higher temperature (> 400°C) generally exhibits a higher pH than biochar from the same source prepared at a low temperature (< 400°C). Regarding different feedstock types, Ji et al. (Ji et al., 2022) reported that wood-derived biochar has a lower pH compared to biochar from crop residue and organic waste. Crop residue, such as straw biomass, contains a higher level of alkaline salts. These are separated from the biomass during pyrolysis, hence an increase in the pH. Consequently, straw biochar has a higher pH than wood biochar and willow biochar (Pariyar et al., 2020). Various biochar properties depend on pH, including CEC, and ash content (Ding et al., 2016). The EC of biochar generally increases with an increase in temperature. This increase may be attributed to a loss of biomass volatiles during carbonisation, an increase in CEC (due to the presence of exchangeable ions on the biochar surface), and augmentation of available nutrients (Chandra and Bhattacharya, 2019).

3.2.1.4. Influence on the elemental composition of biochar. Typically, optimising the pyrolysis process with a temperature in the range of 200°C to 800°C has been employed to control the properties of biochar. With an increase in pyrolysis temperature, the hydrogen content, oxygen content, and H/C and O/C ratios decrease mainly due to dehydration and deoxygenation (Mukome et al., 2013; Weber, K. and Quicker, P., 2018). The H/C and O/C ratios in biochar impact its stability and aromaticity. One study indicates that as the pyrolysis temperature rises, the content of water and oxygen functional groups decreases due to dehydration and deoxygenation (Zhou, Yuwen et al., 2021). The increase in CC and decrease in hydrogen content leads to a reduction in H/C. Biochar is rich in mineral elements such as Na, K, Ca, Fe, and Mg, whose concentrations increase with an increase in pyrolysis temperature. Saletnik et al. reported that the highest P, K, and Mg content was obtained at 500°C (4.3, 9.9, and 2.8 g/kg, respectively), while the highest carbon and nitrogen content was recorded at 400°C (73.6 % and 1.9 %, respectively) (Saletnik et al., 2022). In general, nutrient elements in biochar tend to increase with an increase in pyrolysis temperature. However, at higher pyrolysis temperatures (> 700°C), there may be a loss of P and K in biochar. Although there is minimal loss of phosphorus content in biomass during the pyrolysis process, the absorption of phosphorus from the resulting biochar by plants may slow down as the pyrolysis temperature increases (Laghari et al., 2016). Jindo et al. (Jindo et al., 2020) explained that the higher content of Ca, Mg, P, and K seen in biochar prepared at higher pyrolysis temperatures is due to an increase in the ash content (from approximately 3 % to 32.9 %).

3.2.1.5. Effect on the CEC of biochar. The CEC of biochar is more dependent on the feedstock used than on the temperature applied in pyrolysis. This may be associated with the loss of some acidic functional groups on the surface of biochar at a higher pyrolysis temperature (Zhao et al., 2013). The CEC of different types of biochar tends to decrease slightly with an increase in pyrolysis temperature (Wang, L. et al., 2020; Wang, Z. et al., 2020). According to Agrafioti et al. (Agrafioti et al., 2013), the K, Na, Ca, Mg, and P in the feedstock promote the formation of oxygen-containing functional groups on the biochar surface during pyrolysis, thereby enhancing the value of CEC. Mosharrof et al. (Mosharrof et al., 2021) suggested that the CEC of biochar depends on the distribution and nature of surface oxygen-rich functional groups. The negatively charged sites on the surface of biochar are composed of phenolic and carboxylic acid groups (Fawzy et al., 2021). Rodriguez Correa et al. (Rodriguez Correa et al., 2019) suggested that the positive charge may come from oxygenate groups, while the negative charge can only come from phenolic and carboxylic acid groups. Indeed, studies have found that biochar with a higher SSA has higher surface microporosity and CEC (Das et al., 2021; Jalal et al., 2020).

3.2.1.6. Effect on the surface functional groups of biochar. Differences in the content and intensity of functional groups in biochar are intricately linked to the raw materials used, the pyrolysis medium and, particularly, the pyrolysis temperature used, which play a key role in obtaining the desired functional groups. Common functional groups in biochar (C-C/C-O/C=C/-OH/CH-/Metal-O-, CHO-/COO-, and carbon skeleton) are formed on the surface via oxidation, dehydration, and decarboxylation that occur during pyrolysis (Luo et al., 2015). Breakdown and rearrangement of chemical bonds in biomass occurs at a high pyrolysis temperature, ranging from 300 to 700°C, which generates numerous functional groups (Mia et al., 2017; Reshad et al., 2019). Biochar produced at a lower temperature is predominantly hydrophilic due to a significant presence of oxygen-containing functional groups (Lian and Xing, 2017). At higher temperatures, it may contain more aromatic structures and skeletons (Pignatello et al., 2017). Gezahegn et al. (Gezahegn et al., 2019) investigated the pyrolysis behaviour of 19 types of raw materials obtained from Canadian temperate wood at different pyrolysis temperatures ranging from 300 to 700°C. Their study revealed that as the pyrolysis temperature increased, the concentrations of carboxyl and lactate functional groups decreased while the concentration of phenolic functional groups increased. Zhu et al. (Zhu et al., 2020) studied the effect of pyrolysis temperature (200, 400, and 600°C) on the structure of iron-ion-doped magnetic biochar and found that as the pyrolysis temperature increased, the number of functional groups decreased while the specific surface area and iron oxide content increased.

3.2.1.7. Effect on the stability of biochar. In terms of the biochar production process, pyrolysis temperature stands out as the most important factor influencing aromaticity, aromatic condensation, and the stability of biochar. Numerous studies have indicated that the content of the stable fused aromatic ring structures increases with an increase in pyrolysis temperature, while the size and quantity of unstable non-aromatic structures decrease (Suárez-Abelenda et al., 2017). Almost all research findings indicate that pyrolysis temperature has a strong positive effect on the stability of biochar (Aller, 2016; Wang, J. et al., 2016). Other influencing factors, such as the composition and properties of biomass feedstock, may prove more important than pyrolysis temperature and result in different levels of stability in the biochar (Mašek et al., 2013).

3.2.2. Optimization of pyrolysis temperature and applications of biochar: comprehensive assessment and future prospects

In pyrolysis, the heating rate is defined as the rate of temperature change during the process. A high heating rate (> 10°C/min) increases volatility and porosity, which promotes the generation of other components and reduces the biochar yield. A slow heating rate (below 10°C/min) favours the formation of a stable structure, which increases the biochar yield (Pandey et al., 2020). In the case of safflower seed pyrolysis, an increase in reaction temperature from 400 to 600°C at a heating rate of 10 to 50°C/min, led to a reduction in the SSA of the biomass char (Angın, 2013). Additionally, a lower heating rate helps to preserve structural complexity and prevents thermal breakdown within biomass (Li, Y. et al., 2020). The composition of biochar is also affected by the heating rate applied in pyrolysis. Li et al. (Li, Shuangjun et al., 2021) analysed biochar derived predominantly from lignocellulosic feedstock when employing different pyrolysis heating rates (5, 10, 15, 20°C/min) and reported variations in element content, even when using a constant temperature. As the heating rate increased from 5°C/min to 20°C/min, with a fixed pyrolysis temperature of 700°C, the carbon content decreased from 94 % to 85.4 %, and the hydrogen content varied from 1.2 % to 1.5 %. This suggests an increase in the H/C ratio with an increase in the heating rate, indicating reduced stability of the biochar. It is evident that establishing a clear correlation between the heating rate and other parameters - such as temperature, catalyst and atmosphere - helps to construct more integrated production models, thereby enhancing the efficiency and controllability of the biochar preparation process.

Biochar has attracted considerable attention for its outstanding adsorption and catalytic ability, which makes it suitable for use as a soil amendment and treatment product (Azeem et al., 2019; Han et al., 2018; Kumar et al., 2022; Li, C. et al., 2021). Biochar addition can enhance soil pH, electrical conductivity and water retention capacity, and increase both macro and micronutrient elements in plants, including N, C, P, K, and O (Liu et al., 2019; Qian et al., 2015). The high CEC and large SSA of biochar provide advantages in terms of pollution remediation (Berslin et al., 2022). Ahmad et al. (Ahmad et al., 2014) demonstrated that biochar can adsorb organic pollutants efficiently, including heavy metals. However, the detailed mechanisms of this adsorption process remain unclear, such as adsorption time and the impact of pyrolysis temperature on biochar selection for specific applications and conditions (Issaka et al., 2022). Biochar composites can be prepared to counter this obstacle (Blenis et al., 2023). Studies have also shown that biochar can remove residual pesticides from treated land (Carpio et al., 2021). It can also remove both organic and inorganic pollutants from wastewater, including inorganic ions through various mechanisms such as surface complexation, precipitation, electrostatic interactions, and ion exchange with functional groups (Michalak et al., 2019; Qiu et al., 2022; Wang, H. et al., 2020). The effectiveness of biochar in pollutants removal depends on a number of factors such as environmental pH, the concentration level of the pollutants, and contact time between biochar and pollutants. Investigating these variables and their impact on biodegradation is important in formulating effective biochar-based remediation strategies (Khan et al., 2021; Lv et al., 2022).

Biochar has also garnered widespread attention in the field of advanced energy storage and conversion. It can be designed for use as electrode materials in lithium-ion batteries and supercapacitors or as a catalyst for the redox reaction or hydrogen storage process. Studies have demonstrated the potential of using biochar derived from rice husks and corn cobs as high-performance supercapacitor electrode materials (Teo et al., 2016; Wang, F. et al., 2021). Algae-derived biochar has emerged as a potential material for supercapacitors due to its notable advantages related to specific capacitance and stability. Pourhosseini et al. (Pourhosseini et al., 2018) designed a high-performance asymmetric supercapacitor using functional biochar (FBC) as the anode electrode and iron oxide/carbon composite materials (MBC and FCBC) as the cathode electrode. The results showed that this metal oxide-loaded supercapacitor exhibited a high energy density (41.5 Wh kg^{-1}) and power density (900 W kg^{-1}). Norouzi et al. (Norouzi et al., 2021) further improved the structure by introducing cobalt nanoparticles into the 3D interconnected architecture of Cladophora glomerata algae-derived biochar and used this modified biochar in the fabrication of symmetrical and asymmetrical supercapacitors. However, despite extensive research efforts, most studies on the applications of biochar and its derivatives remain in the experimental stage and require further investigation before commercialization. When considering the use of biochar for soil remediation, careful control of pyrolysis temperature is essential to ensure efficient and effective use. Future research should focus on fine-tuning pyrolysis temperature for specific remediation applications, to allow biochar-treated soil to be temporarily managed by creating a soil-biochar composite and managing residual chemicals in pesticide-contaminated soils. Additional research is needed to address commercial barriers related to resource optimisation, scalability, and life-cycle sustainability assessment, in order to unleash the full potential of biochar as an efficient environmental biodegradation tool. Application-oriented research in the field of energy storage could help enhance and optimise the pore structure, SSA, and surface functional groups of biochar through pyrolysis temperature adjustment to ensure superior performance in energy storage applications. Therefore, the potential application of biochar in the field of energy storage warrants further exploration.

3.2.3. Summary

Pyrolysis temperature has varying degrees of influence on key properties of biochar, such as yield, carbon content, ash content, surface structure, pH and conductivity, elemental composition, cation exchange capacity (CEC), surface functional groups, and stability. A comprehensive understanding of the various impacts of pyrolysis temperature on biochar formation can be attained through an in-depth analysis of these changes. Optimising pyrolysis temperature is crucial for the application of biochar in different fields such as soil improvement, remediation of contaminated soil, water treatment, and energy storage. Future research should consider the effects under complex environmental conditions, particularly in diverse scenarios and in alignment with sustainable development goals, to ensure its sustainability in environmental governance, resource utilization and energy fields.

3.3. Effect of additives and doping

Incorporating various additives and dopant elements is a potent strategy for modifying biochar. This chapter reports on a comprehensive exploration of different types of dopants, including metal oxides, carbon nanomaterials, and elements such as N, S, and P. Through a detailed analysis of their specific effects on the conductivity and chemical reactivity of biochar, the unique contributions of various additives and dopants in enhancing the performance of biochar are unveiled. A comprehensive understanding of the application potential of various dopants in biochar modification is thus provided, and this valuable insight could guide future research and applications in this field.

3.3.1. Additives

Additives can be integrated into the biochar production process to enhance the properties and therefore, the efficiency of the final product. These substances are introduced to facilitate specific chemical reactions, improve process kinetics, and modify the characteristics of biochar (Li, H. et al., 2021). During pyrolysis, additives can affect the decomposition of biomass and facilitate the formation of the desired biochar properties. It has been reported that additives such as zeolites, transition metals, alkali metals and alkaline-earth metals are able to increase the biochar yield, enhance carbon retention, and modify the physical and chemical properties of biochar (Obidike and Yoro, 2022). In hydrothermal carbonisation, additives can expedite reaction kinetics and affect the properties of hydrochar. Alkaline solutions or alkali metals, for example, can improve the carbonisation processes, resulting in hydrochar with a higher carbon content and stability (Zou et al., 2022). The selection and concentration of additives may affect the yield, energy content, and nutrient retention of hydrochar (Deng, C. et al., 2023). The choice of additives depends on the required properties in the biochar produced, the raw material characteristics, and the desired product. Therefore, extensive research and experimentation are necessary to determine the appropriate additives, optimal dosage and application method.

The primary objective of using chemical additives is to enhance the adsorption capacity of biochar by increasing its SSA, surface functional groups, and pore volume (Ding et al., 2016; Duan et al., 2019). During the process of preparing biochar, chemical additives are introduced to inhibit the decomposition of hemicellulose in raw materials like plant residues and wood chips, which promotes dehydration reactions (Yuan et al., 2019). Researchers (Demirbas, 2004; Wang, M. et al., 2018) have demonstrated the use of biochar obtained from watermelon peel and biochar with added $MgCl_2$ before calcination to simulate the removal of Pb (II). The prepared biochar, containing Mg (II), exhibited enhanced removal capacity for Pb (II), which increased from 181 mg/g to 558 mg/g (Fig. 3.3a - d). Zhao et al. (Zhao et al., 2020) examined the efficiency of biochar and sulphur-impregnated biochar obtained from rice husks in removing mercury from contaminated soil (28.3 mg/kg), and reported improved efficiency for the modified biochar (Fig. 3.3k). Biochar prepared by adding H_2O_2 during the production process exhibits a significant amount of oxygen-containing functional groups and effectively removes heavy metals such as copper, nickel, and cadmium from water (Xue et al., 2012). Liquid petroleum coke activated by means of physical (steam and CO_2) and chemical (KOH and H_3PO_4) activation methods have also been prepared (Rambabu et al., 2013), with steam treatment used to produce biochar from tea waste. This resulted in biochar with an enhanced sulfamethoxazole removal capacity (Fig. 3.3e and -3.3f). The addition of nanoparticles (Chausali et al., 2021) further enhances the adsorption capacity and selectivity of nano-composite materials. For example, graphene oxide enhances the adsorption of organic molecules, while zero-valent iron nanoparticles promote a reduction in heavy metals (Noreen and Abd-Elsalam, 2021). Liu et al. (Liu, T. et al., 2016) studied biochar produced from slow pyrolysis of maple biomass pre-treated with CNTs and graphene oxide. The treated biochar exhibited improved SSA and an enhanced adsorption capacity for Pb (II) and Cd (II) in an aqueous solution compared to the original biochar (Liu, T. et al., 2016). (See Fig. 3.3 g and -3.3h).

3.3.2. Doping elements

Doping with heteroatoms can enhance the properties of biomass char significantly, such as enriching heteroatom functional groups and modulating the carbon framework. Heteroatom doping introduces specific functional groups that promote chemical adsorption, which alters the spatial structure of biomass char and enhances physical adsorption (Kaya and Uzun, 2021). Different types of doping elements have different effects on the structure and functionality of biomass char. Doping typically involves the introduction of elements such as N, S, P, which can alter the electrochemical and surface chemical properties of biomass char significantly. For example, the addition of N may enhance the gas adsorption performance of biomass char, as the introduction of N improves the conductivity and electron transfer capacity, and this accelerates electron transfer (Wang, H. et al., 2021; Zhou, X. et al., 2021). In a study, the removal efficiency was increased sevenfold by preparing graphite N and pyridine N with the addition of urea (Zhou, X. et al., 2021). Wu et al. reported a non-thermal plasma technique for generating N-doped biomass char from lotus and lavender seed pods. The introduction of N in a plasma atmosphere increased the N content tenfold. In another study, charge storage showed a significant increase of approximately 65 % and a capacitance of 342 F/g (Wu et al., 2021) (Fig. 3.3i and j). In addition to doping with N, S, doping in biomass char increased the efficiency of persulfate activation (Wan et al., 2021). Bai et al. (Bai et al., 2023) investigated the process of pre-mixing three phosphorus compounds (KH_2PO_4, $Ca(H_2PO_4)_2$, and $NH_4H_2PO_4$) with corn straw to prepare biochar (CSB+K, CSB+Ca, and CSB+N) that showed enhanced carbon (C) sequestration and slow phosphorus (P) release at three temperatures (300, 500, and 700°C). The results indicate that the addition of all phosphorus sources increased C retention significantly in the order: $NH_4H_2PO_4$ (65.6–83.5 %) > $Ca(H_2PO_4)_2$ (60.4–78.2 %) > KH_2PO_4 (50.1–76.1 %). The original retention rate was 47.8–73.6 %. Furthermore, the addition of $Ca(H_2PO_4)_2$ and KH_2PO_4 led to an increase in aromatization and graphitisation compared to the original biochar. (See Fig. 3.4a -3.4c). Boron doping of biomass char is also feasible, with boric acid being one of the B-doping agents used for biomass char modification (Gao et al., 2022).

During the preparation of biomass char, metal elements can be doped to tailor the biochar properties for various applications. Xu et al. (Xu, Y. et al., 2021) investigated the effects of four Ca-based additives (CaO, $CaCO_3$, $Ca(OH)_2$, and $Ca(H_2PO_4)_2$) on the pyrolysis characteristics of swine manure (SM) and the properties of biomass char. The results indicated that CaO outperformed other Ca-based additives in improving gas product composition and biomass char mass (Fig. 3.4d - i). Zhang et al. (Zeng, M. et al., 2023) co-pyrolyzed sludge using different $CaSiO_3$ ratios (0 %, 3 %, 6 %, 9 %, 12 % and 15 %), various pyrolysis temperature levels (300, 400, 500, 600 and 700°C), and various dwell times (15, 30, 60 and 120 min) to investigate the stabilisation of heavy metals in sludge. The results showed that the application of $CaSiO_3$ promoted the formation of crystals associated with heavy metals, such as

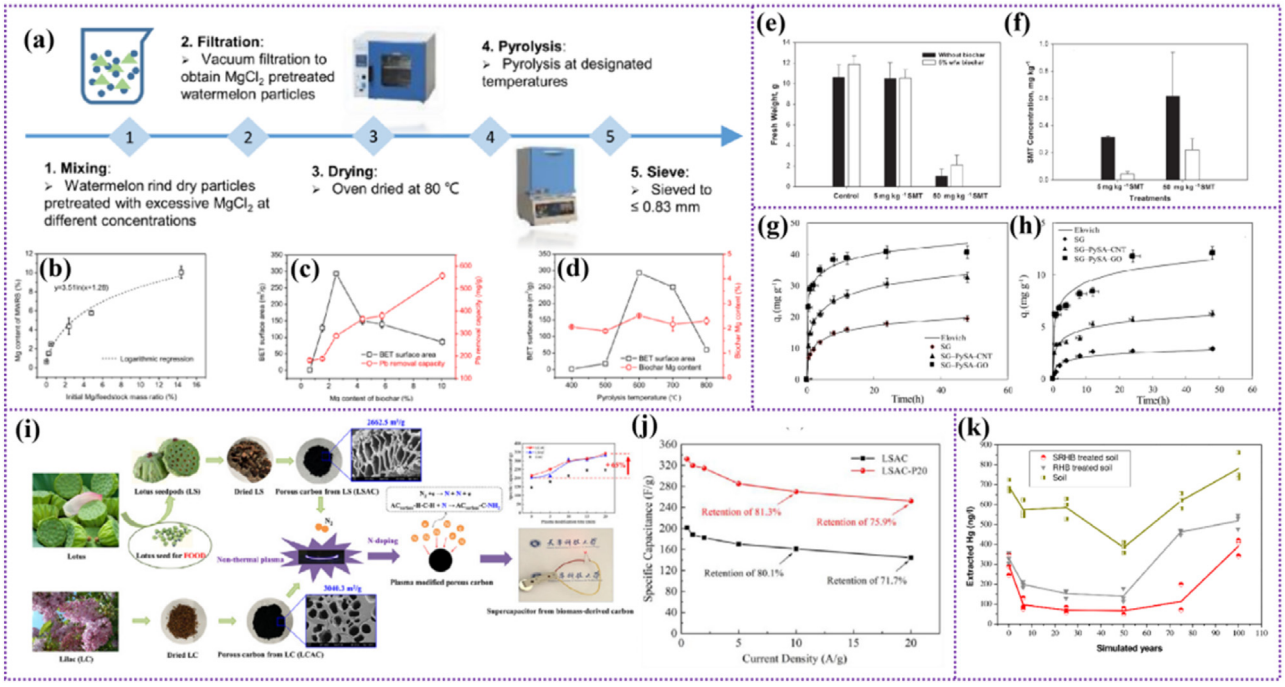

Fig. 3.3. (a) Synthesis of MgO-coated watermelon rind biochar. (b) Coated Mg content vs Mg/feedstock ratio. (c) BET SSA vs coated Mg content, Pb removal capacity coated Mg content. (d) BET SSA vs pyrolysis temperature, Pb removal capacity vs pyrolysis temperature (Zhang, J. et al., 2020). (e) Fresh weight of lettuce samples after the various treatments. (f) Concentration of antibiotic recorded in the lettuce samples after the various treatments (SMT, sulfamethazine) (Rajapaksha et al., 2014). (g) Sorption kinetics of Pb (II) and Cd (II) (h) on biochar samples (Liu, T. et al., 2016). (i) Biochar preparation process diagram. (j) Specific capacitance at different charge-discharge current density levels (Wu et al., 2021). (k) Simulated Hg extraction levels for treatments at different years. Note: SRHB 295 treated soil = 5 % sulphur modified rice husk biochar treated soil; RHB treated soil = 5 ;% rice 296 husk biochar treated soil; soil = control soil with no treatment (Zhao et al., 2020).

$Pb_3(CO_3)_2(OH)_2$ and $CuFe_2(PO_4)_2(OH)_2$, but weakened the intensity of the O-H stretching vibration peaks. This facilitated the formation of aromatic and epoxy ring structures, which enhances the immobilisation of heavy metals (Fig. 3.4j-m). Xu et al. (Xu, Y. et al., 2023) added five chlorine-based additives (Cl additives ($CaCl_2$, $MgCl_2$, KCl, NaCl and PVC) during swine manure pyrolysis and studied the effect on heavy metal volatilisation and the pyrolysis properties of biomass char. Adding $CaCl_2$ increased carbon retention in biomass char significantly (up to 13.1 %), possibly due to CO_2 capture during pyrolysis by the formation of $CaCO_3$ and physical barriers that prevented the release of volatiles by newly-generated mineral substances. This study suggests that co-pyrolysis with $CaCl_2$ is a promising strategy for enhancing carbon retention, the bio-availability of phosphorus, and reducing the bioavailability of heavy metals at higher temperatures (Fig. 3.4j - m).

3.3.3. Effect of additives and doping elements on the structure and applications of biochar

Additives and doping elements can initiate new chemical reactions, such as redox reactions and acid-base neutralisation, thereby further altering the properties and structure of biochar. For example, metal doping can enhance the conductivity of biochar. Modulation of electrochemical active sites and surface functional groups can optimise biochar's performance in electrocatalysis and energy storage (Xu, X. et al., 2020). Using molten salts such as $ZnCl_2/CaCl_2$ as additives can expedite the conversion of biomass to biochar and can be used with a wide range of temperatures. Ionic species in the molten state act as microstructure/pore directors (Egun et al., 2022). Additives and doping can exert a direct influence on the structure of biochar. In one study, coconut shell biochar was prepared at 500°C and subjected to heat treatment at temperatures ranging from 1000 to 1300°C in the presence of Ni. An ordered graphite structure was observed at 1200°C, with interlayer spacings ranging from 0.3369 nm to 0.3376 nm (Destyorini et al., 2021) (Fig. 3.5a and b). Similarly, iron-catalysed graphitisation has been reported in biochar derived from sugarcane bagasse and chestnut shells (Gai et al., 2021; Hunter et al., 2020). Schaefer et al. investigated the effect of heteroatoms on the hydrogen absorption performance of olive pit carbon. Olive pit biochar was activated using KOH, and O functionality was enhanced via ozone oxidation. The hydrogen absorption tendency followed a decreasing order of SSA, average micropore size, surface functionality, and pore size distribution. Nevertheless, the acidic functional groups generated by ozone treatment led to an increase of approximately 26 % in hydrogen absorption capacity compared to carbon without ozone treatment (Schaefer et al., 2020) (Fig. 3.5c). Ying et al. (Ying et al., 2022) used rice husks in pyrolysis and hydrothermal carbonisation to produce biomass char. They observed a significant reduction in the initial potential and an increase in current density when biomass char replaced the anode in the oxygen evolution reaction. Furthermore, the abundant -OH groups in hydrothermal carbonised biomass char contributed to lowering the initial potential (Fig. 3.5d - e). The porous structure and larger SSA of pyrolyzed biomass char enhanced its reactivity at high potentials. The effects of $CaSiO_3$ addition, pyrolysis temperature, and residence time on heavy metal species distribution are shown in Fig. 3.5f-h.

3.3.4. Summary

Different dopants and additives have a significant impact on the composition, pore structure, conductivity, and chemical activity of biochar. By providing a detailed explanation of these effects, a deeper scientific understanding of the biochar preparation process is established, offering strong support for practical applications. For example, in the field of hydrogen and energy storage, introducing specific additives into biochar can notably enhance hydrogen adsorption capacity and improve conductivity, introducing new perspectives for designing hydrogen storage materials. The in-depth analysis lays the groundwork for future research

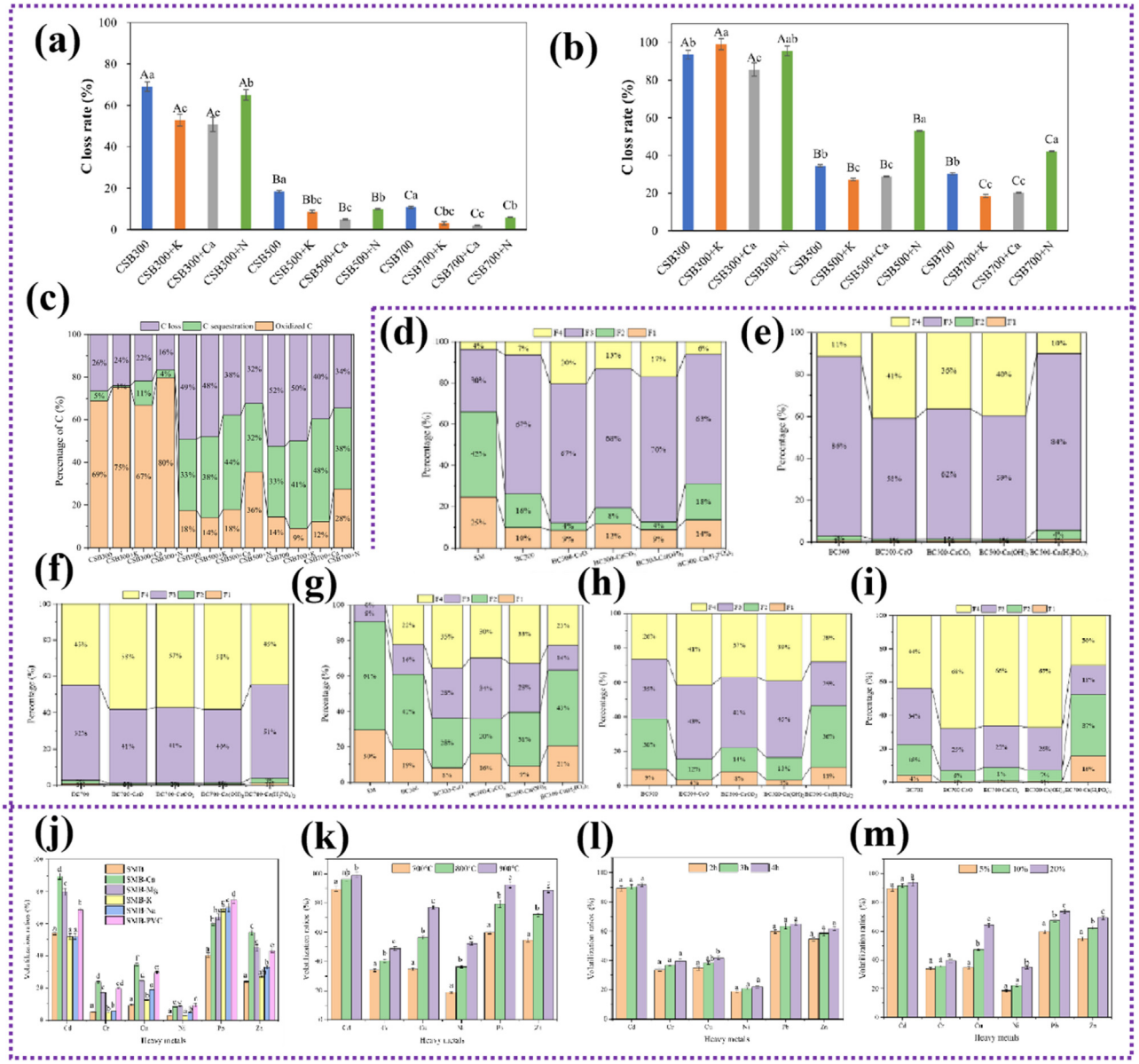

Fig. 3.4. The chemical stability of (a) C in biochar, (b) C oxidized by H_2O_2, (c) C oxidized $K_2Cr_2O_7$, and (d) Total C species (Bai et al., 2023). Chemical fractionation of Cu (d-f) and Zn (g-i) in the resultant biochar (Xu, Y. et al., 2021). The volatilization ratios of heavy metals affected by (j) Cl-additive types and pyrolysis conditions, (k) pyrolysis temperature, (l) reaction time and (m) amount of $CaCl_2$ added (Xu, Y. et al., 2023).

on biochar structural regulation and its application in the field of energy storage.

3.4. Effect of pressure

Pressure is an important factor in the production of biochar, as it plays an indispensable role in reaction conditions and the quality of the biochar that is produced. This section reports on the role of pressure in biochar formation and its impact on biochar quality. The methods used to optimise pressure parameters for enhanced production efficiency are reported to better understand how the variations affect the use of biochar in fields such as soil improvement, water treatment, and energy storage. The aim of the investigation into the effect of pressure on biochar was to provide new insight and guidance for optimising the production of biochar and its broader use in various fields.

3.4.1. Effect on biochar yield and fixed carbon content

Biochar is produced under anaerobic or oxygen-limited conditions. With the exception of hydrothermal pyrolysis, all other types of pyrolysis are conducted in an inert gas environment (Li et al., 2014). N_2 is typically used as the inert gas in the reactor chamber to ensure an oxygen-deficient condition for feedstock pyrolysis (Park et al., 2014). The pressure and flow rate of the inert gas affect pyrolysis and biochar formation significantly. High pressure can extend the residence time of pyrolysis vapors by reducing their flow rate, promoting more prolonged interaction with reactor surfaces and enhancing secondary reactions such as condensation , which increases the decomposition rate (Li, Y. et al., 2020). It has also been reported that biochar yield increases with pressure. The positive impact on both the yield and quality of biochar is attributed to a higher temperature under high pressure, which leads to rapid decomposition of biomass components and, consequently, the generation of an abundance of high-quality char. Pyrolysis of biomass containing more volatile matter under high pressure has been

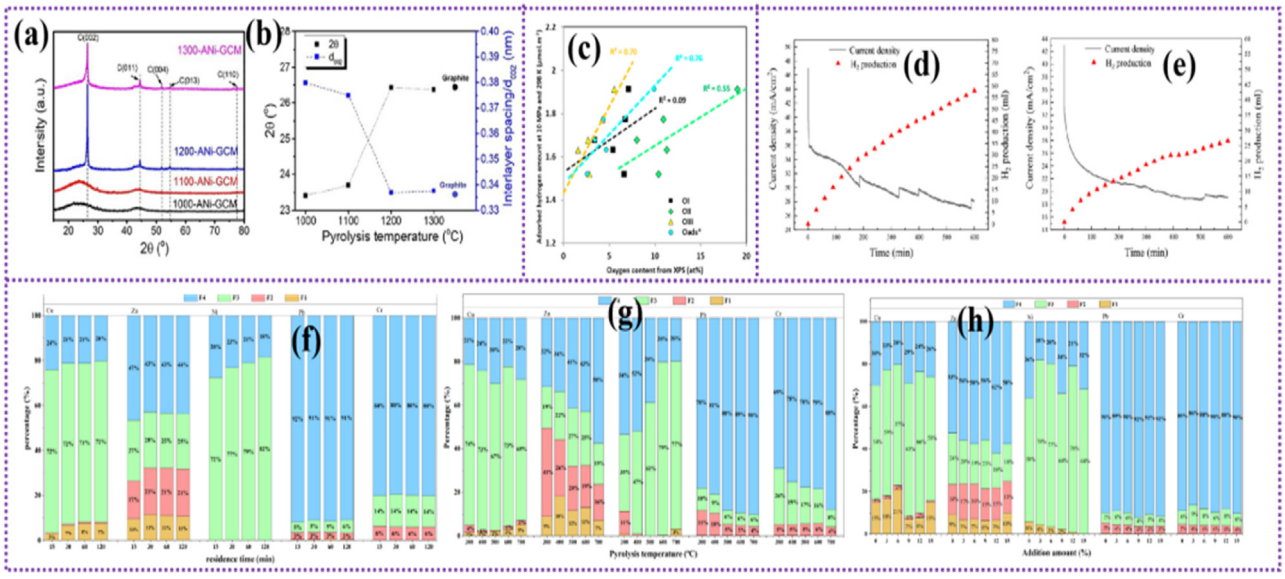

Fig. 3.5. (a) XRD patterns; (b) 2θ and d-spacing value of graphitic carbon materials (1000-ANi-GCM, 1100-ANi-GCM, 1200-ANi-GCM, 1300-ANi-GCM) (Destyorini et al., 2021). (c) Correlation between the amount of oxygen from XPS and the amount of adsorbed hydrogen per unit of surface area (10 MPa, 298 K) (Schaefer et al., 2020). Variation in current density and hydrogen production with time during BAWE of (d) PB800 and (e) HB200 (Ying et al., 2022). (f) Effect of adding $CaSiO_3$ on the distribution of heavy metal species, (g) Effect of pyrolysis temperature on the distribution of heavy metal species ($CaSiO_3$ addition 9 %, residence time 60 min). The percentage of metal components not shown in the graph is less than 1 %. (h) Effect of residence time on the distribution of heavy metal species ($CaSiO_3$ addition 9 %, pyrolysis temperature 600 °C). The percentage of metal components not shown in the graph is less than 1 %, (Zeng, M. et al., 2023).

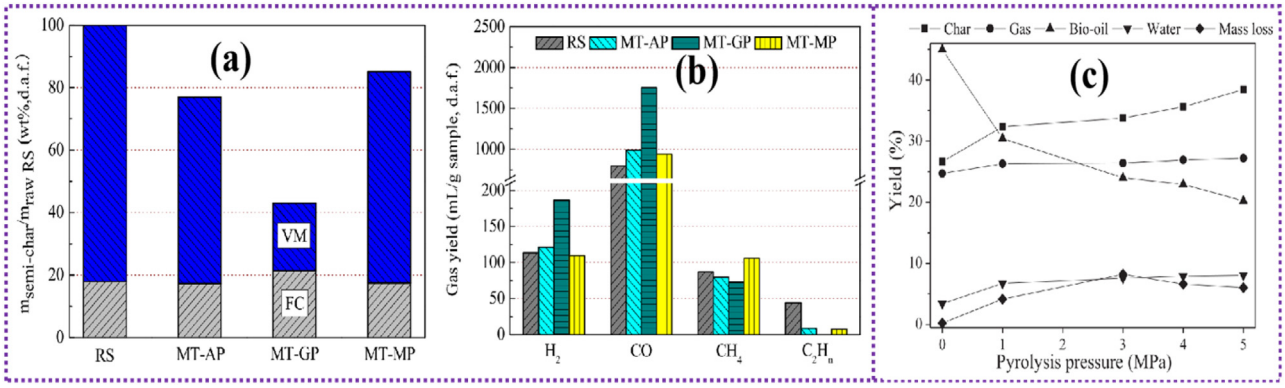

Fig. 3.6. (a) Fixed carbon and volatile matter content of the MT semi-chars on a raw RS basis and (b) Yield of H_2, CO, CH_4 and C_2H_n of CO_2 gasification of raw RS and MT semi-chars at 900 °C (Xiao et al., 2015). (c) Effect of pyrolysis pressure on product distribution (Xu and Li, 2017).

shown to increase the biochar yield (Tripathi et al., 2016). Xiao et al. (Xiao et al., 2015) conducted straw baking pyrolysis under mechanical pressure at 10 MPa using temperatures ranging from 200 to 280°C. They reported a significant increase in carbon yield when baking under mechanical pressure (Fig. 3.6a and b). Recent research done by Setkit et al. (Setkit et al., 2021) suggests that applying mechanical pressure during the pyrolysis process also has a positive impact on the biochar. They reported a pre-treatment method involving applying mechanical pressure (10–70 MPa) at 250°C to investigate its effect on the pyrolysis of tulipwood (LC). The results indicated that applying mechanical pressure during pyrolysis increased the carbon char yield significantly at 900°C. In the literature, however, different conclusions have been drawn on the effect of pressure on pyrolysis. Previous studies reported that the fixed carbon content in biochar increases with a higher pyrolysis pressure (Van Wesenbeeck et al., 2016). However, studies have also found that this enhancement can be achieved by simply increasing the gas residence time in the pyrolysis reactor (Elyounssi and Halim, 2010). Therefore, the impact of pressure should be evaluated while keeping the gas residence time constant. Research revealed that biochar produced at 1 MPa pressure had a lower carbon content, H/C, O/C, average pore size and SSA, and a higher fixed carbon content than that produced at 0.1 MPa pressure (Manyà et al., 2016) (Fig. 3.7a-d). Similar conclusions were drawn by Melligan et al. (Melligan et al., 2011), who reported that as pressure increased, the content of biochar decreased, when using biochar obtained from miscanthus pyrolysis. They also reported that as atmospheric pressure increased from 0.6 to 2.6 MPa, the molar ratio of O/C and H/C gradually decreased, the SSA reduced, and the aromatic C proportion increased. Under high-pressure conditions, the quality of the biochar improves due to the increased surface-deposited carbon enhancing its energy density (Anand et al., 2022; Manyà et al., 2013). While high temperature and pressure reduce the biochar yield, they also increase pyrolysis gases, carbon content, and CEC (Ferreira et al., 2019; Wang, K. et al., 2020). Azuara et al. (Azuara et al., 2016) investigated the effects of different temperature and pressure levels on corn straw biochar, and reported that increased pressure reduces the O:C ratio and increases the fixed carbon content. The impact of pressure on biochar yield is relatively minor, and further research is needed to assess the suitability of pressurized pyrolysis systems for optimising reaction con-

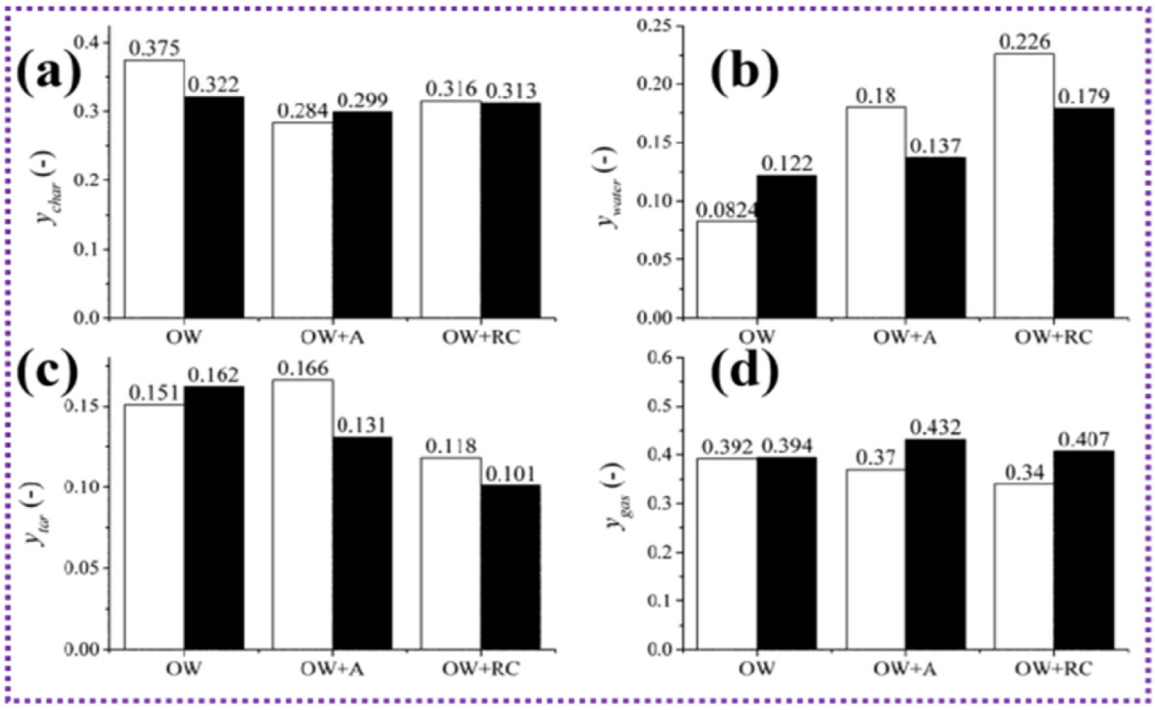

Fig. 3.7. Mass yield of (a) char, (b) tar, (c) produced water and (d) gas. The white columns indicate pyrolysis runs at 0.1 MPa; the black columns indicate runs conducted at 1.0 MPa, (Manyà et al., 2016).

ditions and pressure control (Ferreira et al., 2019); (Wang, K. et al., 2020).

3.4.2. Effect on the surface properties of biochar

During biochar preparation, the pyrolysis pressure conditions also affect the textural characteristics of the resulting biochar. Increased pressure leads to a reduction in the SSA and therefore, high pressure limits the formation of biochar with high SSA and the required porosity (Manyà, 2012). Choi et al. (Choi et al., 2017) studied the effect of temperature (350, 450 and 520°C) and vacuum pressure (0.09, 0.7 and 3 kPa) on the physicochemical properties of biochar obtained from vacuum pyrolysis of ash larch. The results indicated that the effect of vacuum pressure on product properties depended on the pyrolysis temperature (Fig. 3.8a-d). Xu et al. (Xu and Li, 2017) conducted pressurised pyrolysis experiments on pine sawdust using a homemade pressure pyrolysis reactor and studied the effect of pyrolysis pressure (within the range of 0–5 MPa) on product distribution and characteristics. The results showed that pressure affected biomass pyrolysis significantly by increasing the yield of gaseous products and biochar (Fig. 3.6c). In a study done on pine wood, the SSA exhibited a consistent downward trend as pressure increased from 1 to 20 bar (Cetin et al., 2005). Melligan et al. (Melligan et al., 2011) reported similar results, i.e. the SSA decreased from 161.7 to 0.137 m^2/g with the pressure increasing from 1.013 to 26 bar. High pressure may impede the release of volatiles and disrupt the microporous structure, as large spherical voids are formed, which is unfavourable for obtaining a high SSA. Therefore, it is recommended that the appropriate atmospheric pressure is used.

3.4.3. Effect on polycyclic aromatic hydrocarbons in biochar

Polycyclic aromatic hydrocarbons (PAHs) are highly condensed aromatic structures that are generated during the biomass pyrolysis process, with their final concentration in biochar typically ranging from less than 0.1 to over 10,000 mg/kg (Wang et al., 2017; Zhang, C. et al., 2019). These compounds may be present on the surface of biochar. Due to their persistent existence in the environment and their carcinogenic, mutagenic and teratogenic effects on human health, PAHs have drawn public and scientific attention (Mahler et al., 2012). Among the various pyrolysis methods used, slow pyrolysis is preferred when a higher biochar yield and lower PAH is required (Quilliam et al., 2013). Research has demonstrated that adopting low-temperature slow pyrolysis (< 500°C) can reduce the total concentration of PAHs in biochar and decrease the levels of highly toxic PAH species (Hale et al., 2012). Pyrolysis temperature and gas residence time are the primary factors affecting the formation and release of PAHs (Buss et al., 2016; Madej et al., 2016). Compared to the effect that pyrolysis temperature and gas residence time has on PAHs, the effect of pressure appears to be relatively minor (De la Rosa et al., 2008; Fabbri et al., 2013). Greco et al. (Greco et al., 2021) evaluated the impact of pressure, gas residence time and type of carrier gas on the pyrolysis behaviour of untreated wood waste and the properties of the resulting biochar (including its PAHs content). The results indicated that increasing pressure leads to a significant reduction in PAHs, possibly due to the higher carrier gas velocity under pressurised conditions, which inhibits the condensation and aggregation of PAHs. In one study (Balmuk et al., 2023), two biomass materials (grapevine shoots - VS and corn stover - CS) were subjected to 60 min of pyrolysis at different temperature (350 and 500 °C) and pressure levels (0.1 and 0.5 MPa). The research focused on the effect of temperature and pressure on the concentration of PAHs in the resulting products. The study revealed that temperature and pressure affected the concentration of PAHs in corn stover biochar but had no impact on biochar produced from grapevine shoots.

3.4.4. Summary

The impact of pyrolysis pressure on biochar is highly complex. Firstly, pressure can influence the yield and fixed carbon content of biochar, which provides some guidance for future production optimisation. Secondly, increasing pressure contributes to improving the carbon fixation effect, which lays the foundation for using biochar in various applications. Pressure also affects the surface properties of biochar, especially changes in specific surface area, which is crucial for the effectiveness of the application. Additionally, increasing pyrolysis pressure significantly reduces the concentration of PAHs in biochar, which helps

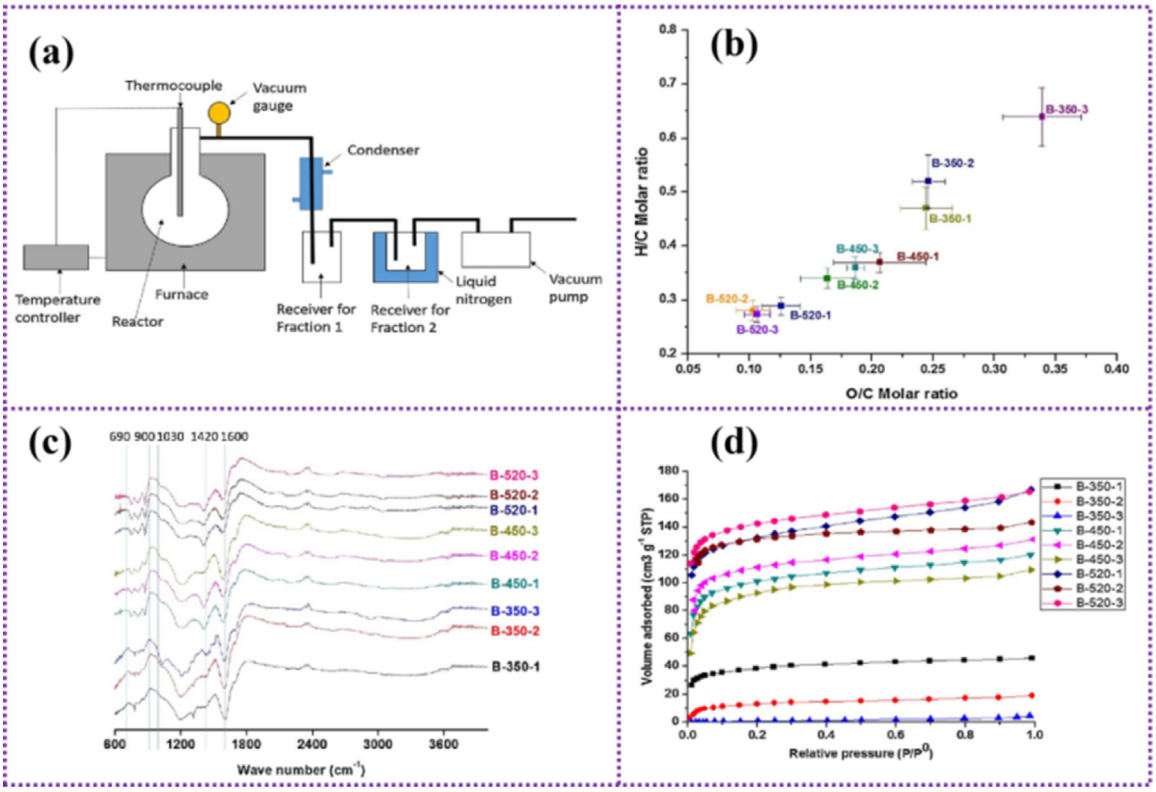

Fig. 3.8. (a) Scheme for the vacuum pyrolysis experimental setup. (b) Van Krevelen plot for biochar derived using different pyrolysis conditions. (c) FTIR spectra of biochar obtained using different pyrolysis conditions. (d) Nitrogen adsorption isotherms of biochar obtained using different pyrolysis conditions (Choi et al., 2017).

to mitigate environmental and human health risks. Therefore, future research and production should focus on pressure regulation to optimise the properties of biochar and ensure environmental and safety attributes.

3.5. *Influence of heating method*

Biochar is mainly produced by biomass cracking under heated conditions. Temperature, heating rate and residence time have a strong effect on the yield and physicochemical properties of biochar. As the temperature increases, the biochar yield decreases while the carbon composition and specific surface area in biochar increase. A high heating rate causes secondary cracking of pyrolysis intermediates in biomass, which reduces the biochar yield and affects the properties of biochar, e.g. it can accelerate the gas release and increase the porosity of biochar. Conversely, a low heating rate improves biochar yield.

Biochar production is closely related to the pyrolytic heating method, which depends on the heating rate used to produce the biomass (Table 3.4). Both slow pyrolysis which has a long history and fast pyrolysis, which has gradually developed in recent decades, are traditional techniques. Novel methods are also emerging, such as flash pyrolysis, vacuum pyrolysis and microwave pyrolysis. Gasification, torrefaction and hydrothermal carbonisation should also not to be ignored, although these are the less common methods employed in biochar production. Depending on the type of feedstock and its possible use, it is possible to customise the production of biochar with different properties by selecting a specific heating method.

3.5.1. *Biochar production by pyrolysis*

Carbon materials prepared from forestry and agricultural biomass by slow pyrolysis have widely been used as adsorbents, catalyst carriers, and fuel (Kumar Mishra et al., 2023). Slow pyrolysis that yields biochar as the main product generally takes several hours or even days to complete the decomposition and carbonisation process (Zhu, X. et al., 2018). Slow pyrolysis typically has a low heating rate (typically less than 10 °C/min), a long residence time (hours to days), and a low pyrolysis temperature (300–600 °C). The relatively long residence time and suitable temperature mean the biomass pyrolysis vapour has a long residence time, and this promotes secondary cracking. The main products from slow pyrolysis are biochar (35–55 %), bio-oil (25–35 %) and syngas (20–30 %). Pyrolysis temperature and heating rate are key process parameters that affect the distribution of biomass pyrolysis products. The biochar yield from biomass is higher when the heating rate is low. In general, the quality of biochar is related to properties such as carbon content, pH, specific surface area, porosity and nutrients. Carbon content is an important parameter, as a low heating rate favours adequate heat transfer, which facilitates the deposition of the carbon fraction and thus, increases the biochar yield. Slow pyrolysis combined with a higher pyrolysis temperature improves the quality of biochar, as more volatiles are removed from the material, hence, an increase in carbon content. However, a low heating rate increases the stability of biochar. Wood vinega is a by-product of slow pyrolysis. It contains mainly acids, esters, ketones and phenols, which can be extracted and used as value-added products.

Fast pyrolysis is an efficient thermal conversion method that usually requires only a few seconds to achieve biomass cracking (Lakshman et al., 2021). Fast pyrolysis has a very high heating rate of about 1000 °C/min, a pyrolysis temperature of about 500 °C, and a residence time for the pyrolysis vapour that is typically less than 2 s. With most types of biomass, a fast pyrolysis temperature of about 500 °C is appropriate. The advantages of fast pyrolysis are high conversion efficiency and a high product recovery rate. During fast pyrolysis, biomass particles undergo rapid cracking, with the main product being bio-oil, rather than biochar (usually less than 20 %). Biochar is a by-product of the rapid pyrolysis of biomass. The main product, bio-oil, is the condens-

Table 3.4
Biochar production technologies (Rathore et al., 2021; Wang, D. et al., 2020; Yaashikaa, P.R. et al., 2020; Zhou, Y. et al., 2021).

Heating method	Temperature (˚C)	Heating Rate	Residence Time	Atmosphere	Main Product	Biochar Yield (%)
Slow pyrolysis	300–600	< 10 ˚C/min	Hours to days	Oxygen free or limited	Biochar	35–55
Fast pyrolysis	400–600	1000 ˚C/min	2 s	Oxygen free or limited	Bio-oil	< 20
Flash pyrolysis	400–700	1000 ˚C/s	2 s	Oxygen free or limited	Bio-oil	< 30
Vacuum pyrolysis	400–600	< 50 ˚C/min	Min to hours	Oxygen free	Bio-oil	< 30
Microwave pyrolysis	400–600	Up to 330 ˚C/s	Several min	Oxygen free or limited	Bio-oil	< 40
Gasification	800–1600	1000 ˚C/min	Several second	–	Syngas	< 25
Torrefaction	200–300	< 50 ˚C/min	Min to hours	Oxygen free or limited	Torrefied biochar	60–80
Hydrothermal carbonization	150–300	< 10 ˚C/min	Min to hours	–	Biochar	> 50

able component of the pyrolysis vapour collected in the condenser. Similarly, a high pyrolysis temperature promotes the volatilisation of volatile components, which also reduces the amount of biochar produced by fast pyrolysis. Fast pyrolysis has a high heating rate where biomass is heated rapidly, and the pyrolysis vapours are quickly removed from the reaction system. The shorter residence time and faster rate of vapour removal also reduce the carbon deposition reaction, hence reducing the biochar yield. Although biochar is a by-product of fast pyrolysis of biomass, fast pyrolysis is suitable for processing large quantities of biomass and therefore, the overall amount of biochar generated is not insignificant. The effect of heating rate on the quality of biochar during fast pyrolysis is also a complex process. It has been reported that biochar produced at a high heating rate results in biochar with a more pronounced pore structure and specific surface area, due to the rapid release of volatile matter. However, contrary conclusions have also been reported, depending on the biomass feedstock and pyrolysis conditions used (Chen, D. et al., 2016a).

Flash pyrolysis is a modified form of fast pyrolysis, with heating rates in excess of 1000 ˚C/s (Nzihou et al., 2019). This method has received much attention due to the high heating rate used. The temperature range for flash pyrolysis is typically 400 to 700 ˚C, which means that the target temperature can be reached in less than a second. Cracking of biomass in the flash pyrolysis process is accomplished almost instantly, typically in the range of 0.1 to 0.5 s. Such high heating rates and reaction temperatures combined with the short vapour residence time can increase the bio-oil yield significantly, i.e. to about 65–75 wt %. However, this also reduces biochar yield. Furthermore, the yield of the various products in flash pyrolysis is closely related to the type of biomass used, and it is also affected by temperature, the residence time of the vapour in the system and the gas flow rate. Generally, flash pyrolysis is carried out in fluidised beds or twin-screw hybrid reactors. Biochar is also a by-product in flash pyrolysis; however, the yield can be even lower than the biochar yielded via fast pyrolysis.

Vacuum pyrolysis is the thermal degradation of biomass under vacuum or low pressure (Yadav et al., 2016). Generally, vacuum pyrolysis is carried out at a pressure below 0.05 MPa and a temperature in the range of 400 to 600 ˚C. As with conventional pyrolysis, the heating rate applied in vacuum pyrolysis is low. Although the pyrolysis conditions are similar to the conditions used for slow pyrolysis, the product distribution and quality can be quite different. This is due to the rapid release of vapour during vacuum pyrolysis. In vacuum pyrolysis, the interaction between volatiles and biochar has a significant effect on the bio-oil fraction. In addition, the vapour generated during pyrolysis is only associated with vacuum or low pressure, which reduces the transfer of solid particles such as ash, and this has significant benefits in terms of biochar quality and yield. Vacuum pyrolysis technology facilitates the production of biochar with high porosity, which can be widely used as an adsorbent and soil conditioner.

Microwave pyrolysis used in the production of biochar is an advanced technology that has received more attention recently (Lv et al., 2022). Mari et al. (Selvam S and Paramasivan, 2022) compared the performance of microwave-assisted pyrolysis with that of conventional pyrolysis in terms of product yield, characteristics and energy consumption, and found that biochar as a “hot spot” in microwave pyrolysis plays an important role in improving product selectivity and quality. Also, microwave pyrolysis at low temperatures produces a uniform thermal gradient, which helps in the production of engineered biochar for use in gasification, energy storage, etc. Gabriela et al. (Durán-Jiménez et al., 2021) demonstrated a simple, fast and flexible microwave processing method to produce biochar for CO_2 adsorption thus avoiding the use of any form of catalyst or chemical activation. Emily et al. (Kostas et al., 2020) used microwave pyrolysis to recover value-added products from natural waste resources such as olive pomace, revealing the superiority of microwave heating in pyrolysis systems and emphasizing that this is a novel and promising pathway. Microwave heating has excellent application prospects due to its fast startup and shutdown, high selectivity and high energy efficiency. Compared to the traditional heating method, microwave heating has more advantages in terms of heat transfer. Microwave heating generates heat energy through dielectric heating, and the heat source is in direct contact with the reactants, which heats the raw materials more quickly, hence accelerating the decomposition process. The fundamental difference between microwave heating and conventional heating is the difference in the heating mechanism, with microwave heating causing more hot spots inside the biomass feedstock. Microwave heating has a higher heating rate. There are also differences between microwave heating and conventional heating in terms of product distribution. Since the heat in microwave heating is generated inside the biomass, it is more favourable for cracking the feedstock and releasing the products. Microwave heating also reduces the sintering temperature, which improves vapour release. In addition, with conventional pyrolysis, the moisture in biomass will have an unfavourable effect on the pyrolysis process; however, in microwave pyrolysis, moisture is favourable, as it improves the efficiency of microwave heating. This is due to the fact that moisture absorbs microwaves better than biomass. In addition, microwave absorbers are generally needed during microwave pyrolysis to enhance the absorption of microwaves and therefore, increase the heating rate. Microwave absorbers can also be combined with catalysts to further modulate the pathway for generating biomass pyrolysis products. Microwave technology is also attracting attention in the industrial fields due to its outstanding thermal properties of fast, selective, uniform heating. Biochar produced at lower temperatures via microwave heating can show similar results or even better performance than conventionally pyrolyzed biochar.

3.5.2. Biochar production using other heating methods

Gasification is a technology employed to produce syngas from different carbonaceous materials. Although the main product of biomass gasification is syngas, the gasification process also results in the generation of biochar (approximately 10 %). Unlike conventional pyrolysis, gasification temperatures are typically above 800 °C. At the same time, depending on the desired syngas composition, gasification agents such as water vapour or air are introduced into the reaction system. Gasification agents facilitate the production of effective components of syngas (such as hydrogen and CO), and the formation of porous biochar. In general, the quality and yield of syngas are the main focus of biomass gasification. While assessing the quality of syngas, attention is also given to the quality of biochar. The carbon content and yield of biochar are closely related to the equivalence ratio of the gasification parameters, feedstock type, gasifier and pressure. Among them, the equivalence ratio is the most important parameter in gasification. The optimal value of the equivalence ratio is 0.2–0.4. Increasing the equivalence ratio decreases the yield and carbon content of the biochar. The higher the equivalence ratio, the higher the amount of oxygen in the gasifier, which affects the gasification process. At the same time, an increase in the equivalence ratio promotes gas yield, which facilitates the formation of micropores in the biochar, hence increasing the specific surface area. A high equivalence ratio leads to more complete combustion of the biochar, which reduces its mechanical strength and increases the ash content.

Torrefaction is a special thermochemical process used in the pretreatment of feedstock at temperatures typically in the range of 200–300 (Zhu et al., 2021). During torrefaction, an inert atmosphere, and low heating rate (below 50 °C/min) and long residence time (tens of minutes to several hours) are generally employed. Depending on the final temperature, typically 10–30 % of the volatile components are released. Torrefaction improves the quality of the biomass and contributes to further pyrolysis and combustion processes. The solid product produced after biomass torrefaction can also be viewed as a special type of biochar. The product of torrefied biochar is generally a brown solid with better energy density than biomass. This indicates that torrefied biochar has a good potential for use as fuel. In addition, torrefied biochar can continue to be used as a special biomass feedstock in processes such as pyrolysis and gasification. The physicochemical properties of the biomass feedstock have an important influence on the quality of the torrefied biochar and also affect the energy requirements of the torrefaction process (Shao et al., 2020). In general, hemicellulose in biomass is the first to crack and volatilise, while lignin is relatively stable. Torrefaction temperature and residence time are the most important factors in the torrefaction process. As the temperature increases, the yield of torrefied biochar decreases and the carbon content in biochar increases. After the biomass has been torrefied, most of the moisture is removed, which can significantly reduce transportation costs and increase storage time. Torrefied biochar also has better grindability. Torrefied solids, such as soil conditioners, can also be used for carbon sequestration, as they have physicochemical properties similar to biochar.

Hydrothermal carbonisation is an effective treatment for feedstocks with high moisture content (Zhu, Xiefei et al., 2023). Typical feedstocks include sewage sludge and animal manure. Generally, during hydrothermal carbonisation, water is kept in a state below the critical point. There is no need to dry the biomass prior to hydrothermal carbonisation, which can significantly reduce the energy consumed during the overall process. Reaction temperatures applied in hydrothermal carbonisation are typically in the range of 150–300 °C where a pressure of about 2–10 MPa is required. Hydrothermal carbonisation degrades the feedstock mainly through hydrolysis, which includes dehydration, decarboxylation or condensation reactions. Firstly, the hemicellulose (T > 180°C), cellulose (T > 200°C) and lignin (T > 220°C) in the biomass are degraded via hydrolysis into small fragments, which facilitates decarboxylation and dehydroxylation. In general, biomass can be hydrolysed to reduce the H/C and O/C ratios in the solid products. The decarboxylation reaction removes carboxyl and carbonyl groups, which releases gaseous products such as CO_2 and CO. Dehydration also releases more water in the reaction medium. In addition, some highly reactive intermediates are further polymerised through a condensation reaction to form large polymers. These are the building blocks of hydrothermal solid products, which are relatively stable. The reactions in hydrothermal carbonisation do not occur in a certain order.

Similar to pyrolysis, solid products, liquid products and gas products are also obtained through hydrothermal carbonisation. The biochar product, also known as hydrochar, can be used as fuel to replace conventional coal or for soil improvement purposes. The liquid product is complex and contains mainly acids, phenols, aldehydes and alcohols, in addition to significant amounts of water. These high value chemicals can be upgraded via further separation. Gaseous products mainly contain CO_2, CO, CH_4 and H_2 and etc., with CO_2 generally accounting for more than 90 % (Zeng, M. et al., 2023). Organic matter in the feedstock is mainly dissolved in liquids and retained in solid products. Depending on the adjustments made to the different reaction conditions, various carbonaceous materials of different sizes, shapes, surface textures and functional groups can be prepared. In addition, HTC-produced biochar retains nutrients such as nitrogen and phosphorus, which contribute to soil fertility. Improvement of the hydrophobicity and abrasive capacity of biochar is also important. Hydrothermally produced biochar can also be widely used as an adsorbent or in soil amendment and carbon sequestration.

3.5.3. Summary

The quantity and quality of biochar produced depends on a number of factors such as carbonisation temperature, heating rate, pressure and heating method. The heating method will generally determine the type of reactor, while the carbonisation temperature, heating rate, and pressure will be selected according to the actual operation and the type of biochar required. It is difficult to keep the carbonisation temperature, heating rate and pressure identical when applying different heating methods, so it is difficult to evaluate the exact effects of different heating methods on biochar. Generally, a comparatively favourable heating method can be opted for according to the required biochar yield and quality.

3.6. Other factors affecting biochar production

Biochar production has gained global attention due to its use in environmental bioremediation and energy storage. The biochar preparation process is affected by a myriad of factors, including those mentioned previously, such as feedstock, pyrolysis temperature, pressure, additives, and dopants. This section reports on the research done on other key factors, such as feedstock moisture content, pretreatment methods, particle size, catalysts, heating rate, type of inert gas used, and flow rate and residence time (Nsamba Hussein Kisiki 2015) (Fig. 3.9). This section serves to provide a more comprehensive understanding of the biochar preparation process.

3.6.1. Impact of moisture of feedstock

Moisture plays an important role in the pyrolysis process. The effect of humidity on product distribution depends on the specific process and reaction conditions. High humidity can contribute to the formation of water-based liquid by-products through enhanced hydrolysis or condensation reactions, while low humidity may reduce these effects and favour processes such as carbonization or combustion, leading to a higher yield of solid residues like ash, depending on the feedstock and operational parameters (Bridgwater et al., 1999). Moisture affects the energy and temperature required for biochar synthesis (Yaashikaa et al., 2019). For slow pyrolysis, feedstock with a 40–60 % moisture content is considered suitable for biochar production, while moisture levels of 10 % or below are preferred for fast pyrolysis (Pandey et al., 2020). Hydrothermal carbonization (HTC) produces biochar, and using feedstock with a high moisture content enables the preparation of biochar

Fig. 3.9. Schematic representation of additional factors impacting biochar production.

rich in active functional groups (Mäkelä et al., 2015); Nizamuddin et al., (Nizamuddin et al., 2016). The biochar yield also varies with variations in moisture content (Murtaza et al., 2021; Sun et al., 2018). Eke et al. (Eke et al., 2020) investigated pyrolysis in a bubbling fluidised bed reactor reported at 500˚C with 2.69 wt %, 5 wt %, and 10 wt % moisture content. They concluded that the organic yield varied from 15.2 wt % to 19.6 wt % and decreased with an increase in moisture content. One study indicates that, under high-pressure conditions, high-moisture raw materials (i.e. 40–60 %) result in a higher biomass char yield, while a moisture level below 10 % is preferred for rapid pyrolysis because the energy expended in achieving a higher gasification temperature is minimised (Daful and Chandraratne, 2020).

3.6.2. *Impact of pre-treatment method on feedstock*

Pre-treating feedstock before pyrolysis can affect the properties of biochar (Adeniyi et al., 2022). Different pretreatment methods have different effects. For example, steam pretreatment can increase the density of sawdust particles (Alizadeh et al., 2022), while hydrothermal pretreatment can facilitate easier grinding of sawdust and increase its energy density (Dai et al., 2018). In one example, magnetic biochar derived from poplar catkins under $FeCl_3$ and $ZnCl_2$ pretreatment conditions exhibited a large SSA and excellent magnetic properties via one-step pyrolysis (Liu et al., 2019). Another study reported that adding H_2SO_4 and oxalic acid increases the specific surface area of biochar up to 250 times that of non-activated biochar (Vithanage et al., 2015). Alkaline treatment can increase the hydrophobicity of the feedstock and thus enhance the stability of biomass char. Ephraim et al. (Ephraim et al., 2018) assert that adding KOH alters the pore structure of biomass char, which increases its adsorption capacity. Upon pre-modification, the material had an enriched porous structure, especially the microporous structure, which resulted in a notable increase in SSA. Treatment with potassium carbonate (K_2CO_3) has a strong effect on the porosity of biochar, as it affects the distribution of internal micropores and mesopores, which, in a study, led to a fivefold increase in SSA (Zhu, L. et al., 2018).

3.6.3. *Impact of raw particle size*

Biomass is characterised by poor thermal conductivity, which can impede the rate of heat flow through the feedstock during co-pyrolysis. Therefore, particle size is particularly important in terms of variations in reactor requirements and the effect on biochar yield (Table 3.5). An increase in particle size is linked to an increase in the distance for heat to reach the core of the biomass material, which decelerates the rate of heat flow and increases the solid biochar yield (Akhtar et al., 2012; Encinar et al., 2000). In the pyrolysis process, as particle size increases from 17 to 20 mm, water content increases from 40 to 55 %, and the carbon content of solid biomass char decreases from 78.5 to 75 %. Larger particles are also associated with higher humidity and a lower carbon content (Wang et al., 2005). However, some researchers have found an opposite correlation between particle size and biochar yield or no significant impact (Ertaş and Hakkı Alma, 2010; Yaashikaa, P.R. et al., 2020). Some studies have assessed the impact of particle shape on biochar yield and suggest that biomass particles with a cylindrical or plate shape, yield better biochar than spherical particles (Park et al., 2010). Additionally, vertically arranged charcoal particles produce a greater biochar yield. Yorgun and Yıldız (Yorgun and Yıldız, 2015) analysed the effect that particle size in paulownia wood had on the biochar production rate. Experiments were conducted using a constant temperature (773 K) and heating rate (50 K/min) for particles of the following in sizes (mm): 0.224–0.425, 0.425–1, 1–1.8, >1.8. The highest biochar yield was obtained with a particle size of 0.224–0.425 mm. Septien et al. (Septien et al., 2012) conducted pyrolysis experiments using wood with a particle size of 0.35–0.8 mm. They noted that a higher biochar yield was achieved with a particle size of 0.8 mm. Demiral and Şensöz (Demiral and Şensöz, 2006) experimented with hazelnut shells, with various particle sizes (from 0.224–0.425 mm to 0.85–

Table 3.5
Influence of particle size on biochar yield and properties.

Feedstock	Reaction Conditions	Particle Size (mm)	Yield (%)	Water Content (%)	SSA (m^2/g)	Ref
Pine, beech, bamboo, demolition wood	T: 450–550 °C; RT: 0.25–6s	17–20	78.5–75	40–55	—	(Wang et al., 2005)
Dry wood spheres	T: 365–606 °C	—	31–17	—	—	(Park et al., 2010)
Paulownia wood	T: 350–600 °C; HR: 10–50 K/min	0.425–1	34.5–25.4; 29.5–24;	—	—	(Yorgun and Yıldız, 2015)
	T: 500 °C; HR: 50 K/min	0.224–1.8	27.3–25.9	—	—	
	T: 500 °C; HR: 50 K/min; GFR: 100–300 mL/min	0.224–1.8	25.5–22.6	—	—	
Wood	T: 1200 °C	0.35–0.80	11.8–13.7	—	—	(Septien et al., 2012)
Hazelnut bagasse	T: 350–550 °C; HR: 10 °C/min	0.425–0.600	35.09–26.82	—	—	(Demiral and Şensöz, 2006)
	T: 350–550 °C; HR: 50 °C/min	0.425–0.600	33.59–26.17	—	—	
Rice husk, tea waste, woodchips	T: 450 °C; HR: 20 °C/min	1–0.053	—	—	5.2–51.1	(Fazeli Sangani et al., 2020)

Table 3.6
Effect of type of catalyst on biochar yield.

Feedstock	Reaction conditions	Catalyst	Yield (%)	Ref
Hazelnut shell	Temperature: 500/650 °C	$CaCO_3$	33/25	(Aydinli and Caglar, 2012)
		Perlite	33/30	
		$K_2Cr_2O_7$	24/21	
Polyethylene		$CaCO_3$	1/0	
		Perlite	9/0	
		$K_2Cr_2O_7$	0/4	
Polyethylene oxide		$CaCO_3$	0/0	
		Perlite	5/4	
		$K_2Cr_2O_7$	3/1	
Pine wood/ Cottonstalk/ Fir wood	Temperature: 700 °C	Untreated	17/26/18	(Wang et al., 2006)
		Na_2CO_3	34/30/35	
		NaOH	36/34/32	
		NaCl	30/31/28	
		Na_2SiO_3	31/38/31	
		TiO_2	21/29/23	
		HZSM-5	23/27/21	
Corncob	Temperature: 550 °C; Gas flow rate: 3.4 L/min	HZSM-5	23.2–20.1	(Zhang et al., 2009)

1.8 mm), using a temperature of 500°C and a heating rate of 10°C/min. The highest biochar yield (27.90 %) was achieved with a particle size of 0.425 mm. Particle size typically affects the physical properties (rather than the element properties of biochar), which control the rate of heat and mass transfer during the process. For example, one study reported that when the particle size decreased from 1 mm to 0.053 mm, the SSA of biochar increased from 5.2 m^2/g to 51.1 m^2/g, with a slight decrease in the porosity (Fazeli Sangani et al., 2020). It has also been reported that the CEC and anion exchange capacity (AEC) of biochar increases as the particle size decreases from 0.25 mm to 0.053 mm (Liao and Thomas, 2019).

3.6.4. Impact of catalysts

In science and engineering, catalysts are materials that can reduce the time required to reach equilibrium conditions (Valle et al., 2018). Biochar elements, such as ash, can also act as catalysts, but they do not increase the biochar yield (Samolada et al., 2000). The effect of the type of catalysts used on biochar is indicated in Table 3.6. Catalysts can increase the biochar yield by accelerating the pyrolysis reaction, and increase pore density and SSA (Aydinli and Caglar, 2012; Hwang et al., 2015). Catalysts commonly used in biomass pyrolysis include alkaline catalysts (e.g. KOH, NaOH, K_2CO_3, and Na_2CO_3), metal oxides (e.g. Fe_2O_3, Al_2O_3, ZnO, CaO, and TiO_2), and activated carbon (AC) (Alipour Moghadam Esfahani et al., 2017; Chen, W. et al., 2020). Wang et al. (Wang et al., 2006) studied the carbon yield using sodium-based catalysts Na_2CO_3, NaOH, NaCl, and Na_2SiO_3. They found that all the catalysts increased the biochar yield with pine wood and fir wood. The reduction in carbon yield was attributed to the insolubility of ZSM-5 in water, which means it is difficult to ensure it disperses uniformly. When using cotton stalks, all catalysts except Na_2SiO_3 reduced the carbon yield. The choice of catalyst is influenced by the type of raw material and the properties required in the biochar that is produced. The ZSM-5 catalyst was found to be superior to the aluminium oxide and sodium carbonate catalysts in terms of biochar yield (Smets et al., 2013). Chattopadhyay et al. (Chattopadhyay et al., 2016) found that using catalysts with a higher cobalt loading during co-pyrolysis reduced the solid char and coke formation with all mixed materials.

3.6.5. Effect of inert gas type and flow rate

During pyrolysis, the gas flow rate in the reactor chamber affects the formation of biochar, primary steam generation, and secondary biochar formation (Beis et al., 2002). The impact of inert gases on biochar is described in Table 3.7. The common carrier gases are Ar, N_2, CO_2, and steam (Araki et al., 2021); however, N_2 is widely used in commercial

Table 3.7
Influence of inert gas on biochar.

Feedstock	Reaction conditions	Inert gas	Yield (%)	FCC (%)	EC (%)	Ref
Tropical timber	T: 700 °C; HR: 10 °C/min; GFR: 100 mL/min	N_2/Ar/He/CO_2	38.5/37.6/36.2/41.2	—	—	(Araki et al., 2021)
Coffee residue	T: 700 °C; HR: 10 °C/min; GFR: 20/100/200/600/ 1200/2000 mL/min	N_2	37.6/36.8/40/32/33.3	—		
Laurel (Laurus nobilis L.)	T: 300 °C; HR: 50/150/250 °C/min; RT: 30 min	N_2	—	—	C: 74.08/74.82/73.57; H: 5.60/5.45/5.60; O: 11.42/11.65/11.69	(Pathomrotsakun et al., 2020)
		CO_2	—	—	C: 73.73/74.06/74.50; H: 5.80/5.75/5.74; O: 13.83/13.29/13.12	
Straw pellet	T: 500 °C; GFR: 50/100/200/ 300/400 mL/min	N_2	28.4–27	—	—	(Ertaş and Hakkı Alma, 2010)
Wood pellet	T: 650 °C; HR: 5 °C/min; GFR: 0/330/660 mL/min; RT: 40 min	N_2	52.4/48.8/48.4	62.9/59.3/61.8	C: 73.2/71.4/72.5; H: 1.2/1.1/1.3; O: 3.5/4.6/3.0	(Crombie and Mašek, 2015)
			48.5/47.5/44.1	91.3/89.4/89.1	C: 90.0/90.2/87.4; H: 2.0/1.8/1.8; O: 5.9/6.4/9.6	
Corncob	T: 550 °C; GFR: 1.2/2.3/3.4/4.5 L/min	N_2	24.4/23.2/23.2/22.6	—	—	(Zhang et al., 2009)
Safflower (Charthamus tinctorius L.) seed	T: 5000 °C; HR: 50 °C/min; GFR: 50/100/150/200 cm^3/min	N_2	27.5/25.3/25.0/24.8	—	—	(Şensöz and Angın, 2008)
Sugar cane bagasse	T: 500 °C; GFR: 0/50/350/700 mL/min	N_2	32/27/24/22.5	—	—	(Katyal et al., 2003)

pyrolysis operations due to its inert behaviour, easy availability, and cost-effectiveness. Increasing the gas flow rate can enhance the yield of stable carbon in biochar (Crombie and Mašek, 2015), and many studies have reported the effect that the carrier gas flow rate has on the final product distribution. Zhang et al. found that increasing the N_2 flow rate from 1.2 to 4.5 L min-1 resulted in a slight decrease in biochar yield, i.e. from 24.40 % to 22.60 % (Zhang et al., 2009). Erts and Alma (Ertaş and Hakkı Alma, 2010) reported that increasing the nitrogen flow rate from 50 to 400 mL min-1 led to a decrease in biochar yield of 28.48 % - 27.21 %. Choi et al. (Choi et al., 2012) found that the biochar yield decreases with an increase in the N_2 flow rate. These results suggest that reducing the flow rate reduces the biochar yield; however, the effect is not severe, and the yield only decreases slightly.

The gas flow rate used during the pyrolysis process also affects the formation of polycyclic aromatic hydrocarbons (PAHs) in biochar. Madej et al. (Madej et al., 2016) noted that using a relatively high flow rate for the carrier gas (N_2) resulted in biochar with a lower PAH content (below 1.5 mg kg^{-1}) when using various types of biomass sources. The gas flow rate used also has an impact on the pore structure and SSA of biochar. Increasing the gas flow rate helps with the emission of volatile substances, which promotes pore formation, and this increases SSA and total pore volume (Liu et al., 2018). However, if the carrier gas flow rate is too high, it may lower the temperature of the biochar, which leads to a reduction in the reaction rate and less volatile substances being released, hence a decrease in SSA and total pore volume (Lua et al., 2006). Therefore, it is recommended that a moderate gas flow rate (50–150 mL/min) is used during pyrolysis in practical operations. It should also be noted that an extremely high gas flow rate can reduce the biochar yield and pore volume (Bouchelta et al., 2012); therefore, it is advisable to maintain a moderate gas flow rate of 150 to 300 mL/min to obtain optimal characteristics.

3.6.6. Impact of residence time

Residence time refers to the period of time that the feedstock is exposed to a high temperature during the pyrolysis process (Chen et al., 2022). It is an important operational parameter in the biochar preparation process. The effect this has on the biochar that is produced is summarised in Table 3.8. This indicates that a balance between pyrolysis temperature and kiln residence time is necessary to ensure that carbonisation and biochar are stable (Cross and Sohi, 2013).

3.6.6.1. Effect of residence time on biochar yield. Residence time affects the yield of biochar to a certain extent. Liang et al. (Liang et al., 2016) confirmed this by demonstrating that increasing the residence time at a lower temperature (300°C) reduces the biochar yield; increasing it at a temperature exceeding 600°C has almost no effect on the biochar yield. The temperature employed during pyrolysis is a primary variable that affects residence time, as a higher temperature generally results in a shorter residence time. However, other factors can also affect residence time, such as feedstock type, particle size and heating rate. Due to the interactions with temperature, it is challenging to draw a specific conclusion on the singular impact that residence time has on the biochar

Table 3.8
Effect of residence time on biochar.

Feedstock	Reaction conditions	Yield (%)	SSA (m^2/g)	Fixed C (%)	Ref
Pinus pinaster	T: 450 °C; RT: 15/30/60 min	35.3/30.55/32.56	—	—	(Fassinou et al., 2009)
	T: 750 °C; RT: 15/30/60 min;	16.77/17.87/20.35	—	—	
Pruning residues	T: 300/500 °C	55/36	6.1095/174.55	54.88/72.03	(Liang et al., 2016)
Rapeseed stem	T: 500 °C; HR: 20 °C/min; RT: 10–100 min	29.6–28.6	—	—	(Zhao et al., 2018)
Cow manure	T: 500 °C; HR: 10 °C/min; RT: 30/60/90 min	—	—	42.22/38.43/41.85	(Guo et al., 2021)
Wheat straw	T: 300 °C; RT: 30/60/120/	58.2–18.8	—	28.3/33.1/38.4/43.4/44.9/45.8	(Sun et al., 2017)
Free leaves of apricot tree	240/480/1440 min;	—	—	18.3/20.3/22.7/23.9/31.3/33.9	
Platane wood		—	—	25.4/34.3/43.4/50.5/59.5/62.1	
Empty fruit bunch	T: 442.15 °C; RT: 6/8/10/12 min	26.67/26.65/25.88/25.47	—	—	(Mohamed et al., 2013)
Radix isatidis	T: 300 °C & RT: 0/90/180 min; T: 500 °C&RT: 0/90/180 min; T: 700 °C&RT: 10/90/180min	—	2.32/3.78/4.45; 3.63/5.89/8.50; 5.57/8.68/11.8	46.67/45.49/45.23; 59.64/62.49/65.94; 66.73/72.37/70.47	(Yuan et al., 2014)
Rubber wood sawdust	T: 300 °C&RT: 60/180 min; T: 400 °C&RT: 60/180 min; T: 500 °C&RT: 60/180 min; T: 600 °C&RT: 60/180 min; T: 700 °C&RT: 60/180 min	—	1.8/1.9; 1.4/2.1; 2.2/2.0; 2.7/1.9; 2.3/5.5;	—	(Shaaban et al., 2014)
Rice husks	T: 500 °C; RT: 15–90 min; HR: 10 °C/min	40.58–38.06	—	64.17/64.9/65.59/66.85	(Abbas et al., 2018)
	T: 500 °C; RT: 60 min; GFR: 20–200 Sccm	39.14–36.09	—	65.59/64.59/62.28/60.67	
Saccharina japonica	T: 380 °C; RT: 1–5 min	87–59	—	—	(Kim, S.-S. et al., 2012)

Note: T: temperature. RT: residence time., HR: heating rate., GFR: gas flow rate. SSA: specific surface area.

yield (Anuar Sharuddin et al., 2016). Research indicates that a longer residence time may lead to a lower concentration of volatile organic compounds, which results in improved stability and water retention capacity of biochar (Bi et al., 2022). However, the benefits of increasing the residence time are limited since, at a certain point, the additional heating time may not improve the quality of the biochar further and could even lead to a decrease in quality due to an increase in the ash content (Guo et al., 2021).

3.6.6.2. Effect of residence time on the surface characteristics of biochar. Residence time can affect the SSA, micro- and macro-pore distribution, and morphology of biochar. Extending the residence time up to 2 h during the biochar production process has a positive impact on the SSA and pore volume, while a residence time that exceeds 2 h has an adverse effect (Kumar et al., 2020). Extending the residence time enhances feedstock reactions (Tripathi et al., 2016) and increases the SSA, total pore volume, and total organic carbon content of biochar (Yavari et al., 2017; Zhao et al., 2018). However, the yield of biochar prepared at a low temperature may decrease with a prolonged residence time. One study reported that when residence time increased from 1 to 5 min, the biochar yield produced from Sargassum horneri at 380°C decreased from 87 % to 59 % (Kim, S.-S. et al., 2012). Overall, the effect of residence time on the pyrolysis process is intertwined with biomass quality, pyrolysis temperature, heating rate and other parameters (Rangabhashiyam, 2019).

3.6.7. Summary

The yield and properties of biochar are influenced by multiple factors, including the moisture content of the feedstock, preprocessing methods, particle size, catalysts, gas type and flow rate, and residence time (Uddin et al., 2018). Precise control of moisture content has a profound impact on the yield and properties of biochar, as well as on the economic and environmental aspects of overall biomass energy production. Different preprocessing methods applied to the feedstock lead to varying effects, particularly recommending the use of dry biomass for enhancing biochar yield and conversion rates, especially for wet biomass. Moreover, the impact of catalyst types on biochar yield varies with different biomass types and warrants further in-depth investigation. Literature reports suggest that acidic catalysts generally increase the biochar yield and reduce tar formation, while alkaline catalysts tend to decrease the biochar yield (Akhtar et al., 2012). Therefore, optimising process parameters is essential for achieving optimal biochar yield. Additionally, the type of inert gas and its flow rate are crucial factors affecting biochar yield and properties. Although CO_2 shows promising results as an alternative gas, a balance is required in gas flow rate to achieve efficient and environmentally friendly biochar production, con-

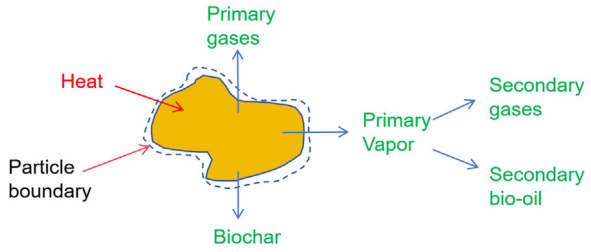

Fig. 3.10. Biomass conversion mechanism.

sidering volatile emissions, surface area, and pore volume. Lastly, residence time plays a significant role in the biochar preparation process, directly impacting pyrolysis progress and biochar properties. Precise control of residence time allows for process optimisation, resulting in biochar of superior quality and stability.

3.7. Biochar production mechanisms

Biomass is made up mainly of biopolymers such as lignin, cellulose and hemicellulose. Breaking and reorganizing the various chemical bonds of these polymers involves complex transformation pathways for producing biochar. Conversion of biomass to biochar mainly involves depolymerisation, fragmentation and char formation (Shan Ahamed et al., 2021). In general, biomass conversion reactions can be categorised into primary and secondary reactions. As biomass materials are heated, the chemical structure of the polymers within their residue matrix changes. Heating and rearrangement reactions release volatile compounds. After these primary reactions, some unstable, volatile compounds are further transformed (Collard and Blin, 2014).

The biomass particles are subjected to external heat and subsequently undergo several physical and chemical changes (Fig. 3.10). Depolymerisation of biomass by heat leads to the gradual breakdown of biomass constituents into smaller independent units. During the heat treatment, the extent of the polymerisation of biomass decreases, and some molecules become volatile components. The various monomers of the polymer are linked by covalent polymeric bonds. The fragmentation reaction further releases several non-condensable gases and a variety of small-chain organic compounds.

Biomass undergoes some degree of depolymerisation and bond breaking that leaves a solid residue known as biochar. The formation pathway is mainly inter- and intra-molecular reorganisation of the molecular structure, which results in a residue with a high thermal stability and filamentary structure (Zhang, B. et al., 2021). Biochar has a polycyclic aromatic structure, and the formation of benzene rings helps to stabilise biochar. The interaction between volatile pyrolysis gases and biochar during the formation of biochar should not be neglected. The secondary reaction of volatiles contributes to pore formation in biochar.

3.7.1. Primary conversion mechanisms of pyrolysis

Lignin, cellulose, and hemicellulose, commonly known as biopolymers, are the core ingredients in biomass. The conversion reaction of these compounds presents the foremost characteristics. The three pathways that break the various chemical bonds are explained below.

The solid residue left after the thermal heating of biomass is called char. The char has a polycyclic aromatic structure. The formation pathway is mainly inter- and intra-molecular reorganisation of the molecular structure, which results in higher thermal stability and a filamentary structure in biochar. The formation of benzene rings and the grouping of the rings are the main mechanisms in this pathway (Zeng, L. et al., 2023). The rearrangement results in the release of non-condensable gases and moisture from the biomass material.

The depolymerisation phenomenon in this pathway involves breaking the biopolymers (lignin, cellulose, and hemicellulose) down into separate units called monomers. The degree of polymerisation is reduced until the molecules formed become volatile. The molecules condense at room temperature and form a liquid fraction (Shao, L. et al., 2018). Fragmentation involves the polymer covalent bonds (Verziu et al., 2018). The linkages also occur between various monomers of the polymer. This pathway is responsible for releasing many incondensable gases and various small organic compounds that condense at room temperature.

3.7.2. Secondary conversion mechanisms of pyrolysis

Reaction temperature is important in the second conversion mechanism of biomass. When the temperature in the reactor is maintained at a high temperature, unstable, volatile compounds undergo further secondary reactions such as cracking or recombination. Cracking breaks down the volatile compounds further into lower molecular weight compounds. Recombination or condensation is the reverse process of cleavage and leads to the formation of higher molecular weight compounds. The re-formed compounds are difficult to volatilise and cleave again at normal temperatures, which leads to the production of more char.

3.7.3. Pyrolysis mechanisms of biomass components

Lignocellulosic biomass is the most abundant non-food biomass. It consists mainly of forestry and agricultural waste, such as wood chips and rice straw. Lignocellulosic biomass has three main components - cellulose, hemicellulose and lignin plus small amounts of extractives and ash. These three main components are unevenly distributed in the cell wall and serve as the skeleton, connecting material and hard solid, respectively.

Cellulose macromolecules regularly aggregate to form tough microfibres, which serve as the skeleton material of the cell wall, while the internal space is crowded with amorphous hemicellulose and lignin connecting materials. Cellulose is connected to hemicellulose or lignin molecules mainly by hydrogen bonding, whereas the connections between hemicellulose and lignin include both hydrogen and covalent bonds. Carbohydrates and lignin are tightly linked together in the lignin-carbohydrate complex, which results in residual carbohydrate or lignin fragments in the extracted lignin or hemicellulose samples. The content of cellulose, hemicellulose and lignin in biomass varies greatly depending on the type of biomass. The content can be as high as 40–60 % for cellulose, hemicellulose 15–30 % for hemicellulose, 10–25 % for lignin. Generally, during biomass pyrolysis, when the components of lignocellulosic materials such as cellulose, hemicellulose and lignin are heated to a certain temperature, reactions such as depolymerisation, fragmentation and cross-linking take place, which produce solid, liquid and gaseous products. Bio-oil and biochar are the main products, while hydrogen, carbon monoxide and carbon dioxide are by-products in the gaseous state. Some C1-C2 hydrocarbons are also included. During biomass pyrolysis, hemicellulose, cellulose and lignin decompose at different temperatures. Hemicellulose decomposes between 200°C and 320°C, cellulose decomposes between 320°C and 450°C, and lignin exists in a wide decomposition range between 150°C and 900°C.

The possible pyrolysis mechanism of cellulose is shown in Fig. 3.11. The mechanism of cellulose decomposition is determined by two reactions that reduce the degree of polymerisation: 1) Slow pyrolysis, which consists of the decomposition of cellulose with longer residence times and lower heating rate, and 2) Levoglucan is produced by fast pyrolysis, which involves rapid volatilisation at a high heating rate (Zong et al., 2020). In addition to producing the solid biochar product, levoglucan undergoes a dehydration process to produce hydroxymethylfurfural, which can be decomposed to produce liquid and gaseous products such as bio-oil and syngas. The specific reaction pathway for the formation of biochar is generally as follows. Cellulose is first depolymerised to form oligosaccharides, which are then cleaved through glycosidic bonds to form d-glucose. d-glucose is further rearranged intermolecularly to form levoglucan, which is dehydrated to form levoglucenone. Finally, levoglucenone can be re-generated into solid biochar through reactions such as aromatisation, condensation and polymerisation.

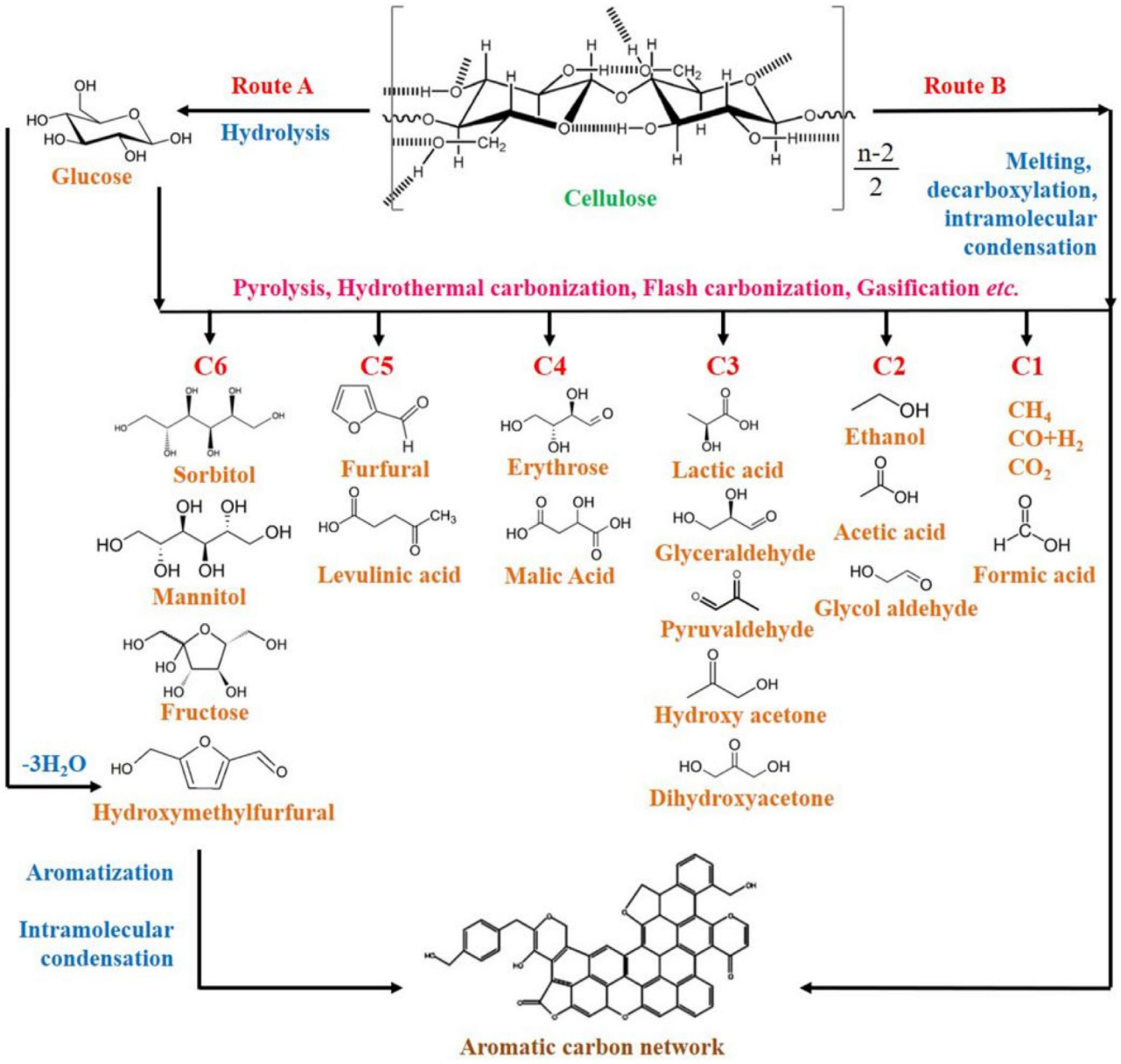

Fig. 3.11. The cellulose conversion mechanism (Qin et al., 2022).

The possible pyrolysis mechanism of hemicellulose is shown in Fig. 3.12. The decomposition mechanism of hemicellulose is similar to that of cellulose. The hemicellulose undergoes depolymerisation to form oligosaccharides. This can occur through a series of reactions including decarboxylation, intramolecular rearrangement, depolymerisation and aromatisation, which produces biochar or compounds that break down into syngas and bio-oil (Ma, Z. et al., 2019).

Unlike the decomposition mechanism of cellulose and hemicellulose, the lignin decomposition mechanism is complex. The proposed pyrolysis mechanism of the lignin model compound is shown in Fig. 3.13. Breaking the β-O-4 linkage of lignin generates free radicals (Yuan, J.-M. et al., 2022), which move to other molecules for chain propagation. These free radicals capture protons from other species, which results in the formation of decomposing compounds.

3.8. *Influence of reactor*

The properties of biochar depend on the type of feedstock and pyrolysis temperature; however, they are also linked to the type of reactor used. Typical reactors used in biochar production are shown in Table 3.9 and Fig. 3.14. The reactor selected for biochar production is generally closely related to the heating method. Although a wide variety of heating methods exist, as described above, that are capable of producing high quality biochar, some of these methods are limited because of the design and manufacture of the reactor and cannot be used to prepare biochar on a large scale. Small scale biochar producers can be used to customize high quality biochar by varying the reaction conditions. In contrast, large-scale, continuous production of biochar is essential for processing large quantities of biomass and is also necessary to ensure viable production of biochar.

There are various types of reactors capable of producing biochar, but pyrolysis reactors are generally used. They can be categorised as fast and slow pyrolysis reactors based on the rate of heating and the time the pyrolysis vapour remains in the reactor. The main product of a slow pyrolysis reactor is biochar, while the main product of a fast pyrolysis reactor is bio-oil. The by-product of fast pyrolysis is biochar, but it is not carbonised as thoroughly as biochar produced by slow pyrolysis. In addition, fast pyrolysis has certain requirements in terms of the

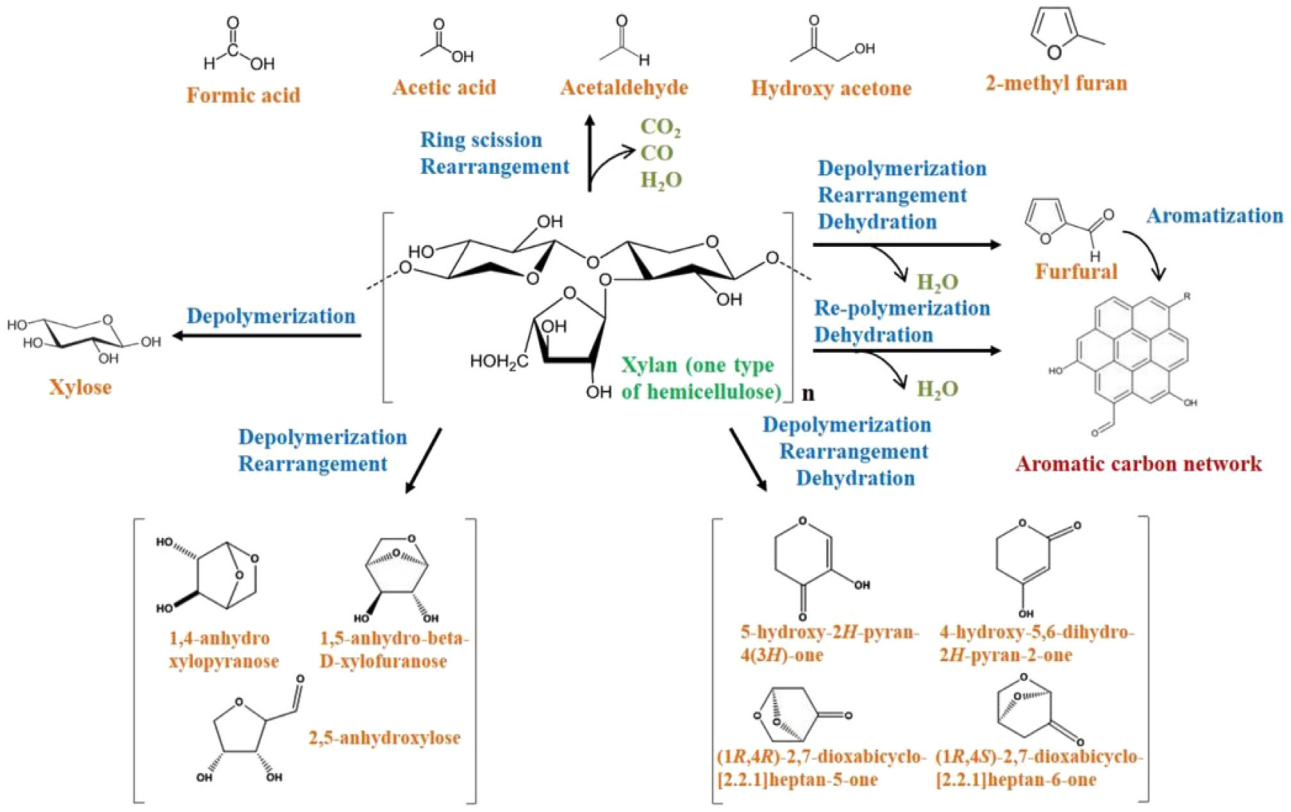

Fig. 3.12. The hemicellulose conversion mechanism (Qin et al., 2022).

Table 3.9
Typical reactors used for biochar production.

Reactor type	Temperature range (°C)	Capacity	Ref
Muffle furnace	500–600	300 *g*	(Januševičius et al., 2022)
Vacuum tube furnace	300–600	30 *g*	(Yadav et al., 2016)
Programmable batch reactor	200–700	3 *g*	(Zhu, X. et al., 2018)
Microwave reactor	250–450	10 *g*	(Li, X. et al., 2022)
Gasification reactor	850	10 kg	(Dissanayake et al., 2020)
Hydrothermal carbonization reactor	200–300	10 *g*	(Zhu, X. et al., 2023)
Auger reactor	425–575	600 *g*	(Lakshman et al., 2021)
Drum kiln	350–500	40 kg	(Sangsuk et al., 2020)
Fluidised bed reactor	450–850	400 *g*	(Liu, Y. et al., 2020)
Fixed bed reactor	450–600	100 *g*	(Yue et al., 2016)
Earthen kiln	400–600	1 t	(Paz-Ferreiro et al., 2017)
Rotary kiln	400–600	600 kg	(Khodaei et al., 2024)
Spouted bed reactor	400–600	20 *g*	(Niksiar and Nasernejad, 2017)

granularity of the raw material. For example, the diameter of the raw material particles should be less than 2 mm. With slow pyrolysis, the shape of the raw material is less important, and larger pieces of wood can be used.

Slow pyrolysis reactors are generally not able to produce continuously, as the reaction time is very long, which limits the rate at which biochar is produced. Fast pyrolysis reactors are generally equipped with a continuous feeder, which allows for continuous pyrolysis of biomass, so large amounts can be processed. There are various classifications of biomass pyrolysis, based on different heating mechanisms, such as slow pyrolysis, fast pyrolysis, microwave pyrolysis and hydrothermal carbonisation. Reactors can also be classified as batch reactors or continuous reactors, depending on the mode of operation. Other classifications are vacuum reactor, atmospheric reactor and pressurised reactor, if classified according to the pressure under which the equipment operates. Stationary and mobile rector categories are also used when classifying reactors according to the movability of the reaction bed. Although the type of pyrolysis reactor and its operating conditions largely determine the quality of the final target product, the quality of the product is determined by a combination of different conditions.

3.8.1. Muffle and tube furnace

The muffle and tube furnace type of reactor is widely used in laboratories to produce biochar for scientific research due to its simplicity of operation and programmable temperature increase. However, the capacity of the muffle and tube furnace is relatively small, usually ranging from a few grams to several hundred grams. They are typical stationery and batch reactors with limited biomass capacity. They allow for controlled experimental conditions and good consistency between different batches of biochar produced, which means that the required quality of the biochar can be ensured. This facilitates the exploration of biochar properties and applications. As the capacity of the reactor increases,

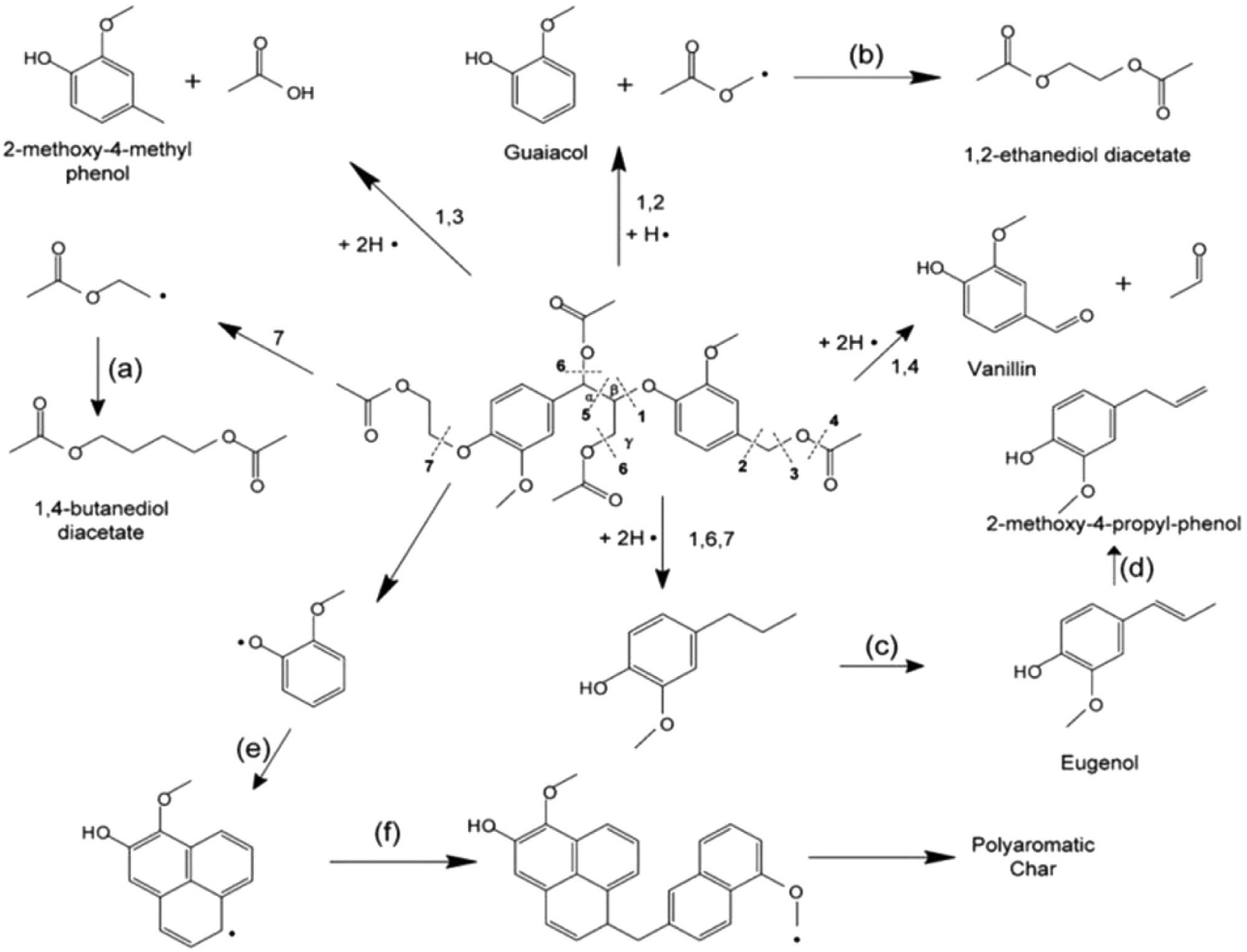

Fig. 3.13. The proposed pyrolysis mechanism of the lignin model compound (Chu et al., 2013).

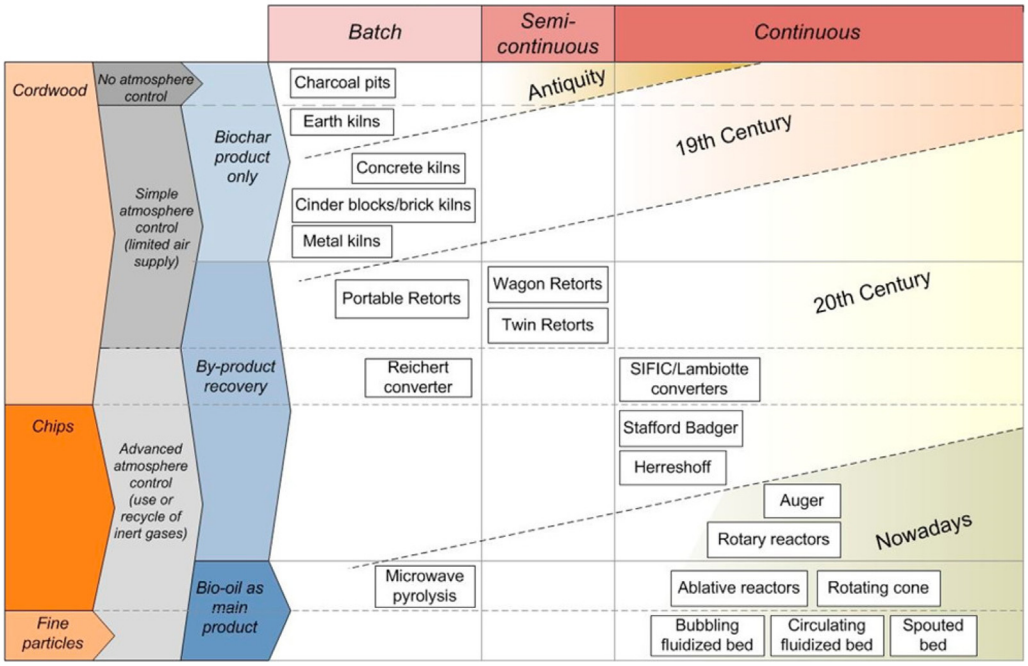

Fig. 3.14. Historical developments of pyrolysis reactors (Garcia-Nunez et al., 2017).

biochar properties gradually become differentiated, even when using the same conditions, which may be due to the increase in capacity affecting the heat and mass transfer of the biomass feedstock.

3.8.2. Microwave reactor

The heating principle of the microwave reactor is different from that of the tube furnace. A tube furnace heats its contents primarily through thermal radiation and convection, while the microwave heat source relies on the interaction between microwaves and the feedstock, such as Joule heating and induction heating (Suresh et al., 2021). Microwaves can act directly on the raw material, thus reducing the heat lost during the transfer process. However, it is more difficult to regulate the temperature by modulating the generation of microwaves compared to temperature regulation in resistance heating. The size of the microwave reactor is limited by the electrical power available and the microwave frequency. In pyrolysis, the microwave frequency generally chosen is 2.45 GHz. Although, the frequency can be adjusted, this will increase the difficulty and cost of manufacturing microwave reactors. Also, electrical power is limited by the installation site of the reactor. Therefore, the capacity of microwave pyrolysis reactors is also limited, usually to less than 1 kg (Luo, H. et al., 2021). The specific heating method of the microwave heating reactor depends on the characteristics of the raw materials. Wave-absorbing materials can be added to the microwave pyrolysis reactor to enhance microwave pyrolysis. Although microwave reactors have widely been used to study biomass pyrolysis, the scale of microwave reactors is still limited due to the high cost of design and manufacturing. In general, microwave reactors can accelerate biomass cracking as microwaves can act directly on biomass particles and so further enrich the pore structure of biochar.

3.8.3. Hydrothermal carbonization reactor

With the hydrothermal carbonisation reactor, the cracking reaction of the feedstock occurs in the liquid phase, which is different from what happens in a typical gas-solid phase reactor such as a muffle furnace. Although the heat transfer method also involves feedstock cracking through heat conduction, the heat exchange between the reactor and the feedstock inside the reactor is mainly realised through the liquid medium. In the process of heating, the liquid in the hydrothermal carbonisation reactor is heated to produce steam, while the pressure inside the reactor is further increased due to the gas generated by pyrolysis. Some of the organic matter is dissolved in the liquid medium, while the rest exists as solids that form a lignite-like product (Xue et al., 2022). The capacity of the hydrothermal carbonisation reactor is also small due to the limited heat transfer capacity. Also, considering the reaction pressure, higher requirements are needed in manufacturing, thus limiting its larger scale up. The high pressure also helps decompose the feedstock further. In addition, the lower temperature of hydrothermal carbonisation compared to conventional pyrolysis results in relatively suppressed cracking of the feedstock, which results in a better biochar yield. At the same time, the milder reaction conditions result in richer functional groups on the surface of biochar. The pore structure of biochar is related to the reaction temperature and pressure. In general, the pores of biochar prepared using hydrothermal reactors are smaller than those of biochar prepared by pyrolysis.

These types of reactors include the gasification reactor, auger reactor, fluidised bed reactor, spouted bed, and rotary kiln. They can be designed to different biochar production capacity requirements, depending on the application (Porat et al., 2022). In the laboratory, these units generally have a capacity of several kg, while commercial units can have a capacity of several tonnes per day. There is a difference in the heat and mass transfer achieved by reactors of the same type but with different capacity levels, even though the structures are similar. Therefore, the properties and yield of biochar produced by the same type of reactor may be different with different capacities. Many different types of reactors can be used for biochar production, each having a different capacity, so maintaining consistency in biochar quality is sometimes difficult. Furthermore, the physiochemical properties of biochar produced by different equipment may vary.

3.9. Pilot and large-scale production of biochar

Although biochar is produced using different methods, large-scale production is still limited by reactor design, fabrication, and investment. Typical reactors suitable for large-scale biochar production include fixed beds, earthen kilns, rotary kilns, fluidised beds, auger reactors and spouted beds. (Fig. 3.15 and Fig. 3.16). Different scales of production can be achieved by adjusting the capacity of the reactor. The choice of reactor for large-scale biochar production mainly depends on the type of biomass and the availability of biomass. Although these reactors are used in large-scale biochar production, they are employed in different scenarios and are associated with different drawbacks.

3.9.1. Earthen kiln

As a traditional biochar production facility, the earthen kiln has a long history and is still used in some developing countries. There are three types of earthen kilns: vertical, horizontal and improved kilns. Earthen kilns are simple in structure, have a low level of technical difficulty and low investment cost, are simple to operate and can be easily constructed in places where biomass feedstock is abundant. The capacity of an earthen kiln can be adjusted according to the source of the biomass used and the biochar required. The produced biochar has a high heating value and is widely used as a solid fuel to replace coal. The biochar yield of an earthen kiln is generally 20 % lower since some of the biomass is burned as fuel to supply thermal energy to the kiln during the process start-up and throughout the pyrolysis process. Earthen kilns can also release smoke and some organic matter into the atmosphere. This is why earthen kilns are gradually being phased out in some regions. Earthen kilns are generally used to process larger wood chips and are less effective in carbonising biomass in granular form. In addition, earthen kilns offer poor control over the carbonisation conditions, and it is difficult to ensure a consistent quality of biochar across batches. A long residence time also limits the scale of production offered by earthen kilns.

3.9.2. Fixed bed reactor

The fixed bed reactor is commonly used for the pyrolysis of biomass and the preparation of biochar due to its simplicity of fabrication, low cost and ease of operation. It is widely used in laboratories; however, it is also suitable for small-scale biochar production operations. Nevertheless, fixed bed reactors do have certain limitations, as they can only be operated in batch mode, which restricts the scale of biochar production. These reactors can be categorised into externally heated fixed-bed pyrolytic carbonisation furnaces and internally combusted fixed-bed pyrolytic carbonisation furnaces based on the heat source. The externally heated fixed-bed pyrolysis carbonisation furnace mainly consists of two parts: the heating furnace and the pyrolysis reactor, and the externally heated furnace body provides the energy required for cracking to the pyrolysis reactor. The externally heated fixed-bed pyrolysis carbonisation furnace can regulate the external heat source, which allows for precise temperature control and, hence, better control of the quality of biochar. However, the heat from the furnace is transferred from outside to inside, and the temperature in the centre of the reactor is generally lower than at the reactor wall. This means that the biomass particles may not be heated uniformly in the reactor. The heat and mass transfer performance of the reaction system is also limited, which results in poor energy efficiency. Internal combustion fixed-bed pyrolytic carbonisation furnaces rely on the combustion of part of the feedstock to supply heat. The heat provided *via* conduction, convection and radiation has a high thermal efficiency. However, the pyrolysis reaction temperature of the internal combustion fixed bed is not easy to control.

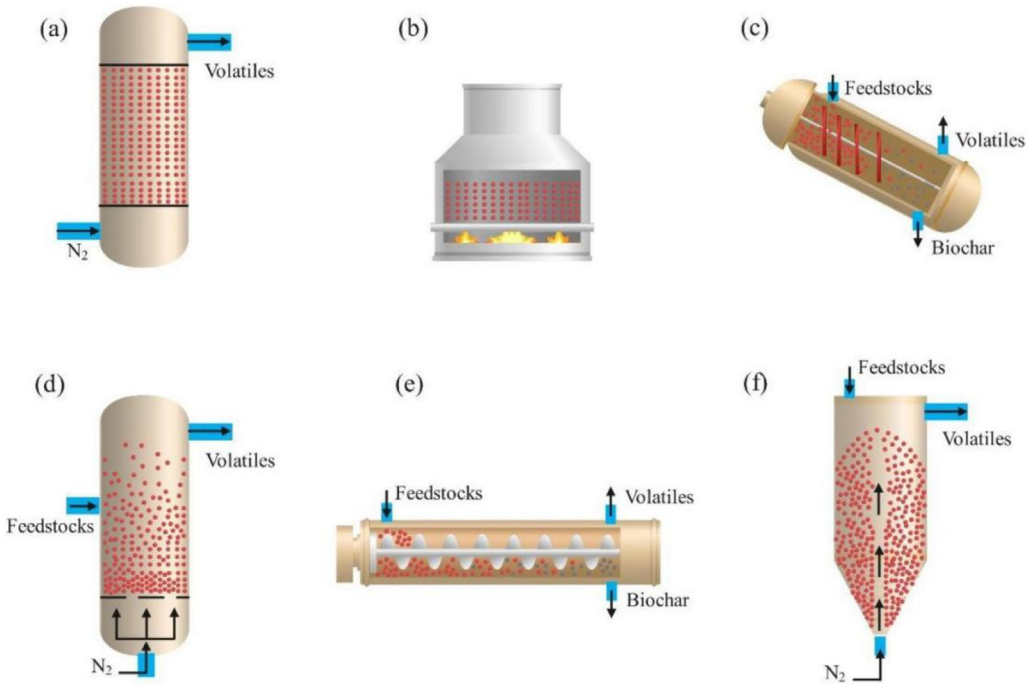

Fig. 3.15. Typical biochar production reactors: (a) fixed bed, (b) earthen kiln, (c) rotary kiln, (d) fluidised bed, (e) auger reactor, and (f) spouted bed (Zhu, X. et al., 2022).

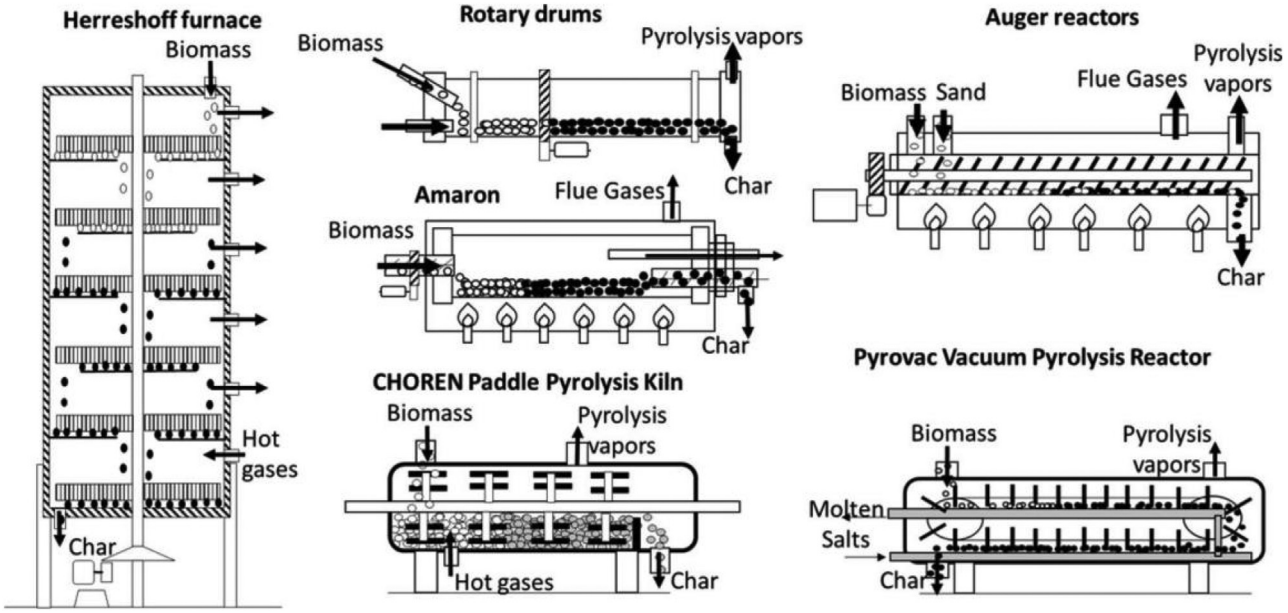

Fig. 3.16. Schematics of typical reactors used to process of biomass (Garcia-Nunez et al., 2017).

3.9.3. Rotary kiln

The design of the rotary kiln has been optimised to serve as a reliable reactor type for biochar production (Khodaei et al., 2024). The residence time of biomass in a reactor can be adjusted by adjusting the angle and speed of the rotary kiln. The structure of the rotary kiln is simple: it consists mainly of a round-centre steel tube and a sequence of radial steel fins. By rotating the drum, biochar and gaseous products can be discharged by two outlets at the end of the reactor. The rotary reactor is simple to operate and can be designed for direct and indirect heating through combustion, but the thermal efficiency needs to be improved further. The required biochar and bio-oil yields can be realised by adjusting the operating parameters of the rotary kiln. The rotary kiln can also be designed to have the requisite capacity to suit large-scale biochar production.

3.9.4. Fluidized bed reactor

Fluidised bed reactors are commonly used in biomass pyrolysis. This reactor mainly utilises convection and conduction to achieve heat transfer between the heat carrier (e.g. sand) and the biomass particles. The fluidised bed reaction system has a high heat transfer rate and gas-solid uniformity, while the continuous operation of the fluidised bed makes large-scale processing of biomass and large-scale production of biochar a reality. The raw material particles in a fluidised bed should generally be less than 2 mm, to ensure better heat transfer (Darweesh and

Weis, 2024). Fluidised bed reactors are mainly used for the production of bio-oil, with yields reaching 65 %. As a by-product of the pyrolysis of biomass in the fluidised bed, biochar can be entrained by the gas flow and leave the reaction area; gas-solid separation can then be realised under the action of a cyclone separator. The biochar yield varies within 10–40 % depending on the feedstock and experimental conditions. In addition, fluidised beds can be designed as self-heating reactors if needed, using pyrolysis gas and biochar as fuel for combustion to provide heat for the entire reaction system. Circulating fluidised beds have been developed following the design of fluidised bed reactors. The difference between the circulating fluidised beds and fluidised beds is mainly that the heat carrier obtained from pyrolysis is fed directly to the bottom of the fluidised bed reactor together with biochar, then the heat carrier is heated with the heat from biochar combustion, and the heat carrier is returned to the fluidised bed to provide the heat required for pyrolysis. High temperature flue gas is used as the fluidisation medium; however, the temperature of this flue gas needs to be controlled to below 600 ˚C to avoid overheating. Fluidised bed reactors are widely used in biomass pyrolysis due to their advantages, which include good temperature control, simple gas-solid separation, and continuous production. They can be designed to have a capacity ranging from tens of kg per hour to hundreds of tons per day, depending on the supply of raw materials. Fluidised bed reactors also have some disadvantages, however. The extensive use of inert gases in these reactors results in dilution of the combustible gas component of the pyrolysis syngas. A higher gas velocity leads to the wearing of the heat carrier and biochar, while complex gas-solid hydrodynamic phenomena are present. In addition, these reactors are associated with high investment costs in terms of design and operation.

3.9.5. Auger reactor

The design of the auger reactor is more complicated than the earthen kiln; however, it is associated with better heat transfer efficiency. Also, auger reactors are comparatively easier to operate. Auger reactors generally have a hopper or feed screw, which gradually feeds the biomass into the pyrolysis section of the reactor. The products gradually move out of the reaction area with the rotation of a screw. In an auger reactor, the screw feed rate can be adjusted to control the residence time of the biochar and pyrolysis vapour in the reactor, enabling both slow and fast pyrolysis. Heat carriers such as hot sand, steel or ceramic balls can also be used in the auger reactor to achieve better heat transfer to the biomass. The heat carriers and biochar are discharged from the reactor by gravity. Auger reactors are similar to fluidised bed reactors in that the yield of biochar is typically 10–30 %, depending on the feedstock and operating conditions. The auger reactor also allows for continuous production and, therefore, can process a large quantity of biochar.

3.9.6. Spouted bed

Spouted bed reactors are similar to fluidised bed reactors in terms of structure and layout, boasting a high heat transfer rate and gas-solid contact. The main product of the spouted bed reactor is also bio-oil, while biochar is only a by-product. Unlike fluidised beds, which require high granularity of biomass feedstock, spouted beds can handle irregular particles. With the traditional spouted bed, the central spouted zone and the annular fluidisation zone can be separated by optimising the structure of the spouted bed. This prevents mutual interference between the spouted zone and the fluidisation zone and maintains the stability of the gas and solid state during the spouted process. By optimising the structure of the spouted bed, gas-solid slip velocity increases, which increases the gas-solid time and enhances heat and mass transfer, hence improving the effect of biomass pyrolysis. It is also easier to control the solid-phase retention time and increase the carbon conversion rate, which results in a lower biochar yield. Spouted beds can be further developed into circulating spouted beds, enabling in-situ heat supply.

3.9.7. Summary of reactor selection

The selection of a scale-up pyrolysis reactor depends on feedstock, operating conditions and the process viability. Finding a dedicated sustainable reactor design solution for most scenarios is difficult, as there is flexibility in terms of selecting a reactor for large-scale production of biochar. In general, commercial production of biochar demands optimum yield, which can adversely affect the quality of biochar. In addition, costs and thermal efficiency are key design factors in developing pyrolysis reactors. These reactors and industrial plants show different advantages and features. Generally, the most suitable reactor will be selected based on different application scenarios, reaction conditions and product requirements.

3.10. Conclusion

Biochar has demonstrated unique application potential in various fields, including environmental management, energy production, and soil amendment. This article provides a comprehensive analysis of biochar production technologies, key factors influencing its characteristics, and its performance under different application contexts, with a particular focus on the significant role of reactor design in the biochar production process.

(1) The selection of feedstock is decisive in determining the final properties of biochar. Different types of biomass feedstock, such as woody materials, herbaceous plants, agricultural waste, and animal manure, lead to significant differences in the porosity, SSA, and chemical reactivity of the produced biochar due to their distinct chemical compositions and structural characteristics. The introduction of additives and doping elements, such as metal oxides, carbon nanomaterials, and elements like nitrogen, sulphur, and phosphorus, can further modulate the electrical conductivity and chemical activity of biochar, enhancing its performance in catalysis and energy storage. Additionally, the moisture content, particle size, and pre-treatment methods of the raw materials significantly impact the properties of the final biochar.
(2) Biochar production is influenced by thermochemical treatment methods, such as slow pyrolysis, fast pyrolysis, microwave pyrolysis, vacuum pyrolysis, hydrothermal carbonisation and so on. Controlling parameters such as pyrolysis temperature, heating rate, gas flow rate and reaction time significantly affect the yield, carbon content, pore structure, and surface chemical properties of biochar. Pyrolysis temperature is a key factor in adjusting the characteristics of biochar, directly influencing its stability and adsorption capacity.
(3) Pressure is an important parameter in the pyrolysis process, and it significantly impacts the yield and fixed carbon content of biochar. Studies have shown that increasing pressure can enhance the carbon retention rate and the yield of pyrolysis gases, but it may also lead to a reduction in the specific surface area of biochar. Furthermore, the choice of the pyrolysis method is crucial for the yield and characteristics of biochar, as different methods, with their unique operational conditions and reaction kinetics, result in variations in the quality and application potential of biochar products.
(4) The design of the reactor is equally crucial for the quality and yield of biochar. Different reactor types, such as fixed beds, fluidised beds, rotary kilns, and screw reactors, have a significant impact on the physicochemical properties of biochar due to their distinct operational conditions and reaction kinetics. The design of reactors must consider the continuous production capacity and scalability requirements for biochar, ensuring the consistency and reproducibility of biochar products.

In conclusion, as a versatile material, biochar holds broad application prospects in various fields. An in-depth exploration of the correlation between the chemical and physical structure of biochar and its environmental and energy applications, along with the optimisation of

biochar production conditions to enhance its performance in soil amendment, pollutant removal, and energy storage, is essential. For the commercialisation and large-scale production of biochar, a comprehensive consideration of cost-effectiveness, sustainability, and potential environmental impact is necessary to support the achievement of sustainable development goals.

4. Biochar activation

Activation increases the surface area, porosity, and adsorption capacity, introduces functional groups, improves thermal stability and durability, and supports beneficial microbial activity, making it a versatile and valuable material. As shown in Fig. 4.1, the process of preparing porous activated carbon (PAC) from biomass mainly includes three paths. The first path is that PAC can be prepared through the biomass one-step pyrolysis activation method. The second path is that biomass is first carbonized and then activated to prepare PAC through a two-step process. The third path is biomass conversion to liquid to produce viscous heavy bio-oil containing high carbon content, which is difficult for direct applications, making it an ideal raw precursor for preparing carbon materials. The heavy oil is then used to prepare PAC through one or two-step methods. Carbon materials can be activated via physical, chemical and physicochemical techniques.

4.1. Physical activation

Physical activation, also known as gaseous activation, is a technique used to develop activated biochar by employing oxidizing agents (Chen et al., 2025). Typical oxidizing agents include steam, CO_2, air, etc. The process involves heating biochar under these gaseous conditions, typically at temperatures exceeding 700°C. These oxidizing agents infiltrate the internal structure of biochar and gasify the carbon atoms, leading to the generation and expansion of pores (Dalai and Azargohar, 2007). Such activation conditions yield activated biochar with a high specific surface area and abundant pore volume. The parameters of activation processes discussed in typical studies are shown in Table 4.1. These activated biochar products, as prepared, hold significant potential for a wide range of applications (Jia et al., 2024; Sajjadi et al., 2019; Yuan et al., 2024).

Physical activation offers a more environmentally friendly method of activation compared to the commonly used chemical activation technique (Ajien et al., 2023; Bushra and Remya, 2020; Li, S. et al., 2022). The chemical activation method relies on the application of chemical agents, a topic that will be thoroughly discussed in the next section. In contrast, physical activation can avoid the environmental challenges associated with these chemical agents, as evidenced by certain life-cycle assessments of commercial-scale physical activation production (Azzi et al., 2019; Wang, Junyao et al., 2023). This advantage is also a key factor contributing to the considerable research attention that physical activation is currently receiving.

4.1.1. Role of activation agent

Steam and CO_2 are frequently employed in the physical activation of biochar. They are considered the most commonly used activation agents due to their comparatively lower costs and the ease of controlling the oxidation process (Contescu et al., 2018). CO_2 facilitates the formation of micropores, while steam promotes a wider range of pore sizes, leading to an increase in both micropores and mesopores (Molina-Sabio, M et al., 1996; Sun and Chun Jiang, 2010; Yuan, Xiangzhou et al., 2023).

Steam activation uses steam as an activation agent, and the process typically involves a series of partial gasification processes of carbon-rich materials (Sajjadi et al., 2019). The chemical reaction of steam activation was expressed as Eq. 4.1 and 4.2 (Tan et al., 2017). During the partial gasification process, some carbon molecules on the surface of biochar are exposed and react with water molecules, resulting in the elimination of volatile matter ($C_xH_yO_z$) from the structure, together with the formation of new surface oxides (C(O)) on the surface of biochar (Tan et al., 2017). At the same time, some carbon molecules are exposed to steam, converting into CO and H_2. In this series of steam activation reactions, owing to the removal of uncarbonized biomass or trapped products, a large number of new pores are generated, while simultaneously enlarging the existing pores (Santos et al., 2015). At the same time, the number of aromatic compounds increases, accompanied by an increase in surface oxygen-containing functional groups (Sizmur, Tom et al., 2017).

$$C+H_2O \leftrightarrow CO+H_2, \Delta H = +117 kJ/mol \quad \text{(Eq. (4.1))}$$

$$CO+H_2O \leftrightarrow CO_2+H_2, \Delta H = +41 kJ/mol \quad \text{(Eq. (4.2))}$$

The partial gasification of biochar by CO_2 gas typically occurs through the reaction of CO_2 with the amorphous carbon in the biochar, producing C(O) chemical moieties and CO gases (Bushra and Remya, 2020). The process follows Boudouard's reaction, as described in

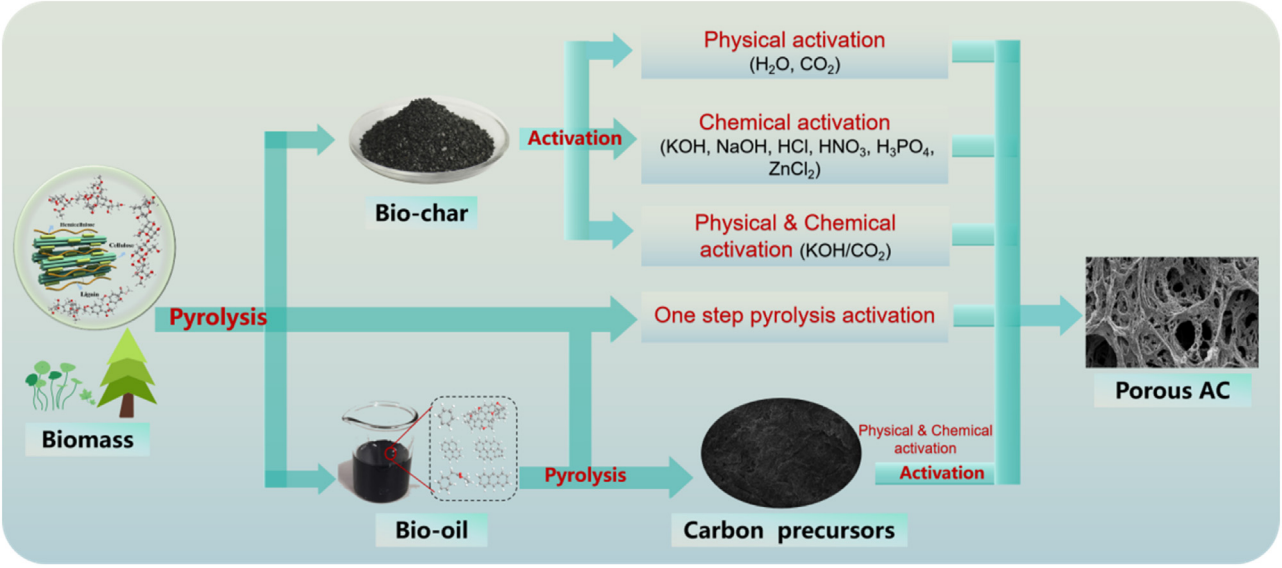

Fig. 4.1. Three key methods in preparing porous carbon materials from biomass.

Table 4.1
Physical activation of biochar from various feedstock under different activation conditions.

Precursor	Agent	Gas flow rate (mL/min)	Ramping rate (°C/min)	Temperature (°C)	Holding time (h)	Ref
α-Cellulose	Steam, CO_2, steam/CO_2	100	5	700, 800	1	(Ming et al., 2023)
Wood panel	CO_2/N_2	3000	–	750, 850, 950	–	(Hachicha et al., 2023)
Corncobs/Coconut shells/Walnut husks/Pistachio husks	CO_2	167	–	800	0.5, 1	(Januszewicz et al., 2023)
Sewage sludge	Steam, CO_2	300	–	650, 800, 950	0.5, 1	(Deng, W. et al., 2023)
Miscanthus straw	CO_2	100	–	800, 850, 900	1.5	(C et al., 2023)
	Steam	15 mg/h	–	900	1	
Microcrystalline cellulose	CO_2	20	10	600	1, 3, 16	(Biti et al., 2023)
Argan shells	CO_2	500	15	900	1.5, 2, 2.5	(Afailal et al., 2023)
Coffee grounds	CO_2	150–250	5	600–800	1–2	(Mukherjee et al., 2022)
Palm oil residues	CO_2	12	10	900	6.5–18.83	(Moliner et al., 2022)
Mantis shrimp shells	CO_2	250	5	600, 650, 700, 750	1	(Ding et al., 2021)
Light yard waste	steam	–	10	650, 750, 850	1	(Xu, Z. et al., 2021)
	CO_2	–	10	650, 750, 850	1	

Eq. 4.3 (Cho et al., 2015). During this process, C(O) will be desorbed from the porous surface of biochar, enabling further development of the existing porous structure. This phenomenon is also a primary reason for the increase in micropores caused by CO_2 activation. As the process progresses, CO gas may be absorbed by the carbon active sites on the surface of biochar, thus slowing down the partial gasification caused by CO_2 (Sajjadi et al., 2019).

$$C + CO_2 \rightarrow 2CO, \Delta H = +172.47 kJ/mol \quad \text{(Eq. (4.3))}$$

Simultaneously, there has been a common practice of comparing the activation processes of biochar using steam and CO_2. Carbonized cellulose has been subjected to activation using steam, CO_2, or a combination of both. The findings indicate that employing CO_2 as the activation agent can result in higher yields. The activation process using steam induces greater weight loss, potentially leading to enhanced efficiency in oxidizing the aliphatic structures within the activated biochar, thereby further enhancing the performance of the desired products (Ming et al., 2023). The physical activation of carbonized sewage sludge was carried out using steam and CO_2. Due to the higher diffusion coefficient of CO_2, a higher rate of activation was observed using CO_2 (Deng, W. et al., 2023). From the perspective of the performance of obtained activated biochar, carbons derived from Miscanthus biochar are effective for the adsorption and separation of NO. In the production of samples using physical activation processes, steam has been demonstrated to exhibit stronger reactivity compared to CO_2 (Díaz-Maroto et al., 2023). Alternatively, other oxidizing gases, such as air or ozone, can be used as in physical activation. These agents are effective in creating surface oxides on biochar; however, the more complex mechanisms involved require careful selection in practical applications (Smith, 2011; Suliman et al., 2016).

It must be acknowledged that existing research has indicated that physical activation processes using different activation agents may weaken the stability of activated biochar (Xu, Z. et al., 2021), particularly in terms of chemical oxidation resistance, thereby potentially impacting its practical performance adversely.

4.1.2. Impact of activation temperature

Activation temperature is an essential parameter in the physical activation process, directly impacting the properties of the activated biochar produced. Previous studies have demonstrated the significant role of activation temperature in enhancing the specific surface area and total volume of the final products (Zhang et al., 2014). At excessively low activation temperatures, the microspore surface may not be discernible, as the formation of new pores cannot be completed due to insufficient activation temperatures. Conversely, excessively high activation temperatures may result in a lower carbon yield, making the development process less economical. Hence, selecting an appropriate activation temperature is crucial for producing activated biochar tailored to specific applications.

Consequently, the link between activation temperature and the properties of the prepared samples has been researched well. In the physical activation treatment of wood panel-derived biochar, activation temperatures as high as 950°C have been employed. Such an optimal activation temperature facilitated the development of samples with the best textural properties reported in the study: 866 m^2/g specific surface area, 0.411 cm^3/g total pore volume, 0.272 cm^3/g micropore volume, and 0.139 cm^3/g mesopore volume (Hachicha et al., 2023). In the development of activated biochar derived from mantis shrimp shells, various activation temperatures have been explored. The results demonstrated that the smallest specific surface area and micropore volume (i.e. 172.4 m^2/g and 0.023 cm^3/g, respectively) were obtained at the lowest activation temperature of 600°C. The optimum values for these two textural properties (i.e. 484.5 m^2/g and 0.291 cm^3/g, respectively) were achieved at an activation temperature of 700°C. In this study, it was demonstrated that the reaction intensity between the carbon and the activation agent was slow, while increasing the temperature accelerated the rates of reaction and pyrolysis. Notably, further increasing the activation temperature (raised to 750°C in this study) did not result in a further increase in specific surface area. However, both the micropore volume and proportion could be further enhanced (Ding et al., 2021). In the optimization of the physical activation process using response surface methodology (RSM), activation temperature is frequently selected as a key independent variable. Its impact on specific surface area and carbon yield is deemed essential (Mukherjee et al., 2022). Higher specific surface area and increased carbon yield are crucial for ensuring the effectiveness and economic viability of the activated biochar development process. Therefore, selecting the appropriate activation temperature is essential for optimizing the process.

Lower activation temperatures result in higher carbon yields but may lead to poorer textural properties; conversely, higher activation temper-

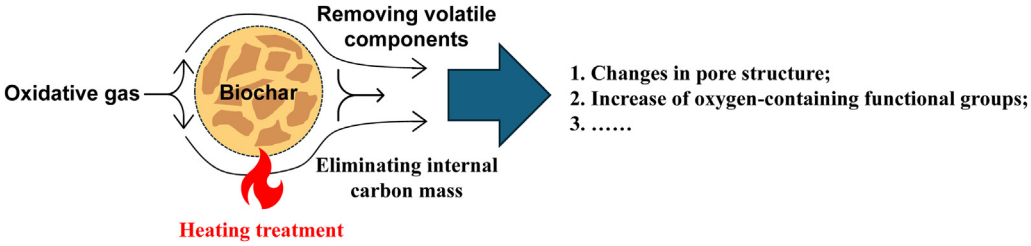

Fig. 4.2. Schematic diagram of mechanism and effect of physical activation method (Sangon et al., 2018).

atures can yield higher specific surface areas and pore volumes but at the expense of lower yields. Considering these trade-offs, target-driven process optimization is often relied upon when selecting an appropriate activation temperature.

4.1.3. Impact of activation time

The application of an appropriate holding time in the activation process can affect the overall extent of burn-off. Sufficient holding time ensures the full reaction between biochar and activation agents under high-temperature conditions. However, excessively long activation times will inevitably lead to a decrease in carbon yield. Therefore, considering the varied characteristics of the treated biochar, selecting an appropriate holding time for activation treatment is also of significant importance.

In the physical activation treatment of microcrystalline cellulose-derived biochar, an experimentally determined burn-off condition of 40 % was observed, with the longest holding time of 24 hours. Burn-off conditions ranging from 10 to 30 % have been achieved, with holding times ranging from 1 to 16 hours. This represents a relatively long activation time, which is not commonly employed in research (Biti et al., 2023). Palm oil residues have also been converted into biochar, where the preparation and activation processes of activated biochar involve the utilization of holding time as a crucial parameter to achieve varying degrees of burn-off. In this study, activation times of up to 19 hours were examined. With activation times of 6.5 and 19 hours, the burn-off rates were measured at 23.13 and 39.57 %, respectively. Moreover, longer activation times have been demonstrated to produce samples with higher specific surface areas and total pore volumes, resulting in enhanced performance in practical applications (as reported in this study, improved CO_2 adsorption performance) (Moliner et al., 2022). The more common activation temperatures typically range between 0.5 and 2.5 hours (Januszewicz et al., 2023). Within this activation time range, it is typically ensured that there is sufficient reaction to guarantee the product possesses a satisfactory specific surface area and total pore volume while still maintaining a reasonable yield. In the physical activation of argan shell-derived biochar, three different activation times of 1.5, 2, and 2.5 hours were tested. The sample prepared using the longest activation time was characterized by the highest specific surface area (up to 1500 m^2/g), the largest total pore volume (up to 0.68 cm^3/g), and the highest carbon content (up to 95 wt. %) (Afailal et al., 2023).

It is evident that different biochar may necessitate significantly varied activation times during the physical activation process, underscoring the importance of selecting an appropriate holding time to optimise samples with desirable textural properties. Furthermore, holding time is closely linked to carbon yield and therefore, the application of suitable holding times is the most practical method of controlling carbon yield directly. Consequently, in the industrial production of targeted activated biochar, a thorough understanding and control of holding time is deemed critical.

4.1.4. Mechanisms of physical activation

The modification of biochar pore structure through physical activation is achieved by removing volatile components and eliminating internal carbon mass, as depicted in Fig. 4.2 (Sangon et al., 2018). As mentioned, the changes in pore structure achieved through physical activation provide biochar with more contact surface for adsorption. Simultaneously, it increases the presence of oxygen-containing functional groups such as -COOH and -OH on the biochar surface (up to a certain temperature), thereby enhancing adsorption efficiency (Sakhiya et al., 2021; Yuan, X. et al., 2022). The activation process involves the penetration of the activating gas into the sample's surface openings, followed by pore diffusion, reaction with the carbonaceous network, and the generation of additional gas reaction products – a process ultimately shaping the final porous structure (Biti et al., 2023).

A number of theoretical models describing the process of physical activation of biochar to activated carbon have also been proposed. Simple and general models have been developed and validated to describe the physical activation process. The establishment of these models can be seen as a comprehensive description of the mechanisms of physical activation. Several models have been developed to estimate gas yield and adapted to describe biochar activation. These models include the volume reaction model (VRM), the shrinking core model (SCM), and others (Lin et al., 2012; Zhao, S. et al., 2021). A new model has been proposed with the primary assumption that the activation process deepens but does not widen the pores, successfully predicting both the carbon yield and specific surface area of the produced activated biochar. A possible explanation for this reasonable assumption is as follows: the pores formed during the initial pyrolysis stage may serve as channels for the evacuation of hot gases during the physical activation process. These pores may become obstructed by heavy tars formed in the later stages of pyrolysis, which are still present at the initial stages of physical activation. Subsequently, during the activation process, oxidative gases would preferentially react with these heavy tars, clearing these channels (Colomba et al., 2022). The principles of the reaction between oxidative gases and the carbonaceous components in biochar under high-temperature conditions are well understood. However, the focus on how the carbon yield and specific surface area, among other performance indicators of activated biochar, are ultimately determined in this process, remains a critical component of studying the mechanism of physical activation.

Itt is evident that current research primarily focuses on investigating the effects of key activation conditions such as activating agents, activation temperature, and activation time on the properties of the final product. This holds practical significance in guiding the optimisation of experimental conditions. Moreover, by proposing realistic assumptions and establishing corresponding models to describe the physical activation process quantitatively, and subsequently validating these models with experimental data, the mechanisms of physical activation can be further realised in more depth.

4.2. Chemical activation

Chemical activation is the activation treatment of pristine biochar to modify porous network, surface chemistry, primarily surface functional groups and surface alkalinity. Chemical activation can be done via one-step or two-step activation. In one-step activation, carbonisation and activation of biomass occur in situ in the presence of chemical reagents (Zhang, Ying et al., 2020). However, two-step activation involves car-

Table 4.2
Characteristics of activated biochar using different chemical activators.

Feedstock	Activator	Temperature (°C)	Time (h)	Activator/BC	Surface area (m^2/g)	Pore volume (cm^3/g)	Application	Ref.
Pine wood	KOH	700	1	6: 1	3733	1.41	Energy storage	(Lü et al., 2022)
Rice husk	NaOH	700	2	1: 4	307.42	N/A	Supercapacitor	(Ray et al., 2023)
Bio-oil	NaOH	800	2	3: 1	2826	1.78	Supercapacitor	(Zhu, Y.W. et al., 2022)
Fern	H_3PO_4	400	1	3: 1	1212	1.43	Capacitor Electrode	(Trinh et al., 2020)
Spirulina	$ZnCl_2$	400	2	1: 1	235	0.13	Adsorbent	(Moon et al., 2023)
Rice husk	HNO_3	600	2	—	33.1	0.08	Catalyst	(Wang, Y. et al., 2021)
Corn stalk	K_2CO_3	450	2	—	57.8	0.081	Adsorbent	(Zhu, L. et al., 2018)
		600			541.91	0.339		
		750			814.89	0.478		
Poplar chips	$AlCl_3$	550	2	20:1	418.14	0.413	Adsorbent	(Yin et al., 2018)
Wood residues	KOH	900	2	1:1	1700	0.75	Adsorbent	(Braghiroli et al., 2019)
Bio-oil	CaO	800	2	1: 1	1688	1.68	Energy storage	(Li, Xiaowen et al., 2020)
Bio-oil	MgO	800	2	2: 1	1409	1.689	Supercapacitor	(Li, J. et al., 2019)
Bio-oil	Calcium citrate	800	2	2: 1	922	0.182	Adsorbent	(Zhang, H.Y. et al., 2022)
Waste phoenix leaves	KOH	700	2	2: 1	1344.45	0.637	Energy storage	(Lv et al., 2024)
	$ZnCl_2$				1297.35	0.826		
	H_3PO_4				1062.74	1.077		
	K_2CO_3				891.38	0.427		

bonisation of the feedstock and subsequent activation of the carbonised product using chemical reagents or pretreatment of the biomass using chemical reagents before carbonisation (Cheng, J. et al., 2021).

4.2.1. Impact of activation agent

The type of activating agent used is directly linked to the functional groups created (Table 4.2). Common chemical activations include acid activation (Fu et al., 2024), alkali activation (Peter et al., 2021), and metal and metal oxide activation (Manfrin et al., 2021). Acid treatment of biochar serves two purposes. Firstly, acid treatment can remove impurities from the biochar surface and enhance its physicochemical characteristics, such as porosity and available surface area (Jia et al., 2024). HCl is an effective inorganic acid that has been employed at different stages of biochar activation. Lu et al. found that treating wheat straw biochar with HCl increased its specific surface area from 4.36 to 43.86 m^2/g, as well as the accessible pore space. This led to a 60 % increase in the adsorption capacity of nitrobenzene (Lu et al., 2022). Secondly, acid activation introduces several oxygen-containing functional groups (such as amino and carboxyl) to the biochar's surface. In another study, HNO_3 treatment was shown to improve the number of carboxyl, carbonyl, hydroxyl, and nitro functional groups in biochar, which enhanced the removal of Na^+ from the salt solution (up to 81.92 % removal) (Tan et al., 2023). In addition, HNO_3 modified biochar retains more adsorption sites and enhances chemisorption (Liu, C. et al., 2021). Compared to other acidic chemical activators, H_3PO_4 is less corrosive, leaves less harmful residue after activation, and is more environmentally friendly. A possible chemical reaction pathway for H_3PO_4 activation was first proposed by Yang et al. As is shown in Fig. 4.3, H_3PO_4 preferentially reacts with reactive oxygen-containing groups, followed by further reaction with carbon fragments, resulting in the removal of significant amounts of oxygen and carbon from biomass, while creating new vacancies. H_3PO_4 then introduces phosphorus and new oxygen moieties into the phosphorus-doped biochar, forming abundant phosphorus-containing groups (including C-O-P, C-P-O, C_3-P-O groups), and simultaneously creating a highly developed mesoporous structure (i.e. 1089.33 m^2/g) (Yang, H. et al., 2022).

Alkaline activation is achieved by soaking or mixing biochar or biomass at different alkali concentrations for about 6–24 hours at 25–100°C, depending on the specific raw material (Panwar and Pawar, 2020). Commonly used alkaline activators mainly include sodium hydroxide and potassium hydroxide. Alkaline activation of biochar enhances surface area and porosity, while generating additional oxygenated functional groups on the biochar surface (Yuan, X. et al., 2022). Chen et al. elucidated the chemical activation process of KOH and presented a potential reaction pathway between KOH and oxygenated functional groups. KOH reacted with oxygen-containing groups in the biomass during pyrolysis, resulting in the formation of multiple vacancies. In addition, KOH interacts with carbon pieces that are more stable to create empty spaces. The OH^- ions from KOH fill these empty spaces, forming significant new oxygen-containing functional groups, namely C=O, -OH, C-O, O-C=O, and -COOH groups. When KOH reacts with biomass at elevated temperatures, it produces several gaseous products and potassium substances (K_2CO_3, K_2O), which form well-developed pores, resulting in a noticeable increase in specific surface area (from 26.98 to 1351.13 m^2/g). The oxygen-containing groups were further converted into more stable -OH, C-O, and -COOH groups (Chen, W. et al., 2020). Compared to KOH, NaOH is less corrosive and more economically viable for carbon activation. Activation of rice husk biochar with NaOH resulted in a narrow range of pores in the samples with a specific surface area seven times higher than that of the pristine biochar (Ray et al., 2023). It is worth noting that NaOH has an excellent chemical activation effect on biochar and also has a positive activation effect on the production of activated carbon from heavy components of bio-oil (HCBO). Zhu et al. employed NaOH as the activating agent and HCBO derived from rice husk pyrolysis as a carbon source to prepare high-performance hierarchical porous carbon (PC) via a two-step activation process (pyrolysis followed by activation) (Zhu, Y.W. et al., 2022). When the mass ratio of NaOH to heavy bio-oil-derived carbon precursor was 3:1, porous carbon exhibited the highest specific surface area (2826 m^2/g), maximum total pore volume (1.78 cm^3/g), and abundant oxygen-containing functional groups.

Similarly, the impregnation of biochar with metals/metal oxides can also enhance oxygen-containing functional groups and pore properties. It has been reported that impregnating biochar with metal oxides (such as MnO, ZnO, CaO, MgO and FeO) and metal salts (e.g., $AlCl_3$, $LaCl_3$, $MgCl_2$, KCl, $FeCl_3$, and Calcium citrate) might boost the adsorption capacity of negative ions (dos Reis et al., 2022; Sizmur, T. et al., 2017; Wang, S. et al., 2015). Recently, Lee and Shin modified biochar via acidic and alkaline treatment, and impregnation with manganese oxide (MnO_x), and iron oxide (FeOx) (Lee and Shin, 2021). The results showed that manganese oxide impregnation led to significant changes in functional groups (e.g. aromatic rings, Mn-O, -OH) and specific surface area. The biochar prepared by MnO impregnation showed excellent adsorption capacity for heavy metals (> 9.15 mg/g). The effect of different metal salts ($AlCl_3$, $FeCl_3$, and $MgCl_2{\cdot}6H_2O$) on the impregnation of biochar and its ability to capture CO_2 was investi-

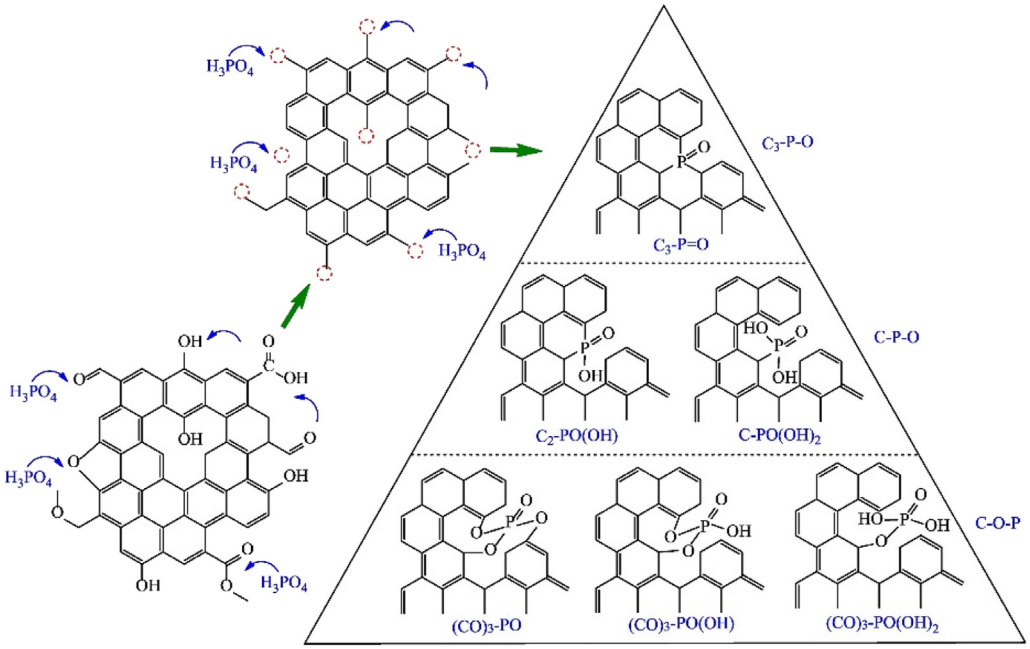

Fig. 4.3. Possible chemical reaction pathways for H_3PO_4 activation during biomass pyrolysis (Yang, H. et al., 2022).

gated in a study by Gao et al. The metal-biochar composites showed higher CO_2 capture capacity compared to pristine biochar (MgO-biochar: 63.69 mg/g, AlOOH-biochar: 71.05 mg/g, Fe_2O_3-biochar: 66.57 mg/g).

Notably, despite the largest surface area of Fe_2O_3-biochar, AlOOH-biochar showed the highest adsorption. It is due to the microporous volume of AlOOH-biochar (0.37 cm^3/g) compared to Fe_2O_3-biochar (0.33 cm^3/g), and the higher number of smaller micropores contributing to CO_2 capture (Creamer et al., 2016). Li et al. used CaO to activate HCBO to prepare PC, and investigated their hydrogen storage performance (Li, X.W. et al., 2020). At 0.1 MPa and 77 K, the hydrogen adsorption capacity of PC could reach up to 199.79 cm^3/g, surpassing the H_2 adsorption performance of commercial activated carbon. Li et al. used MgO and HCBO to prepare PC via a simple and economical one-step activation method, which were then applied as electrode materials in the field of energy storage (Choudhary et al., 2019). It is worth noting that PC obtained by activation at 800 °C for 2 hours demonstrated a large specific surface area (1167–1409 m^2/g), well-defined hierarchical porous structure, and abundant oxygen-containing functional groups. It is clear that metal oxides have excellent activation properties for the preparation of porous carbon from heavy oil, while organic salts also display positive effects. Zhang et al. utilised organic calcium salts (calcium citrate) as activators to prepare PC via a one-step templating method, which were then used in adsorbing large molecule dyes (Methylene Blue, MB) from wastewater (Zhang, H.Y. et al., 2022). When the mass ratio of template agent to heavy oil was 2:1, the specific surface area and total pore volume of PC reached their maximum values upon activation at 800 °C, reaching 922 m^2/g and 0.182 cm^3/g, respectively. At pH = 12, PC exhibited the maximum adsorption capacity for MB (411 mg/g), surpassing commercial activated carbon by 28 %.

Yuan et al. compared the environmental impacts of three activation pathways for producing waste PET plastic-derived porous carbon (Yuan, X. et al., 2022). Combining the results of life-cycle assessment (LCA) and techno-economic assessment (TEA) showed that the physical CO_2 activation pathway had a lower environmental impact (in terms of CO_2 equivalent emitted) and was more economically viable for industrial-scale applications than the two chemical activation pathways studied (KOH, KOH/urea).

4.2.2. *Impact of activation temperature*

During the chemical activation of biochar, the activation temperature affects the surface structure of biochar. Deng et al. investigated the effects of different carbonization and activation temperatures on the properties of gas and solid products (Deng, L. et al., 2024). The results showed that the emission of CO, CH_4, and H_2 were significantly affected by the activation temperature and the degree of carbonization. In addition, the activation temperature could increase the nanopore size. The specific surface area of the biochar increased with increasing activation temperature, with the optimum sample displaying a surface area of 3567.33 m^2/g. Notably, the oxygen concentration decreased with increasing activation temperature, and the oxygen-containing structure could be constructed by raising the carbonization level.

Also, Patra et al. investigated how activators such as steam and KOH, temperatures ranging from 700 to 900°C, and activation period between 60 and 120 min, affect the activation of biochar. Among these, the activator and activation temperature were realised to have a more pronounced effect on surface area (Patra et al., 2021). Similarly, Wang et al. found that the self-gasification reaction activity of biochar was closely related to the activation temperature and atmosphere (Wang, D. et al., 2019). Oxygen activation at lower temperatures favoured self-gasification and volatile reforming of biochar.

4.2.3. *Impact of activation time*

Variation in activation time has a strong effect on the structure of biomass. An excessive activation time may reduce the overall pore volume and average pore size, potentially leading to pore collapse. Activation time is an important parameter that affects the capacity of biochar. A study by Iberahim et al. showed an increase in the adsorption capacity of biochar for activation times ranging from 30 to 60 min reaction time (Iberahim et al., 2019). However, the adsorption capacity decreased with an activation time of more than 90 min. The study found that the activation time may severely influence and potentially control the pore size distribution of biochar adsorbents. Prolonged activation time can also lead to impaired surfaces (Iberahim et al., 2019). Similarly, Genuino et al. examined how varying KOH content, activation temperature, and activation time impacted the specific surface area of activated biochar (Genuino et al., 2018). They discovered that initially,

the activation period did not influence the biochar pore volume. However, extending the activation time to 90 min resulted in a significant reduction in pore volume caused by charcoal sintering.

Tan et al. explored the interaction effect of different independent variables on the efficiency of Na^+ removal by biochar after HNO_3 treatment (Tan et al., 2023). The results showed that activation time and temperature were important parameters affecting the Na^+ removal capacity of biochar. The significant interaction effect between HNO_3 concentration and treatment temperature was reflected in the small area of the contour plot (Fig. 4.4a). Low HNO_3 concentration and longer activation time exhibited higher Na^+ removal efficiency (Fig. 4.4b). The optimal interaction between activation temperature and activation time had a positive effect on the maximum removal efficiency of Na^+ from the salt solution (Fig. 4.4c) (Tan et al., 2023).

4.2.4. Effect of chemical loading

Chemical loading can significantly affect biochar activation. In a study, the surface area and micropores of biochar were seen to initially increase with the loading of chemicals and reduced upon further increase in loading (Li, S. et al., 2021). Ding and Liu discovered that excessive activation caused the disintegration of the char wall structure and a reduction in the specific surface area (Ding and Liu, 2020). As the ratio of KOH to biomass increased from 1:1 to 1:4, the biochar's specific surface area reduced from 60.2 m^2/g to 16.4 m^2/g, and the total pore volume decreased from 0.16 cm^3/g to 0.07 cm^3/g.

Lin et al. created a high-capacitance material from rice husk by activating it with KOH. Here, both specific surface area and specific capacitance were initially improved, but they suffered a reduction as the KOH ratio increased. The most specific surface area achieved was 3263 m^2/g, whereas the highest specific capacitance reached was 330 F/g. Notably, the activating reaction was accelerated and led to the formation of more micropores due to the higher ratio of KOH to biochar and therefore, increasing the specific surface area and specific capacitance. However, when the ratio of KOH to biochar exceeded 4:1, the activation process occurred too fast, resulting in severe etching and damage to the pores that were created (Liu, D. et al., 2016).

4.2.5. Mechanisms of chemical activation

The mechanism of chemical activation of biochar refers to the process of introducing a series of activators (e.g. H_3PO_4, $ZnCl_2$, KOH) to influence the pyrolysis reaction during the preparation of biochar and to transform the original carbon material into activated carbon with specific structure and properties (Sajjadi et al., 2019). The activator plays a number of key roles in the process (Fig. 4.5): 1. Catalytic effect: The activator can reduce the activation energy of the pyrolysis reaction so that the reaction can be carried out at a lower temperature. It helps generate more volatile gases, hence enhancing the pore structure and specific surface area of the biochar. 2. Charcoal structure rearrangement: In the process of chemical activation, the charcoal structure of biochar will also be rearranged. This rearrangement can make the carbon structure of biochar more orderly and improve thermal and chemical stability. 3. Etching: Some elements in the activator (e.g. P, Zn, K) can react with the carbon atoms in the biomass to form a new chemical bonding structure. During the pyrolysis process, these elements will escape from the biochar, leaving a large number of holes in the carbon matrix, hence further improving the porosity of the biochar (Lee and Kim, 2023). 4. Surface modification: Chemical activation can alter the kind and quantity of functional groups present on biochar's surface. Functional groups such as carboxyl, hydroxyl, and carbonyl can improve the adsorption performance of biochar, making it more adsorptive to specific chemical species (Zhang, C. et al., 2023).

In summary, the chemical activation mechanism of biochar involves various aspects, including thermal catalysis, carbon structure rearrangement, etching, and surface modification. These processes together determine the performance and end application potential of the produced biochar. An in-depth study of these mechanisms can provide theoretical and technical support for biochar preparation and application.

4.3. Combined physical and chemical activation

The combination of physical and chemical activation methods is commonly referred to as physicochemical activation, as depicted in Fig. 4.6. This approach often yields activated biochar with textural and chemical characteristics that differ from those obtained through the use of chemical or physical activation methods alone. Based on the discussions in the preceding sections, it is evident that chemical activation typically requires substantial quantities of toxic and corrosive chemical activating agents (Yuan, X. et al., 2023), while physical activation may result in biochar with a lower specific surface area (Zhang, Z. et al., 2020). Consequently, the employment of a physicochemical activation method aims to address the shortcomings of both aforementioned activation techniques. The synergy of these activation methods is believed to have the capability to produce activated biochar with adjustable porosity and higher yields, making it more versatile and holding significant promise for practical applications (Nasri et al., 2015).

The most common method for preparing activated biochar through physicochemical activation involves impregnating biochar with chemical activating agents, followed by CO_2 or steam activation (Kong et al., 2022). During this activation process, both the chemical activating agents and oxidizing gases are employed simultaneously, thereby influencing the final characteristics of the resulting activated biochar. From a perspective of sustainability and cost-efficiency, the use of physicochemical activation methods can reduce the consumption of corrosive chemical activating agents without compromising the micro-porosity of materials (Adlak et al., 2021). Furthermore, the combination of chemical and physical activation methods plays a vital role in achieving the desired specific surface area and pore volume of the prepared activated biochar (Adlak et al., 2021). This hybrid activation method has extensively been discussed, and its specific mechanisms have also been reported. Taking the common sequence of chemical activation followed by physical activation as an example, in the chemical activation stage, metallic ions permeate the char's matrix, creating a porous network primarily composed of micropores. Subsequently, in the continued use of the physical activation method, activating gases diffuse within the micropores, enlarging the micropores into mesopores or even macropores, ultimately achieving the desired pore characteristics (Alharbi et al., 2022; Yuan, X. et al., 2023). This preparation process is versatile and can be used with various precursors, with the resulting activated biochar having potential applications in different areas (Hu et al., 2003; Yuan, X. et al., 2022).

The process of blending precursors or carbonized products with chemical activating agents, subjecting them to heat treatment, followed by cooling to room temperature, cleaning, and drying, and subsequently undergoing physical activation in an oxidizing gas atmosphere can be succinctly described as a typical two-step physicochemical activation process. Table 4.3 summarises some of the works done adopting this approach. It is noticeable that the temperature remains relatively low during the chemical activation step, whereas higher temperatures are frequently applied in the physical activation step. Physicochemical activation consistently yields samples with a larger proportion of mesopores, primarily attributed to the subsequent physical activation phase, which allows the primary pore structure created during chemical activation to further develop (Prauchner and Rodríguez-Reinoso, 2008). In a study, peach stones were initially treated with H_3PO_4 during the chemical activation step, followed by further physical activation at elevated temperatures using CO_2. The resultant granular activated carbons exhibited a wide range of pore size distribution, and in comparison to the chemical activation method, the samples prepared using the two-step physicochemical approach demonstrated a higher proportion of mesopores (up to 1.3 cm^3/g) (Molina-Sabio, M. et al., 1996) in research involving seed hulls as precursors, a chemical activation process employing K_2CO_3 as the chemical activating agent was followed by physical activation with

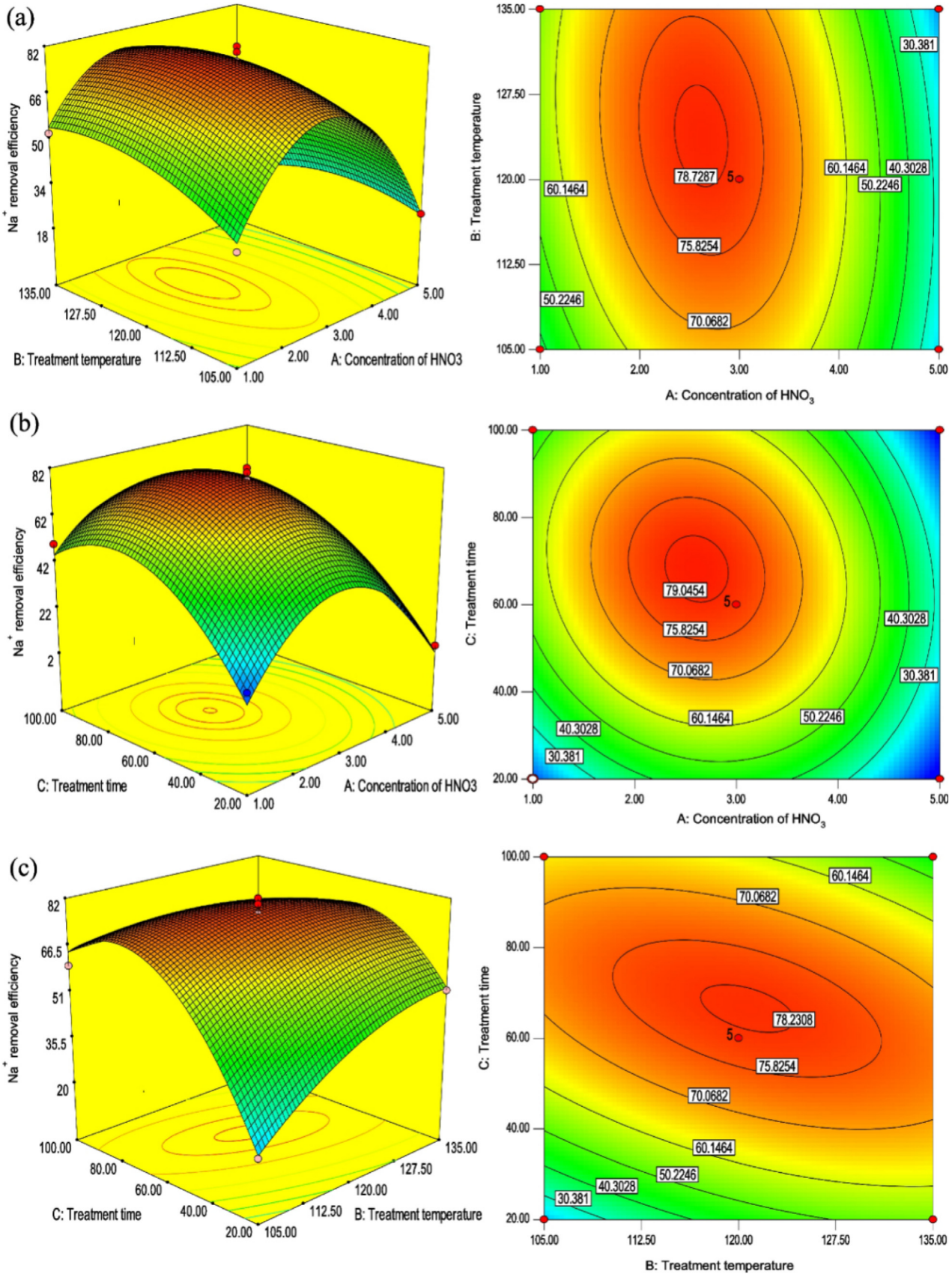

Fig. 4.4. Interaction diagram of Na^+ removal efficiency of biochar after HNO_3 treatment (Tan et al., 2023). Reproduced with permission from ref. 46. Copyright 2023, Springer Link.

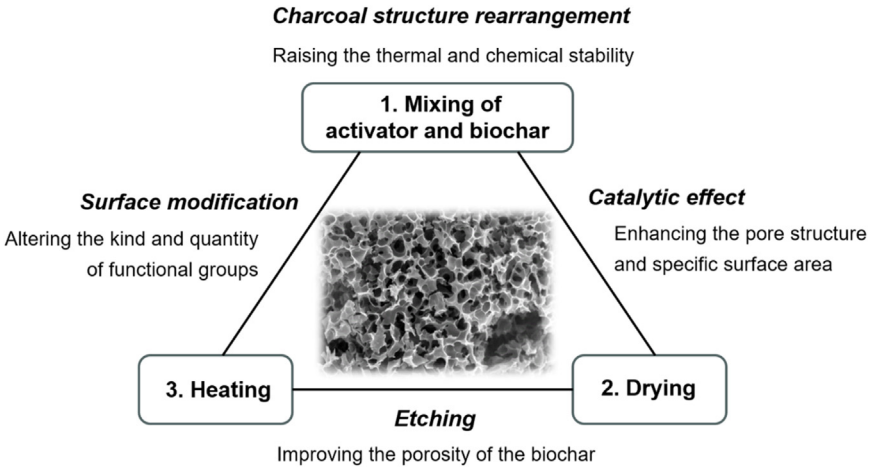

Fig. 4.5. Chemical activation enhances the properties and performance of biochar (Rajapaksha et al., 2016).

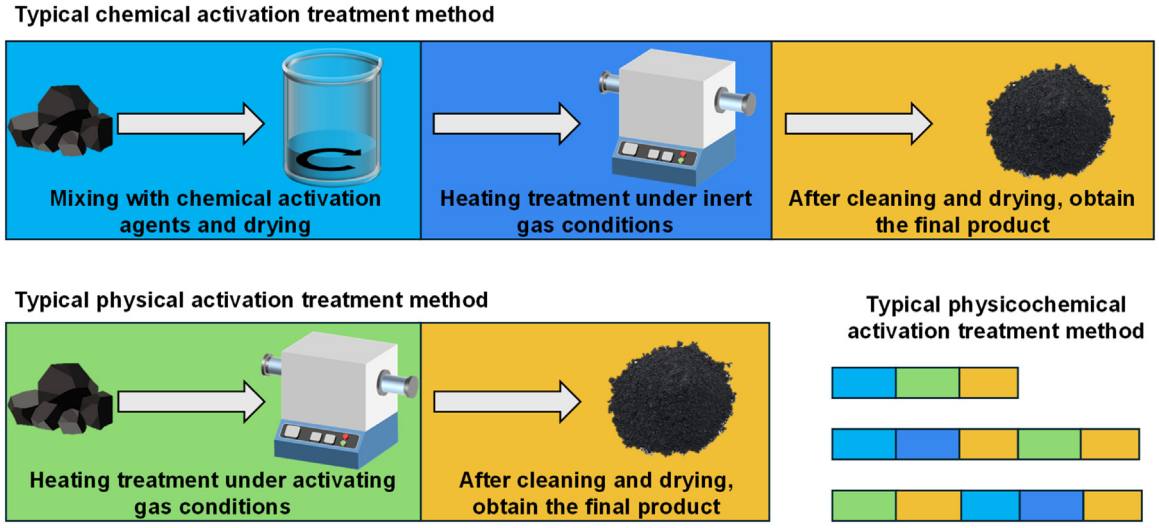

Fig. 4.6. Schematic diagram of typical physicochemical activation methods and their relationship with chemical and physical activation methods (Li, W. et al., 2022).

Table 4.3
List of recent studies on two-step physicochemical activation method.

Precursor	Chemical activation					Physical activation				Application	Ref
	Agent	Mixing mass ratio	Ramping rate (°C/min)	Activating temperature (°C)	Holding time (h)	Agent	Ramping rate (°C/min)	Activating temperature (°C)	Holding time (h)		
Peach stones	H_3PO_4	0.66, 0.95, 1.08, 1.14, 2.88	–	450	4	CO_2	–	825	3–20	–	(Molina-Sabio, M. et al., 1996)
Olive stones	H_3PO_4	0.66, 0.89, 1.11, 1.33	1	800	2	CO_2	–	750	–	Storage of methane.	(Molina-Sabio et al., 2003)
Coconut shell	H_3PO_4	0.28	1	450	2	CO_2	5	750	–	Adsorption of methane.	(Prauchner and Rodríguez-Reinoso, 2008)
	$ZnCl_2$	0.52		500							
Seed hulls	K_2CO_3	0.5–2	–	600	–	CO_2	–	650–850	0.5–2	Adsorption of malachite green dye.	(Garba et al., 2015)
Empty fruit bunch fiber	H_2SO_4	0.75, 1, 1.5, 2, 4	10	400	1	CO_2	10	900	1	Adsorption of urea.	(Ooi et al., 2017)

CO_2. Characterization results similarly indicated that the produced activated biochar was mostly mesoporous, with a substantial specific surface area and high monolayer adsorption capacity (Garba et al., 2015). Some studies also suggest that after undergoing further physical activation, the produced activated biochar exhibits an increase in micropore volume. However, this is accompanied by a decrease in bulk density, meaning that performing physical activation at high temperatures can significantly reduce the yield of the final product (Molina-Sabio et al., 2003). In the preparation process of activated carbon fibres, a two-step physicochemical activation method was applied, resulting in materials with uniform macropores and thick channel walls (Ooi et al., 2017). Characterisation of the samples and performance comparisons consis-

Table 4.4
Details in typical research using one-step physicochemical activation method.

Precursor	Chemical activation				Physical activation		Application	Ref
	Agents	Mixing ratio	Ramping rate (°C/min)	Activating temperature (°C)	Agent	Holding time (h)		
Coconut shells and palm seeds	$ZnCl_2$	0.25–3	10	800	CO_2	2–3	–	(Hu and Srinivasan, 2001)
Fir wood	KOH	1	10	780	CO_2	0, 0.25, 0.5, 1	Adsorption of dyes and phenols from water.	(Wu and Tseng, 2006)
Coconut husk	KOH	0.01, 1, 2.45, 3.90, 4.89	10	698.87, 750, 825, 900, 951.13	CO_2	0.32, 1, 2, 3, 3.68	Removal of methylene blue from aqueous solutions.	(Tan et al., 2008)
Rambutan peel	KOH	2.9	–	778	CO_2	1.7	Removal of malachite green dye from aqueous solution.	(Ahmad and Alrozi, 2011)
Coffee grounds	KOH	1	5	800	CO_2	1	Adsorption of phenol and methylene blue.	(Laksaci et al., 2017)
Rice husk	KOH	2, 3, 4	5	600, 700, 800	CO_2	0.5, 1	Removal of copper.	(Cuong et al., 2019)
Coconut shells	H_3PO_4	0, 0.5, 1, 2	5,10	800	CO_2	–	Adsorption of benzene.	(Zhang, Zongbo et al., 2020)
Oil palm shells	H_3PO_4	0.6–3.4	10	601–799	Steam	3	–	(Kouotou et al., 2013)
Neem wood	KOH	1	10	800	Steam	1	Adsorption of methane.	(Adlak et al., 2021)

tently provide clear insights into the role of incorporating the physical activation step. This approach allows for the selection of more suitable preparation process parameters for practical application scenarios.

In comparison to the two-step method, the one-step physicochemical activation process is straightforward. The general procedure involves mixing precursor materials or carbonized products with chemical activating agents. Initially, the mixture is heated to a specified temperature in an inert gas atmosphere such as N_2. Subsequently, the gas is switched to the corresponding oxidizing gas, such as CO_2 or steam. Therefore, one-step physicochemical activation methods often opt for higher heating temperatures to align with the conditions required for physical activation. General experimental results consistently demonstrate that the one-step physicochemical activation process can yield activated biochar samples with a high surface area. It is noteworthy that samples obtained through this treatment typically exhibit substantial mesopore content. For example, coconut shell- and palm seed-derived biochar have been simultaneously activated by $ZnCl_2$ and CO_2, with both surface area and pore contents being controlled by adjusting the preparation conditions. Adsorption experiments involving different-sized adsorbates (including phenol, methylene blue, and erythrosine red) have been conducted, revealing high capacities for larger adsorbates, confirming the presence of samples with significant mesopores (up to 1.364 cm^3/g) (Hu and Srinivasan, 2001). Activated biochar prepared by heating H_3PO_4-loaded coconut shells in a CO_2 flow has also exhibited superior mesopore volume (up to 0.929 cm^3/g), in addition to a large surface area and pore volume (Hu et al., 2003). Comparative experiments in this context have established that both chemical and physical activation contribute to the development of activated biochar, with the latter playing a more dominant role. The synergistic effect of KOH and CO_2 activation has also been observed to substantially enhance the microporosity of the prepared samples, as documented in existing literature. Specifically, research has demonstrated that when coffee ground-derived biochar is activated using KOH in the presence of CO_2, there is a noticeable enhancement in the porous structure, including increased pore volume and specific surface area. Furthermore, this activation process has been shown to boost microporosity and augment the adsorption capacity of organic molecules (Laksaci et al., 2017). Activated biochar prepared from oil palm shells via physicochemical activation was predominantly found to be microporous and mesoporous, with H_3PO_4 and steam serving as the chemical and physical activation agents, respectively (Kouotou et al., 2013).

Further details regarding the utilisation of the one-step physicochemical activation method can be found in Table 4.4. In summary, the porosity characteristics of the resulting samples, including specific surface area, pore volume, and meso/micropore ratio, can be finely tuned by controlling key process parameters during the activation process. The use of one-step physical activation methods provides considerable flexibility in this regard. Notably, it has been reported that activated biochar derived from rice husks with a high specific surface area and a predominantly mesoporous structure can be achieved by adjusting the KOH impregnation ratio, activation time, and temperature under a CO_2 atmosphere (Cuong et al., 2019). In similar studies, it has been observed that CO_2 activation leads to an increase in both pore volume and surface area, with the activation time using CO_2 impacting the surface chemistry of the resulting activated biochar samples (Wu and Tseng, 2006). It has been reported that, compared to activation time, CO_2 activation temperature has a more pronounced impact on the yield of activated biochar (Tan et al., 2008). These findings collectively underscore that process parameters employed in the CO_2 activation step significantly influence the properties of the product in the one-step physicochemical method. In another study, it was noted that the contribution of CO_2 activation to pore development in samples is greater than that of chemical activation using H_3PO_4 (Zhang, Zongbo et al., 2020). Consequently, the use of physicochemical activation methods not only reduces the reliance on harmful chemical agents but also ensures enhanced sample properties, potentially resulting in higher specific surface area and porosity compared to chemical activation alone (Adlak et al., 2021). Physicochemical activation is linked to excellent adsorption performance, especially liquid phase adsorption (Ahmad and Alrozi, 2011; Tan et al., 2008; Wu and Tseng, 2006; Zhang, Zongbo et al., 2020).

Adoption of physical activation followed by chemical activation to prepare activated biochar have less commonly been studied. Waste palm shells were used as the precursor in steam activation at temperatures ranging from 550 to 600°C. This was then followed by mixing the activated sample with KOH and heating to complete the chemical activation step. The results revealed that the activated biochar obtained through the physicochemical activation method exhibited the highest pore surface area and dichlorination efficiency (Shi et al., 2022). Empty fruit bunches have also been used as precursors, undergoing physical activation followed by chemical activation to obtain activated biochar. The high surface area products obtained were considered valuable for use

in sustainable environmental remediation (Kong et al., 2022). Steam activation is generally carried out at lower temperatures compared to CO_2 activation, making subsequent chemical activation at higher temperatures more feasible. For this reason, CO_2 activation is generally less desirable in physicochemical activation processes.

5. Biochar modification

The properties and cost of biochar determine its ultimate applications. Original biochar often yields poor performance due to its unsatisfactory surface morphology and the scarcity of surface functional groups (Huang et al., 2021). The characteristics of biochar, such as its morphology, porosity, and surface chemistry, cannot be effectively controlled using traditional conversion methods, limiting its widespread application (Cheng et al., 2017). Therefore, biochar is often modified to alter its surface properties, endowing it with varied physicochemical characteristics and enhancing the activity of specific functional groups within it. This allows for improved performance in specific applications while reducing costs (Cheng, N. et al., 2021). The primary aim of modification is to load other elemental functional groups onto biochar. This can be categorized into three main types: heteroatom doping, heteroatom-metal co-doping, and metal atom doping. Among these, heteroatom doping, particularly focusing on the elements N, S, P, and B, has been the most extensively researched, including scenarios where these elements are co-doped. Metal atom doping can be subdivided into ordinary metal oxide, hydroxide biochar materials, and magnetic biochar materials (Son et al., 2018). Co-doping represents a combination of the two methods above, where heteroatom-metal co-doping can endow biochar with more active sites. Oxygen functional groups could be insertion points for doping heteroatoms, and metal doping serves as an effective approach to enhance the functionality of biochar (Li, R. et al., 2019).

5.1. Doping heteroatom

Doping with heteroatoms in biochar can alter its morphology and physical and chemical properties. The doping of biochar with heteroatoms can be categorized into single-atom doping and multi-atom doping. Research on single-atom doping primarily focuses on four elements: nitrogen, sulfur, phosphorus, and boron. Similarly, multi-atom doping research is concentrated on various combinations of these elements. The forms and uses of typical heteroatoms doped into biochar are shown in Fig. 5.1.

5.1.1. Doping single heteroatom

5.1.1.1. Nitrogen doping. As a neighbour to carbon in the periodic table and possessing a similar atomic size and chemical properties to carbon, nitrogen doping is the most extensively studied heteroatom doping in biochar, which is shown in Fig. 5.1(I) (Ma, X. et al., 2019). Nitrogen can form relatively stable chemical bonds with carbon atoms in biochar (Li et al., 2018), and the chemical bonds formed between nitrogen and carbon do not significantly alter the spatial structure of the original biochar (Yuan et al., 2016). Therefore, N doping can avoid the side effects caused by excessive deformation of the biochar structure (Bamdad et al., 2021). Biomass rich in N elements can incorporate N-containing functional groups into biochar through direct pyrolysis. N-rich biomass leads to higher nitrogen content in biochar (Wang, Y. et al., 2023). Amino acids tend to transform into NH_3, while protein-N or other N-containing components can increase the content of N-containing functional groups in biochar (Sun, Z. et al., 2023). Biomass with low nitrogen content requires introducing an external nitrogen source for N doping in biochar (Xu, Y. et al., 2023), such as using urea, melamine, and NH_3 (Shao, J. et al., 2018). Also, biomass can be impregnated with other nitrogen-containing substances before pyrolysis, or biochar can be ball-milled with ammonium hydroxide (Xu et al., 2019). After N doping, the N-containing functional groups on the biochar surface mainly exist as five-membered rings, six-membered rings, and heterocycles. Inorganic N-containing functional groups mainly include NH_4−N, NO_2−N, and NO_3−N. In contrast, organic N-containing functional groups have pyridinic-N, pyrrolic-N, quaternary-N, pyridine-N-oxide, graphitic-N, amine-N, amide-N, nitrile-N, etc. (Chen et al., 2018). These N-containing functional groups are primarily formed through direct cyclization reactions, dimerization reactions, dehydration, dehydrogenation, and deamination (Chen, W. et al., 2017; Chen et al., 2018).

Several factors can influence the amount of N-containing functional groups on the biochar surface. As the pyrolysis temperature increases, the nitrogen content in biochar tends to decrease, leading to a reduction in the N/C ratio (Chen, J.-M. et al., 2017). This change is accompanied by increased aromaticity and decreased polarity (Wei et al., 2015), with unstable nitrogen species transforming into more stable ones (Chen, W. et al., 2017). For instance, at higher temperatures, the transformation of pyrrolic-N into pyridinic-N and quaternary-N, as well as the conversion of C=N and C=O groups into C−N groups, is facilitated through polymerization and condensation reactions (Yu et al., 2018). This phenomenon becomes more pronounced at higher temperatures (Wang, X. et al., 2015). Similarly, higher pressure leads to the polymerization and cyclization of N-containing functional groups, developing more stable N-containing components. Excessively high pyrolysis pressure can cause the volatilization of some N-containing functional groups, forming HCN and NH_3, thereby reducing the nitrogen content in biochar (Chen et al., 2019).

The content and types of N-containing functional groups in biochar are closely related to its application performance. N doping can enhance the performance of biochar in adsorption, catalysis, and as an electrode material. For example, Wang et al. (Wang, H. et al., 2016) demonstrated that N-doped carbon quantum dot solar cells prepared by pyrolysis of different ratios of ammonia and citric acid achieved a higher power conversion efficiency of 0.79 % under AM 1.5 G full sunlight, the higher efficiency in carbon quantum dot solar cells to date. He et al. (He et al., 2023) used urea to introduce abundant nitrogen elements and N-containing functional groups into biochar, finding that the adsorption capacity for SO_2 was closely related to quaternary-N, C−N, and N−H groups (Li et al., 2024). The adsorption capacity for CO_2 largely depends on the content of N-containing functional groups. The presence of amine-N significantly influences the adsorption of heavy metals and CO_2, primarily through electrostatic attraction, hydrogen bonding, chelation, and collateralization, providing active sites for heavy metal adsorption (Guo et al., 2023). Ho et al. (Ho et al., 2019) used Spirulina residue extracted from C-phycocyanin (C-CP) as a raw material. They prepared N-doped biochar through pyrolysis and proved that high-salt Spirulina residue could be perfectly transformed into a green N-doped biochar catalyst for PDS activation and SMX oxidation. Guo et al. (Guo et al., 2016) demonstrated that the specific capacitance of layered porous N-doped biochar, using ammonia as the nitrogen source, was significantly higher than that of non-N-doped porous and non-active N-doped biochar.

5.1.1.2. Sulfur doping. Sulfur doping biochar is gradually gaining attention in current discussions. However, the sulfur content in biomass itself is relatively low. S in biomass can be categorized into organic S (organic compounds with carbon-sulfur bonds such as C–S, –C–S–C–, C=S, thiophene, sulfone, sulfoxide, cysteine, and protein) and inorganic S (such as sulfates, sulfides, bisulfites), and elemental S (Zhang, Zhiming et al., 2020). These S forms transform into S-functional groups in organisms and participate in the metabolic activities of life (Johansen et al., 2011). Consequently, it's generally not feasible to directly enrich biochar with sulfur content through biomass pyrolysis. Therefore, S doping is an effective method to increase the sulfur content and abundance in biochar. Park et al. (Park, J.-H. et al., 2019) prepared woodchip-based biochar at 600°C using elemental sulfur as a co-pyrolysis reagent, increasing the biochar's sulfur content from 0.02 wt. % to 8.72 wt. %. Another method involves adding S elements during secondary pyrolysis, incorporating S-functional groups.

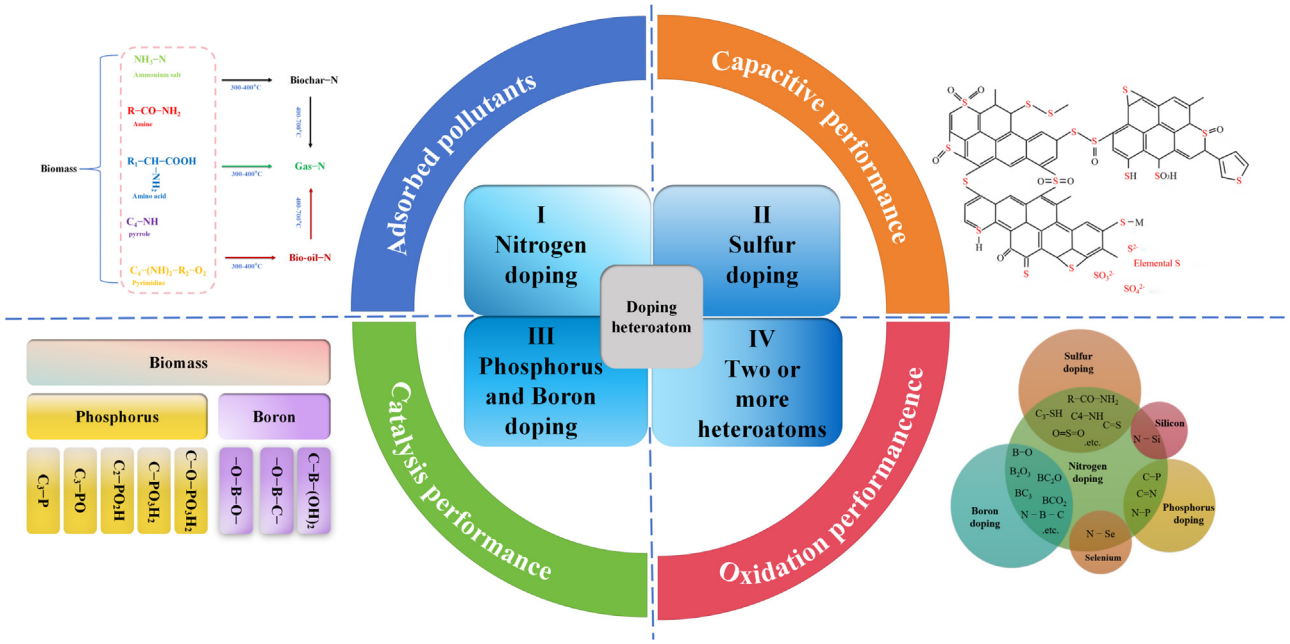

Fig. 5.1. Diagram of common doped heteroatom forms and expected uses of biochar.

David et al. used rice husk-based biochar as a material and, after adding elemental S, increased its S content from 0.2 % to 13.4 % following secondary pyrolysis (post-treatment of biochar) (O'Connor et al., 2018). During pyrolysis, the organic and inorganic S in biomass exhibit different transformation trends. New types of S-impregnation are often used to prepare metal adsorbents and solid acid catalysts (Huang et al., 2019). Additionally, plasma methods have been used to dope S into biochar. In thermal plasma treatment, high reactivity and temperatures lead to the dissociation of injected plasma gases. Plasma forms functional groups by disrupting and regenerating molecular bonds (Zhang, H. et al., 2019). The typical forms of sulfur in biochar include the carbon-sulfur bond (C–S and C=S), carbon-sulfur bridge (C–S–C), poly-sulfur chain (R–S–S–), sulfonic acid (R–SO_3H), sulfoxide (R2–S=O), sulfone (R–SO_2–R) or oxidized sulfur (R–SO_x, x = 2), thiol (R–SH), thioether group (R–S–S–OR), thiophene (C_4H_4S), sulfur-metal (S–M), elemental sulfur (S), sulfite (SO_3^{2-}), sulfate (SO_4^{2-}), and sulfide (S^{2-}), which is shown in Fig. 5.1(II) (Saha and Kienbaum, 2019). Most sulfur in biochar exists in the form of stable metal sulfides (inorganic S). Consequently, only a tiny portion of sulfur is released into the gas phase with low sulfur content (Liu, W.-J. et al., 2017).

Several factors influence the content of S-functional groups in biochar, such as the type of raw material (Zhang, Zhiming et al., 2020), the impact of inorganic elements or silicates in biomass (Liu, W.-J. et al., 2017), and pyrolysis conditions, including pyrolysis temperature (Cheah et al., 2014), residence time, pyrolysis atmosphere, and heating rate (Knudsen et al., 2004). S-doping has numerous industrial applications. Park et al. (Park, J.-H. et al., 2019) reported that wood-based biochar modified with elemental sulfur increased mercury (Hg^{2+}) adsorption capacity from 57.8 mg/g to 107.5 mg/g in aqueous solutions. S-doped biochar has also been used to adsorb heavy metal ions like Cd (Rajendran et al., 2019) and Ni (Higashikawa et al., 2016). S-doped biochar can produce solid acids and catalysts, and it is widely applied in various chemical reactions (Hara et al., 2004). Biochar with sulfur exhibits considerable catalytic performance, and S-doped biochar can serve as cathodes in lithium-sulfur batteries (Li et al., 2020). Zhang et al. (Zhang, H. et al., 2019) modified biochar in an H_2S plasma environment to form various S-containing functional groups, including C–S, S=O, organic sulfides, thiophenes, and sulfates. The modified biochar showed 3–4 times higher efficiency in removing mercury (Hg^{2+}) than untreated biochar. Abd et al. (Abd El-Mageed et al., 2020) found that S-doped biochar significantly increased the chlorophyll content in chili peppers and promoted crop growth. The soil organic matter concentration increased proportionally by adding biochar (Wu et al., 2019).

5.1.1.3. Phosphorus doping. Phosphorus doping in biochar is a promising type of biochar material due to its lower electronegativity and larger covalent radius compared to N-doped and S-doped biochar (Cheng et al., 2023). The low electronegativity and sizeable atomic radius of phosphorus are conducive to electron transfer and introduce more defect sites in carbon materials (Suo et al., 2019). Doping with P atoms leads to lattice distortion in carbon, where defect sites often have higher electron cloud density, thereby increasing the conductivity (Yang, H. et al., 2022). These defect sites lower the energy barrier for catalytic reactions. The pentavalent electrons of P atoms can form strong covalent bonds with surrounding carbon atoms, endowing them with a solid electron-donating ability (Yu et al., 2022). This enhances the reactivity of carbon materials and alters their hydrophobicity, making phosphorus an excellent doping element (Puziy et al., 2020). P covalently binds with carbon and oxygen in five-membered forms, such as C_3–P, C_3–PO, C2–PO_2H, C–PO_3H_2, and C–O–PO_3H_2 which is shown in Fig. 5.1(III) (Su et al., 2022). These P-containing functional groups endow P-doped biochar materials with many characteristics.

Compared to biochar materials without heteroatoms, P-doped biochar materials have a hydrophilic acidic surface, and doping with P improves the chemical stability of biochar materials. Introducing P into the biochar structure can be categorized into three main approaches. The first approach involves the thermal treatment of biomass precursors mixed or chemically bonded with P-containing compounds. The second approach includes modifying biochar materials with P-containing compounds, usually at high temperatures. The third method involves the co-deposition of carbon and P in the gas phase (Cheng et al., 2014). Other factors influencing the P content include the atmosphere used during the activation/modification process, biochar reactivity, porosity, surface chemical properties, and the type of activator (Puziy et al., 2017).

P-doped biochar materials significantly impact electrode materials, catalysis, and pollutant adsorption. Li et al. used potassium phosphate (K_3PO_4) to impregnate soybean straw to prepare P-doped biochar,

achieving pollutant removal from water and utilizing biofuel (Li, R. et al., 2023). The resulting biochar demonstrated sufficient adsorption capacity for sulfamethazine, and its calorific value makes it a viable coal substitute. Zhou et al. adopted phosphoric acid treatment of furfural residue (FR) and rapid pyrolysis to prepare P-doped biochar materials with an ultra-high mesopore ratio, narrow pore size distribution and large specific surface area (Zhou, X. et al., 2022). The adsorption removal rate for methylene blue reached 97.2 %. Huang et al. (Huang et al., 2023) added KH_2PO_4 to the phosphorus doping process of biochar, resulting in P-doped biochar that showed highly efficient activation of PS and degradation of γ-HCH, which was 10.5 times more effective than biochar without P-doping. Su et al. (Su et al., 2022) catalyzed the co-pyrolysis of Chlorella and waste cooking oil using P-doped biochar, enhancing the formation of aromatics and hydrogen. The P-doped biochar catalyst maintained good catalytic performance even after four cycles of reuse. Liang et al. (Liang et al., 2022) used phosphoric acid to impregnate rice husk biomass. They prepared P-doped biochar through a one-step pyrolysis method, which showed high adsorption efficiency for 2,4-D and other pesticide pollutants in the solution. Zhou et al. (Zhou, M. et al., 2022) doped biochar with P from H_3PO_4 using a one-step pyrolysis method to remove elemental mercury (HgO) from coal combustion flue gas. The P-doped biochar surface generated more organic functional groups, particularly C–P=O and C=O groups, leading to a much higher mercury removal efficiency. The C–P=O, C=O, and O–C=O groups can act as electron acceptors, accelerating the electron transfer process in the oxidation of HgO.

5.1.1.4. Boron doping. Boron doping biochar also has a relatively broad range of applications, which is shown in Fig. 5.1(III). The element boron possesses advantages such as being environmentally friendly, safe, and cost-effective. It has a lower electronegativity and a similar atomic size to carbon atoms (Gao et al., 2022), facilitating the formation of covalent bonds with C and O atoms more efficiently during the high-temperature preparation process (Qu et al., 2022). This makes it easier for B atoms to be doped into the carbon lattice, enhancing graphitization (Xing, L. et al., 2022). Different from doping elements like N and S, the electronegativity of B atoms is lower than that of carbon, leading to the distribution of positive charges around carbon atoms when B is doped into biochar (Keru et al., 2015). Unlike n-type dopants such as P, S, and F, boron is a p-type dopant that can inhibit non-radiative transitions through the electron absorption effect (Yuan et al., 2020). The formation of B–C and B–O bonds can introduce new defect edges and active sites, modulating the electronic structure and chemical stability of the carbon surface (Gao et al., 2022). B doping generally employs boric acid as a precursor, incorporating B into biomass via a one-step or distributed pyrolysis method. Phenylboronic acid is also used due to its relatively high carbon content, making it an excellent carbon source (Shen and Xia, 2014).

The most advanced B-doped biochar has been widely applied in multiple research areas, such as supercapacitors (Balaji et al., 2018), oxygen reduction reactions (ORR), photocatalysis (Wang, Z. et al., 2018), and electrochemical catalysis (Sawant et al., 2022). B-doped biochar has potential applications in the field of optical sensors and can also be used for information encryption and anti-counterfeiting applications (Fu et al., 2023). Liu et al. (Liu, B. et al., 2020) studied the preparation of B-doped graphitic porous biochar for activating persulfate to remove sulfamethoxazole. Introducing B species enhanced the surface affinity for PDS, increasing the electron transfer rate and resulting in excellent catalytic capability while providing outstanding long-term durability. Yang et al. (Yang et al., 2023) synthesized B-doped biochar using a one-step method with boric acid H_3BO_3. B doping optimized the textural properties of the biochar, enhancing surface electron density and exhibiting excellent adsorption performance for BSM. Pan et al. (Pan et al., 2023) successfully synthesized B-doped biochar using tea seed shells and boric acid through a thermal activation method, identifying –O–B–O– groups as the primary active sites. This greatly influenced the reactivity of the biochar catalyst. The B atoms, acting as electron-deficient centres, significantly changed the electron cloud density around the surrounding atoms, serving as adsorption sites and electron transfer channels for PMS, thus accelerating electron transfer.

5.1.2. Doping two or more heteroatoms

Doping with heteroatoms in biochar isn't limited to single-atom doping. It also includes dual-atom or multi-atom doping methods. Through various combinations, many multi-atom doping methods can be achieved. Currently, the most extensively studied approach involves co-doping with N atoms and other atoms, such as N/S and N/P co-doping, along with many other co-doping forms, which is shown in Fig. 5.1(IV).

Nitrogen/sulfur (N/S) co-doped biochar is one of the most common co-doping methods. N has a higher electronegativity than carbon, while S has a larger valence orbital, which can polarize on the graphite plane. The coexistence of S and N in the biochar structure has been proven to significantly alter its physical and chemical properties (Duan et al., 2015). Computational analyses of the structure of N/S co-doped biochar have shown that the presence of sulfur near pyridinic-N can enhance electron transfer along the internal structure of the biochar (Yang, J. et al., 2021). Moreover, N can also affect the characteristics of S in biochar. For instance, pyrrolic-N can induce nearby S atoms to protrude from the graphite plane, causing a change in the hybridization state of sulfur from sp_2 to sp_3 (Chen, L. et al., 2017). Other changes caused by N/S co-doping may include a decrease in surface area (due to a significant sulfur component blocking pores) and an increase in defect sites. While an increase in defect sites is beneficial, reducing surface area could decrease the number of catalytic active sites (Sun, Y. et al., 2023). Due to the synergistic interaction between N and S, co-doping with N and S can significantly improve the activation performance of undoped and singly doped biochar in removing dyes, drugs, and phenolic compounds (Oh et al., 2021). However, excessive S inhibit catalytic activity. When an excess amount of sulfur is introduced into biochar, charge density can significantly decrease, leading to the loss of active sites. Therefore, a balanced amount of S and N is necessary to enhance the catalytic effect of the biochar (Ding et al., 2020).

Nitrogen/boron (N/B) co-doped biochar has also garnered significant attention from researchers. Unlike N with five valence electrons, B only has three. Co-doping biochar with B and N provides opportunities to disrupt the electronic structure, creating electron-deficient environments and active sites. If the coordination between B and N becomes more robust, the electronegativity difference between these two atoms could lead to significant polarization of B, resulting in partly positive B that can act as adsorption sites for various electron-rich molecules (Choong et al., 2022). The defect level in N/B co-doped biochar increases with rising temperature, and the variation in bond distances enhances the asymmetry in the electronic distribution of biochar. Hung et al. (Hung et al., 2022) found that in N/B co-doped biochar, B is doped in forms such as B–O, B_2O_3, BC_2O, and B_2O_3. The co-doping of N and B promotes the reduction of biochar particle size and facilitates graphitization. This leads to the decomposition of carbonaceous material around the heteroatoms, with B mainly doped in the form of B–C in biochar.

N/B co-doped biochar also has numerous industrial applications. Zhang et al. (Zhang, T. et al., 2023) prepared N/B co-doped biochar using diatomaceous earth, urea, and boric acid, with doped B primarily existing in BC_3, BC_2O, and BCO_2. They used it to activate PDS in polluted environments for atrazine removal, finding it highly effective and versatile. Zheng et al. (Zheng et al., 2022) prepared N/B co-doped biochar using activated carbon, nitric acid, and boric acid, which can serve as a promising catalyst in the CTEG process to reduce NA wastewater. Hung et al. (Hung et al., 2023) synthesized N/B co-doped lignin-based biochar using lignin, urea, and boric acid to activate calcium peroxide for enhancing the removal of 4-nonylphenol organic micropollutants from waste-activated sludge. The highest content of BCO_2 and N–B–C in the biochar provided sufficient active centres to activate ROS

production, thereby enhancing the catalytic reaction process for 4-NP removal. Dou et al. (Dou et al., 2022) prepared N/B co-doped biochar from wheat straw, urea, and boric acid, using it as a metal-free activator for persulfate (PDS) to degrade tetracycline, finding that pyridinic-N and the BC_3 configuration might be necessary active sites. Yang et al. (Yang et al., 2023) prepared an N/B co-doped biochar catalyst using corn straw, urea, and boric acid. It was used under various experimental conditions for PDS activation and BSM degradation. Graphitic N and BC_3 were proven to be the main active substances for activating PDS and removing BSM, providing positively charged carbon atoms.

Nitrogen/phosphorus (N/P) co-doped biochar holds excellent potential for various applications. After co-doping with N and P, the biochar primarily exhibits bonding in the forms of C–O/C–P and C=O/C=N, which consumes some oxygen elements to ensure the synergistic effect of N and p-P (Yang, W. et al., 2018). The increase in the proportion of C=C double bonds in N/P co-doped biochar suggests that N/P doping enhances the content of C=C, promoting the graphitization of the biochar. Introducing these two elements changes the connectivity between carbon atoms in the material, facilitating the transition from amorphous carbon to a more ordered crystalline carbon, thus improving the material's strength and hardness. Compared to singly doped biochar, N/P co-doped biochar reduces C=O content, indicating that N and P bonding with carbon atoms replaces the original oxygen atoms in the material. The significant increase in –OH content enhances hydrogen bonding interactions (Zhu, Q. et al., 2022). A rough honeycomb layer, a multi-level porous microstructure, and irregular and developed porosity characterize the surface of N/P co-doped biochar. These layers are thinner and interconnected. This phenomenon is likely due to replacing some carbon atoms with N/P atoms after doping. N atoms are usually smaller than carbon atoms, and these size differences can cause lattice distortion, promoting the formation of a layered structure.

The introduction of N/P elements leads to an increased interlayer spacing within the carbon framework, fostering the creation of defects and active sites during activation. Chen et al. (Chen, A. et al., 2024) used seaweed, K_2CO_3 as an activator, and ammonium polyphosphate as an N/P co-doping agent to synthesize N/P co-doped biochar through a one-step pyrolysis method, significantly enhancing the adsorption of dibutyl phthalate by 25.39 %. Yang et al. (Yang, H. et al., 2022) prepared N/P co-doped biochar by co-pyrolyzing bamboo with ammonia and phosphoric acid, finding that H_3PO_4 activation and NH_3 modification of biomass can produce high N/P content mesoporous biochar with a mesoporous structure. Zheng et al. (Zheng et al., 2020) prepared N/P co-doped biochar from shrimp shells using H_3PO_4 as an activator, showing good oxygen reduction reaction performance. Xie et al. (Xie et al., 2020) obtained N/P co-doped biochar from cellulose using $(NH_4)_2HPO_4$ as a N/P source, with N content of 4.3 at. % and P content of 10.66 at. %, exhibiting excellent catalytic activity for the reduction of p-nitrophenol. Bi et al. (Bi et al., 2021) prepared N/P co-doped biochar from rapeseed cake using melamine and phytic acid as doping agents, combined with K_2CO_3 activation, for use as an electrode material with a capacitance of 358 F/g. Chai et al. (Chai et al., 2017)found that the active N/P groups in N/P co-doped graphene are effective active sites for the oxygen evolution reaction.

In addition, multi-atom doping is mainly focused on nitrogen/sulfur/phosphorus (N/S/P) co-doped biochar. Yu et al. (Yu et al., 2022) prepared N/S/P co-doped biochar by co-pyrolyzing bis(4-hydroxyphenyl) sulfone and triphenylphosphine (PPh) with waste shrimp shells. Co-doping enriches the surface catalytic sites of biochar, enhancing its electron conductivity and enabling rapid activation of PDS through an electron transfer pathway. This non-free radical pathway further endows the N/S/P co-doped biochar system with the ability to degrade pollutants selectively. Other dual heteroatom combinations, such as P/S, P/B, and B/S, may also cause changes in biochar properties. However, reports in these areas are not as numerous, possibly due to the difficulty of developing methods for co-doping biochar with these elements. Although phosphorus has similar properties to N, it is harder to incorporate into the carbon structure due to its larger size. Co-doping with P and S or B is expected to cause more significant perturbation to the biochar structure, thereby synergistically improving its performance. Performance improvements attributed to P/S co-doping have been observed in many applications, including catalyzing oxygen reduction reactions (ORR) (Zhou et al., 2016), catalyzing aerobic oxidation of benzyl alcohol (Patel et al., 2017), supercapacitors (Zhang et al., 2016), and Na^+ adsorption. Concurrently, P/B co-doping on biochar can increase its electronic conductivity. Computational studies on biochar co-doped with P and B indicate that P dopants can form B–P bonds, increasing the spin density around the dopant and reducing the bandgap of biochar as a catalyst, potentially imparting higher activation performance (Shao et al., 2020). Meanwhile, reports of B/S co-doped biochar are scarce, possibly because the electronegativity difference between S and C is relatively small, and its interaction with B is limited. However, B/S co-doping in biochar can enable each to exert its individual effects (Guo et al., 2018).

N can also be co-doped with selenium (Se) and silicon (Si) to enhance the catalytic activity of carbon catalysts. Due to its sizeable atomic size and ease of polarization, Se can increase the defect sites of carbon catalysts. Moreover, doping with Se can improve the electron-donating properties of biochar, making it more conducive to activation reactions. Zhang et al. (Zhang, K. et al., 2021) found that Se atoms have a higher polarization rate and that carbon catalysts co-doped with N/Se exhibit improved catalytic ORR activity compared to those co-doped with N/S.

5.2. Doping metals

The metal doping of biochar has garnered significant attention from researchers due to the ability of certain metals to utilize oxygen functionalities as anchoring sites, resulting in stable metal centres on the surface of biochar (Liu et al., 2022; Rong et al., 2019). The introduction of metals alters the surface electronegativity, dispersibility, and functional groups of biochar (Zhuang et al., 2021). Metal-modified biochar improves its application range and performance (such as pollutant adsorption and catalysis), and also makes it easy to separate from the application system (Chen, Y. et al., 2020; Chen, Y. et al., 2021). The metal doping methods of biochar can be divided into single metal doping and two or more metal doping.

5.2.1. Doping single metal

In terms of doping methods, *in-situ* reduction, impregnation, functionalization, and ultrasonic dispersion can all enable biochar to contact/react with metal solutions, as shown in Fig. 5.2. Subsequently, carbonization is often required to make the metal more effectively doped on the surface of the carbon. Noble metals such as Ag, transition metals such as Fe, Co, Ni, and Cu, and other metals such as Al and Mg, have been reported for use in the doping process of biochar, as shown in Table 5.1.

Precious metals are often regarded as high-performance catalysts, while biochar is often an ideal catalyst support material. Huang et al. found that the oxygen-containing groups on the surface of biomass-based carbon can provide the sites (-OH, -COOH, C-O-C) required for *in-situ* reduction and stabilization of Ag sites (Jiang et al., 2021). The Ag@C catalyst was applied to the conversion of 1-alkynes and N-halosuccinimide (-Cl, -Br and -I) to 1-haloalkynes of diverse structures with good to excellent yields up to 98 % at room temperature. In addition, transition metals such as Fe, Co, and Ni have also been widely studied. Among them, doping of Fe and Co often helps biochar to improve its adsorption/redox ability of heavy metal ions or organic pollutants. Hu et al. (Hu et al., 2024) have prepared $FeCl_3$-modified rice husk biochar, which has higher surface positive charges, oxygen-containing functional groups, and persistent free radicals. Therefore, it effectively enhanced the Cr(VI) removal efficiency by 1.54- to 8.20-fold and the Cr(VI) reduction efficiency by 1.88–9.29 fold compared to those of pristine biochar. Dong et al. found that Co-doped coffee ground biochar ex-

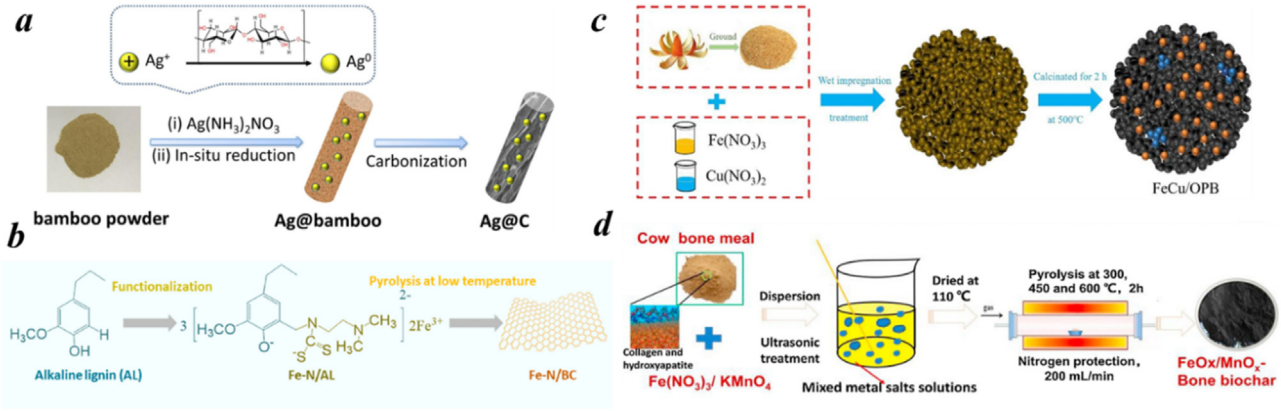

Fig. 5.2. The diagram of metal doping for biochar: (a) In-situ reduction&carbonization (Jiang et al., 2021), (b) Functionalization &carbonization (Guo, L. et al., 2023), (c) Wet impregnation&carbonization (Sun, J. et al., 2023), and (d) Ultrasonic treatment&carbonization (Xiao et al., 2020).

Table 5.1
Summary of existing reports on metal doping for biochar.

Raw material	Type of the metal	Doping method	Annealing conditions	Metal content	Application	References
Bamboo	Ag	*In-situ* reduction & pyrolysis	800°C; 2 h; N_2	6.2–15.5 wt %	Catalyst of halogenation	(Jiang et al., 2021)
Tree residue	Ag	Carbonization & impregnation & drying	700°C; N_2	0.31 wt%	Supercapacitor electrodes	(Kouchachvili and Entchev, 2017)
Olive pit	Ag	Impregnation & pyrolysis	400°C; 15 min; N_2/H_2 (95/5 %) mixture	5.0 at%	Anti-kinetoplast	(Snoussi et al., 2022)
Corn straw	Fe	Impregnation & pyrolysis	600–800°C; 2 h; N_2	23.03–40.35 at %	Metal-cyanide complexes adsorption	(Wei et al., 2023)
Cotton straw biochar	Fe	Impregnation	–	30.66 wt%	Cd(II) and As(V) adsorption	(Zeng, L. et al., 2023)
Local yard waste	Fe	Carbonization & impregnation & carbonization	400–800 °C; 1 h; N_2	7.46–9.00 wt %	Redox of As(III)/Cr(VI)	(Xu et al., 2022)
Kapok fiber biochar	Co	*In-situ* Co-MOF grafting & carbonization	600–800 °C; 2 h; Ar	1.30 wt %	Electromagnetic wave absorption	(Mai et al., 2023)
Rich husk biochar	Ni	Ni loading & calcination & reduction	700°C; 3 h; N_2	6.54–8.58 wt %	Catalytic gasification for H_2 production	(Farooq et al., 2021)
Cellulose	Ni	Impregnation & annealing	500°C; 1 h; N_2	–	Supercapacitor	(Paravannoor, 2018)
Wheat straw	Mn	Pyrolysis & impregnation & pyrolysis/ impregnation & pyrolysis	700°C; 2 h; N_2	0.17/0.40 wt %	Tetracycline adsorption	(Huang et al., 2020)
Sewage sludge	Cu	Impregnation & pyrolysis	450–750°C; 1.5 h; N_2	2.76 at %	Oxidative degradation of bisphenol A	(Yu et al., 2023)
Six types of biomasses	Mg	Impregnation & pyrolysis	430 °C; 4 h	–	Nitrogen and phosphorus adsorption	(Jiang et al., 2019)

hibited marked adsorption capacity and catalyst activity of tetracycline from water (Nguyen et al., 2019). Its maximum adsorption capacity of tetracycline can reach 370.37 mg g^{-1}. Ni often helps catalyze biomass gasification for hydrogen production (Yao et al., 2016). Zhang et al. doped Ni, Fe, or Zn into biochar for wheat straw gasification-catalytic steam reforming process and found that Ni-doped biochar showed ultrahigh carbon conversion efficiency (99.47 %) and high H_2 production efficiency (η: 7.89 g CO_2/g H_2) (Kong et al., 2023). What's more, Mg-doped biochar has a good adsorption effect on phosphorus in water (Shin et al., 2020).

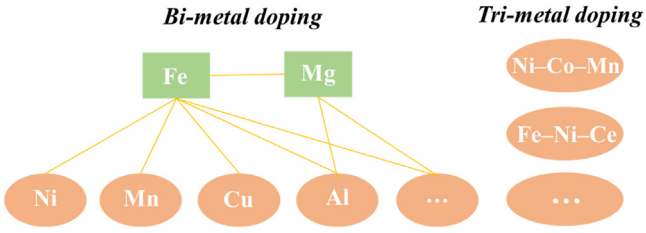

Fig. 5.3. . Common types of two or more metals doping for biochar.

5.2.2. Doping two or more metals

The bimetallic doping of biochar mainly focuses on the combination of Fe and other metals, with magnetic modified biochar as a representative (as shown in Fig. 5.3), such as Fe-Ni doping (Li et al., 2017; Wu et al., 2016; Xing, X. et al., 2022), Fe-Mn doping (Gao et al., 2021; Gao et al., 2021; Xu, L. et al., 2023), Fe-Cu doping (Jin et al., 2023; Peng et al., 2023; Shen, Y. et al., 2023), Fe-Al doping (Peng et al., 2021; Tang et al., 2023), etc. Song et al. (Lin et al., 2017) used Fe-Mn modified biochar for efficient Arsenic removal in an aqueous solution and found that Fe oxide had a strong attraction to As(V), while Mn oxide (Mn_3O_4, Mn_2O_3) promoted the oxidation of As(III) to As(V). Wang et al. (Wang et al., 2024) modified biochar by Fe-Ni nanoparticles loading and amination/hydroxylation, and the maximum adsorption capacity of the modified carbon for Pb(II)/Cd(II) is 4.30–4.79 times that of the pristine biochar. This is due to the introduction of Fe-Ni nanoparticles and O/N-containing groups, which promote complexation and electrostatic interactions during adsorption. Moreover, Fe-based bimetal doped biochar

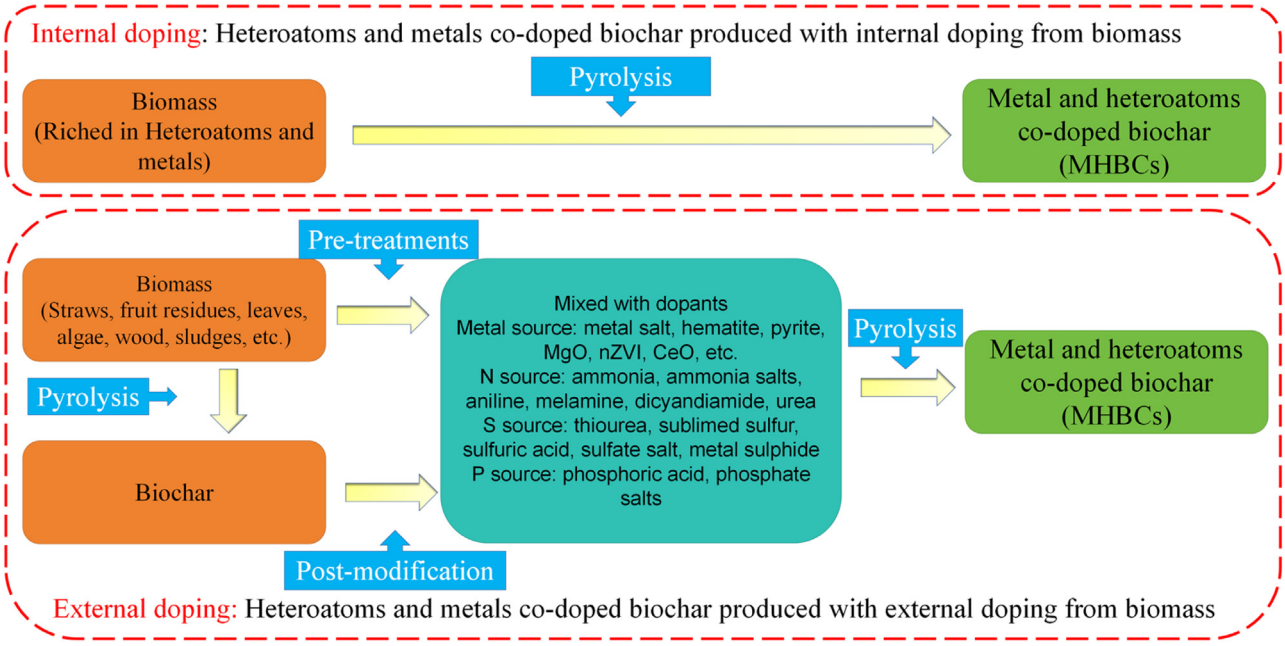

Fig. 5.4. Diagram of the preparation process of biochar co-doped with heteroatoms and metals.

can be used as a bimetallic catalyst (like heterogeneous Fenton-like catalyst) for the degradation of organic pollutants. Zhang et al. used Cu-Fe doped biochar to remove rhodamine B dye through a Fenton-like reaction and found that Cu(I) facilitated the reduction of Fe(III) to Fe(II), resulting in a high catalytic oxidation efficiency (Shen, Y. et al., 2023). In addition to Fe, Mg is often used to dope biochar with other metals, especially in the form of layered double hydroxides (Li, Shuqi et al., 2021; Wang et al., 2021f). Gao et al. (Wan et al., 2017) functionalized and doped biochar with different amounts of Mg-Al and Mg-Fe (3:1) layered double hydroxides, and found that the composite material containing 40 % Mg-Al LDH had the best adsorption effect on phosphate, achieving a 95 % phosphate saturation within 1 hour. However, there is currently not much research on the doping of more metals. Yuan et al. synthesized Fe–Ni–Ce/biochar biomass pyrolysis volatiles catalytic reforming syngas (H_2 + CO) and it showed high catalytic activity (Liu et al., 2023). Shen et al. used spent lithium-ion battery leachate to modify biochar by multi-metal doping, and the as-synthesized Ni-Co-Mn doped carbon catalyst can promote the conversion of large molecular components in cellulose pyrolysis to small molecular gases (Shen and Chen, 2022).

5.3. Co-doping heteroatoms and metals

Compared to biochar doped solely with metals or heteroatoms, biochar co-doped with metals or heteroatoms possesses more active sites and a greater affinity for pollutants. Metals can utilize oxygen functional groups as anchoring points and achieve stable metal centres on the biochar surface. The introduction of metals alters the surface electronegativity, dispersibility, and functional groups of biochar. Doping with heteroatoms, including N, S, or P, effectively enhances biochar functionalities (Li, R. et al., 2019). Metal and heteroatom co-doped biochar (MHBCs) can be divided into two main categories based on the raw materials: internal doping and external doping. Internal doping refers to MHBCs where metals and heteroatoms originate from the biomass waste itself, with specific biomass containing these elements being relatively rare (Yu et al., 2019). If any metal elements and heteroatoms on MHBCs come from external additives, the resulting MHBCs are considered externally doped. Exogenous metal nanoparticles/composites and inorganic metal salts typically provide the metal elements in MHBCs. External doping is more common in the manufacture of MHBCs (Pang et al., 2011). The two preparation processes of heteroatom and metal co-doped biochar are shown in Fig. 5.4.

The pretreatment method for preparing metal and heteroatom co-doped biochar involves treating the biomass with metal or heteroatom substances, followed by the pyrolysis of the pretreated biomass waste. Common additives for N doping in MHBCs include inorganics (such as ammonia and ammonium salts) and organics (such as dicyandiamide, melamine, urea, and aniline). Compared to various nitrogen additives, elemental S is mainly provided by thiourea, sulfuric acid, and sulfates, while P doping in MHBCs is provided by phosphoric acid and phosphates. Additionally, nano-composites containing metals and heteroatoms, such as FeS and MoS_2, can be composite additives for preparing MHBCs (Liu et al., 2022). They mixed aquatic plants with high nitrogen absorption rates in eutrophic water with magnesium chloride solution and rapid pyrolysis to obtain MHBC (MgO/N-biochar). Xu et al. (Xu, L. et al., 2020) prepared MHBC (Fe/N-biochar) by pyrolyzing a mixture of sawdust, $FeCl_3$, and dicyandiamide at 800°C for one hour under an N_2 atmosphere. Besides these methods, heteroatom doping can be achieved under unique gas atmospheres. For example, Zheng et al. (Zheng et al., 2021) prepared (Ga_2S_3/S-modified biochar) by impregnating sugarcane bagasse in gallium nitrate and sulfidizing it at 600°C with a 20 wt. % H_2S/Ar flow rate (30 mL/min) for 3 hours.

The second method involves post-modification of biomass, referring to further modification of the original biochar. Co-doping of metals and heteroatoms on biochar is typically achieved by impregnating the original biochar with external additives. Some MHBCs preparations may require additional treatments. For instance, Yang et al. (Yang et al., 2019) used a homogeneous solution of porous biochar and iron salts for hydrothermal treatment to obtain Fe/Mn/S co-doped biochar, where the porous biochar was produced by pyrolyzing a mixture of corn stalks and $KHCO_3$. Moreover, co-doping in MHBCs might necessitate a second pyrolysis of the impregnated mixture, as done by Shang et al. (Shang et al., 2020), who pyrolyzed a blend of corn-xylan-derived biochar, melamine, and $MgCl_2{\cdot}6H_2O$ at 120°C and 600°C sequentially for 2 hours to produce MHBC (MgO/N-BC). Tang et al. (Tang et al., 2021) considered physical ball milling a simple synthesis method for MHBCs by placing biochar and nano-composites (FeS and FeS_2) in a planetary ball mill for several hours.

The characteristics of MHBCs depend on the manufacturing method, particularly in particle size and composition. The particle size and dop-

ing element amount in MHBCs prepared by pretreatment are not easily controlled. In contrast, MHBCs prepared through post-modification allow for easy adjustment of the size, shape, composition, and loading content of functional active sites on the biochar. Although the relative energy cost of producing MHBCs via post-modification is higher, its excellent controllability makes it more popular than the pretreatment method (Miao and Li, 2021). Choosing the best manufacturing method for MHBCs is crucial based on their intended use. Compared to the original biochar, MHBCs exhibit altered surface characteristics, such as surface morphology, composition, area, graphitization, and functional groups (Zhu, J. et al., 2022). Fe/S co-doped biochar shows a highly similar concave structure to the original biochar, dispersed with small spherical Fe_xS_y particles in the cavities, primarily FeS and Fe_3S_4 particles (Hu et al., 2021).

The functional groups of MHBCs typically originate from the decomposition of biomass waste itself and the contribution of special doping elements (metals and heteroatoms) (He et al., 2022). The metals present in MHBCs mainly exist as metal nanoparticles or metal oxides (Zhao, C. et al., 2021), such as Fe−O, Mn−O, and Fe−S bonds (Ma et al., 2020). Additionally, heteroatoms on MHBCs aid in forming specific functional groups (Wang and Wang, 2020). Different heteroatoms correspond to other functional groups on MHBCs (Zhang, Yuting et al., 2020). Metal and heteroatom co-doped biochar composites (MHBCs) have specific surfaces with many functional groups and unique redox properties. MHBCs demonstrate excellent capability in removing various pollutants from wastewater. The specific pollutant removal mechanisms on MHBCs mainly involve adsorption, redox, and degradation (Xu, L. et al., 2020). The adsorption affinity of MHBCs for pollutants is higher than that of biochar doped only with metals or heteroatoms due to the synergistic effect of co-doping metals and heteroatoms on biochar.

Specific adsorption mechanisms include physical adsorption, ion exchange, electrostatic interactions, surface complexation, and other mechanisms (Mandal and Nanduri, 2020). Li et al. (Li, R. et al., 2019) doped biochar with Mo, Fe, and S, increasing its magnetism and exhibiting excellent stability in acidic and alkaline solutions. MoS_2, Fe_3O_4, and biochar indicate that metal atoms and non-metal heteroatoms form a stable structure doped in biochar, greatly enhancing the adsorption performance of humic acid salts and lead ions in water. Li et al. (Li, Xiang et al., 2020) prepared Fe/N co-doped biochar from wheat straw, urea, and iron salts through pyrolysis for organic pollutant degradation activated by persulfate. Iron oxide doping introduced magnetism for easy separation in biochar and affected its catalytic ability for PS activation. The biochar, loaded with Fe and iron oxides and enlarged in specific surface area and pore volume by urea, catalyzed the reaction. Zhuang et al. (Zhuang et al., 2021) prepared sulfurized nano-zero-valent iron (nZVI) to reduce and adsorb Cr^{2+} ions in polluted water bodies. Sulfur doping allowed for more uniform dispersion of biomass particles and doubled the removal rate. S can effectively inhibit aggregation after loading nZVI particles on biochar, improving biochar's lifespan and recycling times. Cao et al. (Cao et al., 2017) found that sulfide modification effectively increased the crystallinity of Fe on biochar. Only a small amount of iron was oxidized when Fe and S were co-doped in biochar, indicating that surface sulfide modification can enhance the antioxidative properties of Fe embedded in biochar.

Pedino et al. (Penido et al., 2019) prepared P/Mg co-doped biochar by co-pyrolyzing poultry litter (PL), phosphoric acid, and magnesium oxide (MgO), where the addition of phosphoric acid and magnesium oxide enabled Mg loading on biochar, with oxygen and phosphorus functional groups on its surface, enhancing its activation properties and adsorption capacity for degrading Cd ions. Xu et al. (Xu, L. et al., 2020) used a mixture of sawdust, $FeCl_3$, and dicyandiamide for pyrolysis to produce Fe/N co-doped biochar (Fe/N-BC) for activating PMS, exhibiting excellent catalytic and separation performance. The main reactive species promoting PMS activation were the presence of graphitic-N, pyridinic-N, Fe−N_x, Fe_2O_3, and FeO. Co-doping of Fe and N led to distortion in the carbon network and created more defects. The abundance of defects in the carbon-based catalysts, caused by zigzag/armchair edges, vacancies, and functional groups, helped promote the adsorption and activation of PMS.

6. Biochar applications

6.1. Biochar for carbon capture

Biochar, an environmentally friendly adsorbent derived from natural biomass or agricultural wastes, has been identified by the Intergovernmental Panel on Climate Change (IPCC) as a highly promising solution to combating climate change owing to its potential for long-term carbon sequestration potential and various benefits(Liu et al., 2018). Compared with other CO_2 adsorbents, biochar is nearly 10 times cheaper due to its high availability (Gupta and Kua, 2017). The CO_2 uptake of biochar, quantified by the amount of CO_2 adsorbed per unit weight of biochar could be affected by a variety of factors, including the porous structures, surface functional groups, alkali and alkali earth metals, hydrophobicity, polarity, and aromaticity(Dissanayake et al., 2020). These physicochemical properties of biochar are closely related to the type of feedstock used and the thermochemical conditions employed during its production(Sun et al., 2014; Zhang et al., 2014).

6.1.1. Effects of process conditions on physicochemical properties of biochar

6.1.1.1. Effect of feedstocks. The physicochemical properties of biochar are influenced by the type of feedstocks used, and the higher percentage of surface heteroatoms such as N and S contributing to high CO_2 adsorption. Creamer et al. compared biochar produced from the co-pyrolysis of sugarcane bagasse and hickory wood and found that biochar with larger surface areas showed a higher CO_2 adsorption capacity (73.55 mg/g at 25°C) due to more active sites for CO_2 adsorption are provided (Creamer et al., 2016; Creamer et al., 2014). Xu et al. produced biochar from sewage sludge, pig manure, and wheat straw with CO_2 adsorption capacities of 0.41, 0.53, and 0.78 mol/kg, respectively at 25°C (Xu et al., 2016). Igaravesana et al. used a mixture of food waste and wood waste in different proportions to produce biochar and found that when wood wastes occupy the highest proportion, the biochar owned the strongest CO_2 adsorption capacity, while a higher proportion of food wastes in the feedstocks was detrimental to CO_2 adsorption (Igalavithana et al., 2020).

6.1.1.2. Effects of thermochemical conditions. Temperature, heating rate, and residence time are all the parameters that affect the physicochemical properties of biochar (Chatterjee et al., 2020). The effect of temperature on these properties is attributed to the release of volatiles at high temperatures. It has been reported that high pyrolysis temperature leads to increased biochar surface areas (Zhang et al., 2015), higher pH values (Hossain et al., 2011), and higher carbon contents but lower nitrogen contents (Zhang et al., 2017), which sequentially results in an increased CO_2 adsorption capacity. For example, Chatterjee et al. investigated the influence of temperature including 500, 600, 700, and 800°C on the physicochemical properties and the corresponding CO_2 adsorption performance of biochar derived from herbaceous (miscanthus and switchgrass) and agro-industrial (corn stover and sugarcane bagasse) feedstocks (Chatterjee et al., 2020). It is found that when the temperature is increased from 500 to 600°C, the CO_2 uptake is largely enhanced. While further increasing the pyrolysis temperature to 800°C resulted in a decrease of the adsorption capacity due to the decrease of nitrogen content and the destruction of surface porosity at this higher temperature around. As a result, choosing an appropriate pyrolysis temperature involves a trade-off between the surface and chemical properties as described.

The heating rate is another parameter that affects the physicochemical properties of biochar. The increase in the heating rate leads to a

decrease in the yields of biochar. Thus, the low heating rates are usually preferable in terms of yield and stability of biochar, even though they take much longer. In addition, When the process is conducted at a low heating rate, the pyrolysis products and volatile organic matter have enough time to diffuse from the biochar particles. Low heating rates are beneficial in retaining structural complexity, whereas high heating rates result in the loss of structural complexity due to local melting, phase transformation, and expansion of the structure (Angın, 2013).

Pathomrotsakun et al. investigated the effect of residence time including 30, 45, and 60 min on the physicochemical properties of biochar and found that residence time only slightly affected the physicochemical properties of biochar. Zhao et al. found that residence time ranging from 10 to 100 min had a minimal effect on biochar derived from rapeseed stem (Zhao et al., 2018). A near-optimal pyrolysis yield can be obtained in a short residence time. Yaashikaa et al. demonstrated that high-yield biochar can be obtained at a low pyrolysis temperature for longer residence times due to the polymerization and condensation reactions that occurred between the produced solids and vapours (Yaashikaa et al., 2019). Thus, the process conditions including feedstocks, temperature, heating rate, and residence time are closely related to the physicochemical properties of biochar.

6.1.2. Effects of physicochemical properties on CO_2 adsorption of biochar

6.1.2.1. Porous structures. Several studies have assessed the effects of the porous structure including specific surface area, pore size, and pore volume of biochar on its CO_2 capture capacity (Xu et al., 2016). It is found that with the increase of specific surface area, the CO_2 adsorption capacity of biochar could be largely enhanced due to the generation of abundant micropores and more active sites (Fig. 6.1a). As for the pore size, previous studies reported that pores with a diameter of 0.5 nm or less contributed significantly to CO_2 adsorption at low partial pressures, whereas pores with a diameter smaller than 0.8 nm made a higher contribution to CO_2 uptake at 1 bar (Dissanayake et al., 2020). The CO_2 adsorption capacity has a stronger correlation with the micropore surface area (Fig. 6.1b) than the BET surface area (Fig. 6.1a), suggesting that the micropore structure of the biochar significantly affects the CO_2 adsorption capacity (Zhang et al., 2016).

6.1.2.2. Surface functional groups. Surface functional groups including nitrogen-containing functional groups (amide, imide, pyridinic, pyrrolic, and lactam groups) and oxygen-containing functional groups (ketones, pyrones, and chromenes) play an important role in the CO_2 adsorption of biochar through promoting the growth of alkalinity on the surface of biochar and enhancing the affinity between biochar and CO_2 molecules, respectively (Shen and Fan, 2013). For example, Xu et al. obtained nitrogen-doped biochar using ammonium hydroxide ball milling, and the nitrogen functional group species doped onto the surface of the biochar were mainly amine (-NH_2) and nitrile (C≡N). The nitrogen-doped biochar showed a 31.6 %–55.2 % higher adsorption capacity of CO_2 than pristine biochar, due to the strong pole-pole interaction between the large quadrupole moment of the CO_2 species and the polar sites associated with the nitrogen functional (Xu et al., 2019). It is also believed that the introduction of oxygen atoms into the carbon surface to form acidic oxygen-containing functional groups facilitates hydrogen bonding interactions between the carbon surface and CO_2 molecules, particularly carboxyl and hydroxyl groups. Carboxyl and hydroxyl groups increase the polarity of the adsorbent and facilitate the adsorption of CO_2 with the quadrupole moment (Song et al., 2020). Liu et al. concluded that the oxygen-containing functional groups increased CO_2 adsorbed in the microporous structure because the higher electron density around the oxygen-containing functional groups attracts more CO_2 (Liu and Wilcox, 2012).

6.1.2.3. Alkaline and alkaline earth metals. The presence of alkali metals (e.g., K, Na, etc.) and alkaline earth metals (e.g., Ca, Mg, etc.) can enhance the formation of basic sites with a strong affinity for CO_2 and sequentially enhance the CO_2 adsorption capacity of biochar (Xu et al., 2016). Xu et al investigated the influence of alkali metals and alkaline earth metals on the CO_2 adsorption of biochar produced from pig manure, sewage sludge, and wheat straw. It is found pig manure-derived biochar possesses the highest mineral content, including K, Na, Ca, and Mg, which could largely enhance the CO_2 capture capacity (Xu et al., 2016). In addition, Lahijani et al. found that inducing Mg, Al, Fe, Ni, and Ca onto the biochar led to the enhancement of CO_2 capture capacity due to the basic properties of these metals (Lahijani et al., 2018).

6.1.3. Current challenges facing the practical application of biochar-based adsorbents

Although the investigation on biochar for CO_2 capture has attracted considerable attention, there are still great challenges facing the practical application, and more efforts are required as follows:

(1) Compared to the commercial CO_2 adsorbents, the CO_2 adsorption capacity of biochar is still very low and needs to be further improved and optimized. The promising strategies include optimizing the synthesis conditions, selecting suitable feedstocks, creating porous structures, especially micropores, introducing surface function groups, or loading alkali and alkaline earth metals.
(2) Currently, the research on the biochar for CO_2 capture mainly focuses on the simulated gas which is pure CO_2 or a mixture of CO_2

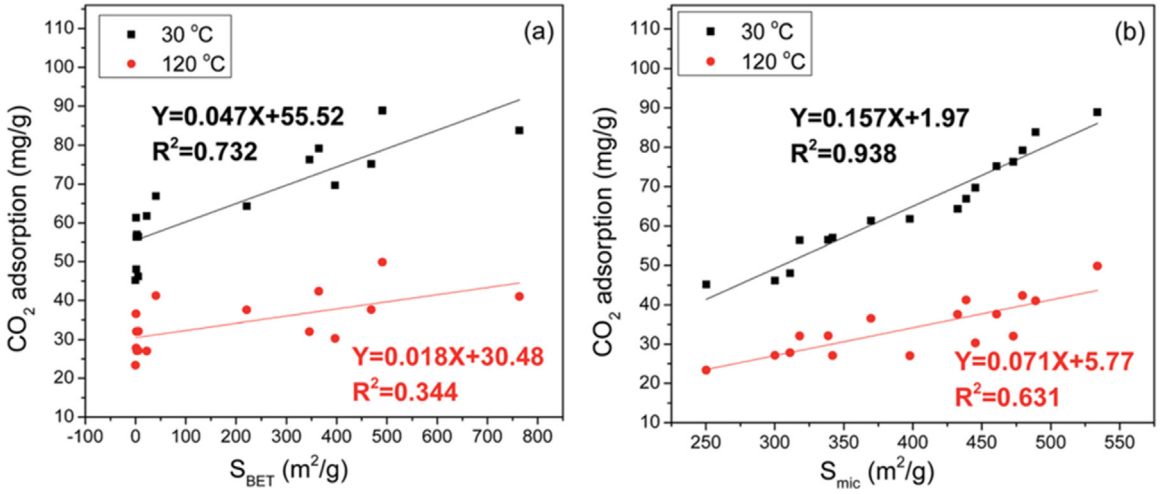

Fig. 6.1. Relationship between CO_2 adsorption capacity and physicochemical properties: (a) SBET and (b) Smic.

and N_2. How about the competitive adsorption of CO_2 compared to other gases? In addition, how about the influence of other containments such as SO_2 and H_2O?

(3) There are four main mechanisms of biochar for CO_2 capture: micropore filling, hydrogen bonding, van der Waals attractions, and Lewis acid-base interactions. To have a better understanding of biochar for CO_2 capture and design efficient physicochemical structures of biochar, it is of great help to have a deep understanding of biochar for CO_2 capture especially the utilization of operando techniques.

6.2. Biochar for energy production through combustion

Biochar, a carbon-rich material derived from the carbonization of biomass wastes, has gained significant attention in recent years for its potential applications in various fields (He et al., 2022; Yuan et al., 2023). With its unique properties such as porous structure, high specific surface area, and high thermal stability, biochar has emerged as a versatile material that can be utilized as a high-performance catalyst for thermal catalysis processes, including hydrothermal, slow pyrolysis, fast pyrolysis, and gasification reactions. Various biochar-based catalysts, such as solid acid, metal-free, and metal loaded catalysts have been developed in recent years. Additionally, biochar is considered a carbon negative material, making it an environmentally friendly option for sustainable energy production and environmental benefits.

Biochar-based solid acid catalyst (BSAC) has been widely used in the hydrolysis of biomass and its derivatives, facilitating the conversion of these renewable substrates into valuable platform chemicals and biofuels through mild hydrothermal reactions. The preparation process typically involves the introduction of sulfonic groups (-SO_3H) onto the biochar surface by using a sulfonating agent (Bhatia et al., 2020; Yue et al., 2020). Bhatia et al. synthesized acidic biochar catalysts by using concentrated H_2SO_4 to attach strong acidic functional groups on the carbon surface (Bhatia et al., 2020). Following acidic treatment, the specific surface area of the biochar decreased from 447 m^2/g to 179 m^2/g, possibly due to the oxidation reaction between carbon and sulfonic molecules, leading to the pores filled with -SO_3H functional groups. The prepared catalysts exhibited high catalytic activity in the production of renewable biodiesel from waste cooking oil through a transesterification reaction. González et al. proposed microwave-assisted heating to strengthen sulfonation and increase the -SO_3H content on the catalyst surface (González et al., 2017). When the sulfonation temperature increases, the corresponding acid density of the catalyst also shows a significant increase, from 3.74 (BS100) to 7.00meq/g (BS140). Consequently, BS140 demonstrated higher yields of biodiesel (90 %) from waste cooking oil at 140°C within a short reaction time (15 min), underscoring the substantial influence of total acidity on the esterification and transesterification of fatty acid methyl ester to produce high-quality biodiesel.

Metal-free biochar catalysts, particularly those that are nitrogen-doped, have shown remarkable catalytic performance. Biochar, a substance obtained through the pyrolysis of biomass, undergoes a complex process where acid intermediates and carbonyl species are produced. These compounds can interact with N species to enable the formation of heteroatom N within the carbon matrix and optimize the electronic structures of the catalysts, ultimately enhancing their efficiency and effectiveness in various chemical processes. Chen et al. prepared N-doped biochar catalysts from bamboo fast pyrolysis at 600°C with flowing NH_3 (Chen, W. et al., 2020). This catalyst has demonstrated the ability to enhance the production of aromatics from bamboo wastes through in situ catalytic pyrolysis. Detailed characterization provides evidence for the formation of N-doped carbon in diverse configurations: pyridinic-N, pyrrolic-N, quaternary-N, and pyridone-N-oxide, exhibiting nitrogen content reaching 3.42 %. The alkaline N-containing groups adsorbed pyrolytic intermediates and then catalyzed them to phenols and aromatics, in which 4-vinyl phenol is the main product with 31 % content, thus greatly improving the quality of bio-oil.

Phosphorus-doped carbon materials also show promise as metal-free catalysts for energy generation through oxidation reactions. The electronegativity of P atoms is lower than that of C atoms, which makes P atoms have a high electron-donating ability and serve as the main active site (Hu, X. et al., 2019). N-, P-, and N, P co-doped carbon catalysts were developed by pyrolyzing pre-treated soluble starch along with urea or/and phosphoric acid. Notably, the P-doped carbon catalyst exhibits high catalytic performance in the aerobic oxidation of benzyl alcohol (at 120 °C with 10 bar O_2 for 24 h), with a high conversion of 89.8 % and an exceptional selectivity of 99 %. The active sites for the oxidation reaction could be attributed to the formation of P-O-C species and the abundant defects induced by P-O doping.

Additionally, boronated carbonaceous catalysts were developed to facilitate the selective conversion of biomass into valuable biomass-derived chemical building blocks, such as furfural and 5-hydroxymethylfurfural (HMF) (Ofrasio et al., 2020). Boron (B), possessing a charge density of 3+, demonstrates a higher ionization potential compared to conventional Lewis acid catalysts such as Al- and Si-based catalysts. The introduction of electron-deficient boron will affect the reactivity of the catalyst, and it can act as a Lewis acid catalyst in various chemical reactions (Liu, W. et al., 2023; Zhou et al., 2022). For B-doped catalyst preparation, boric acid was used as the B precursor, combined with biochar and subjected to calcination at 320°C under an N_2 atmosphere for 5 h (Ofrasio et al., 2020). This study explored the synergistic effects of Lewis acid and Brønsted acid sites generated by boron oxide on the catalyst surface. FTIR spectra revealed B-O stretching vibrations attributed to the formation of either $B(OH)_3$ or B_2O_3, confirming the formation of additional Brønsted acid sites for catalytic reactions. Notably, the catalyst demonstrated high furfural and HMF yields of up to 32 % and 40 %, respectively. Moreover, this catalyst exhibited enhanced recyclability with almost no activity loss after four cycle runs.

Biochar-based catalysts can exhibit significantly improved catalytic performance through the incorporation of noble (Pt, Pd, and Ru) and non-noble metals (Fe, Co, Ni, and Cu) (Maneechakr and Karnjanakom, 2021). Noble metals have demonstrated high efficiency in various reactions such as hydrogenolysis, hydrogenation, and oxidation, particularly in the upgradation of liquid biofuel through mild hydrothermal reactions. A recent study demonstrated the synthesis of glucose-derived biochar with adjustable textural properties through CO_2 activation to support ruthenium (Ru) nanoparticles for converting cellulose to sorbitol, a valuable chemical building block (Rey-Raap et al., 2019). By physically activating the carbon supports derived from glucose, the specific surface area can reach up to 1200 m^2/g, which means a greater direct contact area between metal and carbon supports, thereby creating more active sites. This study underscores the importance of Ru loading, surface area, and acidity of the biochar catalysts in the conversion of cellulose to sorbitol. Ding et al. investigated a N,P-co-doped char (Ru@NP-Char) for the reductive depolymerization of lignin into phenolic monomers (Ding et al., 2022). Melamine (N source) and urea phosphate (N and P sources) were used to modify wood-derived char. The fast electron transfer from Ru particles to the N, P-co-doped char can promote the activation of H_2 and hydrogenate lignin to form monomers, dimers, and oligomers with higher yields. A study comparing the effects of Pd- and Pt -doping on porous carbon derived from Sorghum was conducted in the selective hydrogenation of furfural from biomass to alcohol products (Hu, D. et al., 2019). Different reaction mechanisms were proposed for Pt/C and Pd/C catalysts, with Pd/C showing a preference for transforming the carbonyl group of furfurals into furfuryl alcohol, while Pt/C catalysts acted on the furan ring to produce tetrahydrofurfuryl alcohol.

Non-noble metal-modified biochar catalysts have shown significant potential in enhancing the yield of liquid products during high-temperature pyrolysis reactions. Yuan et al. employed a seaweed char-based support with a high specific surface area (1227.74 m^2/g) to anchor Cu species for the production of high-grade biofuels through the pyrolysis of waste clay oil (Yuan et al., 2021). The Cu-modified

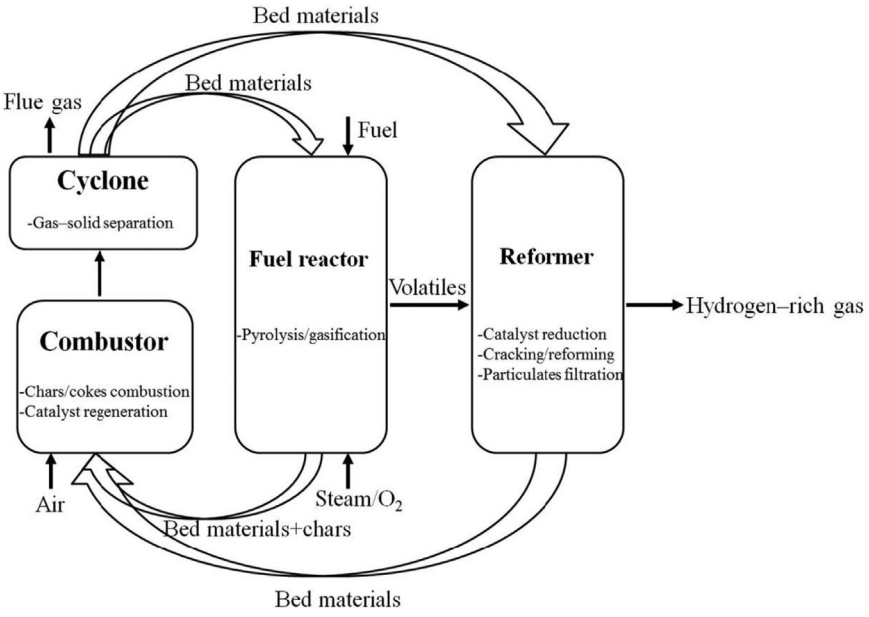

Fig. 6.2. Schematic diagram of DDLG facility (Xiao et al., 2017).

catalysts with 15 % Cu loading were found to promote the decarboxylation of cracked products during catalytic pyrolysis, resulting in the production of high-quality liquid products with a higher heating value up to 48,402 kJ/kg. The catalytic performance of biochar catalysts modified with various metals (Cu, Ni, Zn, or Mg) was systematically studied (Wang et al., 2018). The palm kernel shell (PKS) biochar-based supports were prepared at various temperatures and with different durations of steam activation to optimize their porous structures. Among those catalysts, Mg-biochar exhibited enhanced catalytic performance in the production of aromatics from the mixed PKS/microalgae biomass substrates. Unlike transition metals (Fe, Co, Ni, and Cu), alkaline or alkaline earth metals (Mg and Ca) primarily exist in an oxidized state, offering an abundance of alkaline sites that facilitate the desired reactions (Chen, S.S. et al., 2020; di Bitonto et al., 2020). Wang et al. explored Ni/biochar to further enhance the hydrogenation activity through the optimization of hydrophilicity/hydrophobicity of the catalysts (Wang, Y. et al., 2021). Surface properties play a crucial role in the adsorption/activation of reactants. A two-step treatment of rice husk biochar involving HNO_3 oxidation and subsequent pyrolysis was explored to tailor its overall hydrophobicity. The treated Ni/biochar catalysts predominantly featuring hydrophilic sites favour the adsorption of less polar functionalities such as C=O and C=C bonds in vanillin and eugenol, thereby positively influencing their hydrogenation over the Ni sites. Through systematic research and optimization of catalyst performance, biochar as a carrier supporting various metal species paves the way for the advancement of biofuel production and other catalytic processes.

6.3. Syngas production from biochar reforming

6.3.1. Syngas production from biomass decoupling gasification

Thermochemical conversion is one of the main technical approaches to the utilization of biomass energy (Dayton, 2002), including the pyrolysis of biomass macro molecules, gasification of pyrolysis biochar, steam conversion of gaseous products, secondary cracking of liquid products, oxidation reaction of gas-solid combustible products during gasification. The intermediate and final products are completely mixed under the promotion or inhibition effect of chemical reactions, and it is so difficult to regulate for a single stage of reaction to optimize the overall conversion.

Xu et al. (Xu et al., 2009) and Zhang et al. (Zhang et al., 2010; Zhang et al., 2013) proposed that decoupling ideas could be applied to the field of thermochemical conversion, separating the interrelated chemical reactions through isolation or grading patterns, thereby promoting the improvement of technical effects. The decoupling reaction refers to the pyrolysis of biomass, the reduction of biochar with H_2O/CO_2, and the combustion reaction of gasification biochar, which takes place in different regions. Based on this, many scholars have studied the new thermochemical conversion technology of biomass. Xiao et al. (Xiao et al., 2017) described pine sawdust steam gasification in a novel decoupled dual loop gasification system, as shown in Fig. 6.2. In the system, fuel pyrolysis/gasification, tar cracking/reforming and char combustion are decoupled into three reactors correspondingly, i.e. fuel reactor, reformer Fig. 6.2 and combustor. It has been indicated that the configuration of the system provides an effective way to strengthen the tar cracking/reforming reaction for efficient tar removal. Specifically, a product gas with an H_2 concentration of 40.8 vol. %, dry gas yield of 1.0 Nm^3/kg is obtained at the fuel reactor temperature of 800 ˚C, reformer temperature of 850 ˚C, steam to carbon mass ratio at 1.2 and circulation ratio of 10.

Zhang and Pan (Zhang and Pang, 2017) investigated the correlation between the devolatilization stage and the gasification stage in a 100 kW dual fluidized bed gasifier, as shown in Fig. 6.3(a). The result shows that reaction temperature has a significant impact on the yield and composition of the producer gas from the gasification. With the increase in the reaction temperature, the steam-char reaction is enhanced. At reaction temperatures of up to 750 ˚C, with an increase in CO concentration, more CO_2 could be generated. However, at the higher reaction temperature of 800 ˚C, the equilibrium of water-gas is shifted to the CO side, and thus, CO_2 is consumed, and its yield is reduced.

Combined with the previous studies of biomass cyclone gasification (Sun et al., 2009; Zhao et al., 2012), a composite gasification technology of cyclone pyrolysis-suspension combustion emerged (Zhao et al., 2017). The gasification system mainly consisted of two parts, namely the upper cyclone pyrolysis zone and the lower suspension combustion zone (biochar reduction and combustion), as shown in Fig. 6.3(b). With a secondary air rate (0.20) and bottom air rate (0.50), the gasification efficiency was best, with a gas heating value of 5.15 MJ/Nm^3, carbon conversion rate of 71.50 %, gasification efficiency of 50.80 % and syngas yield of 1.29 Nm^3/kg. Addition of the tar cracking device with biochar

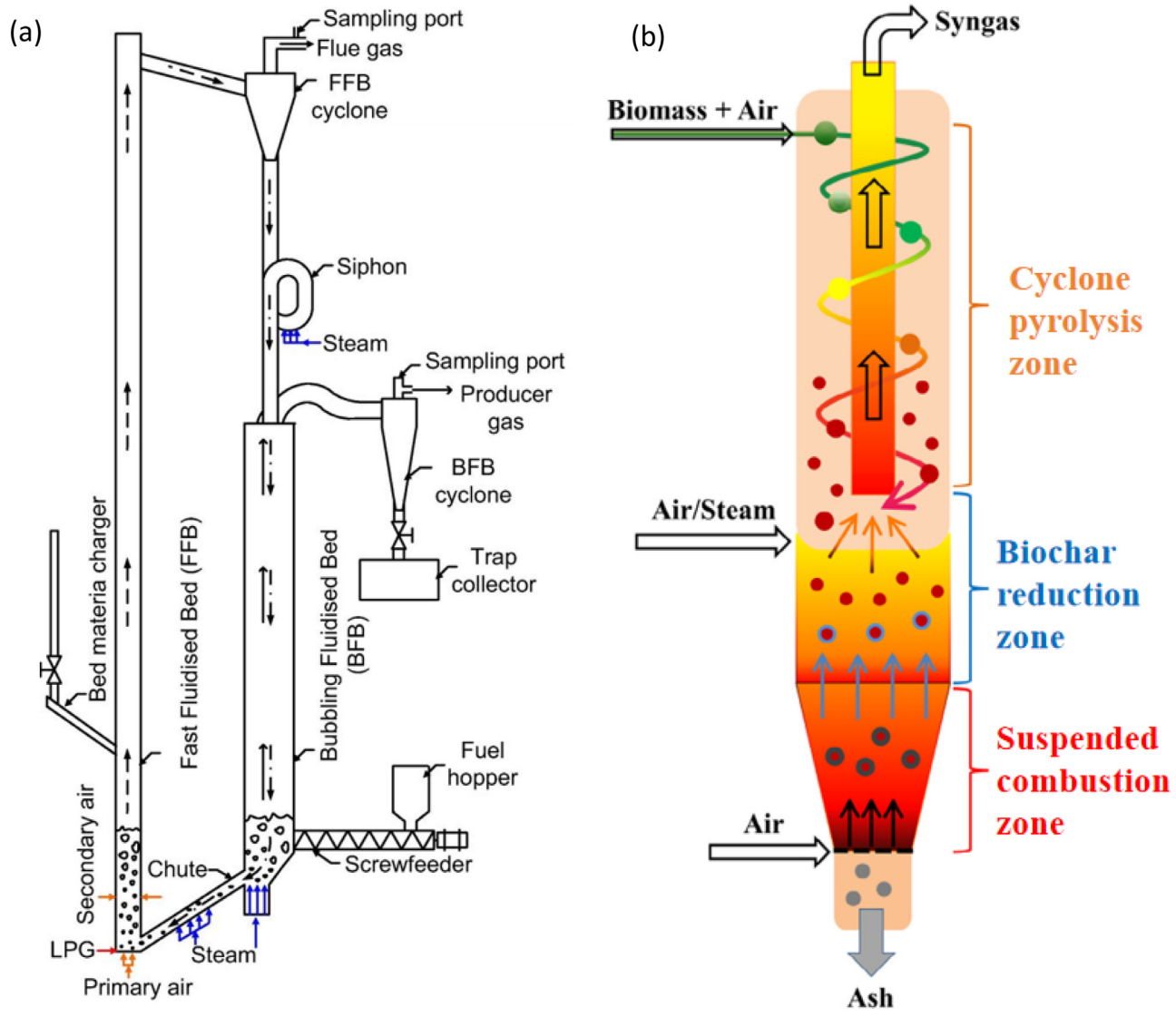

Fig. 6.3. (a) Schematic diagram of dual fluidized bed steam gasifier (Saw et al., 2012; Saw and Pang, 2012); (b) Schematic diagram of cyclone pyrolysis-suspended combustion gasification system (Zhao et al., 2017).

catalyst at the gasifier outlet effectively reduced tar content in syngas, with a minimum value of 1.02 g/Nm^3.

6.3.2. *Catalytic mechanism for biochar gasification*

Gasification, with H_2O/CO_2 as the gasifier agent, is one of the effective thermochemical conversion processes for syngas production (Guan et al., 2016), especially for catalytic gasification (Chun-Zhu and Li, 2006), along with lower emissions of CO_2 and other gaseous pollutants. In previous investigations (Eom et al., 2012; Jiang et al., 2015; Kajita et al., 2010; Lahijani et al., 2013; Yu et al., 2015), it can be seen that the alkali and alkaline earth metallic (AAEM) species, no matter inherent or ion-exchanged in biomass, played a significant catalytic role in producing syngas. According to Shadman et al. (Shadman et al., 1987), the catalytic role of AAEM species would be reflected in three important processes: (i) AAEM redistribution on biochar surface by migration, (ii) loss of AAEM species by vaporization, and (iii) change of biochar structure due to carbon conversion.

The detailed catalytic mechanisms of ion-exchanging AAEMs on biochar during H_2O/CO_2 gasification continue to be developed. Walker and De Lecea (Lecea et al., 1990; Walker et al., 1983) pointed out that the catalytic abilities of AAEM species were different during the gasification of biochar with H_2O and CO_2, due to the various mechanisms between H_2O/CO_2 and biochar. While Meijer et al. (Meijer et al., 1994) observed the result that the effect of K on the H_2O gasification is similar to that on CO_2 one. The AAEM species organically linked to the biomass through ion exchange would promote the biochar gasification to form the gas-liquid-solid products. It can be described that the ion-exchanging AAEM species could enhance the secondary reforming/cracking of macromolecular compounds of volatiles produced from the pyrolysis of biomass and promote their polymerization reactions to form biochar samples with more active physicochemical structures. According to Lang et al. (Lang and Neavel, 1982), K would be mobile and distribute itself during the gasification, and Ca could also be well-dispersed in the sample and transferred to acid sites by ion exchange. Zolin et al. indicated that the AAEM species in wheat straw would volatilize into the gas-phase products and participate in the H_2O gasification reactions of biochar (Zolin et al., 2001). According to Jiang et al. (Jiang et al., 2015), Ca would have a strong effect on the water-gas-shift reaction ($CO + H_2O \leftrightarrow CO_2 + H_2$) of biochar than K. The production of syngas is shown in Fig. 6.4.

According to Perander et al. (Perander et al., 2015), during the CO_2 gasification of biochar, the catalytic effect of Ca was higher than that of

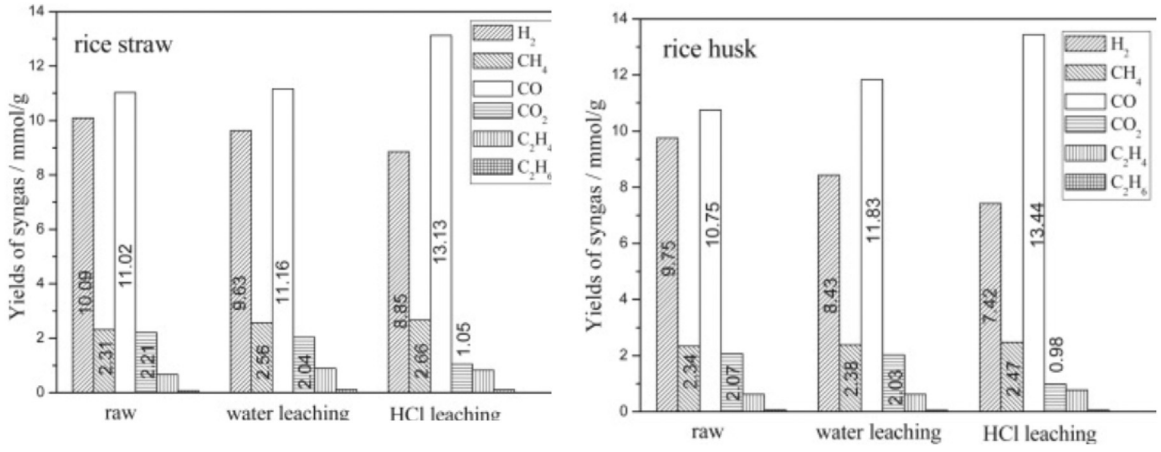

Fig. 6.4. Yields of the syngas of raw and leached samples (Jiang et al., 2015).

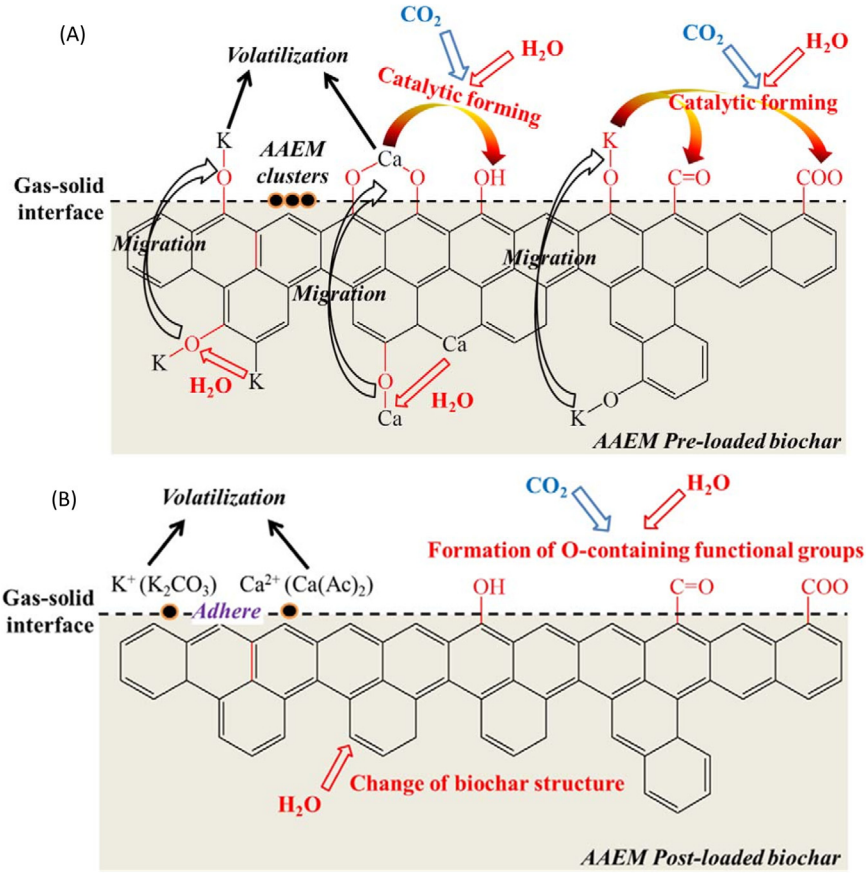

Fig. 6.5. Mechanism of (a) pre-loaded AAEMs and (b) post-loaded AAEMs on biochar (Feng et al., 2018).

K at the early stage of gasification, but the decrease of catalytic ability of Ca would also faster than that of K. The biochar reactivity would be influenced by the ion-exchanging AAEM species, while the differences of biochar initial structures would play an important role during H_2O/CO_2 gasification (Feng et al., 2017). Feng et al. (Feng et al., 2018) obtained more detailed conclusions by loading AAEMs before and after biomass pyrolysis. The results show that the stronger catalytic properties of K and Ca species in the H_2O atmosphere are obtained than those in CO_2. The specific mechanism is shown in Fig. 6.5. The effect of K is mainly on the formation of O-containing functional groups and the transformation from small ring systems to larger ones, while the catalytic effect of Ca is only to increase the proportion of large aromatic ring structures. A better distribution of active sites on biochar surfaces would result in high specific reactivity of biochar during gasification.

6.3.3. Syngas production from biochar as a catalyst for tar reforming

Biomass gasification is gaining attention as a route for the use of biomass energy, but syngas produced by this process usually contain unacceptable levels of tar. Tar control and conversion are key issues for syngas production (Li and Suzuki, 2009). Tar elimination by efficient catalytic conversion by inert carbon-based catalysts an attractive method for commercializing this technique. Feng et al. (Feng et al., 2016) studied the different selectivity of active sites on biochar, the transformation mechanism of biochar structures and the reaction route of tar catalytic reforming. On catalytic reforming of naphthalene and toluene with biochar, in a 15 % H_2O atmosphere, the effect of K is about 10 % greater than that of Ca, while in a pure CO_2 atmosphere, the effect of K is approximately 5 % greater than that of Ca. The specific mechanism is shown in Fig. 6.6.

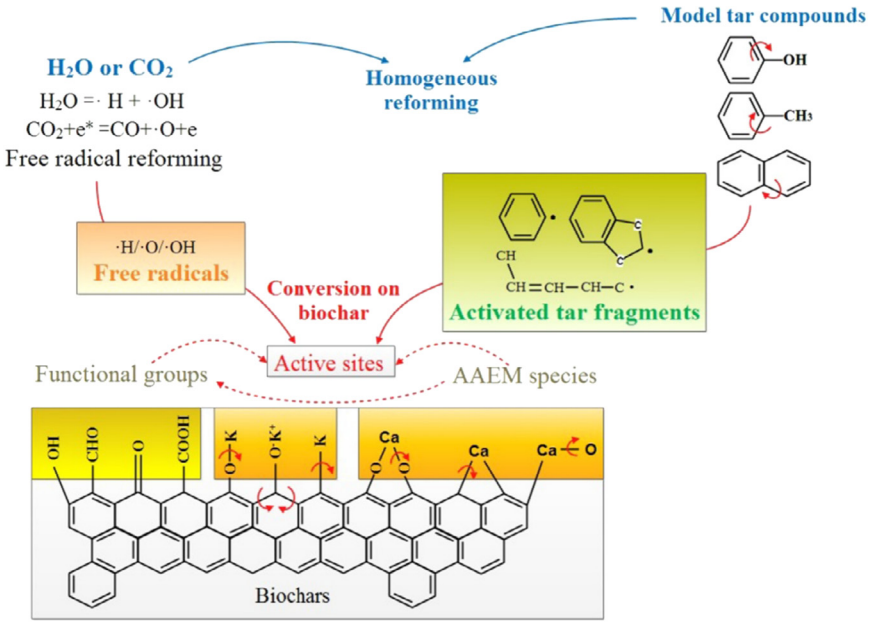

Fig. 6.6. Reforming mechanism of model tar compounds with H-form/K-loaded/Ca-loaded chars under H_2O/CO_2 atmosphere at 800 °C.(Feng et al., 2016).

The biochar surface has a good dispersion of O-containing functional groups and Alkali and alkaline-earth metal species (AAEMs), which makes it excellent for the reforming and removal of tar (Feng et al., 2018; Liu et al., 2020; Stasi et al., 2021; Wang et al., 2022; Zhang, Y. et al., 2022). Wang et al. (Wang et al., 2022) evaluated the role of Ni loading on the biochar surface for the biomass pyrolysis tar reforming. They found that optimum syngas production was obtained with 10 wt. % Ni loaded biochar catalyzing at 650 °C. The addition of 0.3 ml/min of water further improved the hydrogen production. Guo et al. (Guo et al., 2019) explored the effect of different activators on the tar conversion capacity of biochar by employing KOH/ H_3PO_4/$ZnCl_2$ as activators. They summarized that KOH activated biochar had the best catalytic performance for tar removal because of its high surface area and the abundance of metal sites. Chen et al. (Chen et al., 2012) explored the gas-liquid-solid three-phase product characteristics of corn straw pyrolysis with increasing pyrolysis temperature using a packed bed reactor. The hydrogen yield began to increase significantly when the pyrolysis temperature was raised above 600°C. Sun et al. (Sun et al., 2023b) used a two-stage reaction system to investigate the biochar catalytic reforming of corn straw pyrolysis tar. Results show that with some parameter settings, tar is almost completely removed, and the H_2 yield reaches the highest 0.197 L/g. The addition of steam also promotes the reforming of methane steam and the water-gas shift reaction. The H_2 yield is significantly increased. The gas yield data graph is shown in Fig. 6.7.

During the tar reforming, coke inevitably builds up, coating the reactive sites and plugging the pore structure, leading to a degradation of the biochar's catalytic efficiency (Bracciale et al., 2019). The administration of a certain amount of oxygen during tar reforming can help to facilitate the conversion of tar while inhibiting the formation of coke. Many scholars have investigated the effect of oxidation regulation. Lind et al. (Lind et al., 2011) conducted research on the continuous catalytic reforming of biomass gasification tar with $FeTiO_3$ catalysts accompanied by oxidation regeneration at 800°C. They found that the coke deposition can be continuously decomposed by oxidation, thus maintaining the catalyst's activity. Yu et al. (Yu et al., 2016) experimentally studied the partial oxidation's effect on sewage sludge char-catalyzed pine pyrolysis tar reforming. They found that the highest yields of CO and H_2 could be achieved after catalytic reforming at an oxygen equivalent ratio of 0.05, while the tar removal efficiency could reach 98.34 %. Sun et al. (Sun et al., 2023a) investigated the regulation of partial oxidation in biochar catalyzed gasification tar reforming. The results reveal that partial oxidation regulation (0.2 %-0.4 % O_2) can potentially maintain the biochar's catalytic efficiency and facilitate the production of hydrogen in gas (Fig. 6.8). The H_2 yield is also increased to a maximum of 0.523 L/g. When the O_2 concentration is further enhanced (~0.6 %), more H_2 is consumed by oxygen, the H_2 yield is reduced, and the tar conversion capacity of biochar is significantly weakened.

6.4. Biochar for soil amendments

As a typical negative carbon technology, the application of biochar to soil would effectively improve the soil environment and promote crop growth. The regulated pore structure and abundant surface functional groups make it functional in improving soil aggregate structure and retaining water and fertilizer. According to the effect of biochar, its application can be divided into the following four parts: soil characteristic regulation, microbial community improvement, greenhouse gas emission reduction and nutrient increase.

6.4.1. Soil characteristic regulation

The nutrient transport and crop growth of soil are directly affected by its physical and chemical characteristics, and long-term continuous cropping and irrigation will lead to soil compaction, organic matter loss, water retention decline, and other problems. Due to the abundant pore structure and surface functional groups, the application of biochar to soil can effectively improve soil permeability and water retention and enhance soil water absorption capacity and infiltration performance, which is of great significance for water management under agricultural drought conditions. Santos et al. (Araújo Santos et al., 2022) investigated the effect of different biochar on the water-holding capacity (WHC) of sandy soil and found that sugarcane and green coconut biochar would improve the water retention and nutrient transport in the sandy soil by increasing the soil porosity and water transmission. Previous research proved that biochar would present hydrophobic or hydrophilic depending on the presence of different surface functional groups, such as hydroxyl (OH) and alkyl aliphatic (CH) groups (Kamali et al., 2022). The soil environment can be effectively regulated by the addition of biochar, which is conducive to formulating regulatory strategies for the growth environment required by different crop growth cycles. Mao et al. (Mao et al., 2019) compared the effect of biochar with

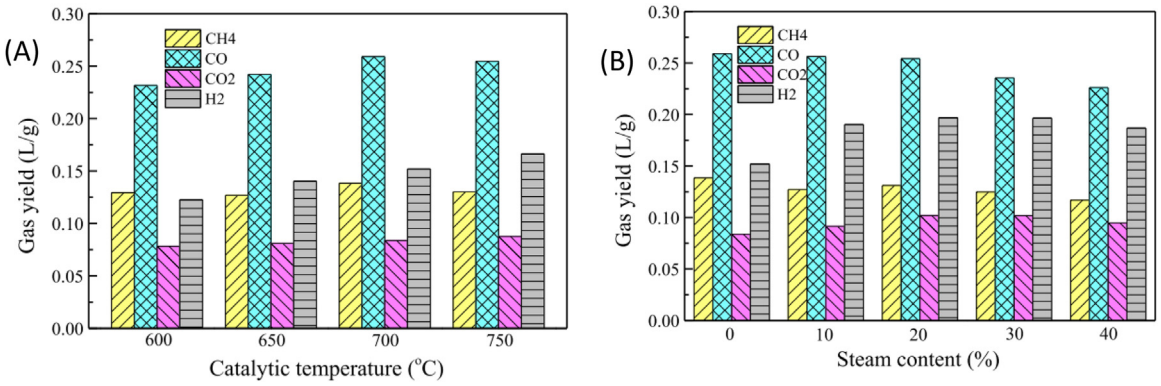

Fig. 6.7. (a) Gas component yield under the influence of catalytic temperature (pyrolysis temperature: 800 °C). (b) Gas component yield under the influence of steam addition (pyrolysis temperature: 800 °C; catalytic temperature: 700 °C).

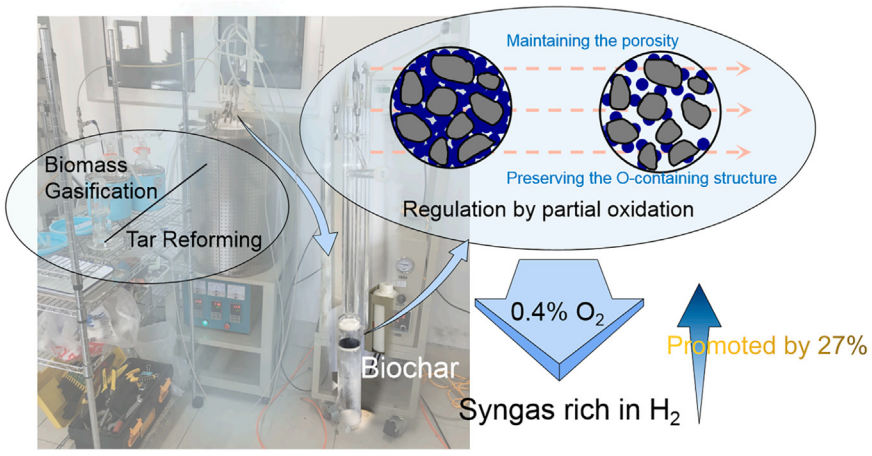

Fig. 6.8. The regulatory mechanism of partial oxidation for biochar-catalyzed biomass gasification tar reforming.

different feedstocks and pyrolysis temperatures to investigate the internal relations of surface functional group distribution characteristics and WHC of biochar and found that increasing the pyrolysis temperature would reduce the content of oxygen functional groups and total organic carbon, which had an obvious effect on barren soil. Xing et al. (Xing et al., 2021) investigated the effect of different biochar percentages on soil water-holding capacity and proposed a multi-objective optimization model to reveal the mechanism. The results illustrated that the addition of biochar would reduce the soil cumulative infiltration and increase the irrigation efficiency. Thus, exploring the mechanism of biochar on soil WHC regulation would improve the soil environment and realize real-time control.

Besides, the application of biochar would influence the soil pH value and salinization with the presence of mineral constituents and pore structure. The exchange of alkali metals and mineral salts with H^+ and Al^{3+} would reduce the ion concentration in the soil, helping to neutralize the acidity of the soil and providing a more suitable growth environment for plants. Shi et al. (Shi et al., 2018) investigated the effect of biochar in increasing the pH buffering capacity of soil and found that the decrease in soil pH and aluminum toxicity was inhibited with the addition of biochar. The main mechanism for the increased pH buffering capacity was the carboxyl protonation. The surface negative charge and microporous structures of biochar ensure the cation adsorption capacity (such as K^+, Ca^{2+} and Mg^{2+}) in the saline-alkali soil treatment. The application of biochar can increase the organic carbon content and ion exchange capacity, reduce the pH and alkalinity degree by adsorbing Cl^- and CO_3^{2-} in the saline-alkali soil, and enhance the nutrient retaining ability. Zhao et al. (Zhao, W. et al., 2020) established a biochar-alkali soil-corn system model and investigated the effectiveness of biochar in improving soil nutrient availability, and found that the application of biochar would promote the formation of soil aggregates and reduce crop salt stress by reducing Na^+ content. Furthermore, the removal of excess Na^+ on soil aggregates would activate the unused phosphorus, iron, calcium and other elements in saline-alkali soil, which plays a positive role in reducing the physiological deficiency of plants (Li and Li, 2022; Zhang, P. et al., 2022).

6.4.2. *Microbial community improvement*

The soil microbial community not only affects plant growth and human health but is also the main source of soil carbon emissions. The addition of biochar can change the soil properties and affect the diversity and activity of soil microorganisms (Xu et al., 2023). Previous research showed that the pore structure of biochar provided shelter for microorganisms, affecting soil ventilation and water retention through macropores and promoting the transport of nutrient molecules through mesoporous and micropores (Yang et al., 2022). This can promote the activity of beneficial microorganisms, such as azotobacter and phosphorolytic bacteria, which can indirectly promote the growth and development of plants (Fig. 6.9). Xu et al. used structural equation modelling to analyze the effect of biochar on microbial community structure and function and found that biochar can improve the stability of the microbial community and the increasing pyrolysis temperature would enhance the effect. Besides, the shelter of biochar to microorganisms can avoid the toxicity of soil pollutants and increase the abundance of microorganisms (Bamminger et al., 2014). Yan et al. (Yan et al., 2021) investigated the effect of biochar on microbial community structure with a 24-month field experiment and found that the addition of biochar increased the complexity of the microbial community. Li et al.

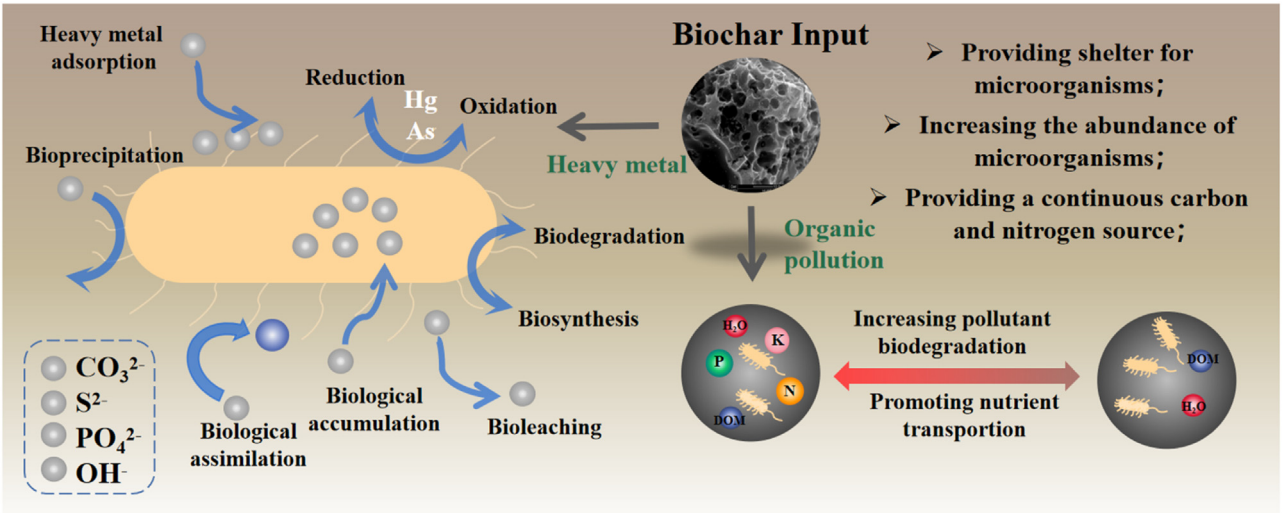

Fig. 6.9. The effects of biochar on soil microbial community improvement.

(Li et al., 2019) studied the effect of biochar on alleviating the toxicity stress of microorganisms caused by polycyclic aromatic hydrocarbons and found the addition of biochar would modulate the total organic carbon and N contents and insulate contaminant contact.

Furthermore, the insoluble organic and inorganic matter of biochar will be adsorbed by microorganisms and promote the proliferation of microbial communities. With the increasing abundance of microbial communities, the aromatic ring carbon structure will be further decomposed, providing a continuous carbon and nitrogen source for microbial reproduction (Li et al., 2022). Quan et al. studied the organic product emission characteristics during biotic ageing and found that biochar had a positive influence on microbial population size, and the organic components like humic acid leaching increased during ageing. Pei et al. (Pei et al., 2021) investigated the long-term effects of biochar on soil organic carbon and microbial activity through the $H_2{}^{18}O$-DNA incorporation method. The results illustrated that biochar ageing would increase microbial carbon use efficiency and promote the microbial carbon utilization cycle due to the increasing pH value of soil during ageing. Then, the contents of soluble carbon black and alkali metal are different in different biochar, such as the dissolved organic matter (DOM) of bamboo at 300 °C (32.33 mg/g) was much higher than coconut (18.47 mg/g), and the content continuously decreased with the increasing pyrolysis temperature (Cao et al., 2022). Exploring the biomass pyrolysis process can customize the physicochemical properties of biochar for different soil needs.

6.4.3. *Greenhouse gas emission reduction*

The application of biochar to soil will indirectly affect the release rate of greenhouse gases such as CO_2, N_2O and CH_4 in the soil (Tao et al., 2023). Regulating the physicochemical properties of biochar can sequester organic carbon and regulate soil greenhouse gas emissions. As for CO_2, the emission of soil consists of the respiration of soil plants, animals and soil. The addition of biochar can improve the water-holding capacity and fertility of soil because of the large surface area and excellent pore structure. The increasing content of carbon and nitrogen creates an environment suitable for the growth and reproduction of microorganisms, thereby improving the activity and respiratory capacity and increasing soil CO_2 emission. Then, due to the high carbon content of biochar, its oxidation effect will increase CO_2 emissions during ageing. Wang et al. (Wang, Lin et al., 2021) investigated the effect of biochar on soil CO_2 emission during ageing and found that the soil minerals would accumulate on the surface of biochar, and the CO_2 and N_2O emission would be continuously inhibited during ageing. In addition, soil pH value increases due to the application of biochar, which will change the microbial community structure in the soil and increase the ratio of bacteria to fungi, thus accelerating the release of soil CO_2. Sheng et al. (Sheng and Zhu, 2018) studied soil CO_2 emission under different pH levels and found that the addition of biochar would increase the DOM utilization and microbial activity, and the increased pH value would enhance the effectiveness of biochar in promoting CO_2 emission. From the perspective of the long-term application of biochar, the soil carbon emission will be effectively reduced because of the decreasing DOM content of biochar in the later period of application; the utilized components will decrease and soil carbon mineralization will be reduced (Hawthorne et al., 2017).

6.4.4. *Nutrients increasing*

The application of biochar can reduce fertilizer utilization and improve nutrient-absorbed efficiency. Carbon-based fertilizers can absorb heavy metals and pesticide residues in soil, which has a positive effect on promoting crop growth and improving crop yield and quality. Liu et al. (Liu, L. et al., 2019) investigated the migration transformation mechanism of nutrient elements and found that the addition of biochar to soil would promote the conversion and absorption of nutrients and supply material conditions for microorganism growth. Due to the characteristics of biochar's easy doping modification, modified biochar can be customized according to different needs. Zhao et al. (Zhao et al., 2024) compared the effect of different biochar on the N, P transformation mechanism and found that plenty of inorganic minerals contained in pig manure and straw co-pyrolysis biochar, the application would increase the total N, P content and promote the conversion to rapidly available minerals. Besides, the surface functional groups and structure will collapse and decompose because of biochar ageing during the long-term application, resulting in the slow release of the internal substances in the soil. The slow-release fertilizer designed based on this mechanism can effectively the absorption efficiency of plants and maintain the soil nutrient content (Fig. 6.10). An et al. (An et al., 2021) developed a new slow-release fertilizer through integrated co-pyrolysis and coating and found that the biochar-based fertilizer would increase the cumulative release concentration of P from 1.68 % for 30 days to 1.14 g/L for 60 days, promote seedling development by 32 %. Fachini et al. (Fachini et al., 2022) evaluated the release of potassium (K) from biochar-based fertilizer enriched with K ions in different forms and found that the slow-release fertilizer would reduce the release rate by up to 77 % compared to pure KCl mineral fertilizer, the release rate would be affected by the particle size and the water content.

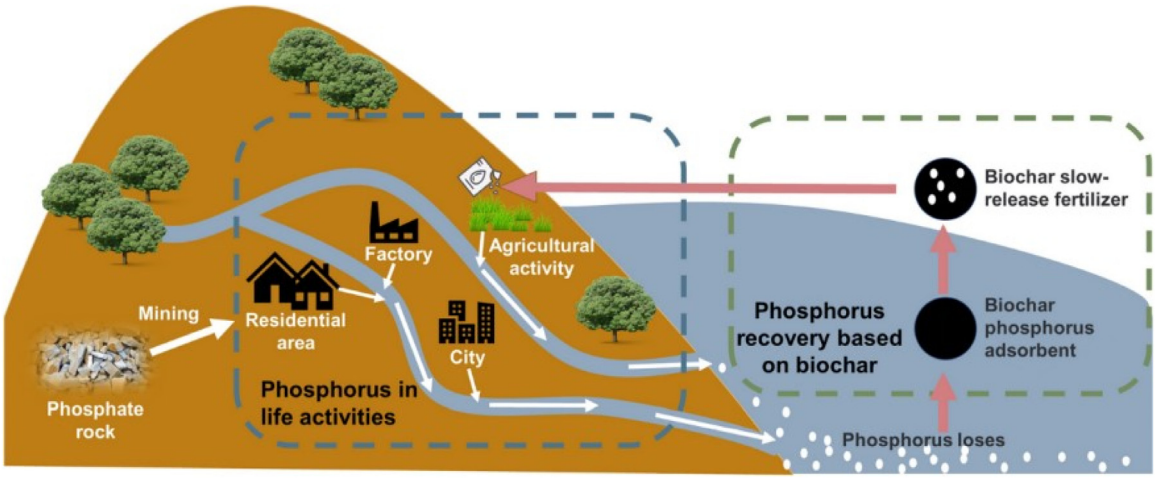

Fig. 6.10. The element release route of phosphorus based slow-release fertilizer (Luo et al., 2023).

6.5. Biochar for contaminant adsorption

In recent years, with the rapid development of industrialization and urbanization, a large amount of wastewater containing heavy metal ions (such as Hg, Cr, Pb, Cd, etc.) has been discharged into nature without complete treatment, seriously affecting the ecology and human health. Excessive intake of heavy metal elements may lead to osteoporosis, skin disease, cardiovascular and cerebrovascular diseases, and even cancer (Asere et al., 2019; Hu et al., 2016; Sherlala et al., 2019). Biochar, as an economic, green and simple adsorbent material, has been widely used in the treatment of heavy metal ions.

6.5.1. Hg removal

Hg is a highly mobile and potent neurotoxic substance, and the Minamata disease incident in Japan in 1956 was caused by Hg poisoning (McNutt, 2013). In order to improve the adsorption capacity of biochar, numerous research has been carried out, and chemical modification is one of the most common methods. Research has shown that the chemical reaction between sulfur and the surface of activated carbon can promote the formation of thiophene, sulfoxide, sulfone, and disulfide groups, which have a higher affinity for mercury (Hadi et al., 2015). Huang et al. (Huang et al., 2019) prepared sulfurized biochar from sublimed sulfur and corn stalks as raw material by co-heating method to remove Hg^{2+}. The result showed that the main forms of sulfur on the sulfurized biochar were alkyl thioether, sulfonyl, thiophene, and inorganic sulfur. Among them, the complexation of C=S and sulfoxide groups with Hg^{2+} to form stable Hg-S and Hg-O bonds is the main reason for the improved adsorption capacity of biochar by sulfurization. The maximum adsorption capacity of biochar for Hg^{2+} increased from 117.7 mg/g before sulfuration to 268.5 mg/g. Park et al. (Park et al., 2019) prepared sulfurized wood biochar (SWB) by directly impregnating elemental sulfur. Compared to the original wood biochar (WB), the higher adsorption capacity of SWB for Hg^{2+} is not only related to the original Hg-Cπ bond but also to the interaction between C-SO_x-C and thiophene groups generated by sulfurization. Benefited by the abundant functional groups, the adsorption performance also improved from the original 57.8 mg/g to 107.5 mg/g. Subsequently, Jeon et al. (Jeon et al., 2020) prepared sulfur-modified pine needle biochar by impregnation method, which further confirmed the promoting effect of thiophene groups generated by sulfurization on Hg^{2+} adsorption. In addition to using elemental sulfur as a sulfur source, organic and inorganic compounds of sulfur can also be used for the sulfurization of biochar. Huang et al. (Huang et al., 2023) used 3-mercaptopropyltrimethoxysilane (3-MPTS) as a thiolation agent to impart more surface S, Si, O, and N elements, as well as more surface negative charges, and more surface defects. This improved the chemical binding process of Hg at the biochar interface, thereby enhancing the adsorption rate and capacity of the adsorbent. Furthermore, the presence of thiol groups can combined with Hg^{2+} and CH_3Hg^+ to promote monolayer adsorption. The results of the performance test showed that thiol modification increased the adsorption capacity for Hg^{2+} and CH_3Hg^+ by 14 times and 19 times, respectively. The surface functional groups of biochar modified with different sulfur sources are shown in Fig. 6.11.

The combining of biochar with magnetic materials is one of the most commonly used methods to improve the recovery efficiency of adsorbents. Li et al. (Li, R.H. et al., 2020) immersed wheat straw in $FeCl_2$ and $FeCl_3$ solutions, followed by calcination and ball milling to obtain magnetized biochar. The adsorbent exhibited excellent adsorption performance (127.4 mg/g) and recovery capacity for Hg^{2+}. Lim et al. (Lim et al., 2023) prepared rice straw-derived biochar by soaking it in iron chloride and ferrous chloride solutions. Unlike the method used by Li et al. (Li, R.H. et al., 2020), the subsequent magnetic adsorbent was prepared by co-precipitation of sodium hydroxide with the mixed solution. The advantage of this scheme is that no heating operation is required during the preparation process. Similarly, combining magnetic materials can also be used to improve recovery efficiency. Mahmoud et al. (Mahmoud et al., 2021) combined magnetic manganese ferrite nanoparticles ($MnFe_2O_4$) with grape stalk biochar (AGB) to obtain an adsorbent with nanometer particle size. The material exhibited a high removal rate of 94.6 % for trace Hg^{2+} (10 mg/L).

6.5.2. Cr removal

Cr has a significant impact on human health, and studies have found that concentrations of Cr in the human body reaching 0.1 mg/g of body weight can cause extreme physical damage or even death (Welling et al., 2015). However, the emission of Cr ions in factories is very high, and it is crucial to reduce treatment costs and enhance the economic advantages of biochar. China's liquor industry generates a large amount of distiller's grains waste every year. Utilizing these waste materials to prepare biochar, achieving the effect of "treating waste with waste," can serve as a new approach to green production. Dong et al. (Dong et al., 2023) used distiller's grains as the raw material for biochar and alkaline solutions (KOH, NaOH, K_2CO_3, etc.) as activators to prepare low-cost, high-adsorption-performance adsorbents with a maximum adsorption capacity of 144.5 mg/g. The team then explored the effect of different proportions of KOH as an activator on the adsorption performance of biochar. The prepared biochar adsorbent was applied to treat wastewater discharged from actual wet-process phosphoric acid production, achieving an adsorption capacity of 426.0 mg/g (Su et al., 2024). Murad et al. (Murad et al., 2022) used peanut shells from household waste as

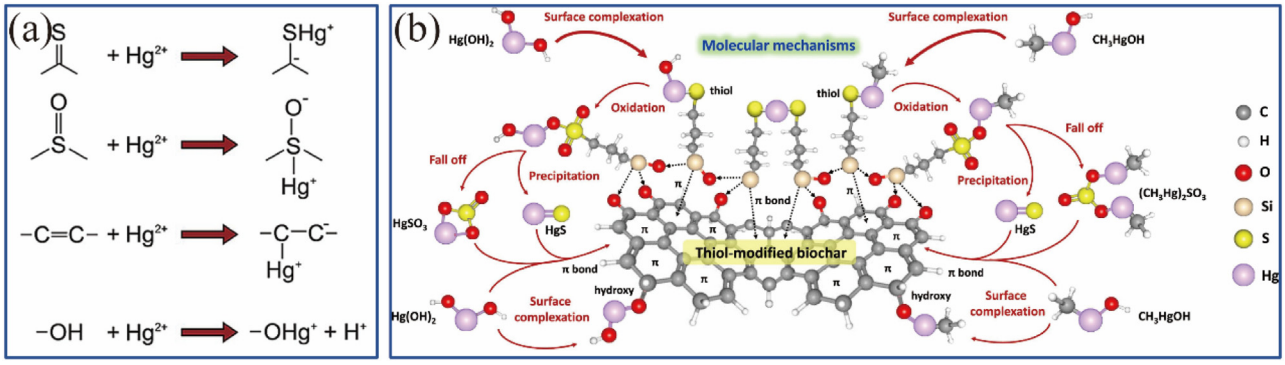

Fig. 6.11. (a) Schematic diagram of the binding of different functional groups with Hg^{2+}(Huang et al., 2019); (b)Underlying molecular mechanisms for Hg^{2+} and CH_3Hg^+ removal (Huang et al., 2023).

the raw material and cetyltrimethylammonium bromide (CTAB) as the activator to prepare engineered biochar that achieved a Cr(VI) removal rate of 79.35 %.

Moreover, the adsorption performance of biochar for Cr is closely related to the activating agent. Truong et al. (Truong et al., 2024) believe that $KHCO_3$, as a weak alkaline salt, has lower corrosivity compared to other activators such as KOH and NaOH, and has the potential for safer and larger-scale applications. The activated biochar has a higher specific surface area and richer binding sites, increasing its adsorption performance from 18.2 to 153.8 mg/g. In addition to alkaline substances, acidic materials can also serve as activators. Lu et al. (Lu et al., 2021) used phosphoric acid to activate biochar, followed by ammonia modification treatment, which resulted in a certain degree of increase in specific surface area and pore volume. The -NHCO-, P=O, and C=N functional groups generated during the modification process were all involved in the removal of Cr(VI). The removal rate of Cr(VI) by the acidified biochar was 76.73 %, while it increased to 85.67 % after ammonia modification.

6.5.3. Pb removal

Due to its significant health hazards to humans, especially infants and young children, lead is classified as the second most toxic metal in the world and is included in the priority list of hazardous substances. Plenty of cases of mental retardation in children are caused by excessive Pb intake (Bellinger et al., 2017). Study shows that the pyrolysis temperature used during the preparation of biochar has a significant impact on Pb adsorption performance. Xu et al. (Xu et al., 2021) prepared phosphorus-containing biochar (BCP) by co-pyrolysis of poplar sawdust and potassium dihydrogen phosphate at 300, 500, and 700 °C. The study found that the higher the pyrolysis temperature, the larger the specific surface area and pore volume of the biochar. However, the adsorption performance did not increase with the temperature due to the higher complexation ability of the $(PO^{3-})_n$ chain generated at 300 °C with Pb^{2+} compared to the P-O-C and C-P bonds formed at 500 and 700 °C. Yun et al. (Yun et al., 2022) pyrolyzed corn stalks at 200 and 600 °C to prepare biochar, and the results also showed higher adsorption performance for Pb^{2+} at the relatively lower pyrolysis temperature of 200 °C. However, the reason for this was different from Xu et al.'s study. This study found that the higher the temperature, the lower the O content in the biochar. The O content is related to the number of oxygen-containing functional groups, and the more oxygen-containing functional groups, the stronger the complexation ability with Pb^{2+} and the better the adsorption performance. In another study, Zhang et al. (Zhang et al., 2020) explored the pyrolysis process of MgO-coated watermelon peels at different temperatures. The specific surface area of the prepared biochar decreased from 293 m^2/g at 600 °C to 59.8 m^2/g at 700 and 800 °C. The adsorption capacity for Pb^{2+} also varied with the temperature, increasing from 81.7 mg/g at 400 °C to 558 mg/g at 600 °C and then decreasing to 368 mg/g at 800 °C.

Moreover, the selection of modification methods and materials also affects the adsorption capacity of biochar for Pb. Ahmed et al. (Ahmed et al., 2021) used H_2O_2 as a green modifier to oxidize and modify biochar prepared from watermelon seeds (HP-BC). The modified biochar had more oxygen-containing functional groups compared to the unmodified biochar, increasing its adsorption capacity from the original 44.32 mg/g to 60.87 mg/g. Similarly, Li et al. (Li, S.H. et al., 2023) prepared biochar from rice straw modified with calcium mercaptoacetate (SRBC). Unlike using H_2O_2 as a modifier, this method resulted in an adsorbent surface with not only oxygen-containing functional groups but also sulfur-containing functional groups, calcium oxalate, and calcium carbonate. The modified biochar had nearly double the adsorption capacity for Pb^{2+} compared to the original biochar, with a maximum adsorption capacity of 124.92 mg/g. The adsorption mechanisms of Pb^{2+} by the two modified biochar are shown in Fig. 6.12. In addition to modifying the prepared biochar, it is also possible to modify the biochar by preprocessing the raw material. Shen et al. (Shen et al., 2021) first immersed bamboo powder in ammonium persulfate solution, followed by drying and roasting to obtain biochar containing N and O functional groups. This adsorbent had an adsorption capacity for Pb^{2+} of up to 175.22 mg/g.

6.5.4. Cd removal

Cd is one of the most common pollutants in industrial wastewater, which causes significant harm to human kidneys and bones and has been listed as a priority pollutant by the United States Environmental Protection Agency (Sharififard et al., 2018; Yin et al., 2021). The treatment of Cd by biochar is affected by many factors, such as raw materials, pyrolysis temperature, and modification methods. Lyu et al. (Lyu et al., 2023) conducted a detailed study on LDH-based magnetic biochar (LMBC) prepared under different influencing factors, including layered double hydroxide (LDH) loading rate (LLR), pyrolysis temperature, and biomass source. This study found that biochar obtained at higher pyrolysis temperatures had a higher specific surface area, and the number of metal/O groups increased with the increase in LLR. The LMBC produced at a 2:1 LLR and 800 °C pyrolysis temperature exhibited the maximum adsorption capacity, which was more than twice that of the LMBC produced at a 0.5:1 LLR and 400 °C pyrolysis temperature. Additionally, LMBC extracted from bamboo showed superior adsorption performance compared to LMBC derived from sewage sludge and garlic. Wu et al. (Wu et al., 2022) found that with the pyrolysis temperature increased, the inherent minerals of the biochar gradually enriched, surface functional groups decomposed, and more structural defects formed at the edges of the graphite-like structure. Biochar prepared at higher temperatures had more significant advantages in complexation and ion exchange with Cd^{2+}.

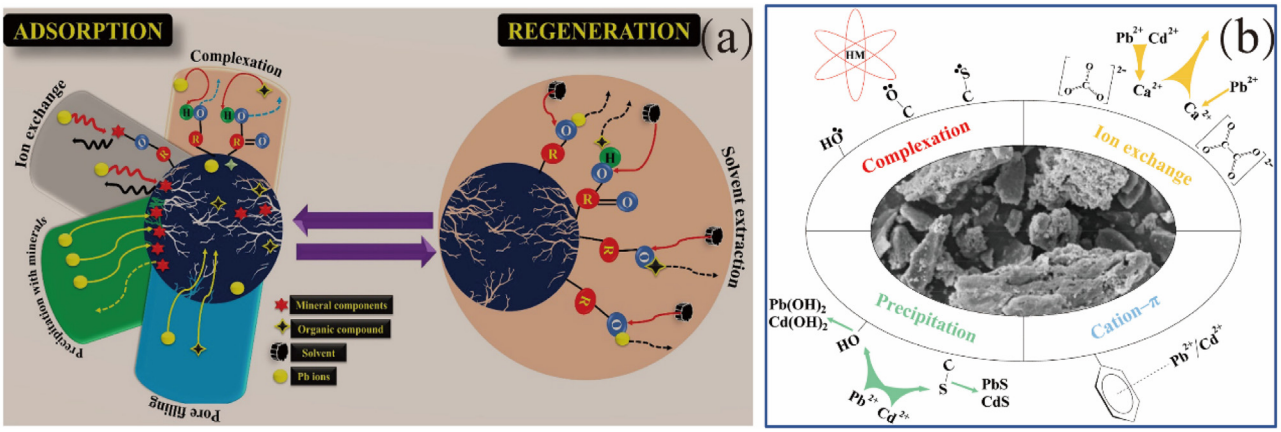

Fig. 6.12. Possible mechanisms of Pb(II) sorption onto (a) HP-BC (Ahmed et al., 2021) and (b) SRBC (Li, S.H. et al., 2023).

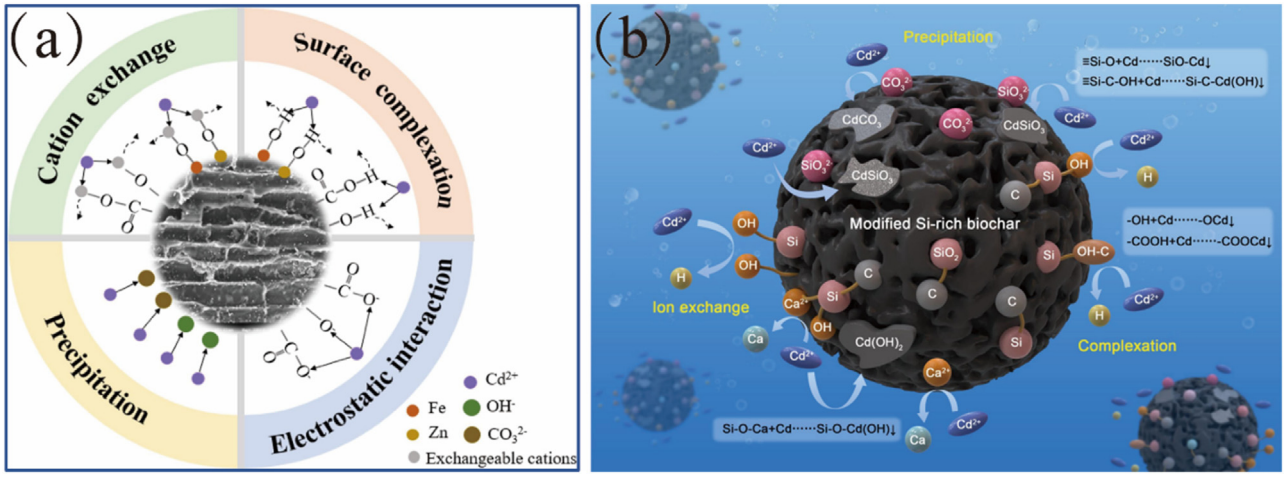

Fig. 6.13. The Cd(II) adsorption mechanism of (a) Fe/Zn-BC (Yang et al., 2021) and (b) MSiWB (Liu, L.A. et al., 2023).

Yang et al. (Yang et al., 2021) used Fe/Zn metal materials as modifiers to optimize Robinia pseudoacacia biochar (RBC) and Durio zibethinus shell biochar (DBC). The resulting CO_3^{2-}, Fe-O, Zn-O, and oxygen-containing functional groups could complex with Cd^{2+}. The maximum adsorption capacity of Fe/Zn-RBC and Fe/Zn-DBC for Cd^{2+} increased by 5 times and 3 times, respectively, compared to the unmodified biochar. In another study, calcium silicate was used as an inorganic modifier for biochar modification. Modified wood biochar (MSiWB) was able to chemically react with Cd^{2+} to form Si-Cd compound precipitates. Some Cd^{2+} was removed through cation exchange with Ca^{2+} or complexation with surface functional groups (Si-O, Si-C). The adsorption efficiency significantly increased from the original 23 % to 57 % after modification (Liu, L.A. et al., 2023). The adsorption mechanisms of Cd^{2+} by the two inorganic material-modified biochar are shown in Fig. 6.13.

6.6. *Biochar for other pollutants removal (e.g. dye, mercury and dioxins)-Biochar for pollutant removal in water*

Biochar for water treatment through adsorption and catalysis has emerged as a highly active and influential research area, as demonstrated by over 7000 publications in the past 15 years (up to May 2024, Fig. 6.14, Web of Science). These studies have garnered an average of more than 30 citations each, underscoring the significant attention and impact this field has achieved within the scientific community.

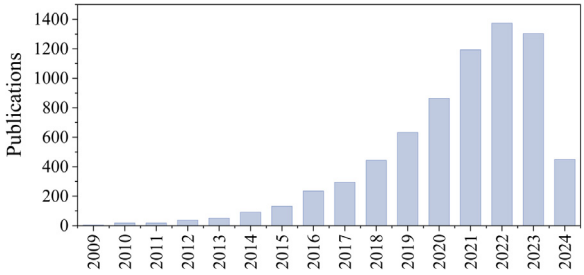

Fig. 6.14. The number of publications from 2009 to 2024 based on a Web of Science search using the terms “Biochar” and “Water treatment”.

6.6.1. *Usages of biochar as absorbers*

Lignocellulosic biomass, such as agricultural and forestry wastes (e.g., hardwood), which contain cellulose (25–50 wt. %), hemicellulose (15–40 wt. %), lignin (10–40 wt. %), and inorganic minerals, were widely used to create biochar for water treatment (Minh et al., 2020; Wan, Z.H. et al., 2021). Lignocellulosic biomass materials are preferred for water treatment because they develop specific pore structures during pyrolysis. The expansion of cellulose, hemicellulose, and lignin results in the formation of numerous micropores, creating a low-density, porous structure suitable for adsorption (Cheng et al., 2022). The porosity of

biomass carbon influences its surface area, which affects the adsorption and transfer of molecules. Additionally, micropores play a crucial role in the adsorption of minerals and pollutants (Xu, Z.B. et al., 2022). Non-lignocellulosic materials derived biochar, including municipal sludge, food residues, and livestock manure, were rich in heteroatoms like N and P (Zhang et al., 2024), exhibited quite different pollutant removal properties with those lignocellulosic feedstocks. Deng et al. developed a cyanobacteria-derived biochar (CN-BC)/PMS system that achieves ultrafast degradation of electron-rich emerging pollutants via a non-radical mechanism dominated by singlet oxygen ($^1O_2$), enhanced electron delocalization, and abundant defect sites, demonstrating strong potential for continuous-flow advanced oxidation processes (Deng, J. et al., 2024). Zhou et al. reviewed sulfate radical-based advanced oxidation processes (SR-AOPs) for the simultaneous removal of antibiotic-resistant bacteria (ARB) and antibiotic resistance genes (ARGs), highlighting various persulfate activation strategies using biochar (Zhou, X. et al., 2024). The study also analyzed key influencing factors and degradation mechanisms, providing valuable guidance for the development of effective SR-AOPs in combating antibiotic resistance in environmental systems. The application of different feedstocks derived biochar for pollutant absorption was summarized in Table 6.1. Despite the good absorption effects on pollutants, it should be noted that the biochar used is difficult to recycle due to the blockage of the absorption sites.

6.6.2. *Usages of biochar as catalysts in advanced oxidation processes*

6.6.2.1. Direct usage of biochar as catalysts. Advanced oxidation processes (AOPs) produce highly reactive oxidative species (ROS) with strong oxidative capabilities to degrade pollutants by using energy assistance or catalysts to activate the common oxidants such as hydrogen peroxide (H_2O_2), hydrogen persulfate (HSO_5^-, PMS) and perdisulfate ($S_2O_8^{2-}$, PDS). ROS can break down pollutants and transform them into less toxic or non-toxic products, thus providing an effective solution for wastewater treatment (Deng and Zhao, 2015). When exposed to enough ROS, organic pollutants can be even mineralized into small inorganic molecules such as CO_2, H_2O and simple inorganic salts. Thus, an efficient generation of ROS is important in AOPs.

Persistent free radicals (PFRs) in biochar have been widely recognized for their roles in electron transfer, which can effectively activate oxidizing agents with peroxy bonds, such as PMS and H_2O_2. With the benefits of improving efficiency, reducing costs, and enhancing environmental sustainability, biochar has been widely used as a catalyst in AOPs to produce strong free radicals or other ROS for pollutant removal (He et al., 2021). Residence time and pyrolysis temperature are the key factors determining the properties of biochar, which are critical for its catalytic properties in AOPs (Gupta, A.D. et al., 2022). Besides PFRs, the wide surface area, rich porosity, good crystallinity and active functional groups of biochar provided wide absorption sites for pollutants' enrichment, facilitating their degradation processes via interfacial catalysis. It is worth mentioning that there are still some problems by using biochar as catalysts directly. Due to the consumption of the PFRs during AOPs, it is difficult to reuse biochar. The modification of biochar by creating recyclable reactive sites for oxidant activation via a load of transition metals and involvement of vacancy is necessary for such a disadvantage.

Zhou et al. provided a comprehensive review of biochar-based single-atom catalysts (SACs), highlighting their synthesis strategies, such as metal salt pre-treatment and pyrolysis of metal-rich biomass, and demonstrating their promising applications in environmental remediation and energy conversion through advanced oxidation and electrocatalysis mechanisms (Zhou, T. et al., 2024). The study emphasizes the advantages of biochar as a low-cost, high-surface-area carbon support for SACs, along with challenges related to stability and future development pathways.

6.6.2.2. Metal-loaded biochar as catalysts. Metal-based biochar, loaded with single or combined metals such as Fe, Cu, Mn, Co, and Mg, effi-

Table 6.1
Usages of biochar as absorbers for pollutant removal in wastewater treatment.

Feedstock	Content (%)			Element content (%)					Pyrolysis methods	Pyrolysis temperature (°C)	Heating rate (°C/min)	Bet Analysis (m^2/g)	Application		Ref.
	Cellulose	Hemicellulose	Lignin	Ash	C	H	O	N	S				Dosage (g/L)	Removal efficiency	
Sugarcane bagasse	37.27	35.80	20.13	1.84	47.50	5.75	41.94	0.48	0.10	Slow pyrolysis	700	10	322.259	0.125	≈100	(Borges et al., 2020; Che et al., 2023; García-Pérez et al., 2002)
Pineapple wood	64.35	13.85	4.60	0.10	47.30	6.03	40.93	1.13	0.21	Slow pyrolysis	500	10	/	/		(Zhao et al., 2022)
Cherry wood	42.00	34.00	24.00	0.00	43.17	5.15	38.05	0.12	0.01	Slow pyrolysis	500	/	118.88			(Trigo et al., 2016)
											700		252.11			
Wheat straw	41.35	27.40	15.70	5.15	41.82	5.67	41.64	0.81	0.15	Slow pyrolysis	800	/-	2944	0.2	60–98	(Shi et al., 2022; Singh et al., 1996)
Rape straw	45.00	19.50	19.00	2.54	44.08	5.41	/	0.07	0.19	Slow pyrolysis	400	/	14.64	0.1, 0.2	98.7	(Huang et al., 2021)
Corn stover	37.40	22.37	16.20	/	44.18	5.52	37.69	0.53	0.10	Slow pyrolysis	800	5	238.30 (cm^2/g)	1.0	85–88	(Zhuo et al., 2022)
Rice hulls	32.40	16.64	28.65	/	38.86	4.86	37.15	0.42	0.06	Slow pyrolysis	550	/	255.78	1, 2, 4	94–96	(Amen et al., 2020; Antal et al., 2000)
Peanut shells	38.85	13.85	26.60	4.95	45.44	6.69	36.06	1.07	0.02	Slow pyrolysis	600	10	61.3	1	97.3	(Song et al., 2023)
Walnut shells	23.30	20.45	42.50	2.41	51.73	6.24	39.01	1.06	0.12	Slow pyrolysis	700	10	737.98	0.2	/	(Xu, H.H. et al., 2022)
Sunflower seed husk	26.70	18.40	27.00	1.62	50.37	5.62	42.64	0.33	0.05	Slow pyrolysis	700	10	1.3	0.625	97	(Nguyen et al., 2023)
Switch grass	33.30	26.00	13.85	16.50	42.09	5.25	33.70	0.69	0.17	Fast pyrolysis	425	/	1.1	1	80–90	(Essandoh et al., 2017)

ciently catalyzes AOPs. These metals provide recyclable reactive sites for activating oxidation agents, while the carbon shell effectively inhibits metal leaching, enhancing the composite's reusability. Fu et al. (2017) reported a Cu based biochar composite for tetracycline degradation via activated H_2O_2 (Fu et al., 2017). The dispersion of Cu nanoparticles on the biochar increased its surface area and pore volume, enhancing adsorption and degradation efficiency. Chen et al. (2018) prepared Co_3O_4 nanoparticles loaded biochar, which exhibited unusual multiphase activation of PMS (Chen et al., 2018). The presence of numerous $CoOH^+$ groups was found on the surface of Co_3O_4-modified biochar, contributing to its abnormally high PMS activity. In particular, Fe-modified biochar can exhibit magnetism, which aids in recycling. Fu et al. (2019) synthesized Fe_3O_4-loaded biochar with a graphitized structure, multiple pores, and strong magnetic properties, which efficiently catalyzed the degradation of organic pollutants in the presence of PMS and demonstrated good recyclability (Fu et al., 2019). Additionally, bimetallic and multi-metals modified biochar offer superior performance, stability, versatility, and recyclability compared to single metal-loaded biochar, making them more effective for AOPs. Bimetallic and multi-metal modified biochar have been increasingly studied in recent years. Liang et al. (2023) investigated a sodium hydroxide modified biochar-loaded Fe-Mn bimetallic loaded biochar for tetracycline removal via activated PMS (Liang et al., 2023). The Fe^{3+}/Fe^{2+} and Mn^{3+}/Mn^{2+} redox cycle promoted free radical production under the synergistic action of Fe-Mn-modified biochar. Comparisons of pollutant removal efficiencies by using different metal-loaded biochar in AOPs are summarized in Table 6.2.

6.6.2.3. Heteroatom-doped biochar as catalysts. Heteroatom-doped biochar has emerged as a promising catalyst for the degradation of various organic pollutants in AOPs. Doping biochar with heteroatoms such as nitrogen, sulfur, phosphorus, and boron enhances its physicochemical properties and catalytic performance. The introduction of these heteroatoms alters the electronic structure and surface chemistry of the biochar, creating vacancies and active sites that facilitate the generation of ROS essential for AOPs. These modifications can also lead to increased surface area, improved porosity, and enhanced electron transfer capabilities, all of which contribute to more efficient pollutant degradation.

Nitrogen doping, for instance, introduces pyridinic, pyrrolic, and graphitic nitrogen species into the biochar matrix, which can significantly improve the catalytic activity by creating vacancies for the activation of oxidants (Wan, Z.H. et al., 2021). Sulfur doping can enhance the electron donor-acceptor properties of biochar, making it more effective in activating oxidizing agents like PMS and H_2O_2. Phosphorus and boron doping also contribute to the generation of additional active sites and the stabilization of transition metal nanoparticles on the biochar surface, further boosting its catalytic performance. The versatility and effectiveness of heteroatom-doped biochar in AOPs make it an attractive alternative to traditional metal-based catalysts. Its potential for recycling and reusability, combined with its ability to reduce the need for precious metals, aligns well with the goals of sustainable and environmentally friendly water treatment technologies.

6.6.2.4. Other biochar modification methods. Besides the metal and heteroatom loadings, the chemical activation with acid/basic treatment or oxidation, physical activation with steam or thermal treatments, surface functionalization, and biochar composites have also been widely employed for biochar modification. Treating biochar with acids (e.g., HCl, HNO_3) or bases (e.g., NaOH, KOH) can increase surface area, porosity, and active sites by removing impurities and creating more functional groups on the surface. Oxidizing agents (e.g., H_2O_2, $KMnO_4$) can introduce oxygen-containing functional groups, enhancing the catalytic properties and adsorption capacity of biochar. Exposing biochar to

Table 6.2
Comparisons of pollutant removal efficiencies by using different metal-loaded biochar in AOPs.

Metal species	Feedstocks	Metal	AOPs		Initial pH	Temperature (°C)	Dosage (g/L)	Reactive species	Removal (%)	Ref.
			Oxidants	Dosage						
Single metal	Shrimp shell	Co^{2+}	PMS	0.4 g/L	6.8	700	0.15	$SO_4^{\cdot-}$, $O_2^{\cdot-}$	~90	(Qin et al., 2022)
	Solid digest	Cu^{2+}	H_2O_2	20 mM	~5.8	/	0.5	$^{\cdot}OH$	97.8	(Fu et al., 2017)
	Wheat husks and paper sludge	Zn^{2+}	Ultrasound	300 W	5.5	90	1.5	$^{\cdot}OH$	96.1	(Gholami et al., 2019)
Single metal oxide	Corn stalks	CuO	PMS	2 mM	7.0	550	0.2	$SO_4^{\cdot-}$, $O_2^{\cdot-}$, $^1O_2$	78–100	(Li, Z.D. et al., 2020)
	Rice straw	Cuo	PDS	50 mg/L	4.3	170	0.3	$SO_4^{\cdot-}$, $O_2^{\cdot-}$, $^1O_2$, $^{\cdot}OH$	86–100	(Li, W. et al., 2020)
	Sludge and sewage sludge	Fe_3O_4	PDS	0.5 g/L	7.0	200 700	0.9	$SO_4^{\cdot-}$, $O_2^{\cdot-}$, $^1O_2$, $^{\cdot}OH$	80–100	(Tong et al., 2023)
	Platanus orientalis leaves	Fe_3O_4	PMS	5 mM	3.0	/	2	$SO_4^{\cdot-}$, $^{\cdot}OH$	100	(Cui et al., 2021)
Multi-metal	Platanus orientalis branches	Fe^{3+}, Mn^{2+}	PMS	0.5 mM	4.8	800	0.5	$SO_4^{\cdot-}$, $O_2^{\cdot-}$, $^1O_2$, $^{\cdot}OH$	97.9	(Liang et al., 2023)
	Maize straw	Fe^{3+}, Cu^{2+}	PMS	2 mM	6.0	600	0.4	$SO_4^{\cdot-}$, $^1O_2$, $^{\cdot}OH$	91–99.8	(Liang et al., 2021)
Multi-metal oxide	Bamboo powder	$CuFe_2O_4$	PDS	0.1 M	7.3	700	2	$SO_4^{\cdot-}$, $O_2^{\cdot-}$, $^1O_2$	90	(Zhao, Y. et al., 2020)
	Rice husk	$CoFe_2O_4$	PMS	0.1 M	7.42	400	5	$SO_4^{\cdot-}$, $O_2^{\cdot-}$, $^{\cdot}OH$	89	(Zhi et al., 2022)
	Peanut shells	$MnFe_2O_4$	PMS	0.2 g/L	7.0	300	0.2	$SO_4^{\cdot-}$, $O_2^{\cdot-}$, $^1O_2$	100	(Xu, S.Y. et al., 2022)

steam at high temperatures can increase porosity and surface area, improving its catalytic and adsorptive properties. High-temperature treatment can enhance the graphitization of biochar, improving its structural stability and electronic properties. Additionally, grafting specific functional groups (e.g., carboxyl, hydroxyl, sulfonic groups) onto the biochar surface can enhance its interaction with pollutants and improve catalytic performance. Coating biochar with polymers, silica, or other materials can provide additional catalytic sites, improve stability, and tailor surface properties for specific applications. Combining biochar with other materials such as activated carbon, carbon nanotubes, or graphene can enhance its structural and catalytic properties. These composites can provide synergistic effects, leading to improved performance in AOPs.

6.6.3. Future outlook on biochar application in water treatment

The application of biochar in water treatment presents a promising future, driven by the necessity for sustainable, efficient, and cost-effective solutions to address water pollution. Key areas poised for significant advancements include:

Enhanced Catalytic Performance: Current limitations, such as the consumption of oxygen-containing functional groups on biochar surfaces, pore clogging, and metal ion dissolution, restrict the reutilization rate of transition metal-based biochar catalysts. Future research will likely focus on incorporating various heteroatoms and transition metals to optimize catalytic performance. Understanding the roles of different biomass components and the formation of active sites will enable the design of highly efficient biochar catalysts. Innovations in synthesis techniques, such as controlled pyrolysis and functionalization processes, will further enhance biochar's reactivity and durability.

Scalability and Industrial Application: The transition from research to industrial-scale application of biochar catalysts faces challenges, including metal dissolution and toxicological concerns. Developing standardized production methods and quality control measures will ensure consistent performance on a large scale. Addressing metal leaching, secondary pollution, and energy consumption during biochar production will be crucial for industrial viability.

Integration with Existing Treatment Systems: Integrating biochar catalysts with existing water treatment systems can enhance efficiency and reduce operational costs. Hybrid systems that combine biochar with other treatment technologies, such as membrane filtration or biological processes, can offer synergistic benefits and improved pollutant removal capabilities.

Environmental and Economic Sustainability: Ensuring the sustainability of biochar applications is essential. Utilizing waste biomass for biochar production can reduce waste and provide a low-cost feedstock. Life-cycle assessments and techno-economic analyses will help evaluate the long-term benefits and feasibility of biochar-based treatments.

Targeted Pollutant Removal: The activity of biochar catalysts is significantly affected by the biomass composition. The relationship between persistent free radical formation and the presence of carbohydrates, cellulose, and lignin in biochar needs further study. Additionally, customizing biochar to target specific pollutants, such as heavy metals, pharmaceuticals, and emerging contaminants, will enhance its effectiveness in diverse water treatment scenarios.

Regulatory and Safety Considerations: Addressing regulatory and safety concerns, particularly regarding the potential toxicity of biochar and its by-products, will be important for widespread adoption. Establishing guidelines and standards for biochar use in water treatment will ensure safe and effective applications.

In conclusion, the future of biochar application in water treatment holds substantial potential for transforming the field. Continued research and innovation will drive the development of advanced biochar catalysts, paving the way for sustainable, efficient, and scalable solutions to meet global water treatment challenges.

6.7. Biochar in building materials

6.7.1. Decarbonization of biochar as binder or aggregate in cementitious materials

Cement and concrete stand as pivotal elements extensively utilized in the construction sector, which is responsible for 5 %-8 % of global anthropogenic CO_2 emissions (Monteiro et al., 2017; Shah et al., 2022). Due to the nature of cement clinker production, the decomposition of calcium carbonates will inevitably generate considerable CO_2 during heating up to 1450 ˚C (Habert et al., 2020). The replacement of partial clinker or aggregate by some mineral admixtures or industrial by-products during concrete production will reduce the overall CO_2 emissions by up to 1.3 Gt (~2.8 % of anthropogenic CO_2 emissions) (Shah et al., 2022), giving to the possibility to achieve the carbon neutrality of construction industry (Miller and Moore, 2020).

To accomplish this objective, integrating carbon-negative materials into concrete could be explored to counterbalance the remaining carbon emissions. Among these materials, biomass-derived biochar can play a pivotal role due to its multifunctional and carbon-negative nature. The first carbon-negative concrete using biochar as fine aggregate was achieved by replacing 30 wt. % of sand (Chen et al., 2022b), resulting in approximately -60 kg CO_2 emissions per tonne of concrete produced, particularly when supplemented with a significant quantity of mineral admixtures.

A comprehensive life-cycle assessment (LCA) of biochar-enhanced cementitious materials was recently performed based on a series of binder types, using biochar as both aggregate and powder (binder phase) (Labianca et al., 2024). Achieving carbon-neutral emissions is estimated to be feasible with the utilization of at least around 20 wt. % biochar (Labianca et al., 2024), though this pursuit entails a trade-off with mechanical properties, representing an ambitious goal. One way to compensate for this sacrifice is to incorporate ultra-fine powder-based biochar as the filler in the cementitious composites, which can reach 60 wt. % replacement ratios, giving approximately -700 kg CO_2 emissions per tonne of concrete products (specified used as 3D printing ink in this case due to its rheological alternations) (Labianca et al., 2024).

6.7.2. Porous biochar serves as the lightweight aggregate or channels in concrete

Due to its porous nature, biochar shows a very low bulk density, which can reduce the volume of the cement paste or aggregate in the matrix. The addition of porous materials naturally will reduce the average density of the final product, giving it the lightweight function of being able to be used in some non-load-bearing structures (such as interior walls, infill walls, partition walls, or curtain walls). Recently, Chen et al. tried to develop lightweight concrete whilst maintaining its high strength by using 20 wt. % food waste digested (FWD) biochar aggregate (Chen et al., 2024). The designed concrete meets the criteria for high-strength lightweight aggregate concrete, demonstrating both low density (< 2 g/cm^3) and high compressive strength (> 40 MPa at 28-d). However, it should be noted that the fineness modulus of biochar particles is only 1.9, which is much smaller than that of normal sand (normally 2.3 - 3.1 according to ASTM C33). Therefore, the amount of binder (i.e., cement paste) used in this concrete product is still high. The higher amount of biochar will inevitably decrease the compressive strength of concrete products, but it is worth trying the high-pressure compression method to produce particleboards, as demonstrated by Chen et al. (Chen et al., 2022a). Attempts were also made to use engineered biochar as part of the binder (similar particle size to Portland cement) to prepare lightweight foamed mortar (Gupta, S. et al., 2022). The findings suggest that the addition of biochar shows a positive effect on the rheological of foamed concrete, giving a 23 %-28 % reduction in its yield stress. Recent trials also confirm that the inclusion of corn husk biochar (CHBC) in the base mix accelerates the formation of flocculation, leading to a reduction in interparticle distance and consequently increasing the yield stress (Xiong et al., 2024).

Importantly, the presence of biochar will further fascinate the carbonation of foamed concrete, giving higher chances to sequestrate CO_2 in the filed application. It is widely found that the addition of biochar will benefit the diffusion of CO_2, and thus, the sequestering amount of CO_2 during curing will be accelerated (Gupta, 2021; Praneeth et al., 2020). Normally, the accelerated carbonation will give 8 %-10 % increase in the mechanical properties of concrete products (Gupta, 2021), which will be further boosted by using an internal carbonation strategy (i.e., using CO_2-saturated biochar), giving up to 30 % increment in compressive strength (Gupta, 2021). It should also be mentioned that the addition of biochar can also facilitate CO_2 curing in not only Portland cement but also magnesia-based cement, giving an additional option for low-carbon construction (Wang, Lei et al., 2021).

Other than being used as an aggregate or a binder, biochar was also used to make lightweight aggregates, which can further be used in concrete, achieving a lightweight foundation. Liu et al. developed a novel CASSAs (cold-bonded artificial steel slag aggregates) with sawdust biochar, which enables the aggregate to stabilize CO_2 even under very low concentrations (Liu, J. et al., 2023), indicating a very high potential to use biochar as the channel to enhance the carbonation effect of steel slag. Further, Wyrzykowski developed the carbon-rich lightweight aggregated (C-LWA) by using the cold bonded method, giving a very high C-sink potential, about −1.05 kg CO_2/kg of C-LWA (Wyrzykowski et al., 2024).

As biochar is a porous material, it can also provide a channel for the moving of internal moisture, giving the internal curing effect to enhance the cement hydration (Chen et al., 2022b) or reduce the shrinkage (Maljaee et al., 2021; Mo et al., 2019), especially in alkali-activated slag system (Prabahar et al., 2021), which typically show a larger shrinkage compared to normal concrete (Zhu et al., 2022; Zhu et al., 2018). In addition, the porous structure will also minimize the wetting-drying cycles of external solution attack, which is believed to be one of the major durability concerns of coastal infrastructures (Li et al., 2021; Li, Q. et al., 2023). Biochar can provide sufficient channels for crystallisation expansion during wetting-drying cycles, as demonstrated by recent work done by Han et al. (Han et al., 2022). The use of biochar to stabilize the coral sand using alkali-activated binder, where the biochar serves as the channel for releasing the crystallisation pressure due to sulphate attack at the coastal area.

6.7.3. Interactions and degradation of biochar in cementitious environments

In any composite material, the interactions between its constituent phases play a crucial role in determining its durability. For instance, the interfacial transition zone (ITZ) between sand and the cement paste matrix is widely recognized as the weakest point in concrete (Scrivener, 2004). Similar interactions will also happen between biochar (carbon-rich materials) and the cement matrix. As shown in Fig. 6.15 (modified from (Zhu et al., 2023)), the brighter region stands for the unreacted clinker in Portland cement, whereas the black parts are the biochar or the defects within the matrix and the grey parts are the hydration products as the results from the reaction. It is evident that from the distribution of grey values of these slices (Fig. 6.15b-d) the hydration degree of these clinkers increased significantly in the region of ITZ.

Two major interactions, i.e., via calcium-rich layer or C-S-H gel layers, are also illustrated using backscattered electron microscopy-energy dispersive X-ray analysis (BSEM-EDX) and X-ray computed tomography (X-CT) for analysing the biochar-cement composites (Zhu et al., 2023). The calcium-rich layer contains mostly calcium hydroxide and some aluminium/calcium-based layered double hydroxides, indicating the concentrated calcium and aluminium will present in the ITZ of biochar-cement. A similar effect was also found in the carbon fibre modified cement, where the oxidised carbon fibre preferred to connect with the cement matrix via Ca-OOC chemical bonds or Al-O bonds (Sugama et al., 1989).

Further, as it is in high alkali condition, the durability of biochar in cementitious materials will also be a critical issue before its real application. The comprehensive study found that environmental exposure diminished Young's modulus and hardness of biochar, attributed to the partial damage of its pore structure and the disruption of its cross-linked network structure by the saponification reaction (Xu et al., 2024). However, the deformation of biochar and its elastic recovery improved in seawater due to salt crystal deposition on its surface or pores (Xu et al., 2024).

6.7.4. Other challenges and future directions

A major challenge in utilizing biochar lies in the need to regulate its properties, given the diverse sources of biomass used as the raw materials for pyrolysis. Even among wood wastes, the resulting biochar exhibits significant variability in performance. Hence, it is crucial to categorize or classify biochar according to its suitability for various functions in construction materials. Secondly, the balance between sacrifice in mechanical properties and carbon sequestration should be systematically evaluated before its real application. Although the LCA predict that carbon emissions will be greatly reduced due to the addition of biochar, the requirements for its mechanical properties are not very high (Labianca et al., 2024). Secondly, the use of high amounts of carbon will generate concerns about fire safety, which will be an important issue to be systematically evaluated. Thirdly, biochar introduces more pores, which will also serve as the channel for external chemicals to ingress, although existing data show the positive effect of the pores under wetting-drying attack (Han et al., 2022). Other conditions, such as full immersion or partial immersion in solutions, should also be considered.

Nevertheless, carbon-negative biochar is a suitable and promising material to offset the carbon emissions from the construction industry, making the buildings the carbon sink (Wyrzykowski et al., 2024). The future direction of biochar-cement composites sheds light on the following aspects: (i) fresh properties (for 3D printing), additive cargo functions of biochar, high-performance concrete, smart monitoring for construction (electrical properties), durability concerns, and field application.

7. Techno-economic analysis of biochar system

7.1. TEA for biochar-based CO_2 capture and energy use

As a potentially renewable solid material, biochar has diverse applications that can replace conventional alternatives, while also providing carbon sequestration benefits. The limited understanding of biochar's economic viability has impeded its practical implementation. Conducting a techno-economic assessment (TEA) is crucial to accelerate the development of innovative technologies using biochar for carbon capture and energy use.

Mukherjee et al. (Mukherjee et al., 2022) investigated the potential of spent coffee grounds as precursors for activated carbon (AC) production via a detailed techno-economic and sensitivity analysis. The results indicate that the price of pristine AC and functionalized AC were lower than the commercially available activated carbon (USD $0.45/kg). Shaheen et al. (Shaheen et al., 2022) evaluated the performance, environmental impacts, and economic considerations of date palm biochar and woody biomass activated carbon. Date palm biochar demonstrated a GHG emission of 1.53 kg CO_2eq/kg, which was less than the 8.96 kg CO_2eq/kg linked to woody biomass activated carbon and other activated carbons derived from different feedstocks found in the literature. The economic analysis revealed that the average production costs for date palm waste biochar and activated carbon were $1.06 per kg and $1.34 per kg, respectively. Haeldermans et al. (Haeldermans et al., 2020) conducted a comparative techno-economic assessment and Monte Carlo risk analysis on large-scale (3 tonne/h) biochar production plants using conventional and microwave pyrolysis, and found that minimum selling prices for conventional biochar

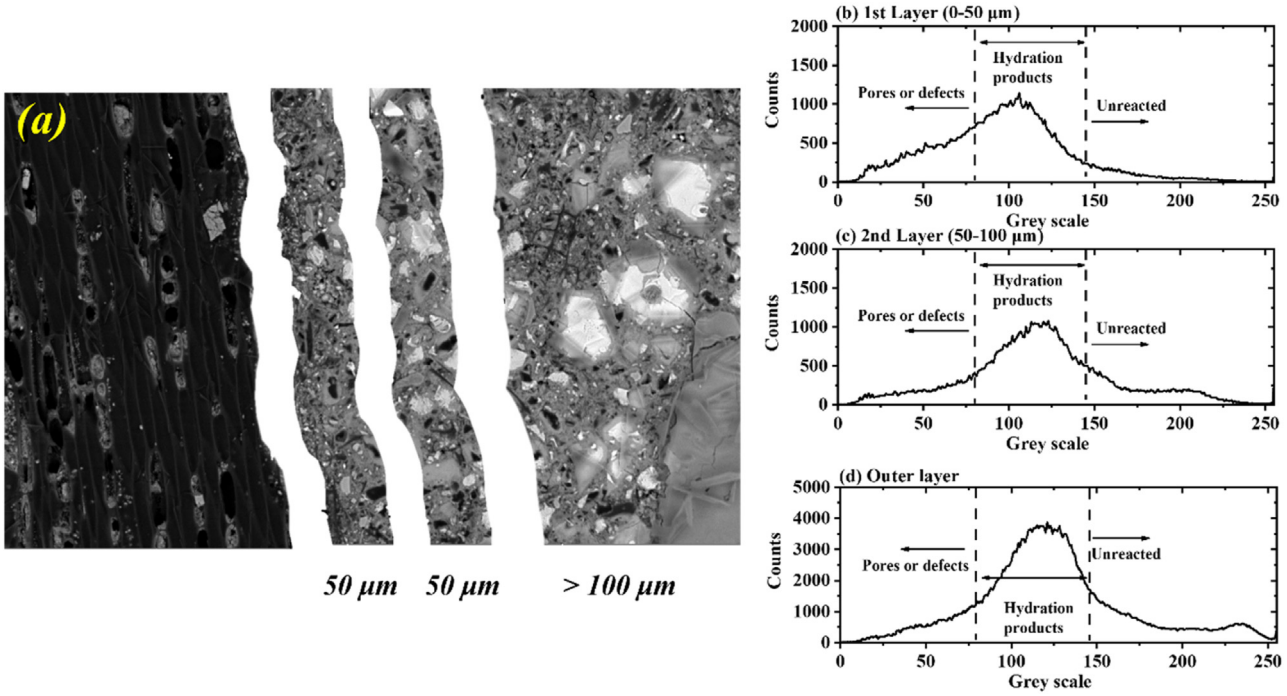

Fig. 6.15. Interfacial transition zone (ITZ) between biochar and the cement matrix: (a) the segment of ITZ; (b-d) the grey values distribution of cement matrix adjective to biochar.

production plants are between €436/tonne and €863/tonne, compared that of €564/tonne and €979/tonne for microwave biochar production. Ganguly et al. (Ganguly et al., 2022) evaluated the economic and environmental performance of conventional fast pyrolysis (FP) and autothermal pyrolysis (ATP) technologies with and without pretreatment of three kinds of biomass to produce sugars, phenolic oil, and biochar as end products while achieving carbon negative emissions. The assessment indicated that the pyrolytic systems are competitive to direct air capture in terms of both net carbon dioxide (CO_2) removal per unit of energy consumption and cost of removing CO_2 which falls between $30 to −$139 per ton CO_2 removed.

Fawzy et al. (Fawzy et al., 2022) conducted a techno-economic-environmental study of atmospheric carbon removal via industrial biochar systems. Using the Puro. Earth methodology, it was realised that 2.68 tCO_2e are permanently removed per tonne of biochar produced (dry basis), considering the entire process's carbon footprint. This equates to 3.26 tCO_2e removed per hour and approximately 24,450 carbon removal certificates (CORCs) issued annually, based on 7500 hours of operation. The economic assessment shows profitability with a CORC price of 110 EUR and biochar price of 350 EUR/tonne, yielding a net present value (NPV) of 3002,358 EUR, an internal rate of return (IRR) of 22.35 %, and a payback period of 8 years.

Huang et al. (Huang et al., 2015) investigated the technical and economic performance of biochar production together with electricity and/or heat from poultry litter waste, demonstrating a break-even biochar selling price (BESP) of around £218/tonne. If the sale of electricity and heat produced is considered to be around £60/MWhe and £5/MWhth, the BESP will decrease to £178/tonne.

It is important to note that the characteristics of biochar are affected by feedstocks and processing conditions, which also determine the respective environmental and economic performances. Current TEA and LCA have lots of uncertainties in terms of process configurations, data sources, assumptions of parameters, and modelling methodologies and therefore, a comprehensive understanding of emerging biochar systems for CO_2 capture and energy use is seen to be critical.

7.2. TEA for biochar soil amendment

As illustrated above, the addition of biochar to soil has been proven to improve soil properties, nutrition availability and water retention, hence promoting crop productivity (Yadav et al., 2019; Yang, K. et al., 2022). With a close long-term economic return for cotton production in northern Benin, biochar amendment is believed to have a greater environmental benefit than mineral fertilizer (Tovihoudji et al., 2022). In a case study of growing pod pepper, Zhang et al. found the net proceeds of biochar-based fertilizers were $543 ha^{-1} in 2018 and $1106 ha^{-1} in 2019, more than those of fertilizers without biochar (Tovihoudji et al., 2022). Moreover, the emission of greenhouse gases can also be offset. However, the cost of biochar is another barrier to its widespread use as soil amendment, hence the importance of assessing the economic viability (Mohammadi et al., 2020). According to a six-year experimental research on paddy field, biochar application may leave adverse impacts on the net ecosystem economic benefit (NEEB), since the high cost of biochar overweighs the income from increased rice production and soil organic carbon storage (Chen, Z. et al., 2024). It should be noted that the duration of the effective lifetime is critical for the profit due to the diluted annual cost of biochar, though the initial investment is still expensive for small-scale farms and low-income countries (Robb et al., 2020).

Basically, the net proceeds generated through biochar soil amendment are predominantly driven by the gross income of harvest and the cost of the biochar, where the gross income is based on the fresh weight in the unit area and the unit price of the fresh crop. The input value of the additive is calculated by the product of biochar price and the feed weight of biochar in the unit area. Since the field output, crop price and the promotion productivity from biochar deployment depend on crop type, the viability of soil amendment should be evaluated under specific conditions. According to a comparison study between biochar amendment for rice and wheat production, although the net economic proceeds by biochar for the two crops were somewhat comparable, i.e. 41–78 % for rice and 34–77 % for wheat, the gross outcomes per unit

area for rice ($899 ha^{-1} on average) were higher than that for wheat ($600 ha^{-1} on average). This means the return of biochar investment would have a longer period for wheat production (Wang, L. et al., 2018). Environmental factors such as climate and soil properties are also critical for biochar deployment (Keske et al., 2020; Shen, J. et al., 2023; Struhs et al., 2020). Considering water capacity, Kroeger et al. claimed that soil and biochar qualities are both important for the realised water holding capacity benefits from biochar soil amendment., pinpointing specific locations in United States for higher performance (Kroeger et al., 2021). Bi et al. evaluated the feasibility of straw biochar amendment with six kinds of soils. Among different fields, the total gains varied widely. The biochar doses applied also led to different impacts on NEEB values (Bi et al., 2019). An interesting application for biochar amendment is to remediate contaminated soil, where the profit is higher than the common cultivation if the harvested crop can meet the standard of livestock feed after the treatment (Wang and Delavar, 2023; Wei et al., 2021). With regard to the dose of biochar, the production may improve quickly at first and then gradually stabilise. The cost, however, rises linearly by a small margin, with a sharp drop in revenue. Latawiec et al. analysed the consumption rate of sunflower husk biochar for soybean production in Poland, where the breakeven prices of biochar were calculated to be $39.22, $38.29 and $23.53 corresponding to doses of 40, 60 and 80 t/ha, and the payback period were 3.19 and 3.26 years for doses of 40 and 60 t/ha, respectively (Latawiec et al., 2021). With an optimum biochar application rate, it is possible to gain both economic benefits for farmers and environmental benefits for the public (Aller et al., 2018; Li, Y. et al., 2023).

Owning to carbon sequestration potentials, if environmental benefits associated with the large-scale application of biochar can lead to the generation of economic revenue through ecological subsidy policies, the expensive cost of biochar can potentially be compensated (Keske et al., 2020; Wang, L. et al., 2018). For a tea plantation ecosystem, Lin et al. compared the effect of an optimistic condition with $160 t^{-1} CO_2-eq to a business-as-usual scenario with the carbon price of $8 t^{-1} CO_2-eq in China, where the NEEB increased 17 % ($14,945 ha^{-1} yr^{-1}) (Lin et al., 2023). At a carbon price of $35/t in Brazil, biochar lacks competitiveness, as it is 617 % more expensive than common fertilizer (Latawiec et al., 2019). Therefore, a market-regulated carbon price reinforced by appropriate ecological compensation is critical to effectively encourage biochar soil amendment (Robb et al., 2020).

In conclusion, soil amendment is a promising application for biochar utilisation from both economic and environmental perspectives, while the return on investment over a long period is still a challenge for users. The income will be further promoted when the biochar amendment is used on high-value crops, and carbon credit can be factored in. In order to optimise the high cost of biochar production, a number of factors need to be carefully taken into account while considering different scenarios and the uncertainty in prices and crop production in order to achieve meaningful techno-economic analysis.

7.3. TEA for H_2-rich syngas production from biomass

Hydrogen, with a calorific value of around 120 - 140 MJ kg^{-}, is widely recognised as clean future energy with a broad range of applications in industries including transportation, electricity, heat and power generation, as well as chemicals (Ghodke et al., 2023). Hydrogen can be produced from syngas via water-gas shift (WGS) reaction (Pal et al., 2018):

$$CO + H_2O \leftrightarrow CO_2 + H_2 \quad \Delta H^{\circ}_{298} = -41.09\,kJ/mol$$

Syngas is a mixture of CO and H_2, which can be used in the synthesis of fuels (e.g. diesel fuel, dimethyether) and value-added chemicals (e.g. methanol) (Rostrup-Nielsen, 2002). The ratio of H_2 to CO in syngas can vary between 3 and 1.2 (Samiran et al., 2016). Syngas is typically produced via gasification (Aydin et al., 2018), catalytic pyrolysis (Wang et al., 2022) and catalytic steam reforming (Chen, G. et al., 2016).

Despite the presence of a number of techno-economic analyses (TEAs) studies on H_2 production, there has been little research on TEAs associated with H_2-rich syngas produced from biomass. Techno-economic assessments could be reflected in the cost, including the capital investments (CAPEX) and/or the operational costs (OPEX), as well as the final cost of the end product. Generally, the CAPEX is composed of direct costs (cost of land, equipment, etc.) and indirect investment (cost of operation, handling, etc.) (Liu, Y. et al., 2017; Wang, Y. et al., 2019). OPEX includes costs associated with maintenance, labour, property taxes, insurance, and administrative expenses, as well as the cost of raw materials used in the process, as well as process utilities (Liu, Y. et al., 2017). It should also be noted that the investment costs usually have an uncertainty ranging from +50 % to −30 % (Brown, 2016). Ahmed AlNouss et al. reported the techno-economic analysis for four different cases of yielding H_2-rich syngas via raw material blending (AlNouss et al., 2020). Oxygen- and oxygen/steam-based gasification with an air separation unit (ASU) was linked to capital costs of around $60 million and operating costs of around $18 million, whereas steam-only gasification was demonstrated with an estimated capital expenditure of approximately $7 million. The operating cost of the steam-based gasification was calculated to be approximately $2 million. It was realised that CAPEX contributed to a bigger share of the overall process costs.

In addition, the technology readiness level (TRL), the size of the plants, and some external factors (i.e. the energy supply and policies) are also critical factors in TEA (Klein-Marcuschamer and Blanch, 2015). The syngas composition is determined by the steam-to-biomass ratio, temperature, and technology employed. Thibaut Lepage et al. have compared the economic aspects of three thermochemical methods, including gasification, partial oxidation, and steam reforming, to produce H_2 from biomass in terms of cost (Lepage et al., 2021). Mature technologies, steam methane reforming and coal gasification (with a CAPEX of 170.95 - 240.20 M€), were found to be most economical with a cost of 0.77 $/kg H_2 (TRL 9) and low feedstock cost. Table 7.1 summarises different technologies for H_2 production using biomass together with their respective CAPEX based on the production capacity. The gasification process requires higher CAPEX and OPEX due to higher operating temperatures (Kannah et al., 2021).

The World Bank Group have reported three benchmarks to gauge process efficiency for biomass processing, including a net present value (NPV), the internal rate of return (IRR) over 10 % and a payback period (PBP) of less than 10 years (Cardoso et al., 2021). Ajay Sharma and Ratnadeep Nath conducted the techno-economic analysis applied to an Indian gasification plant (with syngas production at 500 m^3/day and the capacity of waste processing at 2000 kg/day), designed for the production of H_2-rich syngas using eucalyptus wood sawdust. Based on the life span of 20 years, the results showed that the plant needed a payback period of around 5 years and reflected a minimum of 142 % profit margin (assuming a sale price of 43 INR per kg of hydrogen) (Sharma and Nath, 2023).

J. R. Copa et al. studied the techno-economic analysis of a 15 kWe downdraft gasifier set up in decentralized communities using biomass fuels (Acacia Residues in Portugal and Eucalyptus in Brazil) and its municipal solid waste (MSW) for electricity generation in Portugal and Brazil. The research compared the NPV, IRR and the PBP of the investigated projects. The NPV of acacia was shown to be 29.32 k€ for biomass and 18.99 k€ for MSW, while that of eucalyptus was calculated to be 28.45 k€ and 31.65 k€ for biomass and MSW, respectively. The IRR of acacia was 19.34 % for biomass and 16.88 % for MSW, while that of eucalyptus was 19.28 % and 20.09 % for biomass and MSW, respectively. In terms of PBP, acacia demonstrated a period of 9.2 years and 12.61 years for the MSW, while the eucalyptus project showed 9.38 years for biomass and 8.67 years for MSW. Comparatively, Brazil demonstrated better economic performance due to the higher selling price of elec-

Table 7.1
Cost of different processes of H_2 production using biomass (Lepage et al., 2021).

	Production scale	Methods	CAPEX	Reference
1	2.2 t day^{-1}	Gasification	11 M€	14
2	2.2 t day^{-1}	Steam Reforming	9 M€	14
3	2000 t day^{-1}	Gasification	215M$	15
4	2000 t day^{-1}	Pyrolysis	210 M$	16

tricity (Copa et al., 2020). It was assumed that from the 1st year, the process could produce approximately 36,000 kWh/year of electricity, which leads to an annual profit of 10,500 € on average.

Despite all the efforts, the production of hydrogen-rich syngas is still facing challenges associated with CO_2 emissions (Ayodele et al., 2019). The addition of a carbon capture to the process will affect TEA outcomes. Yaser Khojasteh Salkuyeh et al. have compared the selling price of H_2 with and without carbon capture (Salkuyeh et al., 2018). Production of hydrogen via biomass in a fluidized bed without carbon capture was linked to 3.1 US$/kg of hydrogen, while the H_2 price for the entrained flow process without carbon capture was approximated to be 12 % higher at $3.4 per kg of H_2. With the incorporation of a carbon capture and liquefaction system, hydrogen selling price increased by 3 % in the entrained flow process ($3.8 per kg) and by 11 % in the fluidized bed ($3.5 per kg).

Ahmed AlNouss et al. compared the environmental assessment of four processes using biomass gasification with oxygen/steam and indirect/direct heating to produce H_2-rich syngas, ranging from 0.9 to 1.5 kg of CO_2-e per kg of H_2 (AlNouss et al., 2020). Steam-based gasification with the direct heat source demonstrated the best environmental performance, with 0.9 kg of CO_2-e per kg of H_2. The source of energy could be an important factor affecting the quality of syngas.

In conclusion, the capital cost, NPV, IRR and PBP must be considered to depict an accurate picture of H_2-rich syngas technologies. The influence of the quality of syngas and the coupling and/or addition of a carbon capture system should also be assessed in detail.

7.4. TEA for biochar-based wastewater treatment

A considerable amount of wastewater released by industrial operations is insufficiently treated and requires a cost-effective and technologically sophisticated treatment solution (Paritosh and Hackula, 2024). Investigating the advancement and application of biochar-based materials for wastewater treatment is crucial for environmental protection (El-Shafie et al., 2024; Kang et al., 2023). To assess the technical feasibility, it is essential to examine the adsorption efficiency of contaminants present in wastewater, as well as the regeneration and recyclability of biochar-based materials. The techno-economic analysis should also include a comparison of the capital and operational costs associated with the use of biochar against those of traditional wastewater treatment methods (Kumi et al., 2020; Mian et al., 2024; Tian et al., 2020).

Kumi et al. utilized the pyrolysis process of sewage sludge to produce biochar (BC) adsorbent, which was subsequently modified with eggshell waste, resulting in the creation of eggshell-modified biochar (EMBC). This adsorbent material was applied for the extraction of monoethylene glycol (MEG) from aqueous solutions under a range of adsorption conditions (Kumi et al., 2020). A techno-economic feasibility analysis reveals that the capital costs for producing BC and EMBC adsorbents to treat 1 m^3 of wastewater containing ethylene glycol would amount to US $4.80 and $6.50, respectively. The commercialization of these adsorbents, coupled with the economic benefits associated with tertiary treated water, showed promising annual profitability. The payback periods are estimated to be 12.97 years for the BC option and 6.79 years for the EMBC scenario. Consequently, this study successfully developed effective and cost-efficient adsorbents suitable for the tertiary treatment of petrochemical industrial wastewater that contains hazardous environmental pollutants. In a recent study, Zhang et al. developed a new type of magnetized biochar, referred to as magnetic functionalized carbon microsphere (MF-CMS), through the combined processes of hydrothermal carbonization and pyrolysis activation of starch-rich rice waste, which was utilized for the treatment of wastewater containing tetracycline antibiotics (TCs) (Zhang, F. et al., 2023). The projected expense for the preparation of MF-CMS is approximately US $5.91 per kg. To produce 1 kg of MF-CMS, it is necessary to utilize 8 kg of waste rice, which can effectively treat around 0.55 tons of TCs wastewater. This estimated cost is on par with the prices of commercial adsorbents and other documented adsorbents used for wastewater treatment. In comparison to most commercial adsorbents, the MF-CMS developed in this study demonstrates both efficiency and environmental sustainability for the removal of various TCs, particularly regarding its adsorption capacity and reusability.

The large-scale treatment of polluted wastewater effluents requires the creation of highly efficient and economically viable adsorbents. El-Shafie et al. synthesized a biochar-based adsorbent derived from mandarin peels (MRBC) for the treatment of wastewater effluents containing binary dyes, specifically methylene blue (MB) and basic fuchsin (BF), conducted at both laboratory and large-scale levels (El-Shafie et al., 2024). Large-scale economic analysis demonstrates that the estimated overall cost of MRBC is 3.96 US$/kg, which is greater than that of other biochar varieties, primarily due to the higher expenses associated with unit energy. The total expense for wastewater treatment has been calculated at 10.6 US$/$m^3$ of wastewater effluent over a ten-year lifespan of an adsorption unit with a capacity of 10 m^3. Future research may reduce this cost by exploring innovative methods to enhance the adsorption capacity of MRBC and lower its production expenses. Taslakyan et al. investigated the techno-economic analysis (TEA) of a tertiary water treatment process that employs a large-scale biochar-integrated reactive filtration (RF) system for the removal and recovery of micropollutants through catalytic oxidation (Taslakyan et al., 2023). This advanced system integrates the use of biochar (BC) either alongside or separately from iron-ozone catalytic oxidation (CatOx). The technology achieves total phosphorus removal rates ranging from 90 % to 99 %, facilitates the adsorption of phosphorus onto biochar for recovery purposes, and ensures over 90 % destructive elimination of identified micropollutants. TEA of the biochar catalytic oxidation reactive filtration process indicates an anticipated carbon-neutral process cost of approximately US $0.11/$m^3$ ± 0.01. This estimation pertains to a facility with a capacity of 3780 m^3/day (1 MGD), with the cost of biochar contributing US $0.03/$m^3$ to the overall expense. The large-scale implementation of biochar-integrated wastewater treatment technologies offers a significant opportunity for the decarbonization of the water sector, while simultaneously enhancing the efficiency of pollutant removal and resource recovery. These findings indicate that achieving carbon negativity could establish a performance benchmark for water treatment that is as crucial and achievable as the removal of pollutants and pathogens.

8. Conclusion

This review has provided a systematic analysis of biochar characterization, production, activation, modification, applications, and techno-economic analysis. Biochar characterization is essential for understanding its properties, including elemental composition and distribution, pH, surface area, surface energy, porosity, density, particle size, morphology, functional groups, thermal conductivity, and heat capacity. Advanced analytical methods provide valuable data for enhancing

biochar's effectiveness and developing tailored biochar products for specific applications.

A variety of thermochemical processes for biochar production from biomass, including slow pyrolysis, combustion, hydrothermal carbonisation, and gasification, have been discussed in this work. Each production method is influenced by factors like feedstock type, reactor design, pyrolysis temperature, and the presence of additives, all of which significantly affect biochar's yield and quality. Scaling up biochar production remains challenging, particularly in achieving cost-effective and environmentally sustainable production. Research should focus on optimizing these processes and exploring novel production methods to improve biochar yield and quality while reducing energy requirements.

Biochar activation and modification are important steps for improving the physical and chemical properties of biochar, enhancing its effectiveness across a range of applications, particularly in carbon capture, energy production, soil amendment, heavy metals and pollutants adsorption, and as a binder or aggregate in cementitious materials. Porous activated carbon can be produced through physical, chemical, and physicochemical activation. For specific applications and improved biochar performance, additional functional groups can be incorporated via heteroatom doping, heteroatom-metal co-doping, and metal atom doping. However, the costs, energy requirements, chemical use, and potential environmental impacts of these processes must be balanced with the goal of enhancing biochar's properties for effective environmental and industrial applications.

Limited work has been reported on the techno-economic analysis and life-cycle analysis of the entire chain of biochar production, activation, modification, and application. Such analysis is crucial for understanding biochar's economic and environmental potential before large-scale deployment. To address this gap, future research should focus on comprehensive assessments that integrate cost, energy use, environmental impact, and scalability to guide sustainable biochar production and application strategies.

Overarching perspectives

The authors propose the following recommendations to guide the research community in advancing biochar science and commercialisation, aiming to unlock new opportunities and address current challenges in the field:

(1) Advanced and standardized characterization techniques. Developing and standardizing advanced analytical methods for comprehensive biochar characterization will enhance our understanding of its properties and performance across various applications. Machine learning and computational modelling could accelerate the discovery and customization of biochar for various applications.
(2) Sustainable and energy-efficient biochar production. Biochar production methods should aim to minimize environmental impact, reduce energy consumption, and utilize renewable feedstocks. Advanced reactor design and optimisation of process parameters, such as temperature and residence time, can improve energy efficiency and carbon retention. Additionally, implementing closed-loop systems to capture and reuse by-products (e.g., syngas, bio-oil) can further enhance sustainability and reduce the carbon footprint of biochar production.
(3) Explore novel activation and modification methods. Investigating innovative activation and modification techniques, such as chemical or thermal activation, can enhance the physical and chemical properties of biochar, broadening its utility. Novel approaches like surface functionalization, nanoparticle doping, or impregnation with metal oxides can improve biochar's adsorption capacity, catalytic activity, and conductivity, making it suitable for applications in carbon capture, water purification, catalysis, and energy storage.
(4) Tailored biochar products development. Designing biochar products customized for specific applications, such as carbon capture, soil remediation, pollutant adsorption, or energy storage, can improve both efficacy and commercial appeal. Tailoring biochar's porosity, surface area, and functional groups to match the needs of various industries enables its targeted application, fostering greater industry adoption and versatility across sectors.
(5) Comprehensive techno-economic and environmental analyses. Conducting thorough techno-economic and environmental assessments is essential to evaluate the commercial viability and sustainability of biochar production methods. Analyses should account for the cost of feedstocks, production efficiency, scalability, and environmental impacts, including carbon footprint and potential pollutants. These insights can guide the development of eco-friendly, economically feasible biochar solutions that align with sustainable development goals.
(6) Cross-disciplinary research collaboration. Promoting collaboration across diverse fields, such as materials science, environmental engineering, agriculture, and economics, can address complex challenges in biochar research. Cross-disciplinary efforts can enhance biochar's applications through shared expertise, driving innovation and fostering more holistic approaches to production, characterization, and commercialization. Collaborative projects may accelerate biochar's role in sustainability and contribute to advances in environmental management and clean energy.

Declaration of Interest

Chunfei Wu is the Editor-in-Chief of Carbon Capture Science and Technology and the co-authors Lisa Mingzhe Sun, Lina Liu, Haiping Yang, Hongman Sun, Dongdong Feng, Daxin Liang, Yeshui Zhang, Salman Masoudi Soltani and Shouliang Yi are also editors of the journal; however, none of these individuals have had access to the peer review or editorial process for this article at any point.

Declaration of competing interest

The authors declare that they have no known competing financial interests or personal relationships that could have appeared to influence the work reported in this paper.

CRediT authorship contribution statement

Lisa Mingzhe Sun: Writing – review & editing, Writing – original draft, Methodology, Investigation, Conceptualization. **Sean R. McIntyre:** Writing – original draft, Methodology, Investigation. **Paul Iacomi:** Writing – review & editing, Writing – original draft, Methodology, Investigation, Conceptualization. **Katie Everden:** Writing – review & editing, Writing – original draft, Investigation, Conceptualization. **Paul T. Williams:** Writing – review & editing, Investigation, Conceptualization. **Shuang Zong:** Writing – original draft, Investigation, Conceptualization. **Xinying Liu:** Writing – review & editing, Methodology, Investigation, Conceptualization. **Xiefei Zhu:** Writing – review & editing, Writing – original draft. **Yanke Yang:** Writing – review & editing, Writing – original draft, Conceptualization. **Shuangjun Li:** Writing – review & editing, Writing – original draft, Conceptualization. **Gang Wu:** Writing – original draft, Conceptualization. **Fei Huang:** Writing – original draft, Conceptualization. **Lina Liu:** Writing – review & editing, Formal analysis, Conceptualization. **Xiangzhou Yuan:** Writing – review & editing, Formal analysis, Conceptualization. **Huiyan Zhang:** Writing – review & editing, Supervision, Conceptualization. **Junjie Zhang:** Writing – original draft, Formal analysis, Conceptualization. **Haiping Yang:** Writing – review & editing, Supervision, Conceptualization. **Wei Chen:** Writing – review & editing, Supervision, Investigation. **Hongman Sun:** Writing – review & editing, Writing – original draft, Formal analysis, Conceptualization. **Yang Cao:** Writing – review & editing, Writing – original draft, Investigation, Formal analysis, Conceptualization. **Dongdong Feng:** Writing – review & editing, Formal analysis, Conceptualization. **Zhenyu Cheng:** Writing – original draft, Formal analysis, Conceptualization. **Xiong Zhang:** Writing – review & editing, Supervision, Formal

analysis, Data curation. **Daxin Liang:** Writing – review & editing, Supervision, Investigation, Formal analysis. **Shengkai Liu:** Writing – original draft, Formal analysis, Conceptualization. **Xiaoxiao Zhang:** Writing – review & editing, Writing – original draft, Formal analysis, Data curation, Conceptualization. **Xiaohong Zhu:** Writing – review & editing, Writing – original draft, Data curation, Conceptualization. **Ye Shui Zhang:** Writing – review & editing, Writing – original draft, Formal analysis, Data curation. **Yongliang Yan:** Writing – review & editing, Writing – original draft, Formal analysis, Data curation, Conceptualization. **Jianrui Zha:** Writing – review & editing, Writing – original draft, Formal analysis, Data curation. **Yuanting Qiao:** Writing – review & editing, Writing – original draft, Formal analysis, Data curation, Conceptualization. **Salman Masoudi Soltani:** Writing – review & editing, Investigation, Formal analysis. **Ning Zhang:** Writing – review & editing, Writing – original draft, Formal analysis, Data curation, Conceptualization. **Shouliang Yi:** Writing – review & editing, Writing – original draft, Formal analysis, Data curation. **Chunfei Wu:** Writing – review & editing, Formal analysis, Conceptualization.

References

Abbas, Q., Liu, G., Yousaf, B., Ali, M.U., Ullah, H., Munir, M.A.M., Liu, R., 2018. Contrasting effects of operating conditions and biomass particle size on bulk characteristics and surface chemistry of rice husk derived-biochars. J. Anal. Appl. Pyrolysis. 134, 281–292. doi:10.1016/j.jaap.2018.06.018.

Abd El-Mageed, T.A., Rady, M.M., Taha, R.S., Abd El Azeam, S., Simpson, C.R., Semida, W.M., 2020. Effects of integrated use of residual sulfur-enhanced biochar with effective microorganisms on soil properties, plant growth and short-term productivity of Capsicum annuum under salt stress. Sci. Hortic. 261, 108930. doi:10.1016/j.scienta.2019.108930.

Adeniyi, A.G., Abdulkareem, S.A., Ighalo, J.O., Onifade, D.V., Sanusi, S.K., 2021. Thermochemical Co-conversion of Sugarcane Bagasse-LDPE hybrid waste into biochar. Arab. J. Sci. Eng. 46 (7), 6391–6397. doi:10.1007/s13369-020-05119-9.

Adeniyi, A.G., Abdulkareem, S.A., Iwuozor, K.O., Ogunniyi, S., Abdulkareem, M.T., Emenike, E.C., Sagboye, P.A., 2022. Effect of salt impregnation on the properties of orange albedo biochar. Clean. Chem. Eng. 3, 100059. doi:10.1016/j.clce.2022.100059.

Adewuyi, A., Otuechere, C.A., Ellah, N.H., Kaki, S.S., Fayemi, S.O., Adeosun, C.B., 2021. Evaluation of the hepato-renal functions and antimicrobial activity of fatty amido benzoic acid synthesised from Citrullus colocynthis seed oil. Appl. Biol. Chem. 64 (1), 8. doi:10.1186/s13765-020-00586-y.

Adlak, K., Chandra, R., Vijay, V.K., Pant, K.K., 2021. Physicochemical activation and palletisation of Azadirachta indica wood carbons for increased biomethane adsorbed energy storage. J. Anal. Appl. Pyrolysis. 155. doi:10.1016/j.jaap.2021.105102.

Afailal, Z., Gil-Lalaguna, N., Macías, R.J., Gonzalo, A., Sánchez, J.L., 2023. Production of antioxidant additives and high-quality activated biochar from pyrolysis of Argan shells. BioEnergy Res. 1–14. doi:10.1007/s12155-023-10652-0.

Agrafioti, E., Bouras, G., Kalderis, D., Diamadopoulos, E., 2013. Biochar production by sewage sludge pyrolysis. J. Anal. Appl. Pyrolysis. 101, 72–78. doi:10.1016/j.jaap.2013.02.010.

Ahmad, M.A., Alrozi, R., 2011. Removal of malachite green dye from aqueous solution using rambutan peel-based activated carbon: equilibrium, kinetic and thermodynamic studies. Chem. Eng. J. 171 (2), 510–516. doi:10.1016/j.cej.2011.04.018.

Ahmad, M., Lee, S.S., Dou, X., Mohan, D., Sung, J.-K., Yang, J.E., Ok, Y.S., 2012. Effects of pyrolysis temperature on soybean stover- and peanut shell-derived biochar properties and TCE adsorption in water. Bioresour. Technol. 118, 536–544. doi:10.1016/j.biortech.2012.05.042.

Ahmad, M., Rajapaksha, A.U., Lim, J.E., Zhang, M., Bolan, N., Mohan, D., Vithanage, M., Lee, S.S., Ok, Y.S., 2014. Biochar as a sorbent for contaminant management in soil and water: A review. Chemosphere 99, 19–33. doi:10.1016/j.chemosphere.2013.10.071.

Ahmed, W., Mehmood, S., Núñez-Delgado, A., Ali, S., Qaswar, M., Shakoor, A., Mahmood, M., Chen, D.Y., 2021. Enhanced adsorption of aqueous Pb(II) by modified biochar produced through pyrolysis of watermelon seeds. Science of the Total Environment 784. doi:10.1016/j.scitotenv.2021.147136.

Ahmed, M.B., Zhou, J.L., Ngo, H.H., Guo, W., 2016. Insight into biochar properties and its cost analysis. Biomass Bioenergy 84, 76–86. doi:10.1016/j.biombioe.2015.11.002.

Ajien, A., Idris, J., Md Sofwan, N., Husen, R., Seli, H., 2023. Coconut shell and husk biochar: A review of production and activation technology, economic, financial aspect and application. Waste Manage.. Res. 41 (1), 37–51. doi:10.1177/0734242X2211271.

Akhtar, J., Amin, N.S.J.R., Reviews, S.E., 2012. A review on operating parameters for optimum liquid oil yield in biomass pyrolysis. 16(7), 5101–5109.

Al Masud, M.A., Kumar, A.V.N., Shin, W.S.J.S., Technology, P., 2023. Fe (II) activated calcium peroxide/peroxymonosulfate: A practical system for phenanthrene degradation upholding Ecol. pH. 317, 123902.

Al-Rumaihi, A., Shahbaz, M., Mckay, G., Mackey, H., Al-Ansari, T.J.R., Reviews, S.E., 2022. A review pyrolysis technologies feedstock: A blending approach for plastic biomass towards optimum biochar yield. 167, 112715.

Alharbi, H.A., Hameed, B.H., Alotaibi, K.D., Al-Oud, S.S., Al-Modaihsh, A.S., 2022. Recent methods in the production of activated carbon from date palm residues for the adsorption of textile dyes: a review. Front. Environ. Sci. 10. doi:10.3389/fenvs.2022.996953.

Alipour Moghadam Esfahani, R., Osmieri, L., Specchia, S., Yusup, S., Tavasoli, A., Zamaniyan, A., 2017. H2-rich syngas production through mixed residual biomass and HDPE waste via integrated catalytic gasification and tar cracking plus bio-char upgrading. Chem. Eng. J. 308, 578–587. doi:10.1016/j.cej.2016.09.049.

Alizadeh, P., Dumonceaux, T., Tabil, L.G., Mupondwa, E., Soleimani, M., Cree, D., 2022. Steam Explosion Pre-Treatment Sawdust for Biofuel Pellets. 4(4), 1175–1192.

Aller, D.M., Archontoulis, S.V., Zhang, W., Sawadgo, W., Laird, D.A., Moore, K., 2018. Long term biochar effects on corn yield, soil quality and profitability in the US Midwest. Field. Crops. Res. 227, 30–40.

Aller, M.F., 2016. Biochar properties: transport, fate, and impact. Crit. Rev. Environ. Sci. Technol. 46 (14-15), 1183–1296. doi:10.1080/10643389.2016.1212368.

AlNouss, A., McKay, G., Al-Ansari, T., 2020. Enhancing waste to hydrogen production through biomass feedstock blending: A techno-economic-environmental evaluation. Appl. Energy 266, 114885.

Amalina, F., Abd Razak, A.S., Krishnan, S., Zularisam, A., Nasrullah, M.J.C.M., 2022. A comprehensive assessment method for producing biochar, its characterization, stability, potential applications in regenerative economic sustainability–a review. 3, 100045.

Amen, R., Yaseen, M., Mukhtar, A., Klemes, J.J., Saqib, S., Ullah, S., Al-Sehemi, A.G., Rafiq, S., Babar, M., Fatt, C.L., Ibrahim, M., Asif, S., Qureshi, K.S., Akbar, M.M., Bokhari, A., 2020. Lead and cadmium removal from wastewater using eco-friendly biochar adsorbent derived from rice husk, wheat straw, and corncob. Clean Eng Technol 1, 100006. https://doi.org/ARTN.

Amin, F.R., Huang, Y., He, Y., Zhang, R., Liu, G., Chen, C., 2016. Biochar applications and modern techniques for characterization. Clean. Technol. Environ. Policy. 18 (5), 1457–1473. doi:10.1007/s10098-016-1218-8.

An, X., Wu, Z., Qin, H., Liu, X., He, Y., Xu, X., Li, T., Yu, B., 2021. Integrated co-pyrolysis and coating for the synthesis of a new coated biochar-based fertilizer with enhanced slow-release performance. Journal of Cleaner Production 283, 124642. doi:10.1016/j.jclepro.2020.124642.

Anand, A., Kumar, V., Kaushal, P., 2022. Biochar and its twin benefits: crop residue management and climate change mitigation in India. Renew. Sustain. Energy Reviews 156, 111959. doi:10.1016/j.rser.2021.111959.

Angın, D., 2013. Effect of pyrolysis temperature and heating rate on biochar obtained from pyrolysis of safflower seed press cake. Bioresour. Technol. 128, 593–597. doi:10.1016/j.biortech.2012.10.150.

Angın, D., 2013. Effect of pyrolysis temperature and heating rate on biochar obtained from pyrolysis of safflower seed press cake. Bioresource technology 128, 593–597. https://www.sciencedirect.com/science/article/pii/S0960852412016598.

Antal, M.J., Allen, S.G., Dai, X.F., Shimizu, B., Tam, M.S., Gronli, M., 2000. Attainment of the theoretical yield of carbon from biomass. Industrial & Engineering Chemistry Research 39 (11), 4024–4031. https://pubs.acs.org/doi/full/10.1021/ie000511u.

Antonangelo, J.A., Zhang, H., Sun, X., Kumar, A., 2019. Physicochemical properties and morphology of biochars as affected by feedstock sources and pyrolysis temperatures. Biochar. 1 (3), 325–336. doi:10.1007/s42773-019-00028-z.

Anuar Sharuddin, S.D., Abnisa, F., Wan Daud, W.M.A., Aroua, M.K., 2016. A review on pyrolysis of plastic wastes. Energy Convers. Manage. 115, 308–326. doi:10.1016/j.enconman.2016.02.037.

Aon, M., Aslam, Z., Hussain, S., Bashir, M.A., Shaaban, M., Masood, S., Iqbal, S., Khalid, M., Rehim, A., Mosa, W.F.J.S., 2023. Wheat Straw Biochar Produced at a Low Temperature Enhanced Maize Growth Yield by Influencing Soil Properties Typic calciargid. 15(12), 9488.

Arán, D.S., Deza, M., Monferrán, M.V., Pignata, M.L., Harguinteguy, C.A., 2023. Use of local waste for biochar production: influence of feedstock and pyrolysis temperature on chromium removal from aqueous solutions. Integr. Environ. Assess. Manage. 19 (3), 717–725. doi:10.1002/ieam.4643.

Araújo Santos, J., Isidoria Silva Gonzaga, M., Melo dos Santos, W., José da Silva, A., 2022. Water retention and availability in tropical soils of different textures amended with biochar. CATENA 219, 106616. doi:10.1016/j.catena.2022.106616.

Araki, Y., Matsukawa, Y., Saito, Y., Matsushita, Y., Aoki, H., Era, K., Aoki, T., 2021. Effects of carrier gas on the properties of soot produced by ethylene pyrolysis. Fuel Process. Technol. 213, 106673. doi:10.1016/j.fuproc.2020.106673.

Arenillas, A., Rubiera, F., Parra, J.B., Pis, J.J., 2002. Active surface area of carbon materials determined by different methods. In: Rodriguez-Reinoso, F., McEnaney, B., Rouquerol, J., Unger, K. (Eds.), Studies in Surface Science and Catalysis. Elsevier, pp. 209–216. doi:10.1016/S0167-2991(02)80136-7.

Asere, T.G., Stevens, C.V., Du Laing, G., 2019. Use of (modified) natural adsorbents for arsenic remediation: A review. Science of the Total Environment 676, 706–720. doi:10.1016/j.scitotenv.2019.04.237.

Atienza-Martínez, M., Ábrego, J., Gea, G., Marías, F., 2020. Pyrolysis of dairy cattle manure: evolution of char characteristics. J. Anal. Appl. Pyrolysis. 145, 104724. doi:10.1016/j.jaap.2019.104724.

Aydin, E.S., Yucel, O., Sadikoglu, H., 2018. Numerical and experimental investigation of hydrogen-rich syngas production via biomass gasification. Int. J. Hydrogen. Energy 43 (2), 1105–1115.

Aydinli, B., Caglar, A., 2012. The investigation of the effects of two different polymers and three catalysts on pyrolysis of hazelnut shell. Fuel Process. Technol. 93 (1), 1–7. doi:10.1016/j.fuproc.2011.07.009.

Ayodele, B.V., Mustapa, S.I., Tuan Abdullah, T.A.R.B., Salleh, S.F., 2019. A mini-review on hydrogen-rich syngas production by thermo-catalytic and bioconversion of biomass and its environmental implications. Front. Energy Res. 7, 118.

Azeem, M., Hayat, R., Hussain, Q., Ahmed, M., Pan, G., Ibrahim Tahir, M., Imran, M., Irfan, M., Mehmood ul, H., 2019. Biochar improves soil quality and N2-fixation and reduces net ecosystem CO_2 exchange in a dryland legume-cereal cropping system. Soil Tillage Res. 186, 172–182. doi:10.1016/j.still.2018.10.007.

Azuara, M., Baguer, B., Villacampa, J.I., Hedin, N., Manyà, J.J., 2016. Influence of pressure and temperature on key physicochemical properties of corn stover-derived biochar. Fuel 186, 525–533. doi:10.1016/j.fuel.2016.08.088.

Azzi, E.S., Karltun, E., Sundberg, C., 2019. Prospective life cycle assessment of large-scale biochar production and use for negative emissions in Stockholm. Environ. Sci. Technol. 53 (14), 8466–8476. doi:10.1021/acs.est.9b01615.

Bai, T., Ma, W., Li, W., Jiang, J., Chen, J., Cao, R., Yang, W., Dong, D., Liu, T., Xu, Y., 2023. Effect Different Phosphates on Pyrolysis Temperature-Dependent Carbon Sequestration Phosphorus Release Performance in Biochar. 28(9), 3950.

Balaji, S.S., Karnan, M., Sathish, M., 2018. Symmetric electrochemical supercapacitor performance evaluation of N-doped graphene prepared via supercritical fluid processing. J. Solid State Electrochem. 22 (12), 3821–3832. doi:10.1007/s10008-018-4086-9.

Balmuk, G., Videgain, M., Manyà, J.J., Duman, G., Yanik, J., 2023. Effects of pyrolysis temperature and pressure on agronomic properties of biochar. J. Anal. Appl. Pyrolysis. 169, 105858. doi:10.1016/j.jaap.2023.105858.

Balwant Singh, M.C.-A., Lehmann, Johannes, 2017. Biochar: A Guide to Analytical Methods. CSIRO publishing.

Bamdad, H., Papari, S., MacQuarrie, S., Hawboldt, K., 2021. Study of surface heterogeneity and nitrogen functionalizing of biochars: molecular modeling approach. Carbon 171, 161–170. doi:10.1016/j.carbon.2020.08.062.

Bamminger, C., Zaiser, N., Zinsser, P., Lamers, M., Kammann, C., Marhan, S., 2014. Effects of biochar, earthworms, and litter addition on soil microbial activity and abundance in a temperate agricultural soil. Biology and Fertility of Soils 50 (8), 1189–1200. doi:10.1007/s00374-014-0968-x.

Bartoli, M., Giorcelli, M., Rosso, C., Rovere, M., Jagdale, P., Tagliaferro, A., 2019. Influence of commercial biochar fillers on brittleness/ductility of epoxy resin composites. Appl. Sci..

Beis, S.H., Onay, Ö., Koçkar, Ö.M., 2002. Fixed-bed pyrolysis of safflower seed: influence of pyrolysis parameters on product yields and compositions. Renew. Energy 26 (1), 21–32. doi:10.1016/S0960-1481(01)00109-4.

Bellinger, D.C., Chen, A.M., Lanphear, B.P., 2017. Establishing and Achieving National Goals for Preventing Lead Toxicity and Exposure in Children. Jama Pediatrics 171 (7), 617–618. doi:10.1001/jamapediatrics.2017.0775.

Berslin, D., Reshmi, A., Sivaprakash, B., Rajamohan, N., Kumar, P.S., 2022. Remediation of emerging metal pollutants using environment friendly biochar- review on applications and mechanism. Chemosphere 290, 133384. doi:10.1016/j.chemosphere.2021.133384.

Bhatia, S.K., Gurav, R., Choi, T.R., Kim, H.J., Yang, S.Y., Song, H.S., Park, J.Y., Park, Y.L., Han, Y.H., Choi, Y.K., Kim, S.H., Yoon, J.J., Yang, Y.H., 2020. Conversion of waste cooking oil into biodiesel using heterogenous catalyst derived from cork biochar. Bioresour Technol 302, 122872. doi:10.1016/j.biortech.2020.122872.

Bhatia, S.K., Palai, A.K., Kumar, A., Bhatia, R.K., Patel, A.K., Thakur, V.K., Yang, Y.-H.J.B.T., 2021. Trends in renewable energy production employing biomass-based biochar. 340, 125644.

Bi, Y., Cai, S., Wang, Y., Xia, Y., Zhao, X., Wang, S., Xing, G., 2019. Assessing the viability of soil successive straw biochar amendment based on a five-year column trial with six different soils: views from crop production, carbon sequestration and net ecosystem economic benefits. J. Environ. Manage. 245, 173–186.

Bi, H., He, X., Zhang, H., Li, H., Xiao, N., Qiu, J., 2021. N, P co-doped hierarchical porous carbon from rapeseed cake with enhanced supercapacitance. Renew. Energy 170, 188–196. doi:10.1016/j.renene.2021.01.099.

Bi, D., Huang, F., Jiang, M., He, Z., Lin, X., 2022. Effect of pyrolysis conditions on environmentally persistent free radicals (EPFRs) in biochar from co-pyrolysis of urea and cellulose. Sci. Total Environ. 805, 150339. doi:10.1016/j.scitotenv.2021.150339.

Biti, S., Mccue, A., Dionisi, D., Graça, I., Martín, C.F., 2023. Sustainable microcrystalline cellulose-based activated carbons for a greener carbon capture at post-combustion conditions. Int. J. Greenhouse Gas Control 125, 103876. doi:10.1016/j.ijggc.2023.103876.

Blenis, N., Hue, N., Maaz, T.M., Kantar, M., 2023. Biochar Production, Modification, Its Uses in Soil Remediation: A Review. 15(4), 3442.

Borges, B.M.M.N., Strauss, M., Camelo, P.A., Sohi, S.P., Franco, H.C.J., 2020. Re-use of sugarcane residue as a novel biochar fertiliser-Increased phosphorus use efficiency and plant yield. Journal of Cleaner Production 262, 121406. https://doi.org/ARTN.

Bouchelta, C., Medjram, M.S., Zoubida, M., Chekkat, F.A., Ramdane, N., Bellat, J.-P., 2012. Effects of pyrolysis conditions on the porous structure development of date pits activated carbon. J. Anal. Appl. Pyrolysis. 94, 215–222. doi:10.1016/j.jaap.2011.12.014.

Bracciale, M.P., De Caprariis, B., De Filippis, P., Hernandez, A.D., Scarsella, M., 2019. New synthetic route for the production of mayenite support to enhance Ni resistance to coke deposition in the reforming of tar model compounds. Applied Catalysis A General. https://www.sciencedirect.com/science/article/pii/S0926860X19300511.

Braghiroli, F.L., Bouafif, H., Neculita, C.M., Koubaa, A., 2019. Performance of physically and chemically activated biochars in copper removal from contaminated mine effluents. Water Air Soil Pollut. 230, 1–14.

Brewer, C.E., Chuang, V.J., Masiello, C.A., Gonnermann, H., Gao, X., Dugan, B., Driver, L.E., Panzacchi, P., Zygourakis, K., Davies, C.A., 2014. New approaches to measuring biochar density and porosity. Biomass Bioenergy 66, 176–185. doi:10.1016/j.biombioe.2014.03.059.

Bridgwater, A.V.J.B., bioenergy, 2012. Review fast pyrolysis biomass product upgrading 38, 68–94.

Bridgwater, A.V., Meier, D., Radlein, D., 1999. An overview of fast pyrolysis of biomass. Org. Geochem. 30 (12), 1479–1493. doi:10.1016/S0146-6380(99)00120-5.

Bridgwater, A.J.A.C.A.G., 1994. Catalysis in thermal biomass conversion 116 (1-2), 5–47.

Brown, T., 2016. Engineering economics and economic design for process engineers. CRC press.

Bushra, B., Remya, N., 2020. Biochar from pyrolysis of rice husk biomass—Characteristics, modification and environmental application. BioMass Convers. Biorefin. 1–12. doi:10.1007/s13399-020-01092-3.

Buss, W., Mašek, O., Graham, M., Wüst, D., 2015. Inherent organic compounds in biochar–Their content, composition and potential toxic effects. J. Environ. Manage. 156, 150–157. doi:10.1016/j.jenvman.2015.03.035.

Buss, W., Graham, M.C., MacKinnon, G., Mašek, O., 2016. Strategies for producing biochars with minimum PAH contamination. J. Anal. Appl. Pyrolysis. 119, 24–30. doi:10.1016/j.jaap.2016.04.001.

C, G.D.-M., Saenz de Miera, B., Collado, L., Fermoso, J., Masek, O., Pizarro, P., Serrano, D.P., Moreno, I., Fermoso, J., 2023. Removal of NO at low concentration from air in urban built environments by activated miscanthus biochar. J. Environ. Manage. 336, 117610. doi:10.1016/j.jenvman.2023.117610.

Calvelo Pereira, R., Kaal, J., Camps Arbestain, M., Pardo Lorenzo, R., Aitkenhead, W., Hedley, M., Macías, F., Hindmarsh, J., Maciá-Agulló, J.A., 2011. Contribution to characterisation of biochar to estimate the labile fraction of carbon. Org. Geochem. 42 (11), 1331–1342. doi:10.1016/j.orggeochem.2011.09.002.

Cao, Q., An, T., Xie, J., Liu, Y., Xing, L., Ling, X., Chen, C., 2022. Insight to the physiochemical properties and DOM of biochar under different pyrolysis temperature and modification conditions. Journal of Analytical and Applied Pyrolysis 166, 105590. doi:10.1016/j.jaap.2022.105590.

Cao, X., Pignatello, J.J., Li, Y., Lattao, C., Chappell, M.A., Chen, N., Miller, L.F., Mao, J., 2012. Characterization of wood chars produced at different temperatures using advanced solid-State 13C NMR spectroscopic techniques. Energy Fuels 26 (9), 5983–5991. doi:10.1021/ef300947s.

Cao, Z., Liu, X., Xu, J., Zhang, J., Yang, Y., Zhou, J., Xu, X., Lowry, G.V., 2017. Removal of antibiotic florfenicol by sulfide-modified Nanoscale zero-valent iron. Environ. Sci. Technol. 51 (19), 11269–11277. doi:10.1021/acs.est.7b02480.

Cardoso, J.S., Silva, V., Chavando, J.A.M., Eusébio, D., Hall, M.J., Costa, M., 2021. Small-scale biomass gasification for green ammonia production in Portugal: A techno-economic study. Energy Fuels 35 (17), 13847–13862.

Carpio, M.J., Sánchez-Martín, M.J., Rodríguez-Cruz, M.S., Marín-Benito, J.M., 2021. Effect of organic residues on pesticide behavior in soils: A. Review Laboratory Res. 8 (4), 32.

Cely, P., Gascó, G., Paz-Ferreiro, J., Méndez, A., 2015. Agronomic properties of biochars from different manure wastes. J. Anal. Appl. Pyrolysis. 111, 173–182. doi:10.1016/j.jaap.2014.11.014.

Cetin, E., Gupta, R., Moghtaderi, B., 2005. Effect of pyrolysis pressure and heating rate on radiata pine char structure and apparent gasification reactivity. Fuel 84 (10), 1328–1334. doi:10.1016/j.fuel.2004.07.016.

Cha, J.S., Park, S.H., Jung, S.-C., Ryu, C., Jeon, J.-K., Shin, M.-C., Park, Y.-K.J.J.o.I., Chemistry, E., 2016. Production utilization biochar: A review 40, 1–15.

Chai, G.-L., Qiu, K., Qiao, M., Titirici, M.-M., Shang, C., Guo, Z., 2017. Active sites engineering leads to exceptional ORR and OER bifunctionality in P,N Co-doped graphene frameworks. Energy Environ. Sci. 10 (5), 1186–1195. doi:10.1039/c6ee03446b.

Chan, K.Y., Van Zwieten, L., Meszaros, I., Downie, A., Joseph, S., 2007. Agronomic values of green waste biochar as a soil amendment. Australian J. Soil Res. 45, 629–634. doi:10.1071/SR07109.

Chandra, S., Bhattacharya, J., 2019. Influence of temperature and duration of pyrolysis on the property heterogeneity of rice straw biochar and optimization of pyrolysis conditions for its application in soils. J. Clean. Prod. 215, 1123–1139. doi:10.1016/j.jclepro.2019.01.079.

Chatterjee, R., Sajjadi, B., Chen, W.-Y., Mattern, D.L., Hammer, N., Raman, V., Dorris, A., 2020. Effect of pyrolysis temperature on physicochemical properties and acoustic-based amination of biochar for efficient CO_2 adsorption. Frontiers in Energy Research 8, 85. https://www.frontiersin.org/journals/energy-research/articles/10.3389/fenrg.2020.00085/full.

Chattopadhyay, J., Pathak, T.S., Srivastava, R., Singh, A.C., 2016. Catalytic co-pyrolysis of paper biomass and plastic mixtures (HDPE (high density polyethylene), PP (polypropylene) and PET (polyethylene terephthalate)) and product analysis. Energy 103, 513–521. doi:10.1016/j.energy.2016.03.015.

Chausali, N., Saxena, J., Prasad, R., 2021. Nanobiochar and biochar based nanocomposites: advances and applications. J. Agric. Food Res. 5, 100191. doi:10.1016/j.jafr.2021.100191.

Chaves Fernandes, B.C., Ferreira Mendes, K., Dias Júnior, A.F., da Silva Caldeira, V.P., da Silva Teófilo, T.M., Severo Silva, T., Mendonça, V., de Freitas Souza, M., Valadão Silva, D., 2020. Impact Pyrolysis Temperature on Properties Eucalyptus Wood-Derived Biochar 13 (24), 5841.

Che, H.X., Wei, G.T., Fan, Z.D., Zhu, Y.L., Zhang, L.Y., Wei, Z.Z., Huang, X.L., Wei, L.R., 2023. Super facile one-step synthesis of sugarcane bagasse derived N-doped porous biochar for adsorption of ciprofloxacin. Journal of Environmental Management 335. doi:10.1016/j.jenvman.2023.117566. https://doi.org/ARTN117566.

Cheah, S., Malone, S.C., Feik, C.J., 2014. Speciation of sulfur in biochar produced from pyrolysis and gasification of oak and corn stover. Environ. Sci. Technol. 48 (15), 8474–8480. doi:10.1021/es500073r.

Cheah, S., Jablonski, W.S., Olstad, J.L., Carpenter, D.L., Barthelemy, K.D., Robichaud, D.J., Andrews, J.C., Black, S.K., Oddo, M.D., Westover, T.L.J.G.C., 2016. Effects thermal pretreatment catalyst on biomass gasification efficiency syngas composition 18 (23), 6291–6304.

Chen, Y., Yang, H., Wang, X., Zhang, S., Chen, H., 2012. Biomass-based pyrolytic polygeneration system on cotton stalk pyrolysis: Influence of temperature. Bioresour Technol 107 (none), 411–418. https://www.sciencedirect.com/science/article/pii/S0960852411015628.

Chen, L.W., Yang, S.J., Zuo, X., Huang, Y., Cai, T.M., Ding, D.H., 2018. Biochar modification significantly promotes the activity of CoO towards heterogeneous

activation of peroxymonosulfate. Chemical Engineering Journal 354, 856–865. doi:10.1016/j.cej.2018.08.098.
Chen, S.S., Cao, Y., Tsang, D.C.W., Tessonnier, J.-P., Shang, J., Hou, D., Shen, Z., Zhang, S., Ok, Y.S., Wu, K.C.W., 2020. Effective Dispersion of MgO Nanostructure on Biochar Support as a Basic Catalyst for Glucose Isomerization. ACS Sustainable Chemistry & Engineering 8 (18), 6990–7001. doi:10.1021/acssuschemeng.0c00278.
Chen, L., Zhang, Y., Labianca, C., Wang, L., Ruan, S., Poon, C.S., Ok, Y.S., Tsang, D.C.W., 2022. Carbon-negative cement-bonded biochar particleboards. Biochar 4 (1). doi:10.1007/s42773-022-00185-8.
Chen, L., Zhang, Y., Wang, L., Ruan, S., Chen, J., Li, H., Yang, J., Mechtcherine, V., Tsang, D.C.W., 2022b. Biochar-augmented carbon-negative concrete. Chemical Engineering Journal 431, 133946. doi:10.1016/j.cej.2021.133946.
Chen, G., Yao, J., Liu, J., Yan, B., Shan, R., 2016. Biomass to hydrogen-rich syngas via catalytic steam reforming of bio-oil. Renew. Energy 91, 315–322.
Chen, D., Li, Y., Cen, K., Luo, M., Li, H., Lu, B., 2016a. Pyrolysis polygeneration of poplar wood: effect of heating rate and pyrolysis temperature. Bioresour. Technol. 218, 780–788. doi:10.1016/j.biortech.2016.07.049.
Chen, D., Yu, X., Song, C., Pang, X., Huang, J., Li, Y., 2016b. Effect of pyrolysis temperature on the chemical oxidation stability of bamboo biochar. Bioresour. Technol. 218, 1303–1306. doi:10.1016/j.biortech.2016.07.112.
Chen, J.-M., Zhou, W.-W., Poyarkov Jr., N.A., Stuart, B.L., Brown, R.M., Lathrop, A., Wang, Y.-Y., Yuan, Z.-Y., Jiang, K., Hou, M., Chen, H.-M., Suwannapoom, C., Sang Ngoc, N., Tang Van, D., Papenfuss, T.J., Murphy, R.W., Zhang, Y.-P., Che, J., 2017. A novel multilocus phylogenetic estimation reveals unrecognized diversity in Asian horned toads, genus megophrys sensu lato (Anura: Megophryidae). Mol. Phylogenet. Evol. 106, 28–43. doi:10.1016/j.ympev.2016.09.004.
Chen, L., Li, X., Ma, C., Wang, M., Zhou, J., 2017. Interaction and quantum capacitance of nitrogen/sulfur Co-doped graphene: A theoretical calculation. J. Physical Chem. C 121 (34), 18344–18350. doi:10.1021/acs.jpcc.7b04551.
Chen, W., Chen, Y., Yang, H., Xia, M., Li, K., Chen, X., Chen, H., 2017. Co-pyrolysis of lignocellulosic biomass and microalgae: products characteristics and interaction effect. Bioresour. Technol. 245, 860–868. doi:10.1016/j.biortech.2017.09.022.
Chen, W., Yang, H., Chen, Y., Xia, M., Chen, X., Chen, H., 2017b. Transformation of nitrogen and evolution of N-containing species during algae pyrolysis. Environ. Sci. Technol. 51 (11), 6570–6579. doi:10.1021/acs.est.7b00434.
Chen, W., Chen, Y., Yang, H., Li, K., Chen, X., Chen, H., 2018. Investigation on biomass nitrogen-enriched pyrolysis: influence of temperature. Bioresour. Technol. 249, 247–253. doi:10.1016/j.biortech.2017.10.022.
Chen, W., Yang, H., Chen, Y., Li, K., Xia, M., Chen, H., 2018. Influence of biochar addition on nitrogen transformation during copyrolysis of algae and lignocellulosic biomass. Environ. Sci. Technol. 52 (16), 9514–9521. doi:10.1021/acs.est.8b02485.
Chen, Y., Zhang, L., Zhang, Y., Li, A., 2019. Pressurized pyrolysis of sewage sludge: process performance and products characterization. J. Anal. Appl. Pyrolysis. 139, 205–212. doi:10.1016/j.jaap.2019.02.007.
Chen, W., Fang, Y., Li, K., Chen, Z., Xia, M., Gong, M., Chen, Y., Yang, H., Tu, X., Chen, H., 2020. Bamboo wastes catalytic pyrolysis with N-doped biochar catalyst for phenols products. Appl. Energy 260, 114242. doi:10.1016/j.apenergy.2019.114242.
Chen, W., Gong, M., Li, K., Xia, M., Chen, Z., Xiao, H., Fang, Y., Chen, Y., Yang, H., Chen, H., 2020. Insight into KOH activation mechanism during biomass pyrolysis: chemical reactions between O-containing groups and KOH. Appl. Energy 278, 115730.
Chen, Y., Liu, Y., Li, Y., Chen, Y., Wu, Y., Li, H., Wang, S., Peng, Z., Xu, R., Zeng, Z., 2020. Novel magnetic pomelo peel biochar for enhancing Pb(II) and Cu(II) adsorption: performance and mechanism. Water Air Soil Pollut. 231 (8), 404. doi:10.1007/s11270-020-04788-4.
Chen, J., Wang, P., Ding, L., Yu, T., Leng, S., Chen, J., Fan, L., Li, J., Wei, L., Li, J., Lu, Q., Leng, L., Zhou, W., 2021. The comparison study of multiple biochar stability assessment methods. J. Anal. Appl. Pyrolysis. 156, 105070. doi:10.1016/j.jaap.2021.105070.
Chen, Y., Xu, F., Li, H., Li, Y., Liu, Y., Chen, Y., Li, M., Li, L., Jiang, H., Chen, L., 2021. Simple hydrothermal synthesis of magnetic $MnFe_2O_4$-sludge biochar composites for removal of aqueous Pb^{2+}. J. Anal. Appl. Pyrolysis. 156, 105173. doi:10.1016/j.jaap.2021.105173.
Chen, D., Zhuang, X., Gan, Z., Cen, K., Ba, Y., Jia, D., 2022. Co-pyrolysis of light bio-oil leached bamboo and heavy bio-oil: effects of mass ratio, pyrolysis temperature, and residence time on the biochar. Chem. Eng. J. 437, 135253. doi:10.1016/j.cej.2022.135253.
Chen, Q., Cheng, X., Liu, S., Xia, D., Liu, Y., Zhang, Z., Gu, P.J.D., Materials, R., 2023. Multi-heteroatom self-doped microporous biochar derived from fish scale for boosting uranium immobilization performance, 110052.
Chen, A., Shen, T., Guan, J., Wei, X., Wang, J., Xing, S., 2024. Revolutionizing conventional adsorbents: strengthening dimethyl phthalate adsorption through N/P co-doping macroscopic robust porous carbon. J. Clean. Prod. 434, 140176. doi:10.1016/j.jclepro.2023.140176.
Chen, Z., Han, S., Dong, Z., Li, H., Zhang, A., 2024. Trade-off between soil carbon sequestration and net ecosystem economic benefits for paddy fields under long-term application of biochar. GCB Bioenergy 16 (1), e13116.
Chen, L., Zhao, C., Yuan, X., Zhang, H., Senanayake, M., Mašek, O., He, C., Ok, Y.S., 2025. Sustainable thermochemical plastic valorization towards a circular economy: a critical review. Green Chem. https://doi.org/10.1039/d4gc06070a.
Cheng, Y.Z., Wang, B.Y., Shen, J.M., Yan, P.W., Kang, J., Wang, W.Q., Bi, L.B., Zhu, X.W., Li, Y.B., Wang, S.Y., Shen, L.L., Chen, Z.L., 2022. Preparation of novel N-doped biochar and its high adsorption capacity for atrazine based on π-π electron donor-acceptor interaction. Journal of Hazardous Materials 432, 128757. https://doi.org/ARTN.
Cheng, C., Zhang, J., Mu, Y., Gao, J., Feng, Y., Liu, H., Guo, Z., Zhang, C., 2014. Preparation and evaluation of activated carbon with different polycondensed phosphorus oxyacids (H3PO4, H4P2O7, H6P4O13 and C6H18O24P6) activation employing mushroom roots as precursor. J. Anal. Appl. Pyrolysis. 108, 41–46. doi:10.1016/j.jaap.2014.05.019.
Cheng, B.-H., Zeng, R.J., Jiang, H., 2017. Recent developments of post-modification of biochar for electrochemical energy storage. Bioresour. Technol. 246, 224–233. doi:10.1016/j.biortech.2017.07.060.
Cheng, J., Hu, S.-C., Sun, G.-T., Kang, K., Zhu, M.-Q., Geng, Z.-C., 2021. Comparison of activated carbons prepared by one-step and two-step chemical activation process based on cotton stalk for supercapacitors application. Energy 215, 119144.
Cheng, N., Wang, B., Wu, P., Lee, X., Xing, Y., Chen, M., Gao, B., 2021. Adsorption of emerging contaminants from water and wastewater by modified biochar: A review. Environ. Pollut. 273. doi:10.1016/j.envpol.2021.116448.
Cheng, Y., Yang, J., Shen, J., Yan, P., Liu, S., Kang, J., Bi, L., Wang, B., Zhao, S., Chen, Z., 2023. Preparation of P-doped biochar and its high-efficient removal of sulfamethoxazole from water: adsorption mechanism, fixed-bed column and DFT study. Chem. Eng. J. 468, 143748. doi:10.1016/j.cej.2023.143748.
Chi, N.T.L., Anto, S., Ahamed, T.S., Kumar, S.S., Shanmugam, S., Samuel, M.S., Mathimani, T., Brindhadevi, K., Pugazhendhi, A., 2021. A review on biochar production techniques and biochar based catalyst for biofuel production from algae. Fuel 287, 119411. doi:10.1016/j.fuel.2020.119411.
Cho, D.-W., Cho, S.-H., Song, H., Kwon, E.E., 2015. Carbon dioxide assisted sustainability enhancement of pyrolysis of waste biomass: a case study with spent coffee ground. Bioresour. Technol. 189, 1–6. doi:10.1016/j.biortech.2015.04.002.
Cho, D.-W., Yoon, K., Ahn, Y., Sun, Y., Tsang, D.C., Hou, D., Ok, Y.S., Song, H.J.J.o.h.m., 2019. Fabrication Environ. applications multifunctional mixed metal-biochar composites (MMBC) from red mud lignin wastes 374, 412–419.
Choi, H.S., Choi, Y.S., Park, H.C., 2012. Fast pyrolysis characteristics of lignocellulosic biomass with varying reaction conditions. Renew. Energy 42, 131–135. doi:10.1016/j.renene.2011.08.049.
Choi, J., Nam, H., Carter, S., Capareda, S.C., 2017. Tuning the physicochemical properties of biochar derived from Ashe juniper by vacuum pressure and temperature. J. Environ. Chem. Eng. 5 (4), 3649–3655. doi:10.1016/j.jece.2017.07.028.
Choong, Z.-Y., Lin, K.-Y.A., Lisak, G., Lim, T.-T., Oh, W.-D., 2022. Multi-heteroatom-doped carbocatalyst as peroxymonosulfate and peroxydisulfate activator for water purification: A critical review. J. Hazard. Mater. 426, 128077. doi:10.1016/j.jhazmat.2021.128077.
Choudhary, T.K., Khan, K.S., Hussain, Q., Ahmad, M., Ashfaq, M., 2019. Feedstock-induced changes in composition and stability of biochar derived from different agricultural wastes. Arabian J. GeoSci. 12 (19), 617. doi:10.1007/s12517-019-4735-z.
Chu, S., Subrahmanyam, A.V., Huber, G.W., 2013. The pyrolysis chemistry of a β-O-4 type oligomeric lignin model compound. Green. Chem. 15 (1), 125–136. doi:10.1039/c2gc36332a.
Chun-Zhu, Li, 2006. Special Issue-Gasification: a Route to Clean Energy. Process Safety & Environmental Protection. https://research.monash.edu/en/publications/special-issuegasification-a-route-to-clean-energy.
Ciampi, P., Esposito, C., Bartsch, E., Alesi, E.J., Rehner, G., Morettin, P., Pellegrini, M., Olivieri, S., Ranaldo, M., Liali, G.J.E.R., 2023. A data-driven modeling approach for sustainable remediation persistent arsenic (As) groundwater contamination in a fractured rock aquifer through a groundwater recirculation well (IEG-GCW®) 217, 114827.
CleanAir, 2024. https://www.cleanairfund.org/news-item/deaths-air-pollution-data-hope/.
Collard, F.-X., Blin, J., 2014. A review on pyrolysis of biomass constituents: mechanisms and composition of the products obtained from the conversion of cellulose, hemicelluloses and lignin. Renew. Sustain. Energy Reviews 38, 594–608. doi:10.1016/j.rser.2014.06.013.
Colomba, A., Berruti, F., Briens, C., 2022. Model for the physical activation of biochar to activated carbon. J. Anal. Appl. Pyrolysis. 168, 105769.
Contescu, C.I., Adhikari, S.P., Gallego, N.C., Evans, N.D., Biss, B.E., 2018. Activated carbons derived from high-temperature pyrolysis of lignocellulosic biomass. C 4 (3), 51. doi:10.3390/c4030051.
Conti, R., Fabbri, D., Vassura, I., Ferroni, L., 2016. Comparison of chemical and physical indices of thermal stability of biochars from different biomass by analytical pyrolysis and thermogravimetry. J. Anal. Appl. Pyrolysis. 122, 160–168. doi:10.1016/j.jaap.2016.10.003.
Copa, J., Tuna, C., Silveira, J., Boloy, R., Brito, P., Silva, V., Cardoso, J., Eusébio, D., 2020. Techno-economic assessment of the use of syngas generated from biomass to feed an internal combustion engine. Energies 13 (12), 3097.
CopernicusClimateChangeService, 2024. https://climate.copernicus.eu/?utm_source=pressrelease&utm_medium=referral&utm_campaign=gch24.
Creamer, A.E., Gao, B., Zhang, M., 2014. Carbon dioxide capture using biochar produced from sugarcane bagasse and hickory wood. Chemical Engineering Journal 249, 174–179. https://www.sciencedirect.com/science/article/pii/S1385894714003945.
Creamer, A.E., Gao, B., Wang, S., 2016. Carbon dioxide capture using various metal oxy-hydroxide–biochar composites. Chem. Eng. J. 283, 826–832.
Crombie, K., Mašek, O., 2015. Pyrolysis biochar systems, balance between bioenergy carbon sequestration 7 (2), 349–361. doi:10.1111/gcbb.12137.
Cross, A., Sohi, S.P., 2013. A method for screening the relative long-term stability of biochar. GCB Bioenergy 5 (2), 215–220. doi:10.1111/gcbb.12035.
Cui, X.W., Zhang, S.S., Geng, Y., Zhen, J.Y., Zhan, J.H., Cao, C.B., Ni, S.Q., 2021. Synergistic catalysis by FeO-biochar/peroxymonosulfate system for the removal of bisphenol a. Separation and Purification Technology 276, 119351. https://doi.org/ARTN.
Cui, B., Chen, Z., Wang, F., Zhang, Z., Dai, Y., Guo, D., Liang, W., Liu, Y.J.N., 2022. Facile synthesis magnetic biochar derived from Burley Tobacco stems towards enhanced Cr (VI) removal: Performance mechanism 12 (4), 678.

Cuong, D.V., Liu, N.L., Nguyen, V.A., Hou, C.H., 2019. Meso/micropore-controlled hierarchical porous carbon derived from activated biochar as a high-performance adsorbent for copper removal. Sci. Total. Environ. 692, 844–853. doi:10.1016/j.scitotenv.2019.07.125.

Díaz-Maroto, C.G., de Miera, B.S., Collado, L., Fermoso, J., Mašek, O., Pizarro, P., Serrano, D.P., Moreno, I., Fermoso, J., 2023. Removal of NO at low concentration from air in urban built environments by activated miscanthus biochar. J. Environ. Manage. 336, 117610. doi:10.1016/j.jenvman.2023.117610.

Daful, A.G., Chandraratne, M.R., 2020. Biochar production from biomass waste-derived material. Encycl. Renew. Sust. Mat. 4, 370–378. doi:10.1016/b978-0-12-803581-8.11249-4.

Dai, L., He, C., Wang, Y., Liu, Y., Ruan, R., Yu, Z., Zhou, Y., Duan, D., Fan, L., Zhao, Y., 2018. Hydrothermal pretreatment of bamboo sawdust using microwave irradiation. Bioresour. Technol. 247, 234–241. doi:10.1016/j.biortech.2017.08.104.

Dai, Y., Zhang, N., Xing, C., Cui, Q., Sun, Q., 2019. The adsorption, regeneration and engineering applications of biochar for removal organic pollutants: A review. Chemosphere 223, 12–27. doi:10.1016/j.chemosphere.2019.01.161.

Dalai, A.K., Azargohar, R., 2007. Production of activated carbon from biochar using chemical and physical activation: mechanism and modeling, materials, chemicals, and energy from Forest Biomass. ACS Publications 463–476. doi:10.1021/bk-2007-0954.ch029.

Darweesh, A.H., Weis, M.M., 2024. The impact of particle size in fluidized bed on heat transfer behavior: A review. Adv. Mech. Mater. Eng. 41 (1), 39–46.

Das, S.K., Ghosh, G.K., Avasthe, R.K., Sinha, K., 2021. Compositional heterogeneity of different biochar: effect of pyrolysis temperature and feedstocks. J. Environ. Manage. 278, 111501. doi:10.1016/j.jenvman.2020.111501.

Dayton, D., 2002. Review of the Literature on Catalytic Biomass Tar Destruction: Milestone Completion Report. Journal of Physical Chemistry 97 (48), 7437–7450. https://www.nrel.gov/docs/fy03osti/32815.pdf.

De la Rosa, J.M., Knicker, H., López-Capel, E., Manning, D.A.C., González-Perez, J.A., González-Vila, F.J., 2008. Direct Detection Black Carbon in Soils by Py-GC/MS, Carbon-13 NMR Spectroscopy Thermogravimetric Techniques 72 (1), 258–267. doi:10.2136/sssaj2007.0031.

de Souza Souza, C., Bomfim, M.R., Conceição de Almeida, M.d., Alves, L.d.S., de Santana, W.N., da Silva Amorim, I.C., Santos, J.A.G., 2021. Induced changes of pyrolysis temperature on the physicochemical traits of sewage sludge and on the potential ecological risks. Sci. Rep. 11 (1), 974. doi:10.1038/s41598-020-79658-4.

Deena, S.R., Vickram, A., Manikandan, S., Subbaiya, R., Karmegam, N., Ravindran, B., Chang, S.W., Awasthi, M.K.J.B.T., 2022. Enhanced biogas production from food waste activated sludge using advanced techniques–a review 355, 127234.

Demiral, İ., Şensöz, S., 2006. Fixed-bed pyrolysis of hazelnut (Corylus Avellana L.) bagasse: influence of pyrolysis parameters on product yields. Energy Sources, Part A: Recovery, Utilization, Environ. Effects 28 (12), 1149–1158. doi:10.1080/009083190966126.

Demirbas, A., 2004. Determination of calorific values of bio-chars and pyro-oils from pyrolysis of beech trunkbarks. J. Anal. Appl. Pyrolysis. 72 (2), 215–219. doi:10.1016/j.jaap.2004.06.005.

Deng, Y., Zhao, R.Z., 2015. Advanced Oxidation Processes (AOPs) in Wastewater Treatment. Curr Pollut Rep 1 (3), 167–176. doi:10.1007/s40726-015-0015-z.

Deng, C., Kang, X., Lin, R., Wu, B., Ning, X., Wall, D., Murphy, J.D., 2023. Boosting biogas production from recalcitrant lignin-based feedstock by adding lignin-derived carbonaceous materials within the anaerobic digestion process. Energy 278, 127819. doi:10.1016/j.energy.2023.127819.

Deng, W., Hu, M., Xu, S., Hu, M., Chen, G., Ji, H., Zhou, P., Su, Y., 2023. Pyrolysis of sludge briquettes for the preparation of cylindrical-shaped biochar and comparison between CO_2 and steam activation. Fuel 338, 127317. doi:10.1016/j.fuel.2022.127317.

Deng, J., Chen, J., Zeng, Y., Yang, H., Li, F., Song, B., Yang, Y., Wang, Z., Zhou, C., Wang, W., 2024. Mechanistic insights into ultrafast degradation of electron-rich emerging pollutants by waste cyanobacteria resource utilization. Chem. Eng. J. 499, 155918.

Deng, L., Zhao, Y., Sun, S., Feng, D., Zhang, W., 2024. Preparation of corn straw-based carbon by "carbonization-KOH activation" two-step method: gas–solid product characteristics, activation mechanism and hydrogen storage potential. Fuel 358, 130134. doi:10.1016/j.fuel.2023.130134.

Denoyel, R., Llewellyn, P., Beurroies, I., Rouquerol, J., Rouquerol, F., Luciani, L., 2004. Comparing the basic phenomena involved in three methods of pore-size characterization: gas adsorption, liquid intrusion and thermoporometry. Particle Particle Systems Characterization 21 (2), 128–137. doi:10.1002/ppsc.200400929.

Destyorini, F., Yudianti, R., Irmawati, Y., Hardiansyah, A., Hsu, Y.-I., Uyama, H., 2021. Temperature driven structural transition in the nickel-based catalytic graphitization of coconut coir. Diam. Relat. Mater. 117, 108443. doi:10.1016/j.diamond.2021.108443.

Dhyani, V., Bhaskar, T.J.R.e., 2018. A comprehensive review on pyrolysis lignocellulosic biomass 129, 695–716.

di Bitonto, L., Reynel-Ávila, H.E., Mendoza-Castillo, D.I., Bonilla-Petriciolet, A., Durán-Valle, C.J., Pastore, C., 2020. Synthesis and characterization of nanostructured calcium oxides supported onto biochar and their application as catalysts for biodiesel production. Renewable Energy 160, 52–66. doi:10.1016/j.renene.2020.06.045.

Ding, S., Liu, Y., 2020. Adsorption of CO_2 from flue gas by novel seaweed-based KOH-activated porous biochars. Fuel 260, 116382.

Ding, T., Wu, Y., Zhu, X., Lin, G., Hu, X., Sun, H., Huang, Y., Zhang, S., Zhang, H., 2022. Promoted Production of Phenolic Monomers from Lignin-First Depolymerization of Lignocellulose over Ru Supported on Biochar by N,P-co-Doping. ACS Sustainable Chemistry & Engineering 10 (7), 2343–2354. doi:10.1021/acssuschemeng.1c06335.

Ding, Y., Liu, Y., Liu, S., Li, Z., Tan, X., Huang, X., Zeng, G., Zhou, L., Zheng, B., 2016. Biochar to improve soil fertility. A review. Agronomy for Sustainable Development 36 (2), 36. doi:10.1007/s13593-016-0372-z.

Ding, D., Yang, S., Qian, X., Chen, L., Cai, T., 2020. Nitrogen-doping positively whilst sulfur-doping negatively affect the catalytic activity of biochar for the degradation of organic contaminant. Applied Catalysis B: Environ. 263, 118348. doi:10.1016/j.apcatb.2019.118348.

Ding, Y., Huang, S., Sun, Y., Li, Y., Zhu, L., Wang, S., 2021. Preparation of nitrogen and sulfur Co-doped and interconnected hierarchical porous biochar by pyrolysis of mantis shrimp in CO_2 atmosphere for symmetric supercapacitors. ChemElectroChem. 8 (19), 3745–3754. doi:10.1002/celc.202101151.

Dissanayake, P.D., Choi, S.W., Igalavithana, A.D., Yang, X., Tsang, D.C.W., Wang, C.-H., Kua, H.W., Lee, K.B., Ok, Y.S., 2020. Sustainable gasification biochar as a high efficiency adsorbent for CO_2 capture: A facile method to designer biochar fabrication. Renew. Sustain. Energy Reviews 124, 109785. doi:10.1016/j.rser.2020.109785.

Dissanayake, P.D., You, S., Igalavithana, A.D., Xia, Y., Bhatnagar, A., Gupta, S., Kua, H.W., Kim, S., Kwon, J.-H., Tsang, D.C.W., Ok, Y.S., 2020. Biochar-based adsorbents for carbon dioxide capture: A critical review. Renew. Sustain. Energy Reviews 119, 109582. doi:10.1016/j.rser.2019.109582.

Domingues, R.R., Trugilho, P.F., Silva, C.A., Melo, I.C.N.A.d., Melo, L.C.A., Magriotis, Z.M., Sánchez-Monedero, M.A., 2017. Properties of biochar derived from wood and high-nutrient biomasses with the aim of agronomic and environmental benefits. PLoS. One 12 (5), e0176884. doi:10.1371/journal.pone.0176884.

Dong, H.A., Liang, H., Yang, L., Yang, X.J., Yang, C.L., Hu, G.T., Zhao, T.X., 2023. Porous biochar derived from waste distiller's grains for hexavalent chromium removal: Adsorption performance and mechanism. Journal of Environmental Chemical Engineering 11 (3). doi:10.1016/j.jece.2023.110137.

dos Reis, G.S., Guy, M., Mathieu, M., Jebrane, M., Lima, E.C., Thyrel, M., Dotto, G.L., Larsson, S.H., 2022. A comparative study of chemical treatment by MgCl2, ZnSO4, ZnCl2, and KOH on physicochemical properties and acetaminophen adsorption performance of biobased porous materials from tree bark residues. Colloids Surf. A 642, 128626. doi:10.1016/j.colsurfa.2022.128626.

Dou, J., Cheng, J., Lu, Z., Tian, Z., Xu, J., He, Y., 2022. Biochar co-doped with nitrogen and boron switching the free radical based peroxydisulfate activation into the electron-transfer dominated nonradical process. Applied Catalysis B: Environ. 301, 120832. doi:10.1016/j.apcatb.2021.120832.

Du, J., Zhang, L., Liu, T., Xiao, R., Li, R., Guo, D., Qiu, L., Yang, X., Zhang, Z., 2019. Thermal conversion of a promising phytoremediation plant (Symphytum officinale L.) into biochar: dynamic of potentially toxic elements and environmental acceptability assessment of the biochar. Bioresour. Technol. 274, 73–82. doi:10.1016/j.biortech.2018.11.077.

Duan, X., O'Donnell, K., Sun, H., Wang, Y., Wang, S., 2015. Sulfur and nitrogen Co-doped graphene for metal-free catalytic oxidation reactions. Small. 11 (25), 3036–3044. doi:10.1002/smll.201403715.

Duan, W., Oleszczuk, P., Pan, B., Xing, B., 2019. Environmental behavior of engineered biochars and their aging processes in soil. Biochar. 1 (4), 339–351. doi:10.1007/s42773-019-00030-5.

Dupont, C., Chiriac, R., Gauthier, G., Toche, F., 2014. Heat capacity measurements of various biomass types and pyrolysis residues. Fuel 115, 644–651. doi:10.1016/j.fuel.2013.07.086.

Durán-Jiménez, G., Kostas, E.T., Stevens, L.A., Meredith, W., Erans, M., Hernández-Montoya, V., Buttress, A., Uguna, C.N., Binner, E., 2021. Green and simple approach for low-cost bioproducts preparation and CO_2 capture. Chemosphere 279, 130512. doi:10.1016/j.chemosphere.2021.130512.

Edeh, I.G., Mašek, O., Buss, W.J.S.o.t.T.E., 2020. A meta-analysis on biochar's effects on soil water properties–New insights future Res. challenges 714, 136857.

Egun, I.L., He, H., Hu, D., Chen, G.Z., 2022. Molten salt carbonization and activation of biomass to functional biocarbon. Adv. Sustain. Syst. 6 (12), 2200294. doi:10.1002/adsu.202200294.

Eke, J., Onwudili, J.A., Bridgwater, A.V., 2020. Influence of moisture contents on the fast pyrolysis of trommel fines in a bubbling fluidized bed reactor. Waste BioMass Valorization. 11 (7), 3711–3722. doi:10.1007/s12649-018-00560-2.

El-Bassi, L., Azzaz, A.A., Jellali, S., Akrout, H., Marks, E.A.N., Ghimbeu, C.M., Jeguirim, M., 2021. Application of olive mill waste-based biochars in agriculture: impact on soil properties, enzymatic activities and tomato growth. Sci. Total Environ. 755, 142531. doi:10.1016/j.scitotenv.2020.142531.

El-Gamal, E., Saleh, M., Elsokkary, I., Rashad, M., El-Latif, Abd, 2017. Comparison between properties of biochar produced by traditional and controlled pyrolysis. M., 38, 412–425. doi:10.21608/ASEJAIQJSAE.2017.3720.

El-Shafie, A.S., Rahman, E., GadelHak, Y., Mahmoud, R., El-Azazy, M., 2024. Techno-economic assessment of waste mandarin biochar as a green adsorbent for binary dye wastewater effluents of methylene blue and basic fuchsin: lab- and large-scale investigations. Spectrochimica Acta Part A: Molecular Biomolecular Spectroscopy 306, 123621. doi:10.1016/j.saa.2023.123621.

Elyounssi K, B.J., Halim, M., 2010. High-yield charcoal production by two-step pyrolysis. J. Anal. Appl. Pyrolysis. (87) 138–143.

Encinar, J.M., González, J.F., González, J., 2000. Fixed-bed pyrolysis of Cynara cardunculus L. Product yields and compositions. Fuel Process. Technol. 68 (3), 209–222. doi:10.1016/S0378-3820(00)00125-9.

Eom, I.Y., Kim, J.Y., Kim, T.S., Lee, S.M., Choi, D., Choi, I.G., Choi, J.W., 2012. Effect of essential inorganic metals on primary thermal degradation of lignocellulosic biomass. Bioresource Technology 104 (none), 687–694. https://www.sciencedirect.com/science/article/pii/S0960852411014817.

Ephraim, A., Pham Minh, D., Lebonnois, D., Peregrina, C., Sharrock, P., Nzihou, A., 2018. Co-pyrolysis of wood and plastics: influence of plastic type and content on product yield, gas composition and quality. Fuel 231, 110–117. doi:10.1016/j.fuel.2018.04.140.

Ercan, B., Alper, K., Ucar, S., Karagoz, S., 2023. Comparative studies of hydrochars and biochars produced from lignocellulosic biomass via hydrothermal carbonization, torrefaction and pyrolysis. J. Energy Institute 109, 101298. doi:10.1016/j.joei.2023.101298.

Ertaş, M., Hakkı Alma, M., 2010. Pyrolysis of laurel (Laurus nobilis L.) extraction residues in a fixed-bed reactor: characterization of bio-oil and bio-char. J. Anal. Appl. Pyrolysis. 88 (1), 22–29. doi:10.1016/j.jaap.2010.02.006.

Essandoh, M., Wolgemuth, D., Pittman, C.U., Mohan, D., Mlsna, T., 2017. Phenoxy herbicide removal from aqueous solutions using fast pyrolysis switchgrass biochar. Chemosphere 174, 49–57. doi:10.1016/j.chemosphere.2017.01.105.

Fabbri, D., Rombolà, A.G., Torri, C., Spokas, K.A., 2013. Determination of polycyclic aromatic hydrocarbons in biochar and biochar amended soil. J. Anal. Appl. Pyrolysis. 103, 60–67. doi:10.1016/j.jaap.2012.10.003.

Fachini, J., Figueiredo, C.C.d., Vale, A.T.d., 2022. Assessing potassium release in natural silica sand from novel K-enriched sewage sludge biochar fertilizers. Journal of Environmental Management 314, 115080. doi:10.1016/j.jenvman.2022.115080.

Fang, J., Cheng, L., Hameed, R., Jin, L., Wang, D., Owens, G., Lin, D., 2020. Release and stability of water dispersible biochar colloids in aquatic environments: effects of pyrolysis temperature, particle size, and solution chemistry. Environ. Pollut. 260, 114037. doi:10.1016/j.envpol.2020.114037.

Farooq, A., Jang, S.-H., Lee, S.H., Jung, S.-C., Rhee, G.H., Jeon, B.-H., Park, Y.-K., 2021. Catalytic steam gasification of food waste using Ni-loaded rice husk derived biochar for hydrogen production. Chemosphere 280, 130671. doi:10.1016/j.chemosphere.2021.130671.

Fassinou, W.F., Van de Steene, L., Toure, S., Volle, G., Girard, P., 2009. Pyrolysis of Pinus pinaster in a two-stage gasifier: influence of processing parameters and thermal cracking of tar. Fuel Process. Technol. 90 (1), 75–90. doi:10.1016/j.fuproc.2008.07.016.

Fatnassi, A., Cammarano, C., Oliviero, E., Hulea, V., Brun, N., 2022. Carbon-aerogel-supported noble-metal nanoparticles as hydrogenation catalysts. ACS. Appl. Nano Mater. 5 (10), 14227–14234. doi:10.1021/acsanm.2c03313.

Fawzy, S., Osman, A.I., Yang, H., Doran, J., Rooney, D.W., 2021. Industrial biochar systems for atmospheric carbon removal: a review. Environ. Chem. Lett. 19 (4), 3023–3055. doi:10.1007/s10311-021-01210-1.

Fawzy, S., Osman, A.I., Mehta, N., Moran, D., Ala'a, H., Rooney, D.W., 2022. Atmospheric carbon removal via industrial biochar systems: A techno-economic-environmental study. J. Clean. Prod. 371, 133660.

Fazeli Sangani, M., Abrishamkesh, S., Owens, G., 2020. Physicochemical characteristics of biochars can be beneficially manipulated using post-pyrolyzed particle size modification. Bioresour. Technol. 306, 123157. doi:10.1016/j.biortech.2020.123157.

Feng, D., Zhao, Y., Zhang, Y., Sun, S., Huang, Y., 2016. Effects of K and Ca on reforming of model tar compounds with pyrolysis biochars under H_2O or CO_2. Chemical Engineering Journal 306, 422–432. https://www.sciencedirect.com/science/article/pii/S1385894716310105.

Feng, D., Feng, Y., Zhao, Y., Zhang, Z., Zhang, L., Zhang, 2017. Synergetic effects of biochar structure and AAEM species on reactivity of H_2O-activated biochar from cyclone air gasification. International Journal of Hydrogen Energy. https://www.sciencedirect.com/science/article/pii/S036031991732061X.

Feng, D., Zhao, Y., Zhang, Y., Xu, H., Zhang, L., Sun, S., 2018. Catalytic mechanism of ion-exchanging alkali and alkaline earth metallic species on biochar reactivity during CO_2/H_2O gasification. Fuel 212 (jan.15), 523–532. https://www.sciencedirect.com/science/article/pii/S0016236117312887.

Ferraro, G., Pecori, G., Rosi, L., Bettucci, L., Fratini, E., Casini, D., Rizzo, A.M., Chiaramonti, D., 2021. Biochar from lab-scale pyrolysis: influence of feedstock and operational temperature. BioMass Convers. Biorefin. doi:10.1007/s13399-021-01303-5.

Ferreira, S.D., Manera, C., Silvestre, W.P., Pauletti, G.F., Altafini, C.R., Godinho, M., 2019. Use of biochar produced from elephant grass by pyrolysis in a screw reactor as a soil amendment. Waste BioMass Valorization. 10 (10), 3089–3100. doi:10.1007/s12649-018-0347-1.

Foong, S.Y., Liew, R.K., Yang, Y., Cheng, Y.W., Yek, P.N.Y., Mahari, W.A.W., Lee, X.Y., Han, C.S., Vo, D.-V.N., Van Le, Q.J.C.E.J., 2020. Valorization biomass waste to engineered activated biochar by microwave pyrolysis: Progress, challenges, future directions 389, 124401.

ForestDeclarationAssessmentPartners, 2024. 2024 Forest declaration assessment. www.forestdeclaration.org.

Fu, D., Chen, Z., Xia, D., Shen, L., Wang, Y.P., Li, Q.B.A., 2017. A novel solid digestate-derived biochar-Cu NP composite activating HO system for simultaneous adsorption and degradation of tetracycline. Environmental Pollution 221, 301–310. doi:10.1016/j.envpol.2016.11.078.

Fu, H.C., Zhao, P., Xu, S.J., Cheng, G., Li, Z.Q., Li, Y., Li, K., Ma, S.L., 2019. Fabrication of FeO and graphitized porous biochar composites for activating peroxymonosulfate to degrade p-hydroxybenzoic acid: Insights on the mechanism. Chemical Engineering Journal, 375121980. https://doi.org/ARTN.

Fu, Q., Sun, S., Lu, K., Li, N., Dong, Z., 2023. Boron-doped carbon dots: doping strategies, performance effects, and applications. Chinese Chemical Letters, 109136 doi:10.1016/j.cclet.2023.109136.

Fu, P., Zhang, D., Tang, B., Lin, X., Cai, H., 2024. Targeted production of aromatics from corn stover and high-density polyethylene composite pyrolysis over nitric acid modified biochar catalyst. J. Energy Institute 112, 101447. doi:10.1016/j.joei.2023.101447.

Fuertes, A.B., Arbestain, M.C., Sevilla, M., Maciá-Agulló, J.A., Fiol, S., López, R., Smernik, R.J., Aitkenhead, W.P., Arce, F., Macías, F., 2010. Chemical and structural properties of carbonaceous products obtained by pyrolysis and hydrothermal carbonisation of corn stover. Soil Res. 48 (7), 618–626. doi:10.1071/SR10010.

Gabhane, J.W., Bhange, V.P., Patil, P.D., Bankar, S.T., Kumar, S.J.S.A.S., 2020. Recent trends in biochar production methods its application as a soil health conditioner: a review 2, 1–21.

Gai, L., Li, J., Wang, Q., Tian, R., Li, K., 2021. Evolution of biomass to porous graphite carbon by catalytic graphitization. J. Environ. Chem. Eng. 9 (6), 106678. doi:10.1016/j.jece.2021.106678.

Ganguly, A., Brown, R.C., Wright, M.M., 2022. Techno-economic and greenhouse gas emission assessment of carbon negative pyrolysis technology. Green Chem. 24 (23), 9290–9302.

Gao, M., Chang, X., Xu, Y., Guo, Z., Song, Z., 2021. Effects of Fe–Mn impregnated biochar on enzymatic activity and bacterial community in phthalate-polluted brown soil planted with wheat. Environ. Pollut. 284, 117179. doi:10.1016/j.envpol.2021.117179.

Gao, M., Xu, Y., Chang, X., Song, Z., 2021. Fe–Mn oxide modified biochar decreases phthalate uptake and improves grain quality of wheat grown in phthalate-contaminated fluvo-aquic soil. Chemosphere 270, 129428. doi:10.1016/j.chemosphere.2020.129428.

Gao, S., Wang, Z., Wang, H., Jia, Y., Xu, N., Wang, X., Wang, J., Zhang, C., Tian, T., Shen, W., 2022. Peroxydisulfate activation using B-doped biochar for the degradation of oxytetracycline in water. Appl. Surf. Sci. 599, 153917. doi:10.1016/j.apsusc.2022.153917.

Gao, Y., Gao, Y., Li, A., 2025. Effect mechanism of H3PO4 on the formation and transformation of persistent free radicals in biochar. Biochar. 7 (1), 28.

Garba, Z.N., Rahim, A.A., Bello, B.Z., 2015. Optimization of preparation conditions for activated carbon from Brachystegia eurycoma seed hulls: A new precursor using central composite design. J. Environ. Chem. Eng. 3 (4), 2892–2899. doi:10.1016/j.jece.2015.10.017.

Garcìa-Pèrez, M., Chaala, A., Roy, C., 2002. Co-pyrolysis of sugarcane bagasse with petroleum residue.: Part II.: Product yields and properties. Fuel 81 (7), 893–907.

García-Jaramillo, M., Cox, L., Knicker, H.E., Cornejo, J., Spokas, K.A., Hermosín, M.C., 2015. Characterization selection biochar for an efficient retention tricyclazole in a flooded alluvial paddy soil. (1873-3336 (Electronic)).

Garcia-Nunez, J.A., Pelaez-Samaniego, M.R., Garcia-Perez, M.E., Fonts, I., Abrego, J., Westerhof, R.J.M., Garcia-Perez, M., 2017. Historical developments of pyrolysis reactors: A review. Energy Fuels 31 (6), 5751–5775. doi:10.1021/acs.energyfuels.7b00641.

Genuino, D.A.D., de Luna, M.D.G., Capareda, S.C., 2018. Improving the surface properties of municipal solid waste-derived pyrolysis biochar by chemical and thermal activation: optimization of process parameters and environmental application. Waste Manage.. 72, 255–264.

Gezahegn, S., Sain, M., Thomas, S.C., 2019. Variation in Feedstock Wood Chem. Strongly Influences Biochar Liming Potential 3 (2), 26.

Ghodke, P.K., Sharma, A.K., Jayaseelan, A., Gopinath, K., 2023. Hydrogen-rich syngas production from the lignocellulosic biomass by catalytic gasification: A state of art review on advance technologies, economic challenges, and future prospectus. Fuel 342, 127800.

Gholami, P., Dinpazhoh, L., Khataee, A., Orooji, Y., 2019. Sonocatalytic activity of biochar-supported ZnO nanorods in degradation of gemifloxacin: Synergy study, effect of parameters and phytotoxicity evaluation. Ultrason Sonochem 55, 44–56. doi:10.1016/j.ultsonch.2019.03.001.

Glaser, B., Lehr, V.-I., 2019. Biochar effects on phosphorus availability in agricultural soils: A meta-analysis. Sci. Rep. 9 (1), 9338. doi:10.1038/s41598-019-45693-z.

Glaser, B., Lehmann, J., Zech, W., 2002. Ameliorating physical and chemical properties of highly weathered soils in the tropics with charcoal – a review. Biol. Fertil. Soils. 35. doi:10.1007/s00374-002-0466-4.

Gold, M., Cunningham, M., Bleuler, M., Arnheiter, R., Schönborn, A., Niwagaba, C., Strande, L., 2018. Operating parameters for three resource recovery options from slow-pyrolysis of faecal sludge. J. Water, Sanitation Hygiene for Development 8 (4), 707–717. doi:10.2166/washdev.2018.009.

Gondek, K., Mierzwa-Hersztek, M., 2016. Effect of thermal conversion of pig manure and poultry litter on the content and mobility of Mn and Fe in biochars and in soil after their application. Chilean J. Agric. Res. 76, 343–348.

González, M.E., Cea, M., Reyes, D., Romero-Hermoso, L., Hidalgo, P., Meier, S., Benito, N., Navia, R., 2017. Functionalization of biochar derived from lignocellulosic biomass using microwave technology for catalytic application in biodiesel production. Energy Conversion and Management 137, 165–173. doi:10.1016/j.enconman.2017.01.063.

Gorbounov, M., Diaz-Vasseur, E., Danaci, D., Soltani, S.M., 2024. Chemical activation of porous carbon extracted from biomass combustion bottom ash for CO_2 adsorption. Carbon Capture Sci. Technol. 10, 100151.

Gorbounov, M., Halloran, P., Soltani, S.M., 2024. Hydrophobic and hydrophilic functional groups and their impact on physical adsorption of CO_2 in presence of H_2O: A critical review. J. CO_2 Utilization 86, 102908.

Gorbounov, M., Hecquet-Perrot, L., Ignatova, S., Hewitson, P., Soltani, S.M., 2025. Acidic surface chemical modification of biomass combustion ash-derived activated carbon for CO_2 adsorption. Next Mater. 6, 100321.

Greco, G., Videgain, M., Di Stasi, C., Pires, E., Manyà, J.J., 2021. Importance of pyrolysis temperature and pressure in the concentration of polycyclic aromatic hydrocarbons in wood waste-derived biochars. J. Anal. Appl. Pyrolysis. 159, 105337. doi:10.1016/j.jaap.2021.105337.

Guan, G., Kaewpanha, M., Hao, X., Abudula, A., 2016. Catalytic steam reforming of biomass tar: Prospects and challenges. Renewable and Sustainable Energy Reviews 58 (May), 450–461. https://www.sciencedirect.com/science/article/pii/S1364032115016998.

Gul, S., Whalen, J.K., Thomas, B.W., Sachdeva, V., Deng, H., 2015. Physico-chemical properties and microbial responses in biochar-amended soils: mechanisms and future directions. Agric. Ecosyst. Environ. 206, 46–59. doi:10.1016/j.agee.2015.03.015.

Guo, F.Q., Peng, K.Y., Liang, S., Jia, X.P., Jiang, X.C., Qian, L., 2019. Evaluation of the catalytic performance of different activated biochar catalysts for removal of tar from biomass pyrolysis. Fuel 258. doi:10.1016/j.fuel.2019.116204.

Guo, N., Li, M., Wang, Y., Sun, X., Wang, F., Yang, R., 2016. N-doped hierarchical porous carbon prepared by simultaneous-activation of KOH and NH3 for high performance supercapacitors. RSC. Adv. 6 (103), 101372–101379. doi:10.1039/c6ra22426a.

Guo, Y., Zeng, Z., Zhu, Y., Huang, Z., Cui, Y., Yang, J., 2018. Catalytic oxidation of aqueous organic contaminants by persulfate activated with sulfur-doped hierarchically porous carbon derived from thiophene. Applied Catalysis B: Environ. 220, 635–644. doi:10.1016/j.apcatb.2017.08.073.

Guo, J., Zheng, L., Li, Z., Zhou, X., Cheng, S., Zhang, L., Zhang, Q., 2021. Effects of various pyrolysis conditions and feedstock compositions on the physicochemical characteristics of cow manure-derived biochar. J. Clean. Prod. 311, 127458. doi:10.1016/j.jclepro.2021.127458.

Guo, H., Liu, Y., Lv, Y., Liu, Y., Lin, Y., Liu, M., 2023. Nitrogen doped sinocalamus oldhami lignin-based activated biochar with high specific surface area: preparation and its adsorption for malachite green contaminant. Process Safety Environ. Protect. doi:10.1016/j.psep.2023.12.034.

Guo, L., Lai, X., Peng, L., Li, J., Zhang, W., Shi, B., 2023. Facile synthesis of Fe and N co-coped biochar from low temperature pyrolysis of lignin waste for superefficient Th(IV)/U(VI) separation: performance and mechanism. J. Clean. Prod. 426, 139168. doi:10.1016/j.jclepro.2023.139168.

Gupta, S., Kua, H.W., 2019. Carbonaceous micro-filler for cement: effect of particle size and dosage of biochar on fresh and hardened properties of cement mortar. Sci. Total Environ. 662, 952–962. doi:10.1016/j.scitotenv.2019.01.269.

Gupta, A.D., Singh, H., Varjani, S., Awasthi, M.K., Giri, B.S., Pandey, A., 2022. A critical review on biochar-based catalysts for the abatement of toxic pollutants from water via advanced oxidation processes (AOPs). Science of the Total Environment 849, 157831. https://doi.org/ARTN.

Gupta, S., Kashani, A., Mahmood, A.H., 2022. Carbon sequestration in engineered lightweight foamed mortar – Effect on rheology, mechanical and durability properties. Construction and Building Materials 322, 126383. doi:10.1016/j.conbuildmat.2022.126383.

Gupta, S., 2021. Carbon sequestration in cementitious matrix containing pyrogenic carbon from waste biomass: A comparison of external and internal carbonation approach. Journal of Building Engineering 43, 102910. doi:10.1016/j.jobe.2021.102910.

Habert, G., Miller, S.A., John, V.M., Provis, J.L., Favier, A., Horvath, A., Scrivener, K.L., 2020. Environmental impacts and decarbonization strategies in the cement and concrete industries. Nature Reviews Earth & Environment 1 (11), 559–573. doi:10.1038/s43017-020-0093-3.

Hachicha, H., Dia, M., Bouafif, H., Koubaa, A., Khlif, M., Braghiroli, F.L., 2023. Naturally nitrogen-doped biochar made from end-of-life wood panels for SO2 gas depollution. J. Renew. Mater. 11 (11), 3807–3829. doi:10.32604/jrm.2023.029454.

Hadi, P., To, M.H., Hui, C.W., Lin, C.S.K., McKay, G., 2015. Aqueous mercury adsorption by activated carbons. Water Research 73, 37–55. doi:10.1016/j.watres.2015.01.018.

Haeldermans, T., Campion, L., Kuppens, T., Vanreppelen, K., Cuypers, A., Schreurs, S., 2020. A comparative techno-economic assessment of biochar production from different residue streams using conventional and microwave pyrolysis. Bioresour. Technol. 318, 124083.

Hale, S.E., Lehmann, J., Rutherford, D., Zimmerman, A.R., Bachmann, R.T., Shitumbanuma, V., O'Toole, A., Sundqvist, K.L., Arp, H.P.H., Cornelissen, G., 2012. Quantifying the total and bioavailable polycyclic aromatic hydrocarbons and dioxins in biochars. Environ. Sci. Technol. 46 (5), 2830–2838. doi:10.1021/es203984k.

Han, X., Jiang, N., Jin, F., Reddy, K.R., Wang, Y., Liu, K., Du, Y., 2022. Effects of biochar-amended alkali-activated slag on the stabilization of coral sand in coastal areas. Journal of Rock Mechanics and Geotechnical Engineering 15 (3), 760–772. https://www.sciencedirect.com/science/article/pii/S167477552200107X.

Han, L., Ro, K.S., Wang, Y., Sun, K., Sun, H., Libra, J.A., Xing, B., 2018. Oxidation resistance of biochars as a function of feedstock and pyrolysis condition. Sci. Total Environ. 616-617, 335–344. doi:10.1016/j.scitotenv.2017.11.014.

Hara, M., Yoshida, T., Takagaki, A., Takata, T., Kondo, J.N., Hayashi, S., Domen, K., 2004. A carbon material as a strong protonic acid. Angew. Chem. Int. Ed. 43 (22), 2955–2958. doi:10.1002/anie.200453947.

Hassaan, M.A., Yılmaz, M., Helal, M., El-Nemr, M.A., Ragab, S., El Nemr, A.J.S.R., 2023. Improved methylene blue adsorption from an aqueous medium by ozone-triethylenetetramine modification sawdust-based biochar 13 (1), 12431.

Hassan, M., Liu, Y., Naidu, R., Parikh, S.J., Du, J., Qi, F., Willett, I.R., 2020. Influences of feedstock sources and pyrolysis temperature on the properties of biochar and functionality as adsorbents: A meta-analysis. (1879-1026 (Electronic)).

Hassan, M., Liu, Y., Naidu, R., Parikh, S.J., Du, J., Qi, F., Willett, I.R.J.S.o.T.T.E., 2020. Influences feedstock sources pyrolysis temperature on properties biochar functionality as adsorbents: A meta-analysis 744, 140714.

Hawthorne, I., Johnson, M.S., Jassal, R.S., Black, T.A., Grant, N.J., Smukler, S.M., 2017. Application of biochar and nitrogen influences fluxes of CO_2, CH_4 and N2O in a forest soil. Journal of Environmental Management 192, 203–214. doi:10.1016/j.jenvman.2016.12.066.

He, X., Zheng, N.C., Hu, R.T., Hu, Z.F., Yu, J.C., 2021. Hydrothermal and Pyrolytic Conversion of Biomasses into Catalysts for Advanced Oxidation Treatments. Adv Funct Mater 31 (7), 2006505. https://doi.org/ARTN.

He, P., Liu, Y., Shao, L., Zhang, H., Lü, F., 2018. Particle size dependence of the physicochemical properties of biochar. Chemosphere 212, 385–392. doi:10.1016/j.chemosphere.2018.08.106.

He, Z., Zheng, W., Li, M., Liu, W., Zhang, Y., Wang, Y., 2022. Fe2P/biocarbon composite derived from a phosphorus-containing biomass for levofloxacin removal through peroxymonosulfate activation. Chem. Eng. J. 427, 130928. doi:10.1016/j.cej.2021.130928.

He, Z., Liu, S., Zhao, W., Yin, M., Jiang, M., Bi, D., 2023. Comparative assessment of proportions of urea in blend for nitrogen-rich pyrolysis: characteristics and distribution of bio-oil and biochar. ACS. Omega 8 (1), 1232–1239. doi:10.1021/acsomega.2c06643.

Hekimoğlu, G., Sarı, A., Arunachalam, S., Arslanoğlu, H., Gencel, O., 2021. Porous biochar/heptadecane composite phase change material with leak-proof, high thermal energy storage capacity and enhanced thermal conductivity. Powder. Technol. 394, 1017–1025. doi:10.1016/j.powtec.2021.09.030.

Higashikawa, F.S., Conz, R.F., Colzato, M., Cerri, C.E.P., Alleoni, L.R.F., 2016. Effects of feedstock type and slow pyrolysis temperature in the production of biochars on the removal of cadmium and nickel from water. J. Clean. Prod. 137, 965–972. doi:10.1016/j.jclepro.2016.07.205.

Ho, S.-H., Chen, Y.-d., Li, R., Zhang, C., Ge, Y., Cao, G., Ma, M., Duan, X., Wang, S., Ren, N.-q., 2019. N-doped graphitic biochars from C-phycocyanin extracted Spirulina residue for catalytic persulfate activation toward nonradical disinfection and organic oxidation. Water. Res. 159, 77–86. doi:10.1016/j.watres.2019.05.008.

Hossain, M.K., Strezov, V., Chan, K.Y., Ziolkowski, A., Nelson, P.F., 2011. Influence of pyrolysis temperature on production and nutrient properties of wastewater sludge biochar. J. Environ. Manage. 92 (1), 223–228. doi:10.1016/j.jenvman.2010.09.008.

Hossain, M.Z., Bahar, M.M., Sarkar, B., Donne, S.W., Wade, P., Bolan, N.J.J.o.A., Pyrolysis, A., 2021. Assessment fertilizer potential biochars produced from slow pyrolysis biosolid animal manures 155, 105043.

Hou, D., Al-Tabbaa, A., O'Connor, D., Hu, Q., Zhu, Y.-G., Wang, L., Kirkwood, N., Ok, Y.S., Tsang, D.C., Bolan, N.S.J.N.R.E., Environment, 2023. Sustainable remediation redevelopment brownfield sites 4 (4), 271–286.

Hu, Z., Srinivasan, M.P., 2001. Mesoporous high-surface-area activated carbon. Microporous Mesoporous Mater. 43 (3), 267–275. doi:10.1016/s1387-1811(00)00355-3.

Hu, Y.N., Cheng, H.F., Tao, S., 2016. The Challenges and Solutions for Cadmium-contaminated Rice in China: A Critical Review. Environment International 92-93, 515–532. doi:10.1016/j.envint.2016.04.042.

Hu, X., Fan, M., Zhu, Y., Zhu, Q., Song, Q., Dong, Z., 2019. Biomass-derived phosphorus-doped carbon materials as efficient metal-free catalysts for selective aerobic oxidation of alcohols. Green Chemistry 21 (19), 5274–5283. doi:10.1039/c9gc01910c.

Hu, D., Xu, H., Yi, Z., Chen, Z., Ye, C., Wu, Z., Garces, H.F., Yan, K., 2019. Green CO_2-Assisted Synthesis of Mono- and Bimetallic Pd/Pt Nanoparticles on Porous Carbon Fabricated from Sorghum for Highly Selective Hydrogenation of Furfural. ACS Sustainable Chemistry & Engineering 7 (18), 15339–15345. doi:10.1021/acssuschemeng.9b02665.

Hu, Z., Guo, H., Srinivasan, M.P., Yaming, N., 2003. A simple method for developing mesoporosity in activated carbon. Sep. Purif. Technol. 31 (1), 47–52. doi:10.1016/s1383-5866(02)00148-x.

Hu, Y., Chen, D., Zhang, R., Ding, Y., Ren, Z., Fu, M., Cao, X., Zeng, G., 2021. Singlet oxygen-dominated activation of peroxymonosulfate by passion fruit shell derived biochar for catalytic degradation of tetracycline through a non-radical oxidation pathway. J. Hazard. Mater. 419, 126495. doi:10.1016/j.jhazmat.2021.126495.

Hu, S., Liu, C., Bu, H., Chen, M., Fei, Y.-h., 2024. Efficient reduction and adsorption of Cr(VI) using FeCl3-modified biochar: synergistic roles of persistent free radicals and Fe(II). J. Environ. Sci. 137, 626–638. doi:10.1016/j.jes.2023.03.011.

Huang, Y., Anderson, M., McIlveen-Wright, D., Lyons, G., McRoberts, W., Wang, Y., Roskilly, A., Hewitt, N., 2015. Biochar and renewable energy generation from poultry litter waste: a technical and economic analysis based on computational simulations. Appl. Energy 160, 656–663.

Huang, S., Liang, Q., Geng, J., Luo, H., Wei, Q., 2019. Sulfurized biochar prepared by simplified technic with superior adsorption property towards aqueous Hg(II) and adsorption mechanisms. Mater. Chem. Phys. 238, 121919. doi:10.1016/j.matchemphys.2019.121919.

Huang, D., Zhang, Q., Zhang, C., Wang, R., Deng, R., Luo, H., Li, T., Li, J., Chen, S., Liu, C., 2020. Mn doped magnetic biochar as persulfate activator for the degradation of tetracycline. Chem. Eng. J. 391, 123532. doi:10.1016/j.cej.2019.123532.

Huang, W.-H., Lee, D.-J., Huang, C., 2021. Modification on biochars for applications: A research update. Bioresour. Technol. 319, 124100. doi:10.1016/j.biortech.2020.124100.

Huang, P., Zhang, P., Wang, C., Du, X., Jia, H., Sun, H., 2023. P-doped biochar regulates nZVI nanocracks formation for superefficient persulfate activation. J. Hazard. Mater. 450, 130999. doi:10.1016/j.jhazmat.2023.130999.

Hue, N., 2020. Biochar for maintaining soil health. In: Giri, B., Varma, A. (Eds.), Soil Health. Springer International Publishing, Cham, pp. 21–46. doi:10.1007/978-3-030-44364-1_2.

Hung, C.-M., Chen, C.-W., Huang, C.-P., Yang, Y.-Y., Dong, C.-D., 2022. Suppression of polycyclic aromatic hydrocarbon formation during pyrolytic production of lignin-based biochar via nitrogen and boron co-doping. Bioresour. Technol. 355, 127246. doi:10.1016/j.biortech.2022.127246.

Hung, C.-M., Chen, C.-W., Huang, C.-P., Dong, C.-D., 2023. Nitrogen and boron co-doped lignin biochar for enhancing calcium peroxide activation toward organic micropollutants decontamination in waste activated sludge and related microbial structure dynamics. Bioresour. Technol. 372, 128673. doi:10.1016/j.biortech.2023.128673.

Hunter, R.D., Rowlandson, J.L., Smales, G.J., Pauw, B.R., Ting, V.P., Kulak, A., Schnepp, Z., 2020. The effect of precursor structure on porous carbons produced by iron-catalyzed graphitization of biomass. Mater. Adv. 1 (9), 3281–3291. doi:10.1039/D0MA00692K.

Hwang, H., Oh, S., Choi, I.-G., Choi, J.W., 2015. Catalytic effects of magnesium on the characteristics of fast pyrolysis products – Bio-oil, bio-char, and non-condensed pyrolytic gas fractions. J. Anal. Appl. Pyrolysis. 113, 27–34. doi:10.1016/j.jaap.2014.09.028.

Iberahim, N., Sethupathi, S., Goh, C.L., Bashir, M.J., Ahmad, W., 2019. Optimization of activated palm oil sludge biochar preparation for sulphur dioxide adsorption. J. Environ. Manage. 248, 109302.

Igalavithana, A.D., Choi, S.W., Dissanayake, P.D., Shang, J., Wang, C.-H., Yang, X., Kim, S., Tsang, D.C., Lee, K.B., Ok, Y.S., 2020. Gasification biochar from biowaste (food waste and wood waste) for effective CO_2 adsorption. Journal of hazardous materials 391, 121147. https://www.sciencedirect.com/science/article/pii/S030438941931101X.

Ighalo, J.O., Eletta, O.A.A., Adeniyi, A.G., 2022. Biomass carbonisation in retort kilns: process techniques, product quality and future perspectives. Bioresour. Technol. Rep. 17, 100934. doi:10.1016/j.biteb.2021.100934.

Ighalo, J.O., Iwuchukwu, F.U., Eyankware, O.E., Iwuozor, K.O., Olotu, K., Bright, O.C., Igwegbe, C.A.J.C.T., Policy, E., 2022. Flash pyrolysis biomass: a review recent advances. Clean Techn. Environ. Policy 24 (8), 2349–2363.

Initiative, I.B., 2015. Standardized Product Definition Product Testing Guidelines for Biochar 7 That Is Used in Soil.

Inyang, M., Gao, B., Pullammanappallil, P., Ding, W., Zimmerman, A.R., 2010. Biochar from anaerobically digested sugarcane bagasse. Bioresour. Technol. 101 (22), 8868–8872. doi:10.1016/j.biortech.2010.06.088.

Issaka, E., Fapohunda, F.O., Amu-Darko, J.N.O., Yeboah, L., Yakubu, S., Varjani, S., Ali, N., Bilal, M., 2022. Biochar-based composites for remediation of polluted wastewater and soil environments: challenges and prospects. Chemosphere 297, 134163. doi:10.1016/j.chemosphere.2022.134163.

Jalal, F., Arif, M., Akhtar, K., Khan, A., Naz, M., Said, F., Zaheer, S., Hussain, S., Imtiaz, M., Khan, M.A., Ali, M., Wei, F., 2020. Biochar Integration with Legume Crops in Summer Gape Synergizes Nitrogen Use Efficiency Enhance Maize Yield 10 (1), 58.

Januševičius, T., Mažeikienė, A., Danila, V., Paliulis, D., 2022. The characteristics of sewage sludge pellet biochar prepared using two different pyrolysis methods. BioMass Convers. Biorefin. 14 (1), 891–900. doi:10.1007/s13399-021-02295-y.

Janus, A., Pelfrêne, A., Heymans, S., Deboffe, C., Douay, F., Waterlot, C.J.J.o.e.m., 2015. Elaboration, characteristics advantages biochars for Manage.ment contaminated soils with a specific overview on Miscanthus biochars 162, 275–289.

Januszewicz, K., Kazimierski, P., Cymann-Sachajdak, A., Hercel, P., Barczak, B., Wilamowska-Zawlocka, M., Kardas, D., Luczak, J., 2023. Conversion of waste biomass to designed and tailored activated chars with valuable properties for adsorption and electrochemical applications. Environ. Sci. Pollut. Res. Int. 30 (43), 96977–96992. doi:10.1007/s11356-023-28824-y.

Jeon, C., Solis, K.L., An, H.R., Hong, Y., Igalavithana, A.D., Ok, Y.S., 2020. Sustainable removal of Hg(II) by sulfur-modified pine-needle biochar. Journal of Hazardous Materials 388. doi:10.1016/j.jhazmat.2020.122048.

Ji, M., Wang, X., Usman, M., Liu, F., Dan, Y., Zhou, L., Campanaro, S., Luo, G., Sang, W.J.E.P., 2022. Effects different feedstocks-based biochar on soil remediation: A review 294, 118655.

Jia, W., Li, S., Wang, J., Lee, J.T., Lin, C.S.K., Mašek, O., Zhang, H., Yuan, X., 2024. Sustainable valorisation of food waste into engineered biochars for CO 2 capture towards a circular economy. Green Chem. 26 (4), 1790–1805.

Jia, W., Li, S., Wang, J., Lee, J.T.E., Lin, C.S.K., Mašek, O., Zhang, H., Yuan, X., 2024. Sustainable valorisation of food waste into engineered biochars for CO_2 capture towards a circular economy. Green Chem. 26 (4), 1790–1805. doi:10.1039/d3gc04138g.

Jiang, L., Hu, S., Wang, Y., Su, S., Sun, L., Xu, B., He, L., Xiang, J., 2015. Catalytic effects of inherent alkali and alkaline earth metallic species on steam gasification of biomass. International Journal of Hydrogen Energy 40 (45), 15460–15469. https://www.sciencedirect.com/science/article/pii/S0360319915024003.

Jiang, Y.-H., Li, A.-Y., Deng, H., Ye, C.-H., Wu, Y.-Q., Linmu, Y.-D., Hang, H.-L., 2019. Characteristics of nitrogen and phosphorus adsorption by Mg-loaded biochar from different feedstocks. Bioresour. Technol. 276, 183–189. doi:10.1016/j.biortech.2018.12.079.

Jiang, F.-Y., Zhou, Y.-H., Chen, R., Liu, T.-T., Luo, J.-Y., Huang, Y.-B., 2021. In-situ fabrication of Ag nanoparticles on biomass derived biochar as highly active catalyst for the halogenation of terminal alkynes at room temperature. Appl. Surf. Sci. 560, 150039. doi:10.1016/j.apsusc.2021.150039.

Jin, J., Li, Y., Zhang, J., Wu, S., Cao, Y., Liang, P., Zhang, J., Wong, M.H., Wang, M., Shan, S., Christie, P., 2016. Influence of pyrolysis temperature on properties and environmental safety of heavy metals in biochars derived from municipal sewage sludge. J. Hazard. Mater. 320, 417–426. doi:10.1016/j.jhazmat.2016.08.050.

Jin, H., Li, L., Luo, N., Zhang, X., Niu, H., Cai, Y., 2023. Biochar supported Fe-Cu bimetal composites prepared with waste materials for removal of tetrachloropicolinic acid from high salinity wastewater. Inorg. Chem. Commun. 156, 111141. doi:10.1016/j.inoche.2023.111141.

Jindo, K., Mizumoto, H., Sawada, Y., Sanchez-Monedero, M.A., Sonoki, T., 2014. Physical and chemical characterization of biochars derived from different agricultural residues. BiogeoSci.. 11 (23), 6613–6621. doi:10.5194/bg-11-6613-2014.

Jindo, K., Audette, Y., Higashikawa, F.S., Silva, C.A., Akashi, K., Mastrolonardo, G., Sánchez-Monedero, M.A., Mondini, C., 2020. Role of biochar in promoting circular economy in the agriculture sector. Part 1: A review of the biochar roles in soil N, P and K cycles. Chem. Biol. Technol. Agric. 7 (1), 15. doi:10.1186/s40538-020-00182-8.

Johansen, J.M., Jakobsen, J.G., Frandsen, F.J., Glarborg, P., 2011. Release of K, Cl, and S during pyrolysis and combustion of high-chlorine biomass. Energy Fuels 25 (11), 4961–4971. doi:10.1021/ef201098n.

Jung, J.-M., Lee, S.-R., Lee, J., Lee, T., Tsang, D.C.W., Kwon, E.E., 2017. Biodiesel synthesis using chicken manure biochar and waste cooking oil. Bioresour. Technol. 244, 810–815. doi:10.1016/j.biortech.2017.08.044.

Jyoti, R., Jyoti, S., Pankaj, S., 2019. Biochar: A sustainable approach for improving plant growth and soil properties. In: Vikas, A., Peeyush, S. (Eds.), Biochar. IntechOpen, Rijeka p. Ch. 1 doi:10.5772/intechopen.82151.

Kaal, J., Schneider, M.P.W., Schmidt, M.W.I., 2012. Rapid molecular screening of black carbon (biochar) thermosequences obtained from chestnut wood and rice straw: A pyrolysis-GC/MS study. Biomass Bioenergy 45, 115–129. doi:10.1016/j.biombioe.2012.05.021.

Kajita, M., Kimura, T., Norinaga, K., Li, C.Z., Hayashi, J.I., 2010. Catalytic and Non-catalytic Mechanisms in Steam Gasification of Char from the Pyrolysis of Biomass. Energy & Fuels 24 (jan.-feb), 108–116. https://pubs.acs.org/doi/full/10.1021/ef900513a.

Kamali, M., Sweygers, N., Al-Salem, S., Appels, L., Aminabhavi, T.M., Dewil, R., 2022. Biochar for soil applications-sustainability aspects, challenges and future prospects. Chemical Engineering Journal 428, 131189. doi:10.1016/j.cej.2021.131189.

Kameyama, K., Miyamoto, T., Iwata, Y., Shiono, T.J.S.S., Nutrition, P., 2016. Influences feedstock pyrolysis temperature on nitrate adsorption biochar 62 (2), 180–184.

Kang, Z., Jia, X., Zhang, Y., Kang, X., Ge, M., Liu, D., Wang, C., He, Z.J.S., 2022. A review on application biochar in removal pharmaceutical pollutants through adsorption persulfate-based AOPs 14 (16), 10128.

Kang, K., Hu, Y., Khan, I., He, S., Fatehi, P., 2023. Recent advances in the synthesis and application of magnetic biochar for wastewater treatment. Bioresour. Technol. 390, 129786. doi:10.1016/j.biortech.2023.129786.

Kannah, R.Y., Kavitha, S., Karthikeyan, O.P., Kumar, G., Dai-Viet, N.V., Banu, J.R., 2021. Techno-economic assessment of various hydrogen production methods–A review. Bioresour. Technol. 319, 124175.

Katyal, S., Thambimuthu, K., Valix, M., 2003. Carbonisation of bagasse in a fixed bed reactor: influence of process variables on char yield and characteristics. Renew. Energy 28 (5), 713–725. doi:10.1016/S0960-1481(02)00112-X.

Kaur, D., Bhardwaj, N.K., Lohchab, R.K.J.J.o.C.P., 2018. A study on pulping rice straw impact incorporation chlorine dioxide during bleaching on pulp properties effluents characteristics 170, 174–182.

Kaya, N., Uzun, Z.Y., 2021. Investigation of effectiveness of pine cone biochar activated with KOH for methyl orange adsorption and CO_2 capture. BioMass Convers. Biorefin. 11 (3), 1067–1083. doi:10.1007/s13399-020-01063-8.

Keiluweit, M., Nico, P.S., Johnson, M.G., Kleber, M., 2010. Dynamic molecular structure of plant biomass-derived black carbon (Biochar). Environ. Sci. Technol. 44 (4), 1247–1253. doi:10.1021/es9031419.

Keru, G., Ndungu, P.G., Nyamori, V.O., 2015. Effect of boron concentration on physicochemical properties of boron-doped carbon nanotubes. Mater. Chem. Phys. 153, 323–332. doi:10.1016/j.matchemphys.2015.01.020.

Keske, C., Godfrey, T., Hoag, D.L., Abedin, J., 2020. Economic feasibility of biochar and agriculture coproduction from Canadian black spruce forest. Food Energy Secur. 9 (1), e188.

Khan, N., Chowdhary, P., Gnansounou, E., Chaturvedi, P., 2021. Biochar and environmental sustainability: emerging trends and techno-economic perspectives. Bioresour. Technol. 332, 125102. doi:10.1016/j.biortech.2021.125102.

Khodaei, H., Álvarez-Bermúdez, C., Chapela, S., Olson, C., MacKenzie, M.D., Gómez, M.A., Porteiro, J., 2024. Eulerian CFD simulation of biomass thermal conversion in an indirect slow pyrolysis rotary kiln unit to produce biochar from recycled waste wood. Energy 288, 129895. doi:10.1016/j.energy.2023.129895.

Kim, K.H., Kim, J.-Y., Cho, T.-S., Choi, J.W., 2012a. Influence of pyrolysis temperature on physicochemical properties of biochar obtained from the fast pyrolysis of pitch pine (Pinus rigida). Bioresour. Technol. 118, 158–162. doi:10.1016/j.biortech.2012.04.094.

Kim, S.-S., Ly, H.V., Choi, G.-H., Kim, J., Woo, H.C., 2012b. Pyrolysis characteristics and kinetics of the alga Saccharina japonica. Bioresour. Technol. 123, 445–451. doi:10.1016/j.biortech.2012.07.097.

Kim, K.C., Yoon, T.-U., Bae, Y.-S., 2016. Applicability of using CO_2 adsorption isotherms to determine BET surface areas of microporous materials. Microporous Mesoporous Mater. 224, 294–301. doi:10.1016/j.micromeso.2016.01.003.

Klein-Marcuschamer, D., Blanch, H.W., 2015. Renewable fuels from biomass: technical hurdles and economic assessment of biological routes. AIChE Journal 61 (9), 2689–2701.

Klobes, P., Munro, R., 2006. Porosity and specific surface area measurements for solid materials. Special Publication (NIST SP). National Institute of Standards and Technology, Gaithersburg, MD.

Knicker, H., Müller, P., Hilscher, A., 2007. How useful is chemical oxidation with dichromate for the determination of "Black Carbon" in fire-affected soils? Geoderma 142 (1), 178–196. doi:10.1016/j.geoderma.2007.08.010.

Knudsen, J.N., Jensen, P.A., Lin, W.G., Frandsen, F.J., Dam-Johansen, K., 2004. Sulfur transformations during thermal conversion of herbaceous biomass. Energy Fuels 18 (3), 810–819. doi:10.1021/ef034085b.

Koetlisi, K.A., Muchaonyerwa, P., 2017. Biochar types from latrine waste and sewage sludge differ in physico-chemical properties and cadmium adsorption. Am J Appl Sci 14 (11). doi:10.3844/ajassp.2017.1039.1048.

Kong, K.K., Yek, P.N.Y., Sii, H.S., Lee, M.D., Liew, R.K., Lam, S.S., 2022. Microwave physicochemical activation: an advanced approach to produce activated biochar for palm oil mill effluent treatment. Waste Dispos. Sustain. Energy 4 (4), 323–333. doi:10.1007/s42768-022-00115-1.

Kong, G., Liu, Q., Ji, G., Jia, H., Cao, T., Zhang, X., Han, L., 2023. Improving hydrogen-rich gas production from biomass catalytic steam gasification over metal-doping porous biochar. Bioresour. Technol. 387, 129662. doi:10.1016/j.biortech.2023.129662.

Kostas, E.T., Durán-Jiménez, G., Shepherd, B.J., Meredith, W., Stevens, L.A., Williams, O.S.A., Lye, G.J., Robinson, J.P., 2020. Microwave pyrolysis of olive pomace for bio-oil and bio-char production. Chem. Eng. J. 387, 123404. doi:10.1016/j.cej.2019.123404.

Kouchachvili, L., Entchev, E., 2017. Ag/biochar composite for supercapacitor electrodes. Mater. Today Energy 6, 136–145. doi:10.1016/j.mtener.2017.09.002.

Kouotou, D., Manga, H.N., Baçaoui, A., Yaacoubi, A., Mbadcam, J.K., 2013. Optimization of activated carbons prepared byH3PO4and steam activation of oil palm shells. J. Chem. 2013, 1–10. doi:10.1155/2013/654343.

Krahn, K.M., Cornelissen, G., Castro, G., Arp, H.P.H., Asimakopoulos, A.G., Wolf, R., Holmstad, R., Zimmerman, A.R., Sørmo, E.J.J.o.H.M., 2023. Sewage sludge biochars as effective PFAS-sorbents 445, 130449.

Kroeger, J.E., Pourhashem, G., Medlock, K.B., Masiello, C.A., 2021. Water cost savings from soil biochar amendment: A spatial analysis. GCB bioenergy 13 (1), 133–142.

Krueger, B.C., Fowler, G.D., Templeton, M.R., Moya, B., 2020. Resource recovery and biochar characteristics from full-scale faecal sludge treatment and co-treatment with agricultural waste. Water. Res. 169, 115253. doi:10.1016/j.watres.2019.115253.

Kujawska, J., 2023. Content of heavy metals in various biochar and assessment environmental risk. J. Ecol. Eng. 24 (8), 287–295. doi:10.12911/22998993/166557.

Kumar, A., Kumar, J., Bhaskar, T., 2020. High surface area biochar from Sargassum tenerrimum as potential catalyst support for selective phenol hydrogenation. Environ. Res. 186, 109533. doi:10.1016/j.envres.2020.109533.

Kumar, A., Singh, E., Mishra, R., Kumar, S., 2022. Biochar as environmental armour and its diverse role towards protecting soil, water and air. Sci. Total Environ. 806, 150444. doi:10.1016/j.scitotenv.2021.150444.

Kumar Mishra, R., Jaya Prasanna Kumar, D., Narula, A., Minnat Chistie, S., Ullhas Naik, S., 2023. Production and beneficial impact of biochar for environmental application: A review on types of feedstocks, chemical compositions, operating parameters, techno-economic study, and life cycle assessment. Fuel 343, 127968. doi:10.1016/j.fuel.2023.127968.

Kumi, A.G., Ibrahim, M.G., Fujii, M., Nasr, M., 2020. Synthesis of sludge-derived biochar modified with eggshell waste for monoethylene glycol removal from aqueous solutions. SN. Appl. Sci. 2 (10), 1696. doi:10.1007/s42452-020-03501-8.

Lü, F., Lu, X., Li, S., Zhang, H., Shao, L., He, P., 2022. Dozens-fold improvement of biochar redox properties by KOH activation. Chem. Eng. J. 429, 132203. doi:10.1016/j.cej.2021.132203.

Labianca, C., Zhu, X., Ferrara, C., Zhang, Y., De Feo, G., Hsu, S.C., Tsang, D.C.W., 2024. A holistic framework of biochar-augmented cementitious products and general applications: Technical, environmental, and economic evaluation. Environ Res 245, 118026. doi:10.1016/j.envres.2023.118026.

Laghari, M., Hu, Z., Mirjat, M.S., Xiao, B., Tagar, A.A., Hu, M., 2016. Fast pyrolysis biochar from sawdust improves the quality of desert soils and enhances plant growth. J. Sci. Food Agric. 96 (1), 199–206. doi:10.1002/jsfa.7082.

Laghari, M., Müller-Stöver, D.S., Puig-Arnavat, M., Thomsen, T.P., Henriksen, U.B., 2021. Evaluation of biochar post-process treatments to produce soil enhancers and phosphorus fertilizers at a single plant. Waste BioMass Valorization. 12 (10), 5517–5532. doi:10.1007/s12649-021-01358-5.

Lahijani, P., Zainal, Z.A., Mohamed, A.R., Mohammadi, M., 2013. CO_2 gasification reactivity of biomass char: catalytic influence of alkali, alkaline earth and transition metal salts. Bioresource Technology 144 (Complete), 288–295. https://www.sciencedirect.com/science/article/pii/S0960852413009784.

Lahijani, P., Mohammadi, M., Mohamed, A.R., 2018. Metal incorporated biochar as a potential adsorbent for high capacity CO_2 capture at ambient condition. Journal of CO_2 utilization (26) 281–293. https://www.sciencedirect.com/science/article/pii/S2212982018300027.

Laksaci, H., Khelifi, A., Belhamdi, B., Trari, M., 2017. Valorization of coffee grounds into activated carbon using physic—Chemical activation by KOH/CO 2. J. Environ. Chem. Eng. 5 (5), 5061–5066. doi:10.1016/j.jece.2017.09.036.

Lakshman, V., Brassard, P., Hamelin, L., Raghavan, V., Godbout, S., 2021. Pyrolysis of Miscanthus: developing the mass balance of a biorefinery through experimental tests in an auger reactor. Bioresour. Technol. Rep. 14, 100687. doi:10.1016/j.biteb.2021.100687.

Lang, R.J., Neavel, R.C., 1982. Behaviour of calcium as a steam gasification catalyst. Fuel 61 (7), 620–626.

Latawiec, A.E., Strassburg, B.B., Junqueira, A.B., Araujo, E., D. de Moraes, L.F., Pinto, H.A., Castro, A., Rangel, M., Malaguti, G.A., Rodrigues, A.F., 2019. Biochar amendment improves degraded pasturelands in Brazil: environmental and cost-benefit analysis. Sci. Rep. 9 (1), 11993.

Latawiec, A.E., Koryś, A., Koryś, K.A., Kuboń, M., Sadowska, U., Gliniak, M., Sikora, J., Drosik, A., Niemiec, M., Klimek-Kopyra, A., 2021. Economic analysis of biochar use in soybean production in Poland. Agronomy 11 (11), 2108.

Lecea, C.S.-M.d., Almela-Alarcón, M., Linares-Solano, A., 1990. Calcium-catalysed carbon gasification in CO_2 and steam. Fuel 69 (1), 21–27. https://www.sciencedirect.com/science/article/pii/001623619090253M.

Lee, M.G., Kim, Y., 2023. Enhanced antibiotic removal by waste coffee grounds prepared via water washing and KOH activation. Korean J. Chemical Eng. 40 (10), 2489–2496.

Lee, H.-S., Shin, H.-S., 2021. Competitive adsorption of heavy metals onto modified biochars: comparison of biochar properties and modification methods. J. Environ. Manage. 299, 113651.

Lee, J., Kim, K.-H., Kwon, E.E., 2017. Biochar as a catalyst. Renew. Sustain. Energy Reviews 77, 70–79. doi:10.1016/j.rser.2017.04.002.

Lee, X.J., Ong, H.C., Gan, Y.Y., Chen, W.-H., Mahlia, T.M.I.J.E.C., Management, 2020. State art review on conventional advanced pyrolysis macroalgae microalgae for biochar, bio-oil bio-syngas production 210, 112707.

Legan, M., Gotvajn, A.Ž., Zupan, K., 2022. Potential of biochar use in building materials. J. Environ. Manage. 309, 114704. doi:10.1016/j.jenvman.2022.114704.

Lehmann, J., Joseph, S., 2015. Biochar for Environment Management: Sci., Technol. implementation.

Lehmann, J., Gaunt, J., Rondon, M., 2006. Bio-char sequestration in terrestrial ecosystems – A review. Mitig. Adapt. Strateg. Glob. Chang. 11 (2), 403–427. doi:10.1007/s11027-005-9006-5.

Lehmann, J., Rillig, M.C., Thies, J., Masiello, C.A., Hockaday, W.C., Crowley, D., 2011. Biochar effects on soil biota – A review. Soil Biology BioChem. 43 (9), 1812–1836. doi:10.1016/j.soilbio.2011.04.022.

Leng, L., Huang, H.J.B.t., 2018. An overview effect pyrolysis process parameters on biochar stability 270, 627–642.

Leng, L., Xiong, Q., Yang, L., Li, H., Zhou, Y., Zhang, W., Jiang, S., Li, H., Huang, H., 2021. An overview on engineering the surface area and porosity of biochar. Sci. Total Environ. 763, 144204.

Lepage, T., Kammoun, M., Schmetz, Q., Richel, A., 2021. Biomass-to-hydrogen: A review of main routes production, processes evaluation and techno-economical assessment. Biomass Bioenergy 144, 105920.

Li, Y., Li, G., 2022. Mechanisms of straw biochar's improvement of phosphorus bioavailability in soda saline-alkali soil. Environmental Science and Pollution Research 29 (32), 47867–47872. doi:10.1007/s11356-022-20489-3.

Li, C., Suzuki, K., 2009. Tar property, analysis, reforming mechanism and model for biomass gasification–An overview. Renewable & Sustainable Energy Reviews 13 (3), 594–604. https://www.sciencedirect.com/science/article/pii/S1364032108000063.

Li, Z.D., Liu, D.F., Huang, W.L., Wei, X.C., Huang, W.W., 2020. Biochar supported CuO composites used as an efficient peroxymonosulfate activator for highly saline organic wastewater treatment. Science of the Total Environment 721, 137764. https://doi.org/ARTN.

Li, W., Liu, B.X., Wang, Z.M., Wang, K.X., Lan, Y.Q., Zhou, L.X., 2020. Efficient activation of peroxydisulfate (PDS) by rice straw biochar modified by copper oxide (RSBC-CuO) for the degradation of phenacetin (PNT). Chemical Engineering Journal 395, 125094. https://doi.org/ARTN.

Li, Q., Yang, K., Wang, L., Yi, J., Liu, R., Ming, Y., Mi, T., Zhu, X., Wang, Y., Zhou, G., Yang, C., Bai, Y., 2023. A novel admixture to improve durability of alkali-activated slag by reducing water sorptivity and optimising the process of activation. Cement and Concrete Composites 142, 105193. doi:10.1016/j.cemconcomp.2023.105193.

Li, J., Li, Y., Wu, Y., Zheng, M., 2014. A comparison of biochars from lignin, cellulose and wood as the sorbent to an aromatic pollutant. J. Hazard. Mater. 280, 450–457. doi:10.1016/j.jhazmat.2014.08.033.

Li, H., Qiu, Y.-f., Wang, X.-l., Yang, J., Yu, Y.-j., Chen, Y.-q., Liu, Y.-d., 2017. Biochar supported Ni/Fe bimetallic nanoparticles to remove 1,1,1-trichloroethane under various reaction conditions. Chemosphere 169, 534–541. doi:10.1016/j.chemosphere.2016.11.117.

Li, L., Wang, X.-F., Zhong, J.-J., Qian, X., Song, S.-L., Zhang, Y.-G., Li, D.-H., 2018. Nitrogen-enriched porous polyacrylonitrile-based carbon fibers for CO_2 capture. Ind. Eng. Chem. Res. 57 (34), 11608–11616. doi:10.1021/acs.iecr.8b01836.

Li, J., Xiao, R., Li, M., Zhang, H., Wu, S., Xia, C., 2019. Template-synthesized hierarchical porous carbons from bio-oil with high performance for supercapacitor electrodes. Fuel Process. Technol. 192, 239–249.

Li, R., Deng, H., Zhang, X., Wang, J.J., Awasthi, M.K., Wang, Q., Xiao, R., Zhou, B., Du, J., Zhang, Z., 2019. High-efficiency removal of Pb(II) and humate by a CeO2–MoS2 hybrid magnetic biochar. Bioresour. Technol. 273, 335–340. doi:10.1016/j.biortech.2018.10.053.

Li, Q., Liu, Y., Wang, Y., Chen, Y., Guo, X., Wu, Z., Zhong, B., 2020. Review of the application of biomass-derived porous carbon in lithium-sulfur batteries. Ionics. (Kiel) 26 (10), 4765–4781. doi:10.1007/s11581-020-03694-3.

Li, X., Jia, Y., Zhou, M., Su, X., Sun, J., 2020. High-efficiency degradation of organic pollutants with Fe, N co-doped biochar catalysts via persulfate activation. J. Hazard. Mater. 397, 122764. doi:10.1016/j.jhazmat.2020.122764.

Li, Y., Xing, B., Ding, Y., Han, X., Wang, S., 2020. A critical review of the production and advanced utilization of biochar via selective pyrolysis of lignocellulosic biomass. Bioresour. Technol. 312, 123614. doi:10.1016/j.biortech.2020.123614.

Li, C., Hayashi, J.-i., Sun, Y., Zhang, L., Zhang, S., Wang, S., Hu, X., 2021. Impact of heating rates on the evolution of function groups of the biochar from lignin pyrolysis. J. Anal. Appl. Pyrolysis. 155, 105031. doi:10.1016/j.jaap.2021.105031.

Li, H., Wang, Y., Zhou, N., Dai, L., Deng, W., Liu, C., Cheng, Y., Liu, Y., Cobb, K., Chen, P., Ruan, R., 2021. Applications of calcium oxide–based catalysts in biomass pyrolysis/gasification – A review. J. Clean. Prod. 291, 125826. doi:10.1016/j.jclepro.2021.125826.

Li, L., Zhang, Y.-J., Novak, A., Yang, Y., Wang, J., 2021. Role Biochar in Improving Sandy Soil Water Retention Resilience to Drought 13 (4), 407.

Li, S., Ma, X., Ma, Z., Dong, X., Wei, Z., Liu, X., zhu, L., 2021d. Mg/Al-layered double hydroxide modified biochar for simultaneous removal phosphate and nitrate from aqueous solution. Environ. Technol. Innov. 23, 101771. doi:10.1016/j.eti.2021.101771.

Li, S., Yuan, X., Deng, S., Zhao, L., Lee, K.B., 2021e. A review on biomass-derived CO_2 adsorption capture: adsorbent, adsorber, adsorption, and advice. Renew. Sustain. Energy Reviews 152, 111708.

Li, W., Wang, K., Li, Z., Sun, C., Zhao, S., Zhang, D., Chen, K., Guo, A., 2022. Preparation of high-performance supercapacitors from waste polyurethane-based hierarchical porous carbon. New J. Chem. 46 (48), 23328–23337.

Li, X., Peng, B., Liu, Q., Zhang, H., 2022. Microwave pyrolysis coupled with conventional pre-pyrolysis of the stalk for syngas and biochar. Bioresour. Technol. 348, 126745. doi:10.1016/j.biortech.2022.126745.

Li, L., Long, A., Fossum, B., Kaiser, M., 2023. Effects pyrolysis temperature feedstock type on biochar characteristics pertinent to soil carbon soil health: A meta-analysis 39 (1), 43–52. doi:10.1111/sum.12848.

Li, R., Zhang, C., Chen, W.-H., Kwon, E.E., Rajendran, S., Zhang, Y., 2023. Multistage utilization of soybean straw-derived P-doped biochar for aquatic pollutant removal and biofuel usage. Bioresour. Technol. 387, 129657. doi:10.1016/j.biortech.2023.129657.

Li, Y., Yao, N., Liang, J., Wang, X., Niu, B., Jia, Y., Jiang, F., Yu, Q., Li Liu, D., Feng, H., 2023. Rational biochar application rate for cotton nutrient content, growth, yields, productivity, and economic benefits under film-mulched trickle irrigation. Agric. Water. Manage. 276, 108079.

Li, B., Li, M., Xie, X., Li, C., Liu, D., 2024. Pyrolysis of rice husk in molten lithium chloride: biochar structure evolution and CO_2 adsorption. J. Energy Institute 101526. doi:10.1016/j.joei.2024.101526.
Lian, F., Xing, B., 2017. Black carbon (Biochar) In water/soil environments: molecular structure, sorption, stability, and potential risk. Environ. Sci. Technol. 51 (23), 13517–13532. doi:10.1021/acs.est.7b02528.
Liang, G.W., Yang, Z., Wang, Z.W., Cai, X.W., Zhang, X.L., Xie, X.Y., 2021. Relying on the non-radical pathways for selective degradation organic pollutants in Fe and Cu co–doped biochar/peroxymonosulfate system: The roles of Cu, Fe, defect sites and ketonic group. Separation and Purification Technology 279, 119697. https://doi.org/ARTN.
Liang, F.W., Liu, Z., Jiang, X.D., Li, J.S., Xiao, K.B., Xu, W.C., Chen, X., Liang, J.Z., Lin, Z.F., Li, M., Wu, X.L., Wang, H.L., 2023. NaOH-modified biochar supported Fe/Mn bimetallic composites as efficient peroxymonosulfate activator for enhance tetracycline removal. Chemical Engineering Journal 454, 139949. https://doi.org/ARTN.
Liang, C., Gascó, G., Fu, S., Méndez, A., Paz-Ferreiro, J., 2016. Biochar from pruning residues as a soil amendment: effects of pyrolysis temperature and particle size. Soil Tillage Res. 164, 3–10. doi:10.1016/j.still.2015.10.002.
Liang, X., Guo, N., Zhao, Y., Xue, F., Ren, X., Yang, Z., Yang, Q., 2022. Rapid effectual entrapment of pesticide pollutant by phosphorus-doped biochar: effects and response sequence of functional groups. J. Mol. Liq. 365, 120155. doi:10.1016/j.molliq.2022.120155.
Liao, W., Thomas, S.C., 2019. Biochar Particle Size Post-Pyrolysis Mechanical Processing Affect Soil pH, Water Retention Capacity, Plant Performance 3 (1), 14.
Liao, S., Pan, B., Li, H., Zhang, D., Xing, B., 2014. Detecting free radicals in biochars and determining their ability to inhibit the germination and growth of corn, wheat and rice seedlings. Environ. Sci. Technol. 48 (15), 8581–8587. doi:10.1021/es404250a.
Liao, J., Liu, X., Hu, A., Song, H., Chen, X., Zhang, Z., 2020. Effects of biochar-based controlled release nitrogen fertilizer on nitrogen-use efficiency of oilseed rape (Brassica napus L.). Sci. Rep. 10 (1), 11063. doi:10.1038/s41598-020-67528-y.
Liao, J., Hu, A., Zhao, Z., Liu, X., Jiang, C., Zhang, Z., 2021. Biochar with large specific surface area recruits N2O-reducing microbes and mitigate N2O emission. Soil Biology BioChem. 156, 108212. doi:10.1016/j.soilbio.2021.108212.
Liew, Y.W., Arumugasamy, S.K., Selvarajoo, A., 2022. Potential of biochar as soil amendment: prediction of elemental ratios from pyrolysis of agriculture biomass using artificial neural network. Water Air Soil Pollut. 233 (2), 54. doi:10.1007/s11270-022-05510-2.
Lim, Y., Kim, B., Jang, J., Lee, D.S., 2023. Magnetic rice-straw-derived biochar for adsorptive removal of Hg(II) from aqueous solution: Optimization using response surface methodology. Journal of Environmental Chemical Engineering 11 (3). doi:10.1016/j.jece.2023.110048.
Lin, Y., Cho, J., Davis, J.M., Huber, G.W., 2012. Reaction-transport model for the pyrolysis of shrinking cellulose particles. Chem. Eng. Sci. 74, 160–171. doi:10.1016/j.ces.2012.02.016.
Lin, L., Qiu, W., Wang, D., Huang, Q., Song, Z., Chau, H.W., 2017. Arsenic removal in aqueous solution by a novel Fe-Mn modified biochar composite: characterization and mechanism. Ecotoxicol. Environ. Saf. 144, 514–521. doi:10.1016/j.ecoenv.2017.06.063.
Lin, H., Guo, S., Han, Z., Liu, S., Wang, J., Zou, J., 2023. Can biochar application improve the net economic benefits of tea plantations? Sci. Total Environ. 856, 159029.
Lind, F., Seemann, M., Thunman, H., 2011. Continuous Catalytic Tar Reforming of Biomass Derived Raw Gas with Simultaneous Catalyst Regeneration. Industrial & Engineering Chemistry Research 50 (20), 11553–11562. https://pubs.acs.org/doi/full/10.1021/ie200645s.
Liu, Y., Wilcox, J., 2012. Effects of surface heterogeneity on the adsorption of CO_2 in microporous carbons. Environmental science & technology 46 (3), 1940–1947. https://pubs.acs.org/doi/full/10.1021/es204071g.
Liu, L., Tan, Z., Gong, H., Huang, Q., 2019. Migration and Transformation Mechanisms of Nutrient Elements (N, P, K) within Biochar in Straw–Biochar–Soil–Plant Systems: A Review. ACS Sustainable Chemistry & Engineering 7 (1), 22–32. doi:10.1021/acssuschemeng.8b04253.
Liu, L.A., Yang, X.Z., Ahmad, S., Li, X.L., Ri, C., Tang, J.C., Ellam, R.M., Song, Z.L., 2023. Silicon (Si) modification of biochars from different Si-bearing precursors improves cadmium remediationAfrikaan. Chemical Engineering Journal 457. doi:10.1016/j.cej.2022.141194.
Liu, Z., Zhang, F.-S., Wu, J., 2010. Characterization and application of chars produced from pinewood pyrolysis and hydrothermal treatment. Fuel 89 (2), 510–514. doi:10.1016/j.fuel.2009.08.042.
Liu, X.H., Han, F., Zhang, X.C., 2012. Effect of biochar on soil aggregates in the Loess Plateau: results from incubation experiments. Int J Agric Biol 14, 975–979.
Liu, D., Zhang, W., Lin, H., Li, Y., Lu, H., Wang, Y., 2016a. A green technology for the preparation of high capacitance rice husk-based activated carbon. J. Clean. Prod. 112, 1190–1198. doi:10.1016/j.jclepro.2015.07.005.
Liu, T., Gao, B., Fang, J., Wang, B., Cao, X., 2016b. Biochar-supported carbon nanotube and graphene oxide nanocomposites for Pb(II) and Cd(II) removal. RSC. Adv. 6 (29), 24314–24319. doi:10.1039/C6RA01895E.
Liu, Y., Naidu, R., Ming, H., Dharmarajan, R., Du, J., 2016c. Effects of thermal treatments on the characterisation and utilisation of red mud with sawdust additive. Waste Manage.. Res. 34 (6), 518–526. doi:10.1177/0734242X16634197.
Liu, W.-J., Li, W.-W., Jiang, H., Yu, H.-Q., 2017. Fates of chemical elements in biomass during its pyrolysis. Chem. Rev. 117 (9), 6367–6398. doi:10.1021/acs.chemrev.6b00647.
Liu, Y., Qian, Y., Zhou, H., Xiao, H., Yang, S., 2017. Conceptual design of the coal to synthetic natural gas (SNG) process based on BGL gasifier: modeling and techno-economic analysis. Energy Fuels 31 (1), 1023–1034.
Liu, R., Liu, G., Yousaf, B., Abbas, Q., 2018. Operating conditions-induced changes in product yield and characteristics during thermal-conversion of peanut shell to biochar in relation to economic analysis. J. Clean. Prod. 193, 479–490. doi:10.1016/j.jclepro.2018.05.034.
Liu, P., Lv, J., Shan, F., Liu, Z., Liu, W., 2019. Effects of rib arrangements on the performance of a parabolic trough receiver with ribbed absorber tube. Appl. Therm. Eng. 156, 1–13. doi:10.1016/j.applthermaleng.2019.04.037.
Liu, P., Ptacek, C.J., Blowes, D.W., 2019. Release of nutrients and trace elements from wood-, agricultural residue- and manure-based biochars. Int. J. Environ. Res. 13 (4), 747–758. doi:10.1007/s41742-019-00209-5.
Liu, B., Guo, W., Wang, H., Si, Q., Zhao, Q., Luo, H., Ren, N., 2020. B-doped graphitic porous biochar with enhanced surface affinity and electron transfer for efficient peroxydisulfate activation. Chem. Eng. J. 396, 125119. doi:10.1016/j.cej.2020.125119.
Liu, Y., Song, Y., Ran, C., Siyal, A.A., Chtaeva, P., Dai, J., Jiang, Z., Deng, Z., Zhang, T., Ao, W., Fu, J., 2020. Pyrolysis of furfural residue in a bubbling fluidized bed reactor: biochar characterization and analysis. Energy 211. doi:10.1016/j.energy.2020.118966.
Liu, C., Yin, Z., Hu, D., Mo, F., Chu, R., Zhu, L., Hu, C., 2021. Biochar derived from chicken manure as a green adsorbent for naphthalene removal. Environ. Sci. Pollut. Res. 28, 36585–36597.
Liu, Y., Paskevicius, M., Sofianos, M.V., Parkinson, G., Li, C.-Z., 2021. situ SAXS studies of the pore development in biochar during gasification. Carbon 172, 454–462. doi:10.1016/j.carbon.2020.10.028.
Liu, Y., Chen, Y., Li, Y., Chen, L., Jiang, H., Li, H., Luo, X., Tang, P., Yan, H., Zhao, M., Yuan, Y., Hou, S., 2022. Fabrication, application, and mechanism of metal and heteroatom co-doped biochar composites (MHBCs) for the removal of contaminants in water: A review. J. Hazard. Mater. 431, 128584. doi:10.1016/j.jhazmat.2022.128584.
Liu, J., Qin, T., Li, K., Chen, X., Lu, Q., Deng, J., Luo, X., Yuan, S., 2023. Mechanisms of catalytic reforming of biomass pyrolysis volatiles by Ce promoted Fe–Ni/biochar under N2 and steam atmosphere. J. Energy Institute 111, 101399. doi:10.1016/j.joei.2023.101399.
Lu, Z., Zhang, H., Shahab, A., Zhang, K., Zeng, H.T., Bacha, A.U.R., Nabi, I., Ullah, H., 2021. Comparative study on characterization and adsorption properties of phosphoric acid activated biochar and nitrogen-containing modified biochar employing Eucalyptus as a precursor. Journal of Cleaner Production 303. doi:10.1016/j.jclepro.2021.127046.
Lu, H., Xu, J., Feng, Z., Li, F., Cao, X., Yang, J., 2022. Effects of different modifiers on the sorption and structural properties of biochar derived from wheat stalk. Environ. Sci. Pollut. Res. (36) 29.
Lua, A.C., Lau, F.Y., Guo, J., 2006. Influence of pyrolysis conditions on pore development of oil-palm-shell activated carbons. J. Anal. Appl. Pyrolysis. 76 (1), 96–102. doi:10.1016/j.jaap.2005.08.001.
Luo, D., Wang, L., Nan, H., Cao, Y., Wang, H., Kumar, T.V., Wang, C., 2023. Phosphorus adsorption by functionalized biochar: a review. Environmental Chemistry Letters 21 (1), 497–524. doi:10.1007/s10311-022-01519-5.
Luo, L., Xu, C., Chen, Z., Zhang, S., 2015. Properties of biomass-derived biochars: combined effects of operating conditions and biomass types. Bioresour. Technol. 192, 83–89. doi:10.1016/j.biortech.2015.05.054.
Luo, D., Meng, X., Zheng, N., Li, Y., Yao, H., Chapman, S.J., 2021. The anaerobic oxidation of methane in paddy soil by ferric iron and nitrate, and the microbial communities involved. Sci. Total Environ. 788, 147773. doi:10.1016/j.scitotenv.2021.147773.
Luo, H., Zhang, Y., Zhu, H., Zhao, X., Zhu, L., Liu, W., Sun, M., Miao, G., Li, S., Kong, L., 2021. Microwave-assisted low-temperature biomass pyrolysis: from mechanistic insights to pilot scale. Green Chem. 23 (2), 821–827.
Luo, Z., Yao, B., Yang, X., Wang, L., Xu, Z., Yan, X., Tian, L., Zhou, H., Zhou, Y., 2022. Novel insights into the adsorption of organic contaminants by biochar: A review. Chemosphere 287, 132113. doi:10.1016/j.chemosphere.2021.132113.
Lv, Y., Bao, J., Li, S., Liu, D., Dai, D., Qv, M., Zhu, L., 2022. Biochar amendment of aerobic composting for the effective biodegradation of heavy oil and succession of bacterial community. Bioresour. Technol. 362, 127820. doi:10.1016/j.biortech.2022.127820.
Lv, L., Huang, S., Zhou, H., 2024. Effect of introducing chemically activated biochar as support material on thermal properties of different organic phase change materials. Solar Energy Mater. Solar Cells 264, 112617. doi:10.1016/j.solmat.2023.112617.
Lyu, P., Li, L.F., Huang, J.L., Ye, J., Zhu, C.X., Xie, J.N., Wang, Z.H., Kang, M.Q., Yan, A., 2023. Enhancing sorption of layered double hydroxide-based magnetic biochar for arsenic and cadmium through optimized preparation protocols. Bioresource Technology 388. doi:10.1016/j.biortech.2023.129756.
Lyu, H., Gong, Y., Gurav, R., Tang, J., 2016a. Potential application of biochar for bioremediation of contaminated systems, Biochar application. Elsevier, pp. 221–246.
Lyu, H., Zhang, Q., Shen, B., 2020. Application of biochar and its composites in catalysis. Chemosphere 240, 124842. doi:10.1016/j.chemosphere.2019.124842.
Mäkelä, M., Benavente, V., Fullana, A., 2015. Hydrothermal carbonization of lignocellulosic biomass: effect of process conditions on hydrochar properties. Appl. Energy 155, 576–584. doi:10.1016/j.apenergy.2015.06.022.
Ma, X., Li, L., Zeng, Z., Chen, R., Wang, C., Zhou, K., Li, H., 2019. Experimental and theoretical demonstration of the relative effects of O-doping and N-doping in porous carbons for CO_2 capture. Appl. Surf. Sci. 481, 1139–1147. doi:10.1016/j.apsusc.2019.03.162.
Ma, Z., Yang, Y., Wu, Y., Xu, J., Peng, H., Liu, X., Zhang, W., Wang, S., 2019. In-depth comparison of the physicochemical characteristics of bio-char derived from biomass pseudo components: hemicellulose, cellulose, and lignin. J. Anal. Appl. Pyrolysis. 140, 195–204.
Ma, J., Zhou, B., Zhang, H., Zhang, W., 2020. Fe/S modified sludge-based biochar for tetracycline removal from water. Powder. Technol. 364, 889–900. doi:10.1016/j.powtec.2019.10.107.

Ma, C., Zhang, F., Liu, H., Hu, J., Yang, S., Wang, H.J.F., 2023. Comprehensive investigation on slow pyrolysis product characteristics waste tobacco stem: Pyrolysis reaction mechanism conversion mechanism N 350, 128902.
Mašek, O., Brownsort, P., Cross, A., Sohi, S., 2013. Influence of production conditions on the yield and environmental stability of biochar. Fuel 103, 151–155. doi:10.1016/j.fuel.2011.08.044.
Madej, J., Hilber, I., Bucheli, T.D., Oleszczuk, P., 2016. Biochars with low polycyclic aromatic hydrocarbon concentrations achievable by pyrolysis under high carrier gas flows irrespective of oxygen content or feedstock. J. Anal. Appl. Pyrolysis. 122, 365–369. doi:10.1016/j.jaap.2016.09.005.
Mahler, B.J., Metre, P.C.V., Crane, J.L., Watts, A.W., Scoggins, M., Williams, E.S., 2012. Coal-tar-based pavement sealcoat and PAHs: implications for the environment, Human health, and stormwater management. Environ. Sci. Technol. 46 (6), 3039–3045. doi:10.1021/es203699x.
Mahmoud, M.E., El-Bahy, S.M., Elweshahy, S.M.T., 2021. Decorated Mn-ferrite nanoparticle@Zn-Al layered double hydroxide@Cellulose@ activated biochar nanocomposite for efficient remediation of methylene blue and mercury (II). Bioresource Technology 342. doi:10.1016/j.biortech.2021.126029.
Mai, C., Huang, N., Gao, M., Sun, Y., Yan, J., Zhai, C., Zhao, W., 2023. Natural green raw-based biochar@Co/C composites: simple water bath synthesis and excellent electromagnetic wave absorption properties. J. Alloys. Compd. 968, 171960. doi:10.1016/j.jallcom.2023.171960.
Maljaee, H., Madadi, R., Paiva, H., Tarelho, L., Ferreira, V.M., 2021. Incorporation of biochar in cementitious materials: A roadmap of biochar selection. Construction and Building Materials 283, 122757. doi:10.1016/j.conbuildmat.2021.122757.
Mandal, M., Nanduri, R., 2020. Regularity comparison of fiber cone and associated graded ring. Beiträge zur algebra und geometrie /contributions to algebra. Geometry 61 (2), 219–229. doi:10.1007/s13366-019-00478-3.
Maneechakr, P., Karnjanakom, S., 2021. Improving the Bio-Oil Quality via Effective Pyrolysis/Deoxygenation of Palm Kernel Cake over a Metal (Cu, Ni, or Fe)-Doped Carbon Catalyst. ACS Omega 6 (30), 20006–20014. doi:10.1021/acsomega.1c02999.
Manfrin, J., Gonçalves Jr, A.C., Schwantes, D., Conradi Jr, E., Zimmermann, J., Ziemer, G.L., 2021. Development of biochar and activated carbon from cigarettes wastes and their applications in Pb2+ adsorption. J. Environ. Chem. Eng. 9 (2), 104980.
Mansee, A.H., Abdelgawad, D.M., El-Gamal, E.H., Ebrahim, A.M., Saleh, M.E.J.S.R., 2023. Influences Mg-activation on sugarcane bagasse biochar characteristics its PNP removing potentials from contaminated water 13 (1), 19153.
Manyà, J.J., Roca, F.X., Perales, J.F., 2013. TGA study examining the effect of pressure and peak temperature on biochar yield during pyrolysis of two-phase olive mill waste. J. Anal. Appl. Pyrolysis. 103, 86–95. doi:10.1016/j.jaap.2012.10.006.
Manyà, J.J., Ortigosa, M.A., Laguarta, S., Manso, J.A., 2014. Experimental study on the effect of pyrolysis pressure, peak temperature, and particle size on the potential stability of vine shoots-derived biochar. Fuel 133, 163–172. doi:10.1016/j.fuel.2014.05.019.
Manyà, J.J., Alvira, D., Azuara, M., Bernin, D., Hedin, N., 2016. Effects of pressure and the addition of a rejected material from municipal waste composting on the pyrolysis of two-phase olive mill waste. Energy Fuels 30 (10), 8055–8064. doi:10.1021/acs.energyfuels.6b01579.
Manyà, J.J., 2012. Pyrolysis for biochar purposes: A review to establish current knowledge gaps and research needs. Environ. Sci. Technol. 46 (15), 7939–7954. doi:10.1021/es301029g.
Mao, J., Zhang, K., Chen, B., 2019. Linking hydrophobicity of biochar to the water repellency and water holding capacity of biochar-amended soil. Environmental Pollution 253, 779–789. doi:10.1016/j.envpol.2019.07.051.
Matos, T.T., Mangrich, A.S., Cardoso, E.M., Schultz, J., Fornari, M.R., Wisniewski, A., Carregosa, I.S., 2019. Electron paramagnetic resonance (EPR) spectroscopy as a tool for the characterization of biochar from guava waste. J. Soils. Sediments. 19, 286–295.
McBeath, A.V., Wurster, C.M., Bird, M.I., 2015. Influence of feedstock properties and pyrolysis conditions on biochar carbon stability as determined by hydrogen pyrolysis. Biomass Bioenergy 73, 155–173. doi:10.1016/j.biombioe.2014.12.022.
McNutt, M., 2013. Mercury and Health. Science 341 (6153), 1430. doi:10.1126/science.1245924.
Meijer, R., Kapteijn, F., Moulijn, J.A., 1994. Kinetics of the alkali-carbonate catalysed gasification of carbon: 3. H_2O gasification. Fuel 73 (5), 723–730. https://www.sciencedirect.com/science/article/pii/0016236194900159.
Melligan, F., Auccaise, R., Novotny, E.H., Leahy, J.J., Hayes, M.H.B., Kwapinski, W., 2011. Pressurised pyrolysis of Miscanthus using a fixed bed reactor. Bioresour. Technol. 102 (3), 3466–3470. doi:10.1016/j.biortech.2010.10.129.
Mendonça, F.G.d., Cunha, I.T.d., Soares, R.R., Tristão, J.C., Lago, R.M., 2017. Tuning the surface properties of biochar by thermal treatment. Bioresour. Technol. 246, 28–33. doi:10.1016/j.biortech.2017.07.099.
Mia, S., Singh, B., Dijkstra, F.A., 2017. Aged biochar affects gross nitrogen mineralization and recovery: a 15N study in two contrasting soils. GCB Bioenergy 9 (7), 1196–1206. doi:10.1111/gcbb.12430.
Mian, M.M., Ao, W., Xiao, L., Xiao, J., Deng, S., 2024. Preparation of low-cost sludge-based highly porous biochar for efficient removal of refractory pollutants from agrochemical and pharmaceutical wastewater. J. Hazard. Mater. 478, 135572. doi:10.1016/j.jhazmat.2024.135572.
Miao, Q., Li, G., 2021. Potassium phosphate/magnesium oxide modified biochars: interfacial chemical behaviours and Pb binding performance. Sci. Total Environ. 759. doi:10.1016/j.scitotenv.2020.143452.
Michalak, I., Baśladyńska, S., Mokrzycki, J., Rutkowski, P., 2019. Biochar from A Freshwater Macroalga as A Potential Biosorbent for Wastewater Treatment 11 (7), 1390.
Miller, S.A., Moore, F.C., 2020. Climate and health damages from global concrete production. Nature Climate Change 10 (5), 439–443. https://www.nature.com/articles/s41558-020-0733-0.
Ming, C., Jiang, Y., Li, C., Chen, Q., Zhang, S., Wang, S., Li, B., Cui, Z., Tang, Y., Hu, X., 2023. Activation of cellulose with CO_2 and/or H_2O: evolution of functionalities of the biochar and environmental impacts. Biomass Bioenergy 174, 106811. doi:10.1016/j.biombioe.2023.106811.
Minh, T.D., Song, J.Z., Deb, A., Cha, L.G., Srivastava, V., Sillanpää, M., 2020. Biochar based catalysts for the abatement of emerging pollutants: A review. Chemical Engineering Journal 394, 124856. https://doi.org/ARTN.
Mishra, R.K., 2023. Fresh water availability and its global challenge. British J. Multidisciplinary Advanced Studies 4 (3), 1–78.
Mittal, Y., Srivastava, P., Kumar, N., Kumar, M., Singh, S.K., Martinez, F., Yadav, A.K., 2023. Ultra-fast and low-cost electroactive biochar production for electroactive-constructed wetland applications: A circular concept for plant biomass utilization. Chem. Eng. J. 452, 138587. doi:10.1016/j.cej.2022.138587.
Mo, L., Fang, J., Huang, B., Wang, A., Deng, M., 2019. Combined effects of biochar and MgO expansive additive on the autogenous shrinkage, internal relative humidity and compressive strength of cement pastes. Construction and Building Materials 229, 116877. doi:10.1016/j.conbuildmat.2019.116877.
Mohamed, A.R., Hamzah, Z., Daud, M.Z.M., Zakaria, Z., 2013. The effects of holding time and the sweeping nitrogen gas flowrates on the pyrolysis of EFB using a fixed–Bed reactor. Procedia Eng. 53, 185–191. doi:10.1016/j.proeng.2013.02.024.
Mohammadi, A., Khoshnevisan, B., Venkatesh, G., Eskandari, S., 2020. A critical review on advancement and challenges of biochar application in paddy fields: environmental and life cycle cost analysis. Processes 8 (10), 1275.
Mohanty, P., Nanda, S., Pant, K.K., Naik, S., Kozinski, J.A., Dalai, A.K.J.J.o.a., pyrolysis, a., 2013. Evaluation physiochemical development biochars obtained from pyrolysis wheat straw, timothy grass pinewood: effects heating rate 104, 485–493.
Molina-Sabio, M., Gonzalez, M., Rodriguez-Reinoso, F., Sepúlveda-Escribano, A., 1996a. Effect of steam and carbon dioxide activation in the micropore size distribution of activated carbon. Carbon 34 (4), 505–509. doi:10.1016/0008-6223(96)00006-1.
Molina-Sabio, M., Rodríguez-Reinoso, F., Caturla, F., Sellés, M.J., 1996b. Development of porosity in combined phosphoric acid-carbon dioxide activation. Carbon 34 (4), 457–462. doi:10.1016/0008-6223(95)00209-x.
Molina-Sabio, M., Almansa, C., Rodríguez-Reinoso, F., 2003. Phosphoric acid activated carbon discs for methane adsorption. Carbon 41 (11), 2113–2119. doi:10.1016/s0008-6223(03)00237-9.
Moliner, C., Focacci, S., Antonucci, B., Moreno, A., Biti, S., Hamzah, F., Martinez-Felipe, A., Arato, E., Fernández Martín, C., 2022. Production, activation and CO_2 uptake capacity of a carbonaceous microporous material from palm oil residues. Energies 15 (23), 9160. doi:10.3390/en15239160.
Monteiro, P.J.M., Miller, S.A., Horvath, A., 2017. Towards sustainable concrete. Nat Mater 16 (7), 698–699. doi:10.1038/nmat4930.
Montes-Morán, M.A., Suárez, D., Menéndez, J.A., Fuente, E., 2004. On the nature of basic sites on carbon surfaces: an overview. Carbon 42 (7), 1219–1225. doi:10.1016/j.carbon.2004.01.023.
Moon, S., Lee, Y.-J., Park, S.-J., Lee, C.-G., 2023. Enhanced removal of micropollutants from water using ZnCl2-modified Spirulina sp.-based biochar. J. Appl. Phycol. 1–13.
Mosharrof, M., Uddin, M.K., Jusop, S., Sulaiman, M.F., Shamsuzzaman, S.M., Haque, A.N.A., 2021. Changes in acidic soil chemical properties and carbon dioxide emission due to. Biochar Lime Treatments 11 (3), 219.
Mubarik, S., Saeed, A., Athar, M., Iqbal, d.M.J.J.o.I., Chemistry, E., 2016. Characterization mechanism adsorptive removal 2, 4, 6-trichlorophenol by biochar prepared from sugarcane baggase 33, 115–121.
Mukherjee, A., Okolie, J.A., Niu, C., Dalai, A.K., 2022. Techno–Economic analysis of activated carbon production from spent coffee grounds: comparative evaluation of different production routes. Energy Conversion Manage.ment: X 14, 100218.
Mukherjee, A., Saha, B., Niu, C., Dalai, A.K., 2022. Preparation of activated carbon from spent coffee grounds and functionalization by deep eutectic solvent: effect of textural properties and surface chemistry on CO_2 capture performance. J. Environ. Chem. Eng. 10 (6), 108815. doi:10.1016/j.jece.2022.108815.
Mukome, F.N.D., Zhang, X., Silva, L.C.R., Six, J., Parikh, S.J., 2013. Use of chemical and physical characteristics to investigate trends in biochar feedstocks. J. Agric. Food Chem. 61 (9), 2196–2204. doi:10.1021/jf3049142.
Murad, H.A., Ahmad, M., Bundschuh, J., Hashimoto, Y., Zhang, M., Sarkar, B., Ok, Y.S., 2022. A remediation approach to chromium-contaminated water and soil using engineered biochar derived from peanut shell. Environmental Research 204. doi:10.1016/j.envres.2021.112125.
Murtaza, G., Ahmed, Z., Usman, M., Tariq, W., Ullah, Z., Shareef, M., Iqbal, H., Waqas, M., Tariq, A., Wu, Y., Zhang, Z., Ditta, A., 2021. Biochar induced modifications in soil properties and its impacts on crop growth and production. J. Plant Nutr. 44 (11), 1677–1691. doi:10.1080/01904167.2021.1871746.
Murtaza, G., Ahmed, Z., Dai, D.-Q., Iqbal, R., Bawazeer, S., Usman, M., Rizwan, M., Iqbal, J., Akram, M.I., Althubiani, A.S., Tariq, A., Ali, I., 2022. A review of mechanism and adsorption capacities of biochar-based engineered composites for removing aquatic pollutants from contaminated water. Front. Environ. Sci. 10. doi:10.3389/fenvs.2022.1035865.
Naisse, C., Alexis, M., Plante, A., Wiedner, K., Glaser, B., Pozzi, A., Carcaillet, C., Criscuoli, I., Rumpel, C., 2013. Can biochar and hydrochar stability be assessed with chemical methods? Org. Geochem. 60, 40–44. doi:10.1016/j.orggeochem.2013.04.011.
Nasri, N., Zain, H., Usman, H., Zulkifli, A., Zalilah, S., Nurul, A.S., Nur, L.A., 2015. CO_2 adsorption-breakthrough study on activated carbon derived from renewable oil palm empty fruit bunch. Australian J. Basic Appl. Sci. 9 (26 Special), 67–71.
Nguyen, T.B., Nguyen, T.K.T., Chen, W.H., Chen, C.W., Bui, X.T., Patel, A.K., Dong, C.D., 2023. Hydrothermal and pyrolytic conversion of sunflower seed husk into novel porous biochar for efficient adsorption of tetracycline. Bioresource Technology 373, 128711. https://doi.org/ARTN.

Nguyen, V.-T., Nguyen, T.-B., Chen, C.-W., Hung, C.-M., Huang, C.P., Dong, C.-D., 2019. Cobalt-impregnated biochar (Co-SCG) for heterogeneous activation of peroxymonosulfate for removal of tetracycline in water. Bioresour. Technol. 292, 121954. doi:10.1016/j.biortech.2019.121954.

Nicholas, H.A.-O., Mabbett, I.A.-O., Apsey, H.A.-O., Robertson, I.A.-O., 2022. Physico–chemical properties of waste derived biochar from community scale faecal sludge treatment plants. (2572-4754 (Electronic)).

Niksiar, A., Nasernejad, B., 2017. Activated carbon preparation from pistachio shell pyrolysis and gasification in a spouted bed reactor. Biomass Bioenergy 106, 43–50. doi:10.1016/j.biombioe.2017.08.017.

Nizamuddin, S., Mubarak, N.M., Tiripathi, M., Jayakumar, N.S., Sahu, J.N., Ganesan, P., 2016. Chemical, dielectric and structural characterization of optimized hydrochar produced from hydrothermal carbonization of palm shell. Fuel 163, 88–97. doi:10.1016/j.fuel.2015.08.057.

Noreen, S., Abd-Elsalam, K.A., 2021. Chapter 9 - biochar-based nanocomposites: A sustainable tool in wastewater bioremediation. In: Abd-Elsalam, K.A., Zahid, M. (Eds.), Aquananotechnology. Elsevier, pp. 185–200. doi:10.1016/B978-0-12-821141-0.00023-9.

Norouzi, O., Pourhosseini, S.E.M., Naderi, H.R., Di Maria, F., Dutta, A., 2021. Integrated hybrid architecture of metal and biochar for high performance asymmetric supercapacitors. Sci. Rep. 11 (1), 5387. doi:10.1038/s41598-021-84979-z.

Novak, J.M., Lima, I., Xing, B., Gaskin, J.W., Steiner, C., Das, K.C., Ahmedna, M., Rehrah, D., Watts, D.W., Busscher, W.J., Schomberg, H., 2009. Characterization of designer biochar produced at different temperatures and their effects on a loamy sand. Annals Environ. Sci. 3 (0).

Nsamba Hussein Kisiki, S.E.H., Cornelissen, Gerard, Bachmann, Robert Thomas, 2015. Sustainable technologies for small-scale biochar production-A review. Scientific Res. doi:10.4236/jsbs.2015.51002.

Nzediegwu, C., Naeth, M.A., Chang, S.X., 2021. Elemental composition of biochars is affected by methods used for its determination. J. Anal. Appl. Pyrolysis. 156, 105174. doi:10.1016/j.jaap.2021.105174.

Nzihou, A., Stanmore, B., Lyczko, N., Minh, D.P., 2019. The catalytic effect of inherent and adsorbed metals on the fast/flash pyrolysis of biomass: A review. Energy 170, 326–337. doi:10.1016/j.energy.2018.12.174.

O'Connor, D., Peng, T., Li, G., Wang, S., Duan, L., Mulder, J., Cornelissen, G., Cheng, Z., Yang, S., Hou, D., 2018. Sulfur-modified rice husk biochar: A green method for the remediation of mercury contaminated soil. Sci. Total Environ. 621, 819–826. doi:10.1016/j.scitotenv.2017.11.213.

Obidike, L.I., Yoro, K.O., 2022. Effect of zeolitic nano-catalyst on biodiesel yield and biochar formation during the pyrolysis of tallow. Biofuels. 13 (6), 683–692. doi:10.1080/17597269.2021.1882718.

Ofrasio, B.I.G., de Luna, M.D.G., Chen, Y.-C., Abarca, R.R.M., Dong, C.-D., Chang, K.-L., 2020. Catalytic conversion of sugars and biomass to furanic biofuel precursors by boron-doped biochar in ionic liquid. Bioresource Technology Reports 11, 100515. doi:10.1016/j.biteb.2020.100515.

Oh, W.-D., Zaeni, J.R.J., Lisak, G., Lin, K.-Y.A., Leong, K.-H., Choong, Z.-Y., 2021. Accelerated organics degradation by peroxymonosulfate activated with biochar co-doped with nitrogen and sulfur. Chemosphere 277, 130313. doi:10.1016/j.chemosphere.2021.130313.

Ok, Y.S., Uchimiya, S.M., Chang, S.X., Bolan, N., 2015. Biochar: Production, characterization, and applications. CRC press.

Oleszczuk, P., Jośko, I., Kuśmierz, M., 2013. Biochar properties regarding to contaminants content and ecotoxicological assessment. J. Hazard. Mater. 260, 375–382. doi:10.1016/j.jhazmat.2013.05.044.

Ooi, C.H., Cheah, W.K., Sim, Y.L., Pung, S.Y., Yeoh, F.Y., 2017. Conversion and characterization of activated carbon fiber derived from palm empty fruit bunch waste and its kinetic study on urea adsorption. J. Environ. Manage. 197, 199–205. doi:10.1016/j.jenvman.2017.03.083.

Orlova, T.S., Parfen'eva, L.S., Smirnov, B.I., Gutierrez-Pardo, A., Ramirez-Rico, J., 2016. Thermal conductivity of partially graphitized biocarbon obtained by carbonization of medium-density fiberboard in the presence of a Ni-based catalyst. Physics Solid State 58 (1), 208–214. doi:10.1134/S1063783416010236.

Pal, D.B., Chand, R., Upadhyay, S., Mishra, P., 2018. Performance of water gas shift reaction catalysts: A review. Renew. Sustain. Energy Reviews 93, 549–565.

Palacios, A., Cong, L., Navarro, M.E., Ding, Y., Barreneche, C., 2019. Thermal conductivity measurement techniques for characterizing thermal energy storage materials – A review. Renew. Sustain. Energy Reviews 108, 32–52. doi:10.1016/j.rser.2019.03.020.

Pan, G., Wei, J., Xu, M., Li, J., Wang, L., Li, Y., Cui, N., Li, J., Wang, Z., 2023. Insight into boron-doped biochar as efficient metal-free catalyst for peroxymonosulfate activation: important role of -O-B-O- moieties. J. Hazard. Mater. 445, 130479. doi:10.1016/j.jhazmat.2022.130479.

Pandey, D., Daverey, A., Arunachalam, K., 2020. Biochar: production, properties and emerging role as a support for enzyme immobilization. J. Clean. Prod. 255, 120267. doi:10.1016/j.jclepro.2020.120267.

Pang, Y., Zeng, G., Tang, L., Zhang, Y., Liu, Y., Lei, X., Li, Z., Zhang, J., Xie, G., 2011. PEI-grafted magnetic porous powder for highly effective adsorption of heavy metal ions. Desalination. 281, 278–284. doi:10.1016/j.desal.2011.08.001.

Panwar, N., Pawar, A., 2020. Influence of activation conditions on the physicochemical properties of activated biochar: A review. BioMass Convers. Biorefin. 1–23.

Paravannoor, A., 2018. One-pot synthesis of biochar wrapped Ni/NiO nanobrick composites for supercapacitor applications. J. Electroanalytical Chem. 823, 656–662. doi:10.1016/j.jelechem.2018.04.060.

Paritosh, K., Hackula, A., 2024. Decarbonising distillery wastewater treatment: experimental investigation of biochar-assisted anaerobic conversion and financial assessment. Energy Convers. Manage. 318, 118893. doi:10.1016/j.enconman.2024.118893.

Pariyar, P., Kumari, K., Jain, M.K., Jadhao, P.S., 2020. Evaluation of change in biochar properties derived from different feedstock and pyrolysis temperature for environmental and agricultural application. Sci. Total Environ. 713, 136433. doi:10.1016/j.scitotenv.2019.136433.

Park, W.C., Atreya, A., Baum, H.R., 2010. Experimental and theoretical investigation of heat and mass transfer processes during wood pyrolysis. Combust. Flame 157 (3), 481–494. doi:10.1016/j.combustflame.2009.10.006.

Park, J., Lee, Y., Ryu, C., Park, Y.-K., 2014. Slow pyrolysis of rice straw: analysis of products properties, carbon and energy yields. Bioresour. Technol. 155, 63–70. doi:10.1016/j.biortech.2013.12.084.

Park, H.C., Lee, B.-K., Yoo, H.S., Choi, H.S.J.C.E., 2019. Influence of operating conditions for fast pyrolysis and pyrolysis oil production in a conical spouted-bed reactor. Technol. (Singap World Sci) 42 (12), 2493–2504.

Park, J.-H., Wang, J.J., Zhou, B., Mikhael, J.E.R., DeLaune, R.D., 2019. Removing mercury from aqueous solution using sulfurized biochar and associated mechanisms. Environ. Pollut. 244, 627–635. doi:10.1016/j.envpol.2018.10.069.

Parthasarathy, P., Al-Ansari, T., Mackey, H.R., Narayanan, K.S., McKay, G.J.F., 2022. A review on prominent animal municipal wastes as potential feedstocks for solar pyrolysis for biochar production 316, 123378.

Patel, M.A., Luo, F., Savaram, K., Kucheryavy, P., Xie, Q., Flach, C., Mendelsohn, R., Garfunkel, E., Lockard, J.V., He, H., 2017. P and S dual-doped graphitic porous carbon for aerobic oxidation reactions: enhanced catalytic activity and catalytic sites. Carbon 114, 383–392. doi:10.1016/j.carbon.2016.11.064.

Pathomrotsakun, J., Nakason, K., Kraithong, W., Khemthong, P., Panyapinyopol, B., Pavasant, P., 2020. Fuel properties of biochar from torrefaction of ground coffee residue: effect of process temperature, time, and sweeping gas. BioMass Convers. Biorefin. 10 (3), 743–753. doi:10.1007/s13399-020-00632-1.

Patra, B.R., Nanda, S., Dalai, A.K., Meda, V., 2021. Taguchi-based process optimization for activation of agro-food waste biochar and performance test for dye adsorption. Chemosphere 285, 131531.

Paz-Ferreiro, J., Pandit, N.R., Mulder, J., Hale, S.E., Schmidt, H.P., Cornelissen, G., 2017. Biochar from "Kon Tiki" flame curtain and other kilns: effects of nutrient enrichment and kiln type on crop yield and soil chemistry. PLoS. One 12 (4). doi:10.1371/journal.pone.0176378.

Pei, J., Li, J., Mia, S., Singh, B., Wu, J., Dijkstra, F.A., 2021. Biochar aging increased microbial carbon use efficiency but decreased biomass turnover time. Geoderma 382, 114710. doi:10.1016/j.geoderma.2020.114710.

Peng, Y., Sun, Y., Fan, B., Zhang, S., Bolan, N.S., Chen, Q., Tsang, D.C.W., 2021. Fe/Al (hydr)oxides engineered biochar for reducing phosphorus leaching from a fertile calcareous soil. J. Clean. Prod. 279, 123877. doi:10.1016/j.jclepro.2020.123877.

Peng, X., Yang, Y., Wang, J., Yuan, W., Guo, Y., Hu, W., Yang, X., 2023. Cu/Fe co-modified nitrogen self-doped biochar as a heterogeneous fenton-like catalyst for degradation of organic pollutants: synthesis, performance, and mechanistic study. J. Environ. Chem. Eng. 11 (5), 110866. doi:10.1016/j.jece.2023.110866.

Penido, E.S., Melo, L.C.A., Guilherme, L.R.G., Bianchi, M.L., 2019. Cadmium binding mechanisms and adsorption capacity by novel phosphorus/magnesium-engineered biochars. Sci. Total Environ. 671, 1134–1143. doi:10.1016/j.scitotenv.2019.03.437.

Perander, M., Demartini, N., Brink, A., Kramb, J., Karlstrom, O., Hemming, J., Moilanen, A., Konttinen, J., Hupa, M., 2015. Catalytic effect of Ca and K on CO_2 gasification of spruce wood char. Fuel 150 (jun.15), 464–472. https://www.sciencedirect.com/science/article/pii/S0016236115002100.

Peter, A., Chabot, B., Loranger, E., 2021. Enhanced activation of ultrasonic pre-treated softwood biochar for efficient heavy metal removal from water. J. Environ. Manage. 290, 112569.

Pignatello, J.J., Mitch, W.A., Xu, W., 2017. Activity and reactivity of pyrogenic carbonaceous matter toward organic compounds. Environ. Sci. Technol. 51 (16), 8893–8908. doi:10.1021/acs.est.7b01088.

Pituello, C., Dal Ferro, N., Francioso, O., Simonetti, G., Berti, A., Piccoli, I., Pisi, A., Morari, F., 2018. Effects of biochar on the dynamics of aggregate stability in clay and sandy loam soils. Eur. J. Soil. Sci. 69 (5), 827–842. doi:10.1111/ejss.12676.

Porat, A., Careaga, F.S., Briens, L., Briens, C., 2022. Design development a rotating heater pyrolysis reactor 100 (S1), S25–S37. doi:10.1002/cjce.24099.

Pourhosseini, S.E.M., Norouzi, O., Salimi, P., Naderi, H.R., 2018. Synthesis of a novel interconnected 3D pore network algal biochar constituting iron nanoparticles derived from a harmful marine biomass as high-performance asymmetric supercapacitor electrodes. ACS. Sustain. Chem. Eng. 6 (4), 4746–4758. doi:10.1021/acssuschemeng.7b03871.

Prabahar, J., Vafaei, B., Baffoe, E., Ghahremaninezhad, A., 2021. The Effect of Biochar on the Properties of Alkali-Activated Slag Pastes. Construction Materials 2 (1), 1–14. doi:10.3390/constrmater2010001.

Praneeth, S., Guo, R., Wang, T., Dubey, B.K., Sarmah, A.K., 2020. Accelerated carbonation of biochar reinforced cement-fly ash composites: Enhancing and sequestering CO_2 in building materials. Construction and Building Materials 244, 118363. doi:10.1016/j.conbuildmat.2020.118363.

Prauchner, M.J., Rodríguez-Reinoso, F., 2008. Preparation of granular activated carbons for adsorption of natural gas. Microporous Mesoporous Mater. 109 (1-3), 581–584. doi:10.1016/j.micromeso.2007.04.046.

Prosser, K.E., Walsby, C.J., 2017. Electron paramagnetic resonance as a tool for studying the mechanisms of paramagnetic anticancer metallodrugs. Eur. J. Inorg. Chem. 2017 (12), 1573–1585.

Puziy, A.M., Poddubnaya, O.I., Sobiesiak, M., Gawdzik, B., 2017. Assessment of the structural evolution of polyimide-derived carbons obtained by phosphoric acid activation using fourier transform infrared and Raman spectroscopy. Adsorption Sci. Technol. 35 (5-6), 403–412. doi:10.1177/0263617417693627.

Puziy, A.M., Poddubnaya, O.I., Gawdzik, B., Tascón, J.M.D., 2020. Phosphorus-containing carbons: preparation, properties and utilization. Carbon 157, 796–846. doi:10.1016/j.carbon.2019.10.018.

Qambrani, N.A., Rahman, M.M., Won, S., Shim, S., Ra, C.J.R., Reviews, S.E., 2017. Biochar properties eco-friendly applications for climate change mitigation, Waste Manage.., wastewater treatment: A review 79, 255–273.
Qian, K., Kumar, A., Zhang, H., Bellmer, D., Huhnke, R., 2015. Recent advances in utilization of biochar. Renew. Sustain. Energy Reviews 42, 1055–1064. doi:10.1016/j.rser.2014.10.074.
Qin, F., Zhang, C., Zeng, G., Huang, D., Tan, X., Duan, A., 2022. Lignocellulosic biomass carbonization for biochar production and characterization of biochar reactivity. Renew. Sustain. Energy Reviews 157. doi:10.1016/j.rser.2021.112056.
Qiu, M., Sun, K., Jin, J., Han, L., Sun, H., Zhao, Y., Xia, X., Wu, F., Xing, B., 2015. Metal/metalloid elements and polycyclic aromatic hydrocarbon in various biochars: the effect of feedstock, temperature, minerals, and properties. Environ. Pollut. 206, 298–305. doi:10.1016/j.envpol.2015.07.026.
Qiu, B., Tao, X., Wang, H., Li, W., Ding, X., Chu, H., 2021. Biochar as a low-cost adsorbent for aqueous heavy metal removal: A review. J. Anal. Appl. Pyrolysis. 155, 105081. doi:10.1016/j.jaap.2021.105081.
Qiu, B., Shao, Q., Shi, J., Yang, C., Chu, H., 2022. Application of biochar for the adsorption of organic pollutants from wastewater: modification strategies, mechanisms and challenges. Sep. Purif. Technol. 300, 121925. doi:10.1016/j.seppur.2022.121925.
Qu, Z., Sun, F., Gao, J., Zhao, G., 2022. Activity origin of boron doped carbon cluster for thermal catalytic oxidation: coupling effects of dopants and edges. J. Colloid. Interface Sci. 613, 47–56. doi:10.1016/j.jcis.2022.01.017.
Quilliam, R.S., Rangecroft, S., Emmett, B.A., Deluca, T.H., Jones, D.L., 2013. Is biochar a source or sink for polycyclic aromatic hydrocarbon (PAH) compounds in agricultural soils? 5 (2), 96–103. doi:10.1111/gcbb.12007.
Rafiq, M.K., Bachmann, R.T., Rafiq, M.T., Shang, Z., Joseph, S., Long, R., 2016. Influence of pyrolysis temperature on physico-chemical properties of corn stover (Zea mays L.) biochar and feasibility for carbon capture and energy balance. PLoS. One 11 (6), e0156894. doi:10.1371/journal.pone.0156894.
Rajapaksha, A.U., Vithanage, M., Lim, J.E., Ahmed, M.B.M., Zhang, M., Lee, S.S., Ok, Y.S., 2014. Invasive plant-derived biochar inhibits sulfamethazine uptake by lettuce in soil. Chemosphere 111, 500–504. doi:10.1016/j.chemosphere.2014.04.040.
Rajapaksha, A.U., Chen, S.S., Tsang, D.C., Zhang, M., Vithanage, M., Mandal, S., Gao, B., Bolan, N.S., Ok, Y.S., 2016. Engineered/designer biochar for contaminant removal/immobilization from soil and water: potential and implication of biochar modification. Chemosphere 148, 276–291.
Rajendran, M., Shi, L., Wu, C., Li, W., An, W., Liu, Z., Xue, S., 2019. Effect of sulfur and sulfur-iron modified biochar on cadmium availability and transfer in the soil–rice system. Chemosphere 222, 314–322. doi:10.1016/j.chemosphere.2019.01.149.
Rambabu, N., Azargohar, R., Dalai, A.K., Adjaye, J., 2013. Evaluation and comparison of enrichment efficiency of physical/chemical activations and functionalized activated carbons derived from fluid petroleum coke for environmental applications. Fuel Process. Technol. 106, 501–510. doi:10.1016/j.fuproc.2012.09.019.
Rangabhashiyam, S.a.B., P., 2019. The potential of lignocellulosic biomass precursors for biochar production: performance, mechanism and wastewater application-a review. Ind. Crops. Prod. 128, 405–423. doi:10.1016/j.indcrop.2018.11.041.
Rathore, N.S., Pawar, A., Panwar, N.L., 2021. Kinetic analysis and thermal degradation study on wheat straw and its biochar from vacuum pyrolysis under non-isothermal condition. BioMass Convers. Biorefin. doi:10.1007/s13399-021-01360-w.
Ray, S.K., Pant, B., Park, M., Bastakoti, B.P., 2023. Rice husk-derived sodium hydroxide activated hierarchical porous biochar as an efficient electrode material for supercapacitors. J. Anal. Appl. Pyrolysis. 175, 106207.
Rechberger, M.V., Kloss, S., Rennhofer, H., Tintner, J., Watzinger, A., Soja, G., Lichtenegger, H., Zehetner, F., 2017. Changes in biochar physical and chemical properties: accelerated biochar aging in an acidic soil. Carbon 115, 209–219. doi:10.1016/j.carbon.2016.12.096.
Ren, H.-Y., Wei, Z.-J., Wang, Y., Deng, Y.-P., Li, M.-Y., Wang, B., 2020. Effects of biochar properties on the bioremediation of the petroleum-contaminated soil from a shale-gas field. Environ. Sci. Pollut. Res. 27 (29), 36427–36438. doi:10.1007/s11356-020-09715-y.
Reshad, A.S., Tiwari, P., Goud, V.V., 2019. Thermal and co-pyrolysis of rubber seed cake with waste polystyrene for bio-oil production. J. Anal. Appl. Pyrolysis. 139, 333–343. doi:10.1016/j.jaap.2019.03.010.
Rey-Raap, N., Ribeiro, L.S., Órfão, J.J.d.M., Figueiredo, J.L., Pereira, M.F.R., 2019. Catalytic conversion of cellulose to sorbitol over Ru supported on biomass-derived carbon-based materials. Applied Catalysis B: Environmental 256, 117826. doi:10.1016/j.apcatb.2019.117826.
Ribeiro Carrott, M.M.L., Candeias, A.J.E., Carrott, P.J.M., Ravikovitch, P.I., Neimark, A.V., Sequeira, A.D., 2001. Adsorption of nitrogen, neopentane, n-hexane, benzene and methanol for the evaluation of pore sizes in silica grades of MCM-41. Microporous Mesoporous Mater. 47 (2), 323–337. doi:10.1016/S1387-1811(01)00394-8.
Robb, S., Joseph, S., Abdul Aziz, A., Dargusch, P., Tisdell, C., 2020. Biochar's cost constraints are overcome in small-scale farming on tropical soils in lower-income countries. Land. Degrad. Dev. 31 (13), 1713–1726.
Rodriguez Correa, C., Hehr, T., Voglhuber-Slavinsky, A., Rauscher, Y., Kruse, A., 2019. Pyrolysis vs. hydrothermal carbonization: understanding the effect of biomass structural components and inorganic compounds on the char properties. J. Anal. Appl. Pyrolysis. 140, 137–147. doi:10.1016/j.jaap.2019.03.007.
Rodriguez, J.A., Lustosa Filho, J.F., Melo, L.C.A., de Assis, I.R., de Oliveira, T.S.J.J.o.A., Pyrolysis, A., 2020. Influence pyrolysis temperature feedstock on properties biochars produced from agricultural industrial wastes 149, 104839.
Rondon, M.A., Lehmann, J., Ramírez, J., Hurtado, M., 2007. Biological nitrogen fixation by common beans (Phaseolus vulgaris L.) increases with bio-char additions. Biol. Fertil. Soils. 43 (6), 699–708. doi:10.1007/s00374-006-0152-z.
Rong, X., Xie, M., Kong, L., Natarajan, V., Ma, L., Zhan, J., 2019. The magnetic biochar derived from banana peels as a persulfate activator for organic contaminants degradation. Chem. Eng. J. 372, 294–303. doi:10.1016/j.cej.2019.04.135.
Rostrup-Nielsen, J.R., 2002. Syngas in perspective. Catal. Today 71 (3-4), 243–247.
Rouquerol, J., Llewellyn, P., Rouquerol, F., 2007. Is the bet equation applicable to microporous adsorbents? In: Llewellyn, P.L., Rodriquez-Reinoso, F., Rouqerol, J., Seaton, N. (Eds.) Studies in Surface Science and Catalysis. Elsevier, pp. 49–56. doi:10.1016/S0167-2991(07)80008-5.
Ruan, X., Sun, Y., Du, W., Tang, Y., Liu, Q., Zhang, Z., Doherty, W., Frost, R.L., Qian, G., Tsang, D.C.J.B.t., 2019. Formation, characteristics, applications Environ.ly persistent free radicals in biochars: a review 281, 457–468.
Şensöz, S., Angın, D., 2008. Pyrolysis of safflower (Charthamus tinctorius L.) seed press cake: part 1. The effects of pyrolysis parameters on the product yields. Bioresour. Technol. 99 (13), 5492–5497. doi:10.1016/j.biortech.2007.10.046.
Sørmo, E., Silvani, L., Bjerkli, N., Hagemann, N., Zimmerman, A.R., Hale, S.E., Hansen, C.B., Hartnik, T., Cornelissen, G., 2021. Stabilization of PFAS-contaminated soil with activated biochar. Sci. Total Environ. 763, 144034. doi:10.1016/j.scitotenv.2020.144034.
Saha, D., Kienbaum, M.J., 2019. Role of oxygen, nitrogen and sulfur functionalities on the surface of nanoporous carbons in CO_2 adsorption: A critical review. Microporous Mesoporous Mater. 287, 29–55. doi:10.1016/j.micromeso.2019.05.051.
Sajjadi, B., Chen, W.-Y., Egiebor, N.O., 2019. A comprehensive review on physical activation of biochar for energy and environmental applications. Rev. Chem. Eng. 35 (6), 735–776. doi:10.1515/revce-2017-0113.
Sajjadi, B., Zubatiuk, T., Leszczynska, D., Leszczynski, J., Chen, W.Y., 2019. Chemical activation of biochar for energy and environmental applications: a comprehensive review. Rev. Chem. Eng. 35 (7), 777–815.
Sakhiya, A.K., Anand, A., Kaushal, P.J.B., 2020. Production, activation, applications biochar in recent times 2, 253–285.
Sakhiya, A.K., Baghel, P., Anand, A., Vijay, V.K., Kaushal, P., 2021. A comparative study of physical and chemical activation of rice straw derived biochar to enhance Zn+ 2 adsorption. Bioresour. Technol. Rep. 15, 100774. doi:10.1016/j.biteb.2021.100774.
Saletnik, B., Saletnik, A., Zaguła, G., Bajcar, M., Puchalski, C., 2022. Oak Biomass in Form Wood, Bark, Brushwood, Leaves Acorns in Production Process Multifunctional Biochar 27 (21), 7191.
Salkuyeh, Y.K., Saville, B.A., MacLean, H.L., 2018. Techno-economic analysis and life cycle assessment of hydrogen production from different biomass gasification processes. Int. J. Hydrogen. Energy 43 (20), 9514–9528.
Samiran, N.A., Ng, J.-H., Jaafar, M.N.M., Valera-Medina, A., Chong, C.T., 2016. H2-rich syngas strategy to reduce NOx and CO emissions and improve stability limits under premixed swirl combustion mode. Int. J. Hydrogen. Energy 41 (42), 19243–19255.
Samolada, M.C., Papafotica, A., Vasalos, I.A., 2000. Catalyst evaluation for catalytic biomass pyrolysis. Energy Fuels 14 (6), 1161–1167. doi:10.1021/ef000026b.
Sangani, M.F., Abrishamkesh, S., Owens, G.J.B.t., 2020. Physicochemical characteristics biochars can be beneficially manipulated using post-pyrolyzed particle size modification 306, 123157.
Sangon, S., Hunt, A.J., Attard, T.M., Mengchang, P., Ngernyen, Y., Supanchaiyamat, N., 2018. Valorisation of waste rice straw for the production of highly effective carbon based adsorbents for dyes removal. J. Clean. Prod. 172, 1128–1139. doi:10.1016/j.jclepro.2017.10.210.
Sangsuk, S., Buathong, C., Suebsiri, S., 2020. High-energy conversion efficiency of drum kiln with heat distribution pipe for charcoal and biochar production. Energy for Sustainable Development 59, 1–7. doi:10.1016/j.esd.2020.08.008.
Santos, R.M., Santos, A.O., Sussuchi, E.M., Nascimento, J.S., Lima, Á.S., Freitas, L.S., 2015. Pyrolysis of mangaba seed: production and characterization of bio-oil. Bioresour. Technol. 196, 43–48. doi:10.1016/j.biortech.2015.07.060.
Sarfaraz, Q., Silva, L.S.d., Drescher, G.L., Zafar, M., Severo, F.F., Kokkonen, A., Dal Molin, G., Shafi, M.I., Shafique, Q., Solaiman, Z.M., 2020. Characterization and carbon mineralization of biochars produced from different animal manures and plant residues. Sci. Rep. 10 (1), 955. doi:10.1038/s41598-020-57987-8.
Sato, K., Yamamoto, A., Dyballa, M., Hunger, M., 2022. Molecular adsorption by biochar produced by eco-friendly low-temperature carbonization investigated using graphene structural reconfigurations. Green. Chem. Lett. Rev. 15 (1), 287–295. doi:10.1080/17518253.2022.2048090.
Saw, W.L., Pang, S.S., 2012. Influence of mean gas residence time in the bubbling fluidised bed on the performance of a 100-kW dual fluidised bed steam gasifier. Biomass Conversion&Biorefinery 2 (3), 197–205. https://link.springer.com/article/10.1007/s13399-012-0036-4.
Saw, W., Mckinnon, H., Gilmour, I., Pang, S., 2012. Production of hydrogen-rich syngas from steam gasification of blend of biosolids and wood using a dual fluidised bed gasifier. Fuel 93 (none), 473–478. https://www.sciencedirect.com/science/article/pii/S0016236111005217.
Sawant, S.V., Patwardhan, A.W., Joshi, J.B., Dasgupta, K., 2022. Boron doped carbon nanotubes: synthesis, characterization and emerging applications – A review. Chem. Eng. J. 427, 131616. doi:10.1016/j.cej.2021.131616.
Schaefer, S., Jeder, A., Sdanghi, G., Gadonneix, P., Abdedayem, A., Izquierdo, M.T., Maranzana, G., Ouederni, A., Celzard, A., Fierro, V., 2020. Oxygen-promoted hydrogen adsorption on activated and hybrid carbon materials. Int. J. Hydrogen. Energy 45 (55), 30767–30782. doi:10.1016/j.ijhydene.2020.08.114.
Schlumberger, C., Thommes, M., 2021. Characterization of hierarchically ordered porous materials by physisorption and mercury porosimetry—A tutorial review. Adv. Mater. Interfaces. 8 (4), 2002181. doi:10.1002/admi.202002181.
Schmidt, H.-P., Abiven, S., Kammann, C., Glaser, B., Bucheli, T., Leifeld, J., Shackley, S., 2013. European Biochar Certificate - guidelines for a sustainable production of Biochar. European Biochar Foundation.

Schmidt, H.P., 2023. EUROPEAN BIOCHAR CERTIFICATE.
Scrivener, K.L., 2004. Backscattered electron imaging of cementitious microstructures: understanding and quantification. Cement and concrete Composites 26 (8), 935–945. https://www.sciencedirect.com/science/article/pii/S0958946504000459.
Selvam S, M., Paramasivan, B., 2022. Microwave assisted carbonization and activation of biochar for energy-environment nexus: A review. Chemosphere 286, 131631. doi:10.1016/j.chemosphere.2021.131631.
Senadheera, S., Gupta, S., Kua, H., Hou, D., Kim, S., Tsang, D., Ok, Y.S., 2023. Application of biochar in concrete – A review. Cement Concrete Composites 143, 105204. doi:10.1016/j.cemconcomp.2023.105204.
Senthil, C., Lee, C.W.J.R., Reviews, S.E., 2021. Biomass-derived biochar Mater. as sustainable energy sources for electrochemical energy storage devices 137, 110464.
Septien, S., Valin, S., Dupont, C., Peyrot, M., Salvador, S., 2012. Effect of particle size and temperature on woody biomass fast pyrolysis at high temperature (1000–1400°C). Fuel 97, 202–210. doi:10.1016/j.fuel.2012.01.049.
Setkit, N., Li, X., Yao, H., Worasuwannarak, N., 2021. Torrefaction under mechanical pressure of 10–70 MPa at 250°C and its effect on pyrolysis behaviours of leucaena wood. Bioresour. Technol. 338, 125503. doi:10.1016/j.biortech.2021.125503.
Shaaban, A., Se, S.-M., Dimin, M.F., Juoi, J.M., Mohd Husin, M.H., Mitan, N.M.M., 2014. Influence of heating temperature and holding time on biochars derived from rubber wood sawdust via slow pyrolysis. J. Anal. Appl. Pyrolysis. 107, 31–39. doi:10.1016/j.jaap.2014.01.021.
Shadman, F., Sams, D.A., Punjak, W.A., 1987. Significance of the reduction of alkali carbonates in catalytic carbon gasification. Fuel 66 (12), 1658–1663. https://www.sciencedirect.com/science/article/pii/0016236187903589.
Shah, I.H., Miller, S.A., Jiang, D., Myers, R.J., 2022. Cement substitution with secondary materials can reduce annual global CO_2 emissions by up to 1.3 gigatons. Nat Commun 13 (1), 5758. doi:10.1038/s41467-022-33289-7.
Shaheen, J., Fseha, Y.H., Sizirici, B., 2022. Performance, life cycle assessment, and economic comparison between date palm waste biochar and activated carbon derived from woody biomass. Heliyon. 8 (12).
Shan Ahamed, T., Anto, S., Mathimani, T., Brindhadevi, K., Pugazhendhi, A., 2021. Upgrading of bio-oil from thermochemical conversion of various biomass – Mechanism, challenges and opportunities. Fuel 287, 119329. doi:10.1016/j.fuel.2020.119329.
Shang, H., Li, Y., Liu, J., Wan, Y., Feng, Y., Yu, Y., 2020. Preparation of nitrogen doped magnesium oxide modified biochar and its sorption efficiency of lead ions in aqueous solution. Bioresour. Technol. 314, 123708. doi:10.1016/j.biortech.2020.123708.
Shao, J., Zhang, J., Zhang, X., Feng, Y., Zhang, H., Zhang, S., Chen, H., 2018. Enhance SO_2 adsorption performance of biochar modified by CO_2 activation and amine impregnation. Fuel 224, 138–146. doi:10.1016/j.fuel.2018.03.064.
Shao, L., Zhang, Q., You, T., Zhang, X., Xu, F., 2018. Microwave-assisted efficient depolymerization of alkaline lignin in methanol/formic acid media. Bioresour. Technol. 264, 238–243. doi:10.1016/j.biortech.2018.05.083.
Shao, C., Rui, C., Liu, J., Chen, A., Zhu, K., Shao, Q., 2020. First-principles study on the electronic transport properties of B/P, B/As, and B/Sb Co-doped single-walled carbon nanotubes. Ind. Eng. Chem. Res. 59 (44), 19593–19599. doi:10.1021/acs.iecr.0c03804.
Sharififard, H., Shahraki, Z.H., Rezvanpanah, E., Rad, S.H., 2018. A novel natural chitosan/activated carbon/iron bio-nanocomposite: Sonochemical synthesis, characterization, and application for cadmium removal in batch and continuous adsorption process. Bioresource Technology 270, 562–569. doi:10.1016/j.biortech.2018.09.094.
Sharma, A., Nath, R., 2023. H 2-rich syngas production from gasification involving kinetic modeling: RSM-utility optimization and techno-economic analysis. RSC. Adv. 13 (15), 10308–10321.
Shen, Y., Chen, L., 2022. Catalytic pyrolysis of cellulose with biochar modified by Ni–Co–Mn cathode material recovered from spent lithium-ion battery. Chemosphere 305, 135430. doi:10.1016/j.chemosphere.2022.135430.
Shen, W., Fan, W., 2013. Nitrogen-containing porous carbons: synthesis and application. Journal of Materials Chemistry A 1 (4), 999–1013. https://pubs.rsc.org/en/content/articlehtml/2013/ta/c2ta00028h.
Shen, P., Xia, Y., 2014. Synthesis-modification integration: one-step fabrication of boronic acid functionalized carbon dots for fluorescent blood sugar sensing. Anal. Chem. 86 (11), 5323–5329. doi:10.1021/ac5001338.
Shen, Y., Guo, J.Z., Bai, L.Q., Chen, X.Q., Li, B., 2021. High effective adsorption of Pb(II) from solution by biochar derived from torrefaction of ammonium persulphate pretreated bamboo. Bioresource Technology 323. doi:10.1016/j.biortech.2020.124616.
Shen, J., Huang, G., Yao, Y., Zhang, P., Yin, J., 2023. Challenges and opportunities for the production, utilization and effects of biochar in cold-region agriculture. Sci. Total Environ., 167623.
Shen, Y., Xiao, Y., Zhang, H., Fan, H., Li, Y., Yan, Z., Zhang, W.-H., 2023. Synthesis of magnetic biochar-supported Fe-Cu bimetallic catalyst from pulp and paper mill wastes for the fenton-like removal of rhodamine B dye. Chem. Eng. J. 477, 146823. doi:10.1016/j.cej.2023.146823.
Sheng, Y., Zhu, L., 2018. Biochar alters microbial community and carbon sequestration potential across different soil pH. Science of The Total Environment 622-623, 1391–1399. doi:10.1016/j.scitotenv.2017.11.337.
Sherlala, A.I.A., Raman, A.A.A., Bello, M.M., Buthiyappan, A., 2019. Adsorption of arsenic using chitosan magnetic graphene oxide nanocomposite. Journal of Environmental Management 246, 547–556. doi:10.1016/j.jenvman.2019.05.117.
Shi, R.-y., Hong, Z.-n., Li, J.-y., Jiang, J., Kamran, M.A., Xu, R.-k., Qian, W., 2018. Peanut straw biochar increases the resistance of two Ultisols derived from different parent materials to acidification: A mechanism study. Journal of Environmental Management 210, 171–179. doi:10.1016/j.jenvman.2018.01.028.
Shi, D., Yek, P.N.Y., Ge, S., Shi, Y., Liew, R.K., Peng, W., Sonne, C., Tabatabaei, M., Aghbashlo, M., Lam, S.S., 2022. Production of highly porous biochar via microwave physiochemical activation for dechlorination in water treatment. Chemosphere 309 (Pt 1), 136624. doi:10.1016/j.chemosphere.2022.136624.
Shin, H., Tiwari, D., Kim, D.-J., 2020. Phosphate adsorption/desorption kinetics and P bioavailability of Mg-biochar from ground coffee waste. J. Water. Process. Eng. 37, 101484. doi:10.1016/j.jwpe.2020.101484.
Sigmund, G., Hüffer, T., Hofmann, T., Kah, M., 2017. Biochar total surface area and total pore volume determined by N2 and CO_2 physisorption are strongly influenced by degassing temperature. Sci. Total Environ. 580, 770–775. doi:10.1016/j.scitotenv.2016.12.023.
Singh, K., Honig, H., Wermke, M., Zimmer, E., 1996. Fermentation pattern and changes in cell wall constituents of straw-forage silages, straws and partners during storage. Anim Feed Sci Tech 61 (1-4), 137–153. doi:10.1016/0377-8401(96)00953-4.
Singh, B., Singh, B.P., Cowie, A.L., 2010. Characterisation and evaluation of biochars for their application as a soil amendment. Soil Res. 48 (7), 516–525. doi:10.1071/SR10058.
Singh, S., Chakraborty, J.P., Mondal, M.K., 2020. Pyrolysis of torrefied biomass: optimization of process parameters using response surface methodology, characterization, and comparison of properties of pyrolysis oil from raw biomass. J. Clean. Prod. 272, 122517. doi:10.1016/j.jclepro.2020.122517.
Singhal, A., Konttinen, J., Joronen, T., 2021. Effect of different washing parameters on the fuel properties and elemental composition of wheat straw in water-washing pretreatment. Part 1: Effect of washing duration and biomass size. Fuel 292, 120206. doi:10.1016/j.fuel.2021.120206.
Sizirici, B., Fseha, Y.H., Yildiz, I., Delclos, T., Khaleel, A., 2021. The effect of pyrolysis temperature and feedstock on date palm waste derived biochar to remove single and multi-metals in aqueous solutions. Sustainable Environment Res. 31 (1), 9. doi:10.1186/s42834-021-00083-x.
Sizmur, T., Fresno, T., Akgül, G., Frost, H., Moreno-Jiménez, E., 2017. Biochar modification to enhance sorption of inorganics from water. Bioresour. Technol. 246, 34–47. doi:10.1016/j.biortech.2017.07.082.
Smets, K., Roukaerts, A., Czech, J., Reggers, G., Schreurs, S., Carleer, R., Yperman, J., 2013. Slow catalytic pyrolysis of rapeseed cake: product yield and characterization of the pyrolysis liquid. Biomass Bioenergy 57, 180–190. doi:10.1016/j.biombioe.2013.07.001.
Smith, M., 2011. Evolution of acidic functional groups on biochars by ozone oxidation to improve performance as a soil amendment. Washington State University.
Snoussi, Y., Sifaoui, I., Khalil, A.M., Bhakta, A.K., Semyonov, O., Postnikov, P.S., Michely, L., Pires, R., Bastide, S., Barroso, J.E.-P., Morales, J.L., Chehimi, M.M., 2022. Facile synthesis of silver decorated biochar as a novel and highly active biosourced anti-kinetoplastid agent. Mater. Today Commun. 32, 104126. doi:10.1016/j.mtcomm.2022.104126.
Son, E.-B., Poo, K.-M., Chang, J.-S., Chae, K.-J., 2018. Heavy metal removal from aqueous solutions using engineered magnetic biochars derived from waste marine macro-algal biomass. Sci. Total Environ. 615, 161–168. doi:10.1016/j.scitotenv.2017.09.171.
Song, X., Wang, L.a., Gong, J., Zhan, X., Zeng, Y., 2020. Exploring a new method to study the effects of surface functional groups on adsorption of CO_2 and CH_4 on activated carbons. Langmuir 36 (14), 3862–3870. https://pubs.acs.org/doi/full/10.1021/acs.langmuir.9b03475.
Song, J.Y., Zhao, C.H., Cao, X.Q., Cheng, W.M., 2023. Enhanced catalytic degradation of antibiotics by peanut shell-derived biochar-Co3O4 activated peroxymonosulfate: An experimental and mechanistic study. Process Safety and Environmental Protection 171, 423–436. doi:10.1016/j.psep.2023.01.036.
Song, M., Zhou, Y., Ren, X., Wan, J., Du, Y., Wu, G., Ma, F., 2019. Biowaste-based porous carbon for supercapacitor: the influence of preparation processes on structure and performance. J. Colloid. Interface Sci. 535, 276–286. doi:10.1016/j.jcis.2018.09.055.
Soni, B., Karmee, S.K.J.F., 2020. Towards a continuous pilot scale pyrolysis based biorefinery for production biooil biochar from sawdust 271, 117570.
Stasi, C.D., Cortese, M., Greco, G., Renda, S., Manyà, J.J., 2021. Optimization of the operating conditions for steam reforming of slow pyrolysis oil over an activated biochar-supported Ni–Co catalyst. International Journal of Hydrogen Energy. https://www.sciencedirect.com/science/article/pii/S0360319921020450.
Struhs, E., Mirkouei, A., You, Y., Mohajeri, A., 2020. Techno-economic and environmental assessments for nutrient-rich biochar production from cattle manure: A case study in Idaho. USA. Applied energy 279, 115782.
Stylianou, M., Christou, A., Dalias, P., Polycarpou, P., Michael, C., Agapiou, A., Papanastasiou, P., Fatta-Kassinos, D., 2020. Physicochemical and structural characterization of biochar derived from the pyrolysis of biosolids, cattle manure and spent coffee grounds. J. Energy Institute 93 (5), 2063–2073. doi:10.1016/j.joei.2020.05.002.
Su, K., Hu, G., Zhao, T., Dong, H., Yang, Y., Pan, H., Lin, Q., 2024. The ultramicropore biochar derived from waste distiller's grains for wet-process phosphoric acid purification: Removal performance and mechanisms of Cr(VI). Chemosphere 349, 140877. doi:10.1016/j.chemosphere.2023.140877.
Su, Z., Jin, K., Wu, J., Huang, P., Liu, L., Xiao, Z., Peng, H., Fan, L., Zhou, W., 2022. Phosphorus doped biochar as a deoxygenation and denitrogenation catalyst for ex-situ upgrading of vapors from microwave-assisted co-pyrolysis of microalgae and waste cooking oil. J. Anal. Appl. Pyrolysis. 164, 105538. doi:10.1016/j.jaap.2022.105538.
Suárez-Abelenda, M., Kaal, J., McBeath, A.V., 2017. Translating analytical pyrolysis fingerprints to Thermal Stability Indices (TSI) to improve biochar characterization by pyrolysis-GC–MS. Biomass Bioenergy 98, 306–320. doi:10.1016/j.biombioe.2017.01.021.
Sugama, T., Kukacka, L., Carciello, N., Stathopoulos, D., 1989. Interfacial reactions between oxidized carbon fibers and cements. Cement and Concrete Research 19 (3), 355–365. https://www.sciencedirect.com/science/article/pii/0008884689900252.
Suliman, W., Harsh, J.B., Abu-Lail, N.I., Fortuna, A.-M., Dallmeyer, I., Garcia-Perez, M., 2016. Modification of biochar surface by air oxidation: role of pyrolysis temperature. Biomass Bioenergy 85, 1–11. doi:10.1016/j.biombioe.2015.11.030.

Sullivan, A.L., Ball, R., 2012. Thermal decomposition and combustion chemistry of cellulosic biomass. Atmos. Environ. 47, 133–141. doi:10.1016/j.atmosenv.2011.11.022.
Sun, K., Chun Jiang, J., 2010. Preparation and characterization of activated carbon from rubber-seed shell by physical activation with steam. Biomass Bioenergy 34 (4), 539–544. doi:10.1016/j.biombioe.2009.12.020.
Sun, S., Zhao, Y., Tian, H., Ling, F., Su, F., 2009. Experimental study on cyclone air gasification of wood powder. Bioresource Technology 99 (17), 4047–4049. https://www.sciencedirect.com/science/article/pii/S0960852409000558.
Sun, H., Feng, D., Zhao, Y., Sun, S., 2023a. Optimization of operating parameters for tar reforming/hydrogen upgrading in corn straw pyrolysis polygeneration. Renewable energy. https://www.sciencedirect.com/science/article/pii/S0960148123007802.
Sun, H., Feng, D., Zhao, Y., Sun, S., 2023b. Regulation of partial oxidation in biochar-catalyzed tar reforming for hydrogen upgrading in syngas: The effect of oxygen concentration. Fuel 341, 127671. https://www.sciencedirect.com/science/article/pii/S0016236123002843.
Sun, Y., Gao, B., Yao, Y., Fang, J., Zhang, M., Zhou, Y., Chen, H., Yang, L., 2014. Effects of feedstock type, production method, and pyrolysis temperature on biochar and hydrochar properties. Chem. Eng. J. 240, 574–578. doi:10.1016/j.cej.2013.10.081.
Sun, J., He, F., Pan, Y., Zhang, Z., 2017. Effects of pyrolysis temperature and residence time on physicochemical properties of different biochar types. Acta Agriculturae Scandinavica, Section B — Soil Plant Sci. 67 (1), 12–22. doi:10.1080/09064710.2016.1214745.
Sun, X., Han, X., Ping, F., Zhang, L., Zhang, K., Chen, M., Wu, W., 2018. Effect of rice-straw biochar on nitrous oxide emissions from paddy soils under elevated CO_2 and temperature. Sci. Total Environ. 628-629, 1009–1016. doi:10.1016/j.scitotenv.2018.02.046.
Sun, M., Gu, Q., Hanif, A., Wang, T., Shang, J., 2019. Transition metal cation-exchanged SSZ-13 zeolites for CO_2 capture and separation from N2. Chem. Eng. J. 370, 1450–1458.
Sun, J., Zhang, D., Xia, D., Li, Q., 2023. Orange peels biochar doping with Fe-Cu bimetal for PMS activation on the degradation of bisphenol A: A synergy of SO4−, OH, 1O2 and electron transfer. Chem. Eng. J. 471, 144832. doi:10.1016/j.cej.2023.144832.
Sun, Y., Jia, J., Huo, L., Zhao, L., Yao, Z., Liu, Z., 2023. Heteroatom-doped biochar for CO_2 adsorption: a review of heteroatoms, doping methods, and functions. BioMass Convers. Biorefin. doi:10.1007/s13399-022-03640-5.
Sun, Z., Liu, S., Xu, Y., Lu, J., Shi, H., Li, S., Luo, C., Dong, Q., 2023. Urea impregnation into fungus pretreated corn stover to perform pyrolysis for production of nitrogen-containing bio-oil and nitrogen-doped biochar. Bioresour. Technol. 376, 128921. doi:10.1016/j.biortech.2023.128921.
Suo, F., You, X., Ma, Y., Li, Y., 2019. Rapid removal of triazine pesticides by P doped biochar and the adsorption mechanism. Chemosphere 235, 918–925. doi:10.1016/j.chemosphere.2019.06.158.
Suresh, A., Alagusundaram, A., Kumar, P.S., Vo, D.-V.N., Christopher, F.C., Balaji, B., Viswanathan, V., Sankar, S., 2021. Microwave pyrolysis of coal, biomass and plastic waste: a review. Environ. Chem. Lett. 19 (5), 3609–3629. doi:10.1007/s10311-021-01245-4.
Tag, A., Duman, G., Uçar, S., Yanik, J., 2016a. Effects of feedstock type and pyrolysis temperature on potential applications of biochar. J. Anal. Appl. Pyrolysis. 120. doi:10.1016/j.jaap.2016.05.006.
Tag, A.T., Duman, G., Ucar, S., Yanik, J., 2016b. Effects of feedstock type and pyrolysis temperature on potential applications of biochar. J. Anal. Appl. Pyrolysis. 120, 200–206. doi:10.1016/j.jaap.2016.05.006.
Tahir, A.H., Al-Obaidy, A.H.M., Mohammed, F.H., 2020. Biochar from date palm waste, production, characteristics and use in the treatment of pollutants: A review. In: IOP Conference Series: Materials Science and Engineering. IOP Publishing.
Tan, I., Ahmad, A., Hameed, B., 2008. Optimization of preparation conditions for activated carbons from coconut husk using response surface methodology. Chem. Eng. J. 137 (3), 462–470. doi:10.1016/j.cej.2007.04.031.
Tan, X.-f., Liu, S.-b., Liu, Y.-g., Gu, Y.-l., Zeng, G.-m., Hu, X.-j., Wang, X., Liu, S.-h., Jiang, L.-h., 2017. Biochar as potential sustainable precursors for activated carbon production: multiple applications in environmental protection and energy storage. Bioresour. Technol. 227, 359–372. doi:10.1016/j.biortech.2016.12.083.
Tan, Z., Zou, J., Zhang, L., Huang, Q., 2018. Morphology, pore size distribution, and nutrient characteristics in biochars under different pyrolysis temperatures and atmospheres. J. Mater. Cycles. Waste Manage. 20 (2), 1036–1049. doi:10.1007/s10163-017-0666-5.
Tan, H., Wahab, R.A., Lee, C.T., Goh, P.S., Wong, K.Y., Klemeš, J.J., Ong, P.Y., 2023. Functionalisation of biowaste-derived biochar via accelerated hydrothermal-assisted post-treatment for enhanced sodium ion adsorption. BioMass Convers. Biorefin. 1–18.
Tang, J., Zhao, B., Lyu, H., Li, D., 2021. Development of a novel pyrite/biochar composite (BM-FeS2@BC) by ball milling for aqueous Cr(VI) removal and its mechanisms. J. Hazard. Mater. 413, 125415. doi:10.1016/j.jhazmat.2021.125415.
Tang, J., Ma, Y., Zeng, C., Yang, L., Cui, S., Zhi, S., Yang, F., Ding, Y., Zhang, K., Zhang, Z., 2023. Fe-Al bimetallic oxides functionalized-biochar via ball milling for enhanced adsorption of tetracycline in water. Bioresour. Technol. 369, 128385. doi:10.1016/j.biortech.2022.128385.
Tao, B., Chen, Q., Jiang, Y., Zhang, B., Yuan, H., Wang, Y., 2023. Effect of particle sizes of biochar on CO_2 emissions in a poplar plantation of ancient Yellow River channel, China. Journal of Environmental Management 345, 118721. doi:10.1016/j.jenvman.2023.118721.
Taslakyan, L., Baker, M.C., Strawn, D.G., Möller, G., 2023. Biochar-integrated reactive filtration of wastewater for P removal and recovery, micropollutant catalytic oxidation, and negative CO2e: life cycle assessment and techno-economic analysis. Water Environment Res. 95 (12), e10962. doi:10.1002/wer.10962.
Teo, E.Y.L., Muniandy, L., Ng, E.-P., Adam, F., Mohamed, A.R., Jose, R., Chong, K.F., 2016. High surface area activated carbon from rice husk as a high performance supercapacitor electrode. Electrochim. Acta 192, 110–119. doi:10.1016/j.electacta.2016.01.140.
Thommes, M., Kaneko, K., Neimark, A.V., Olivier, J.P., Rodriguez-Reinoso, F., Rouquerol, J., Sing, K.S.W., 2015. Physisorption gases, with special reference to evaluation surface area pore size distribution (IUPAC Technical Report) 87 (9-10), 1051–1069. doi:10.1515/pac-2014-1117.
Tian, X., Richardson, R.E., Tester, J.W., Lozano, J.L., You, F., 2020. Retrofitting municipal wastewater treatment facilities toward a greener and circular economy by virtue of resource recovery: techno-economic analysis and life cycle assessment. ACS. Sustain. Chem. Eng. 8 (36), 13823–13837. doi:10.1021/acssuschemeng.0c05189.
Tomczyk, A., Sokołowska, Z., Boguta, P., 2020. Biochar physicochemical properties: pyrolysis temperature and feedstock kind effects. Reviews in Environ. Sci. Bio/Technol. 19 (1), 191–215.
Tomczyk, M.M., Boncel, S., Herman, A., Krawczyk, T., Jakóbik-Kolon, A., Pawlyta, M., Krzywiecki, M., Chrobak, A., Minoshima, M., Sugihara, F.J.I.J.o.N., 2020. Oxygen Functional Groups on MWCNT Surface as Critical Factor Boosting T2 Relaxation Rate Water Protons: Towards Improved CNT-Based Contrast Agents 7433–7450.
Tong, S.Q., Chen, D., Jiang, X.B., Xu, Z.X., Liu, X.D., Shen, J.Y., 2023. Persulfate activation by FeO-doped biochar synthesized from Fenton sludge and sewage sludge for enhanced 1-H-1,2,4-triazole degradation. Chemical Engineering Journal 461. doi:10.1016/j.cej.2023.142075. https://doi.org/ARTN142075.
Tovihoudji, G.P., Diogo, R.V.C., Abiola, W.A., Akoha, F.B., Godau, T., 2022. Profitability and agronomic potential of cotton (Gossypium hirsutum L.) under biochar-compost-based amendments in three agroecological zones of northern Benin. Front. Sustain. Food Syst. 6, 1036133.
Tran, H.-T., Bolan, N.S., Lin, C., Binh, Q.A., Nguyen, M.-K., Luu, T.A., Le, V.-G., Pham, C.Q., Hoang, H.-G., Vo, D.-V.N., 2023. Succession of biochar addition for soil amendment and contaminants remediation during co-composting: A state of art review. J. Environ. Manage. 342, 118191.
Trigo, C., Cox, L., Spokas, K., 2016. Influence of pyrolysis temperature and hardwood species on resulting biochar properties and their effect on azimsulfuron sorption as compared to other sorbents. Science of the Total Environment 566, 1454–1464. doi:10.1016/j.scitotenv.2016.06.027.
Trinh, T.K., Tsubota, T., Takahashi, S., Mai, N.T., Nguyen, M.N., Nguyen, N.H., 2020. Carbonization and H3PO4 activation of fern dicranopteris linearis and electrochemical properties for electric double layer capacitor electrode. Sci. Rep. 10 (1), 19974.
Tripathi, M., Sahu, J.N., Ganesan, P., 2016. Effect of process parameters on production of biochar from biomass waste through pyrolysis: A review. Renew. Sustain. Energy Reviews 55, 467–481. doi:10.1016/j.rser.2015.10.122.
Truong, Q.-M., Nguyen, T.-B., Chen, C.-W., Chen, W.-H., Bui, X.-T., Dong, C.-D., 2024. KHCO3-activated high surface area biochar derived from brown algae: A case study for efficient adsorption of Cr(VI) in aqueous solution. Environmental research 247, 118227. doi:10.1016/j.envres.2024.118227.
Tumuluru, J.S., Wright, C.T., Hess, J.R., Kenney, K.L.J.B., Bioproducts, Biorefining, 2011. A review biomass densification systems to develop uniform feedstock commodities for bioenergy application 5 (6), 683–707.
Uchimiya, M., Chang S Fau - Klasson, K.T., Klasson, K.T., 2011. Screening biochars for heavy metal retention in soil: role of oxygen functional groups. (1873-3336 (Electronic)).
Uday, V., Harikrishnan, P., Deoli, K., Zitouni, F., Mahlknecht, J., Kumar, M.J.B.T., 2022. Current trends in production, morphology, real-world Environ. applications biochar for promotion sustainability 359, 127467.
Uddin, M.N., Techato, K., Taweekun, J., Rahman, M.M., Rasul, M.G., Mahlia, T.M.I., Ashrafur, S.M., 2018. An Overview Recent Developments in Biomass Pyrolysis Technologies 11 (11), 3115.
UnitedNations, 2023. UnitedNations. https://news.un.org/en/story/2023/05/1136897.
Valle, B., Aramburu, B., Benito, P.L., Bilbao, J., Gayubo, A.G., 2018. Biomass to hydrogen-rich gas via steam reforming of raw bio-oil over Ni/La2O3-αAl2O3 catalyst: effect of space-time and steam-to-carbon ratio. Fuel 216, 445–455. doi:10.1016/j.fuel.2017.11.151.
Van Wesenbeeck, S., Higashi, C., Legarra, M., Wang, L., Antal Jr., M.J., 2016. Biomass pyrolysis in sealed vessels. Fixed-carbon yields from avicel cellulose that realize the theoretical limit. Energy Fuels 30 (1), 480–491. doi:10.1021/acs.energyfuels.5b02628.
Van Zwieten, L., Kimber, S., Morris, S., Chan, K.Y., Downie, A., Rust, J., Joseph, S., Cowie, A., 2010. Effects of biochar from slow pyrolysis of papermill waste on agronomic performance and soil fertility. Plant Soil. 327 (1), 235–246. doi:10.1007/s11104-009-0050-x.
Vassilev, S.V., Baxter, D., Andersen, L.K., Vassileva, C.G., Morgan, T.J.J.F., 2012. An overview organic inorganic phase composition biomass 94, 1–33.
Verziu, M., Tirsoaga, A., Cojocaru, B., Bucur, C., Tudora, B., Richel, A., Aguedo, M., Samikannu, A., Mikkola, J.P., 2018. Hydrogenolysis of lignin over Ru-based catalysts: the role of the ruthenium in a lignin fragmentation process. Molecular Catalysis 450, 65–76. doi:10.1016/j.mcat.2018.03.004.
Vithanage, M., Rajapaksha, A.U., Zhang, M., Thiele-Bruhn, S., Lee, S.S., Ok, Y.S., 2015. Acid-activated biochar increased sulfamethazine retention in soils. Environ. Sci. Pollut. Res. 22 (3), 2175–2186. doi:10.1007/s11356-014-3434-2.
Walker, P.L., Matsumoto, S., Hanzawa, T., Muira, T., Ismail, I.M.K., 1983. Catalysis of Gasification of Coal-derived Cokes and Chars. Fuel 62 (2), 140–149. https://www.sciencedirect.com/science/article/pii/0016236183901862.
Wan, S., Wang, S., Li, Y., Gao, B., 2017. Functionalizing biochar with Mg–Al and Mg–Fe layered double hydroxides for removal of phosphate from aqueous solutions. J. Industrial Eng. Chem. 47, 246–253. doi:10.1016/j.jiec.2016.11.039.
Wan, Z., Xu, Z., Sun, Y., He, M., Hou, D., Cao, X., Tsang, D.C.W., 2021. Critical impact of nitrogen vacancies in nonradical carbocatalysis on nitrogen-doped graphitic biochar. Environ. Sci. Technol. 55 (10), 7004–7014. doi:10.1021/acs.est.0c08531.
Wang, J., Delavar, M.A., 2023. Techno-economic analysis of phytoremediation: A strategic rethinking. Sci. Total Environ., 165949.

Wang, S., Wang, J., 2020. Peroxymonosulfate activation by Co9S8@ S and N co-doped biochar for sulfamethoxazole degradation. Chem. Eng. J. 385, 123933. doi:10.1016/j.cej.2019.123933.
Wang, L., Gao, C., Yang, K., Sheng, Y., Xu, J., Zhao, Y., Lou, J., Sun, R., Zhu, L., 2021. Effects of biochar aging in the soil on its mechanical property and performance for soil CO and N2O emissions. Science of The Total Environment 782, 146824. doi:10.1016/j.scitotenv.2021.146824.
Wang, L., Chen, L., Poon, C.S., Wang, C.-H., Ok, Y.S., Mechtcherine, V., Tsang, D.C.W., 2021. Roles of Biochar and CO_2 Curing in Sustainable Magnesia Cement-Based Composites. ACS Sustainable Chemistry & Engineering 9 (25), 8603–8610. doi:10.1021/acssuschemeng.1c02008.
Wang, X., Kersten, S.R.A., Prins, W., van Swaaij, W.P.M., 2005. Biomass pyrolysis in a fluidized bed reactor. Part 2: experimental validation of model results. Ind. Eng. Chem. Res. 44 (23), 8786–8795. doi:10.1021/ie050486y.
Wang, J., Zhang, M., Chen, M., Min, F., Zhang, S., Ren, Z., Yan, Y., 2006. Catalytic effects of six inorganic compounds on pyrolysis of three kinds of biomass. Thermochim. Acta 444 (1), 110–114. doi:10.1016/j.tca.2006.02.007.
Wang, Y., Hu, Y., Zhao, X., Wang, S., Xing, G., 2013. Comparisons of biochar properties from wood material and crop residues at different temperatures and residence times. Energy Fuels 27 (10), 5890–5899. doi:10.1021/ef400972z.
Wang, S., Gao, B., Zimmerman, A.R., Li, Y., Ma, L., Harris, W.G., Migliaccio, K.W., 2015a. Removal of arsenic by magnetic biochar prepared from pinewood and natural hematite. Bioresour. Technol. 175, 391–395. doi:10.1016/j.biortech.2014.10.104.
Wang, X., Zhou, W., Liang, G., Song, D., Zhang, X., 2015b. Characteristics of maize biochar with different pyrolysis temperatures and its effects on organic carbon, nitrogen and enzymatic activities after addition to fluvo-aquic soil. Sci. Total Environ. 538, 137–144. doi:10.1016/j.scitotenv.2015.08.026.
Wang, H., Sun, P., Cong, S., Wu, J., Gao, L., Wang, Y., Dai, X., Yi, Q., Zou, G., 2016a. Nitrogen-doped carbon dots for "green" quantum dot solar cells. Nanoscale Res. Lett. 11 (1), 27. doi:10.1186/s11671-016-1231-1.
Wang, J., Xiong, Z., Kuzyakov, Y., 2016b. Biochar stability in soil: meta-analysis decomposition priming effects 8 (3), 512–523. doi:10.1111/gcbb.12266.
Wang, C., Wang, Y., Herath, H.M.S.K., 2017. Polycyclic aromatic hydrocarbons (PAHs) in biochar – Their formation, occurrence and analysis: A review. Org. Geochem. 114, 1–11. doi:10.1016/j.orggeochem.2017.09.001.
Wang, L., Li, L., Cheng, K., Ji, C., Yue, Q., Bian, R., Pan, G., 2018. An assessment of emergy, energy, and cost-benefits of grain production over 6 years following a biochar amendment in a rice paddy from China. Environ. Sci. Pollut. Res. 25, 9683–9696.
Wang, M., Zhu, Y., Cheng, L., Andserson, B., Zhao, X., Wang, D., Ding, A., 2018. Review on utilization of biochar for metal-contaminated soil and sediment remediation. J. Environ. Sci. 63, 156–173. doi:10.1016/j.jes.2017.08.004.
Wang, Z., Chen, M., Huang, Y., Shi, X., Zhang, Y., Huang, T., Cao, J., Ho, W., Lee, S.C., 2018c. Self-assembly synthesis of boron-doped graphitic carbon nitride hollow tubes for enhanced photocatalytic NOx removal under visible light. Applied Catalysis B: Environ. 239, 352–361. doi:10.1016/j.apcatb.2018.08.030.
Wang, D., Li, B., Yang, H., Zhao, C., Yao, D., Chen, H., 2019. Influence of biochar on the steam reforming of biomass volatiles: effects of activation temperature and atmosphere. Energy Fuels 33 (3), 2328–2334.
Wang, Y., Li, G., Liu, Z., Cui, P., Zhu, Z., Yang, S., 2019. Techno-economic analysis of biomass-to-hydrogen process in comparison with coal-to-hydrogen process. Energy 185, 1063–1075.
Wang, D., Jiang, P., Zhang, H., Yuan, W., 2020. Biochar production and applications in agro and forestry systems: A review. Sci. Total. Environ. 723, 137775. doi:10.1016/j.scitotenv.2020.137775.
Wang, H., Wang, H., Zhao, H., Yan, Q., 2020. Adsorption and Fenton-like removal of chelated nickel from Zn-Ni alloy electroplating wastewater using activated biochar composite derived from Taihu blue algae. Chem. Eng. J. 379, 122372. doi:10.1016/j.cej.2019.122372.
Wang, K., Peng, N., Lu, G., Dang, Z., 2020. Effects of pyrolysis temperature and holding time on physicochemical properties of swine-manure-derived biochar. Waste BioMass Valorization. 11 (2), 613–624. doi:10.1007/s12649-018-0435-2.
Wang, L., Ok, Y.S., Tsang, D.C.W., Alessi, D.S., Rinklebe, J., Wang, H., Mašek, O., Hou, R., O'Connor, D., Hou, D., 2020. New trends in biochar pyrolysis and modification strategies: feedstock, pyrolysis conditions, sustainability concerns and implications for soil amendment. Soil. Use Manage. 36 (3), 358–386. doi:10.1111/sum.12592.
Wang, Q., Song, H., Pan, S., Dong, N., Wang, X., Sun, S., 2020. Initial pyrolysis mechanism and product formation of cellulose: an experimental and Density functional theory(DFT) study. Sci. Rep. 10 (1), 3626. doi:10.1038/s41598-020-60095-2.
Wang, Z., Li, J., Zhang, G., Zhi, Y., Yang, D., Lai, X., Ren, T., 2020f. Characterization Acid-Aged Biochar Its Ammonium Adsorption in an Aqueous Solution 13 (10), 2270.
Wang, A., Zou, D., Zeng, X., Chen, B., Zheng, X., Li, L., Zhang, L., Xiao, Z., Wang, H., 2021. Speciation and environmental risk of heavy metals in biochars produced by pyrolysis of chicken manure and water-washed swine manure. Sci. Rep. 11 (1), 11994. doi:10.1038/s41598-021-91440-8.
Wang, C., Sun, R., Huang, R.J.J.o.C.P., 2021. Highly dispersed iron-doped biochar derived from sawdust for Fenton-like degradation toxic dyes 297, 126681.
Wang, F., Zheng, F., Jiang, J., Li, Y., Luo, Y., Chen, K., Du, J., Huang, Y., Li, Q., Wang, H., 2021. Microwave-assisted preparation of hierarchical N and O Co-doped corn-cob-derived activated carbon for a high-performance supercapacitor. Energy Fuels 35 (9), 8334–8344. doi:10.1021/acs.energyfuels.1c00337.
Wang, H., Guo, W., Si, Q., Liu, B., Zhao, Q., Luo, H., Ren, N., 2021d. Multipath elimination of bisphenol A over bifunctional polymeric carbon nitride/biochar hybrids in the presence of persulfate and visible light. J. Hazard. Mater. 417, 126008. doi:10.1016/j.jhazmat.2021.126008.
Wang, T., Zhang, D., Fang, K., Zhu, W., Peng, Q., Xie, Z., 2021f. Enhanced nitrate removal by physical activation and Mg/Al layered double hydroxide modified biochar derived from wood waste: adsorption characteristics and mechanisms. J. Environ. Chem. Eng. 9 (4), 105184. doi:10.1016/j.jece.2021.105184.
Wang, Y., Shao, Y., Zhang, L., Zhang, S., Wang, Y., Xiang, J., Hu, S., Hu, G., Hu, X., 2021g. Co-presence of hydrophilic and hydrophobic sites in Ni/biochar catalyst for enhancing the hydrogenation activity. Fuel 293, 120426.
Wang, Y., Huang, L., Zhang, T., Wang, Q., 2022. Hydrogen-rich syngas production from biomass pyrolysis and catalytic reforming using biochar-based catalysts. Fuel 313, 123006.
Wang, J., Li, S., Deng, S., Cheng, Z., Hu, X., Wan Mahari, W.A., Lam, S.S., Yuan, X., 2023. Upcycling medical plastic waste into activated carbons toward environmental safety and sustainability. Curr. Opin. Environ. Sci. Health 33. doi:10.1016/j.coesh.2023.100470.
Wang, J., Sun, M., Wang, L., Xiong, X., Yuan, W., Liu, Y., Liu, S., Zhang, Q., Liu, J., Wang, Y.J.C., 2023. High-efficient removal arsenic (III) from wastewater using combined copper ferrite@ biochar persulfate. Chemosphere, 139089.
Wang, Y., Yu, G., Xie, S., Jiang, R., Li, C., Xing, Z., 2023. Pyrolysis of food waste digestate residues for biochar: pyrolytic properties, biochar characterization, and heavy metal behaviours. Fuel 353, 129185. doi:10.1016/j.fuel.2023.129185.
Wang, H., Chen, Q., Xia, H., Liu, R., Zhang, Y., 2024. Enhanced complexation and electrostatic attraction through fabrication of amino- or hydroxyl-functionalized Fe/Ni-biochar composite for the adsorption of Pb(II) and Cd(II). Sep. Purif. Technol. 328, 125074. doi:10.1016/j.seppur.2023.125074.
Web of Science, https://www.webofscience.com/wos/woscc/basic-search, Accessed in May 2024.
Weber, K., Quicker, P., 2018. Properties of biochar. Fuel 217, 240–261. doi:10.1016/j.fuel.2017.12.054.
Wei, L., Wen, L., Yang, T., Zhang, N., 2015. Nitrogen transformation during sewage sludge pyrolysis. Energy Fuels 29 (8), 5088–5094. doi:10.1021/acs.energyfuels.5b00792.
Wei, S., Zhu, M., Fan, X., Song, J., Peng, P.a., Li, K., Jia, W., Song, H., 2019. Influence of pyrolysis temperature and feedstock on carbon fractions of biochar produced from pyrolysis of rice straw, pine wood, pig manure and sewage sludge. Chemosphere 218, 624–631. doi:10.1016/j.chemosphere.2018.11.177.
Wei, L., Huang, Y., Huang, L., Huang, Q., Li, Y., Li, X., Yang, S., Liu, C., Liu, Z., 2021. Combined biochar and soda residues increases maize yields and decreases grain Cd/Pb in a highly Cd/Pb-polluted acid Udults soil. Agric. Ecosyst. Environ. 306, 107198.
Wei, Y., Chen, L., Jiao, G., Wen, Y., Liao, Q., Zhou, H., Tang, S., 2023. Enhanced removal of metal-cyanide complexes from wastewater by Fe-impregnated biochar: adsorption performance and removal mechanism. Chemosphere 331, 138719. doi:10.1016/j.chemosphere.2023.138719.
Welling, R., Beaumont, J.J., Petersen, S.J., Alexeeff, G.V., Steinmaus, C., 2015. Chromium VI and stomach cancer: a meta-analysis of the current epidemiological evidence. Occupational and Environmental Medicine 72 (2), 151–159. doi:10.1136/oemed-2014-102178.
Werner, C., Lucht, W., Gerten, D., Kammann, C., 2022. Potential of land-neutral negative emissions through biochar sequestration. Earths. Future 10 (7), e2021EF002583.
Windeatt, J.H., Ross, A.B., Williams, P.T., Forster, P.M., Nahil, M.A., Singh, S.J.J.o.e.m., 2014. Characteristics biochars from crop residues: potential for carbon sequestration soil amendment 146, 189–197.
WMO, 2024. https://wmo.int/media/news/record-carbon-emissions-highlight-urgency-of-global-greenhouse-gas-watch.
Woldetsadik, D., Drechsel, P., Marschner, B., Itanna, F., Gebrekidan, H., 2017. Effect of biochar derived from faecal matter on yield and nutrient content of lettuce (Lactuca sativa) in two contrasting soils. Environ. Syst. Res. (Heidelb) 6 (1), 2. doi:10.1186/s40068-017-0082-9.
Wong, J.W.C., Webber, J.B.W., Ogbonnaya, U.O., 2019. Characteristics of biochar porosity by NMR and study of ammonium ion adsorption. J. Anal. Appl. Pyrolysis. 143, 104687. doi:10.1016/j.jaap.2019.104687.
Wu, F.C., Tseng, R.L., 2006. Preparation of highly porous carbon from fir wood by KOH etching and CO_2 gasification for adsorption of dyes and phenols from water. J. Colloid. Interface Sci. 294 (1), 21–30. doi:10.1016/j.jcis.2005.06.084.
Wu, F.F., Chen, L., Hu, P., Zhou, X., Zhou, H.Q., Wang, D.H., Lu, X.Y., Mi, B.B., 2022. Comparison of properties, adsorption performance and mechanisms to Cd(II) on lignin-derived biochars under different pyrolysis temperatures by microwave heating. Environ Technol Inno 25. doi:10.1016/j.eti.2021.102196.
Wu, J., Yi, Y., Li, Y., Fang, Z., Tsang, E.P., 2016. Excellently reactive Ni/Fe bimetallic catalyst supported by biochar for the remediation of decabromodiphenyl contaminated soil: reactivity, mechanism, pathways and reducing secondary risks. J. Hazard. Mater. 320, 341–349. doi:10.1016/j.jhazmat.2016.08.049.
Wu, C., Shi, L., Xue, S., Li, W., Jiang, X., Rajendran, M., Qian, Z., 2019. Effect of sulfur-iron modified biochar on the available cadmium and bacterial community structure in contaminated soils. Sci. Total Environ. 647, 1158–1168. doi:10.1016/j.scitotenv.2018.08.087.
Wu, L., Cai, Y., Wang, S., Li, Z., 2021. Doping of nitrogen into biomass-derived porous carbon with large surface area using N2 non-thermal plasma technique for high-performance supercapacitor. Int. J. Hydrogen. Energy 46 (2), 2432–2444. doi:10.1016/j.ijhydene.2020.10.037.
Wyrzykowski, M., Toropovs, N., Winnefeld, F., Lura, P., 2024. Cold-bonded biochar-rich lightweight aggregates for net-zero concrete. Journal of Cleaner Production 434, 140008. doi:10.1016/j.jclepro.2023.140008.
Xiang, L., Liu, S., Ye, S., Yang, H., Song, B., Qin, F., Shen, M., Tan, C., Zeng, G., Tan, X., 2021. Potential hazards of biochar: the negative environmental impacts of biochar applications. J. Hazard. Mater. 420, 126611. doi:10.1016/j.jhazmat.2021.126611.
Xiao, Y., Xu, S., Song, Y., Shan, Y., Wang, C., Wang, G., 2017. Biomass steam gasification for hydrogen-rich gas production in a decoupled

dual loop gasification system. Fuel Processing Technology 165, 54–61. https://www.sciencedirect.com/science/article/pii/S0378382017305362.
Xiao, L., Zhu, X., Li, X., Zhang, Z., Ashida, R., Miura, K., Luo, G., Liu, W., Yao, H., 2015. Effect of pressurized torrefaction pretreatments on biomass CO_2 gasification. Energy Fuels 29 (11), 7309–7316. doi:10.1021/acs.energyfuels.5b01485.
Xiao, X., Chen, B.A.-O.X., Chen, Z., Zhu, L.A.-O.X., Schnoor, J.L., 2018. Insight into multiple and multilevel structures of biochars and their potential environmental applications: A critical review. (1520-5851 (Electronic)).
Xiao, J., Hu, R., Chen, G., Xing, B., 2020. Facile synthesis of multifunctional bone biochar composites decorated with Fe/Mn oxide micro-nanoparticles: physicochemical properties, heavy metals sorption behavior and mechanism. J. Hazard. Mater. 399, 123067. doi:10.1016/j.jhazmat.2020.123067.
Xie, T., Sadasivam, B.Y., Reddy, K.R., Wang, C., Spokas, K., 2016. Review of the effects of biochar amendment on soil properties and carbon sequestration. J. Hazardous, Toxic, Radioactive Waste 20 (1), 04015013. doi:10.1061/(ASCE)HZ.2153-5515.0000293.
Xie, X., Shi, J., Pu, Y., Wang, Z., Zhang, L.-L., Wang, J.-X., Wang, D., 2020. Cellulose derived nitrogen and phosphorus co-doped carbon-based catalysts for catalytic reduction of p-nitrophenol. J. Colloid. Interface Sci. 571, 100–108. doi:10.1016/j.jcis.2020.03.035.
Xing, X., Liu, Y., Garg, A., Ma, X., Yang, T., Zhao, L., 2021. An improved genetic algorithm for determining modified water-retention model for biochar-amended soil. CATENA 200, 105143. doi:10.1016/j.catena.2021.105143.
Xing, L., Wei, J., Zhang, Y., Xu, M., Pan, G., Li, J., Li, J., Li, Y., 2022. Boosting active sites of protogenetic sludge-based biochar by boron doping for electro-fenton degradation towards emerging organic contaminants. Sep. Purif. Technol. 294, 121160. doi:10.1016/j.seppur.2022.121160.
Xing, X., Ren, X., Alharbi, N.S., Chen, C., 2022. Biochar-supported Fe/Ni bimetallic nanoparticles for the efficient removal of Cr(VI) from aqueous solution. J. Mol. Liq. 359, 119257. doi:10.1016/j.molliq.2022.119257.
Xiong, Y., Zhang, Z., Zhang, C., Xiao, J., 2024. Foam-stability enhancement in biochar-infused foam concrete: Analyzing ionic strength, interparticle distance, and water state. Journal of Cleaner Production 443, 141231. doi:10.1016/j.jclepro.2024.141231.
Xu, B., Li, A., 2017. Effect of high-pressure on pine sawdust pyrolysis: products distribution and characteristics. AIP. Conf. Proc. 1864 (1). doi:10.1063/1.4992933.
Xu, G., Murakami, T., Suda, T., Matsuzaw, Y., Tani, H., 2009. Two-stage dual fluidized bed gasification: Its conception and application to biomass. Fuel Processing Technology 90 (1), 137–144. https://www.sciencedirect.com/science/article/pii/S0378382008002191.
Xu, X., Kan, Y., Zhao, L., Cao, X., 2016. Chemical transformation of CO_2 during its capture by waste biomass derived biochars. Environmental pollution 213, 533–540. https://www.sciencedirect.com/science/article/pii/S0269749116301944.
Xu, H.H., Han, Y.P., Wang, G.Z., Deng, P.Y., Feng, L.L., 2022. Walnut shell biochar based sorptive remediation of estrogens polluted simulated wastewater: Characterization, adsorption mechanism and degradation by persistent free radicals. Environ Technol Inno 28, 102870. https://doi.org/ARTN.
Xu, S.Y., Wen, L.T., Yu, C., Li, S., Tang, J.C., 2022. Activation of peroxymonosulfate by MnFeO@BC composite for bisphenol A Degradation: The coexisting of free-radical and non-radical pathways. Chemical Engineering Journal 442, 136250. https://doi.org/ARTN.
Xu, W., Zhang, Y., Li, M., Qu, F., Poon, C.S., Zhu, X., Tsang, D.C.W., 2024. Durability and micromechanical properties of biochar in biochar-cement composites under marine environment. Journal of Cleaner Production 449, 141842. doi:10.1016/j.jclepro.2024.141842.
Xu, M., Wu, J., Luo, L., Yang, G., Zhang, X., Peng, H., Yu, X., Wang, L.J.C., 2018. The factors affecting biochar application in restoring heavy metal-polluted soil and its potential applications. Ecology. 34 (2), 177–197.
Xu, X., Zheng, Y., Gao, B., Cao, X., 2019. N-doped biochar synthesized by a facile ball-milling method for enhanced sorption of CO_2 and reactive red. Chem. Eng. J. 368, 564–572. doi:10.1016/j.cej.2019.02.165.
Xu, L., Fu, B., Sun, Y., Jin, P., Bai, X., Jin, X., Shi, X., Wang, Y., Nie, S., 2020. Degradation of organic pollutants by Fe/N co-doped biochar via peroxymonosulfate activation: synthesis, performance, mechanism and its potential for practical application. Chem. Eng. J. 400, 125870. doi:10.1016/j.cej.2020.125870.
Xu, X., Xu, Z., Gao, B., Zhao, L., Zheng, Y., Huang, J., Tsang, D.C.W., Ok, Y.S., Cao, X., 2020. New insights into CO_2 sorption on biochar/Fe oxyhydroxide composites: kinetics, mechanisms, and in situ characterization. Chem. Eng. J. 384, 123289. doi:10.1016/j.cej.2019.123289.
Xu, Y., Qu, W., Sun, B., Peng, K., Zhang, X., Xu, J., Gao, F., Yan, Y., Bai, T., 2021. Effects of added calcium-based additives on swine manure derived biochar characteristics and heavy metals immobilization. Waste Manage.. 123, 69–79. doi:10.1016/j.wasman.2021.01.020.
Xu, Z., He, M., Xu, X., Cao, X., Tsang, D.C., 2021. Impacts of different activation processes on the carbon stability of biochar for oxidation resistance. Bioresour. Technol. 338, 125555. doi:10.1016/j.biortech.2021.125555.
Xu, Z., Wan, Z., Sun, Y., Gao, B., Hou, D., Cao, X., Komárek, M., Ok, Y.S., Tsang, D.C.W., 2022. Electroactive Fe-biochar for redox-related remediation of arsenic and chromium: distinct redox nature with varying iron/carbon speciation. J. Hazard. Mater. 430, 128479. doi:10.1016/j.jhazmat.2022.128479.
Xu, L., He, Z., Wei, X., Shang, Y., Shi, J., Jin, X., Bai, X., Shi, X., Jin, P., 2023. Facile-prepared Fe/Mn co-doped biochar is an efficient catalyst for mediating the degradation of aqueous ibuprofen via catalytic ozonation. Chem. Eng. J. 461, 142028. doi:10.1016/j.cej.2023.142028.
Xu, Y., Qi, F., Yan, Y., Sun, W., Bai, T., Lu, N., Luo, H., Liu, C., Yuan, B., Sheng, Z., Liu, T., 2023. The interaction of different chlorine-based additives with swine manure during pyrolysis: effects on biochar properties and heavy metal volatilization. Waste Manage.. 169, 52–61. doi:10.1016/j.wasman.2023.06.023.
Xue, Y., Gao, B., Yao, Y., Inyang, M., Zhang, M., Zimmerman, A.R., Ro, K.S., 2012. Hydrogen peroxide modification enhances the ability of biochar (hydrochar) produced from hydrothermal carbonization of peanut hull to remove aqueous heavy metals: batch and column tests. Chem. Eng. J. 200-202, 673–680. doi:10.1016/j.cej.2012.06.116.
Xue, Y., Bai, L., Chi, M., Xu, X., Chen, Z., Yu, K., Liu, Z., 2022. Co-hydrothermal carbonization of pretreatment lignocellulose biomass and polyvinyl chloride for clean solid fuel production: hydrochar properties and its formation mechanism. J. Environ. Chem. Eng. 10 (1), 106975. doi:10.1016/j.jece.2021.106975.
Yaashikaa, P.R., Senthil Kumar, P., Varjani, S.J., Saravanan, A., 2019. Advances in production and application of biochar from lignocellulosic feedstocks for remediation of environmental pollutants. Bioresour. Technol. 292, 122030. doi:10.1016/j.biortech.2019.122030.
Yaashikaa, P., Kumar, P.S., Varjani, S., Saravanan, A.J.B.R., 2020. A critical review on biochar production techniques, characterization, stability applications for circular bioeconomy 28, e00570.
Yaashikaa, P.R., Kumar, P.S., Varjani, S., Saravanan, A., 2020. A critical review on the biochar production techniques, characterization, stability and applications for circular bioeconomy. BioTechnol. Reports 28, e00570. doi:10.1016/j.btre.2020.e00570.
Yaashikaa, P.R., Kumar, P.S., Varjani, S., Saravanan, A., 2020. A critical review on the biochar production techniques, characterization, stability and applications for circular bioeconomy. BioTechnol. Reports 28. doi:10.1016/j.btre.2020.e00570.
Yadav, A., Ansari, K.B., Simha, P., Gaikar, V.G., Pandit, A.B., 2016. Vacuum pyrolysed biochar for soil amendment. Resource-Efficient Technologies 2, S177–S185. doi:10.1016/j.reffit.2016.11.004.
Yadav, V., Karak, T., Singh, S., Singh, A.K., Khare, P., 2019. Benefits of biochar over other organic amendments: responses for plant productivity (Pelargonium graveolens L.) and nitrogen and phosphorus losses. Ind. Crops. Prod. 131, 96–105.
Yadav, S.P.S., Bhandari, S., Bhatta, D., Poudel, A., Bhattarai, S., Yadav, P., Ghimire, N., Paudel, P., Paudel, P., Shrestha, J., 2023. Biochar application: A sustainable approach to improve soil health. J. Agric. Food Res. 11, 100498.
Yan, T., Xue, J., Zhou, Z., Wu, Y., 2021. Biochar-based fertilizer amendments improve the soil microbial community structure in a karst mountainous area. Science of The Total Environment 794, 148757. doi:10.1016/j.scitotenv.2021.148757.
Yang, F., Lee, X.-q., Wang, B., 2015. Characterization of biochars produced from seven biomasses grown in three different climate zones. Chinese J. GeoChem. 34 (4), 592–600. doi:10.1007/s11631-015-0072-4.
Yang, W., Yang, W., Kong, L., Song, A., Qin, X., Shao, G., 2018. Phosphorus-doped 3D hierarchical porous carbon for high-performance supercapacitors: A balanced strategy for pore structure and chemical composition. Carbon 127, 557–567. doi:10.1016/j.carbon.2017.11.050.
Yang, Y., Sun, K., Han, L., Jin, J., Sun, H., Yang, Y., Xing, B., 2018. Effect of minerals on the stability of biochar. Chemosphere 204, 310–317. doi:10.1016/j.chemosphere.2018.04.057.
Yang, F., Zhang, S., Cho, D.-W., Du, Q., Song, J., Tsang, D.C.W., 2019. Porous biochar composite assembled with ternary needle-like iron-manganese-sulphur hybrids for high-efficiency lead removal. Bioresour. Technol. 272, 415–420. doi:10.1016/j.biortech.2018.10.068.
Yang, W., Shang, J., Li, B., Flury, M., 2020. Surface and colloid properties of biochar and implications for transport in porous media. Crit. Rev. Environ. Sci. Technol. 50 (23), 2484–2522. doi:10.1080/10643389.2019.1699381.
Yang, C., Liu, J., Lu, S., 2021. Pyrolysis temperature affects pore characteristics of rice straw and canola stalk biochars and biochar-amended soils. Geoderma 397, 115097. doi:10.1016/j.geoderma.2021.115097.
Yang, J., He, X., Dai, J., Chen, Y., Li, Y., Hu, X., 2021. Electron-transfer-dominated non-radical activation of peroxydisulfate for efficient removal of chlorophenol contaminants by one-pot synthesized nitrogen and sulfur codoped mesoporous carbon. Environ. Res. 194. doi:10.1016/j.envres.2020.110496.
Yang, H., Chen, P., Chen, W., Li, K., Xia, M., Xiao, H., Chen, X., Chen, Y., Wang, X., Chen, H., 2022. Insight into the formation mechanism of N, P co-doped mesoporous biochar from H3PO4 activation and NH3 modification of biomass. Fuel Process. Technol. 230, 107215.
Yang, K., Jiang, Y., Wang, J., Cai, X., Wen, Z., Qiu, Z., Qiao, G., 2022. Tobacco straw biochar improved the growth of Chinese cherry (Prunus pseudocerasus) via altering plant physiology and shifting the rhizosphere bacterial community. Sci. Hortic. 303, 111244.
Yang, Y., Kang, Z., Xu, G., Wang, J., Yu, Y., 2023. Degradation of bensulfuron methyl by nitrogen/boron codoped biochar activated peroxydisulfate at lower temperature. J. Clean. Prod. 402, 136816. doi:10.1016/j.jclepro.2023.136816.
Yang, Y., Kang, Z., Xu, G., Yu, Y., 2023. Enhanced adsorption performance of bensulfuron methyl with B doping biochar: mechanism and density functional theory calculations. Bioresour. Technol. 372, 128657. doi:10.1016/j.biortech.2023.128657.
Yao, D., Hu, Q., Wang, D., Yang, H., Wu, C., Wang, X., Chen, H., 2016. Hydrogen production from biomass gasification using biochar as a catalyst/support. Bioresour. Technol. 216, 159–164. doi:10.1016/j.biortech.2016.05.011.
Yao, Z., You, S., Ge, T., Wang, C.-H.J.A.E., 2018. Biomass gasification for syngas biochar co-production: Energy application economic evaluation 209, 43–55.
Yavari, S., Malakahmad, A., Sapari, N.B., Yavari, S., 2017. Sorption properties optimization of agricultural wastes-derived biochars using response surface methodology. Process Safety Environ. Protect. 109, 509–519. doi:10.1016/j.psep.2017.05.002.
Yin, Z., Qiu, D., Zhang, M.Y., 2021. Molecular level study of cadmium adsorption on dithiocarbamate modified chitosan. Environmental Pollution 271. doi:10.1016/j.envpol.2020.116322.

Yin, Q., Ren, H., Wang, R., Zhao, Z., 2018. Evaluation of nitrate and phosphate adsorption on Al-modified biochar: influence of Al content. Sci. Total Environ. 631, 895–903.

Ying, Z., Geng, Z., Zheng, X., Dou, B., Cui, G., 2022. Improving water electrolysis assisted by anodic biochar oxidation for clean hydrogen production. Energy 238, 121793. doi:10.1016/j.energy.2021.121793.

Yorgun, S., Yıldız, D., 2015. Slow pyrolysis of paulownia wood: effects of pyrolysis parameters on product yields and bio-oil characterization. J. Anal. Appl. Pyrolysis. 114, 68–78. doi:10.1016/j.jaap.2015.05.003.

Yu, M.M., Masnadi, M.S., Grace, J.R., Bi, X.T., Lim, C.J., Li, Y., 2015. Co-gasification of biosolids with biomass: Thermogravimetric analysis and pilot scale study in a bubbling fluidized bed reactor. Bioresource Technology 175, 51–58. https://www.sciencedirect.com/science/article/pii/S0960852414014679.

Yu, H., Xu, Y., Chen, G., Chen, D., 2016. Experimental Study on Partial Oxidation Reforming of Pyrolysis Tar over Sewage Sludge Char. Energy & Fuels 30 (11), 9379–9385. https://pubs.acs.org/doi/full/10.1021/acs.energyfuels.6b01037.

Yu, O.Y., Harper, M., Hoepfl, M., Domermuth, D., 2017. Characterization of biochar and its effects on the water holding capacity of loamy sand soil: comparison of hemlock biochar and switchblade grass biochar characteristics. Environ. Prog. Sustain. Energy 36 (5), 1474–1479. doi:10.1002/ep.12592.

Yu, W., Lian, F., Cui, G., Liu, Z., 2018. N-doping effectively enhances the adsorption capacity of biochar for heavy metal ions from aqueous solution. Chemosphere 193, 8–16. doi:10.1016/j.chemosphere.2017.10.134.

Yu, J., Tang, L., Pang, Y., Zeng, G., Wang, J., Deng, Y., Liu, Y., Feng, H., Chen, S., Ren, X., 2019. Magnetic nitrogen-doped sludge-derived biochar catalysts for persulfate activation: internal electron transfer mechanism. Chem. Eng. J. 364, 146–159. doi:10.1016/j.cej.2019.01.163.

Yu, J., Tang, L., Pang, Y., Zhou, Y., Feng, H., Ren, X., Tang, J., Wang, J., Deng, L., Shao, B., 2022. Non-radical oxidation by N,S,P co-doped biochar for persulfate activation: different roles of exogenous P/S doping, and electron transfer path. J. Clean. Prod. 374, 133995. doi:10.1016/j.jclepro.2022.133995.

Yu, C., Yan, C., Gu, J., Zhang, Y., Li, X., Dang, Z., Wang, L., Wan, J., Pan, J., 2023. In-situ Cu-loaded sludge biochar catalysts for oxidative degradation of bisphenol A from high-salinity wastewater. J. Clean. Prod. 427, 139334. doi:10.1016/j.jclepro.2023.139334.

Yuan, C., El-Fatah Abomohra, A., Wang, S., Liu, Q., Zhao, S., Cao, B., Hu, X., Marrakchi, F., He, Z., Hu, Y., 2021. High-grade biofuel production from catalytic pyrolysis of waste clay oil using modified activated seaweed carbon-based catalyst. Journal of Cleaner Production 313, 127928. doi:10.1016/j.jclepro.2021.127928.

Yuan, J.-H., Xu, R.-K., Zhang, H., 2011. The forms of alkalis in the biochar produced from crop residues at different temperatures. Bioresour. Technol. 102 (3), 3488–3497. doi:10.1016/j.biortech.2010.11.018.

Yuan, H., Lu, T., Wang, Y., Huang, H., Chen, Y., 2014. Influence of pyrolysis temperature and holding time on properties of biochar derived from medicinal herb (radix isatidis) residue and its effect on soil CO_2 emission. J. Anal. Appl. Pyrolysis. 110, 277–284. doi:10.1016/j.jaap.2014.09.016.

Yuan, B., Wang, J., Chen, Y., Wu, X., Luo, H., Deng, S., 2016. Unprecedented performance of N-doped activated hydrothermal carbon towards C2H6/CH_4, CO_2/CH_4, and CO_2/H2 separation. J. Mater. Chem. A 4 (6), 2263–2276. doi:10.1039/c5ta08436a.

Yuan, P., Wang, J., Pan, Y., Shen, B., Wu, C., 2019. Review of biochar for the management of contaminated soil: preparation, application and prospect. Sci. Total Environ. 659, 473–490. doi:10.1016/j.scitotenv.2018.12.400.

Yuan, K., Zhang, X., Li, X., Qin, R., Cheng, Y., Li, L., Yang, X., Yu, X., Lu, Z., Liu, H., 2020. Great enhancement of red emitting carbon dots with B/Al/Ga doping for dual mode anti-counterfeiting. Chem. Eng. J. 397, 125487. doi:10.1016/j.cej.2020.125487.

Yuan, J.-M., Li, H., Xiao, L.-P., Wang, T.-P., Ren, W.-F., Lu, Q., Sun, R.-C., 2022. Valorization of lignin into phenolic compounds via fast pyrolysis: impact of lignin structure. Fuel 319. doi:10.1016/j.fuel.2022.123758.

Yuan, X., Kumar, N.M., Brigljević, B., Li, S., Deng, S., Byun, M., Lee, B., Lin, C.S.K., Tsang, D.C., Lee, K.B., 2022. Sustainability-inspired upcycling of waste polyethylene terephthalate plastic into porous carbon for CO 2 capture. Green Chem. 24 (4), 1494–1504.

Yuan, X., Wang, J., Deng, S., Suvarna, M., Wang, X., Zhang, W., Hamilton, S.T., Alahmed, A., Jamal, A., Park, A.-H.A., 2022. Recent advancements in sustainable upcycling of solid waste into porous carbons for carbon dioxide capture. Renew. Sustain. Energy Reviews 162, 112413.

Yuan, X., Wang, J., Deng, S., Suvarna, M., Wang, X., Zhang, W., Hamilton, S.T., Alahmed, A., Jamal, A., Park, A.-H.A., Bi, X., Ok, Y.S., 2022. Recent advancements in sustainable upcycling of solid waste into porous carbons for carbon dioxide capture. Renew. Sustain. Energy Reviews 162. doi:10.1016/j.rser.2022.112413.

Yuan, X., Shen, Y., Withana, P.A., Mašek, O., Lin, C.S.K., You, S., Tack, F.M.G., Ok, Y.S., 2023. Thermochemical upcycling of food waste into engineered biochar for energy and environmental applications: A critical review. Chem. Eng. J. 469. doi:10.1016/j.cej.2023.143783.

Yuan, X., Suvarna, M., Lim, J.Y., Perez-Ramirez, J., Wang, X., Ok, Y.S., 2024. Active learning-based guided synthesis of engineered biochar for CO_2 capture. Environ. Sci. Technol. doi:10.1021/acs.est.3c10922.

Yue, X., Chen, D., Luo, J., Xin, Q., Huang, Z., 2020. Upgrading of reed pyrolysis oil by using its biochar-based catalytic esterification and the influence of reed sources. Applied Energy 268, 114970. doi:10.1016/j.apenergy.2020.114970.

Yue, Y., Lin, Q., Irfan, M., Chen, Q., Zhao, X., 2016. Characteristics and potential values of bio-oil, syngas and biochar derived from Salsola collina Pall. In a fixed bed slow pyrolysis system. Bioresour. Technol. 220, 378–383. doi:10.1016/j.biortech.2016.08.028.

Yun, X., Ma, Y., Zheng, H., Zhang, Y., Cui, B., Xing, B., 2022. Pb(II) adsorption by biochar from co-pyrolysis of corn stalks and alkali-fused fly ash. Biochar 4 (4). https://link.springer.com/article/10.1007/s42773-022-00189-4.

Zeng, K., Gauthier, D., Soria, J., Mazza, G., Flamant, G.J.S.E., 2017. Solar pyrolysis carbonaceous feedstocks: A review 156, 73–92.

Zeng, L., Luo, D., Liu, L., Huang, X., Liu, Y., Wei, L., Xiao, T., Wu, Q., 2023. Alkali/Fe-modified biochar for Cd-As contamination in water and soil: performance and mechanism. Environ. Technol. Innov. 32, 103381. doi:10.1016/j.eti.2023.103381.

Zeng, M., Ge, Z., Ma, Y., Zha, Z., Wu, Y., Hou, Z., Zhang, H., 2023. Hydrothermal carbonization coupled with gasification for collaborative disposal of kitchen waste and yard waste. Energy Convers. Manage. 283, 116864. doi:10.1016/j.enconman.2023.116864.

Zhang, Z., Pang, S., 2017. Experimental investigation of biomass devolatilization in steam gasification in a dual fluidised bed gasifier. Fuel 188, 628–635.

Zhang, J., Wang, Y., Dong, L., Gao, S., Xu, G., 2010. Decoupling Gasification: Approach Principle and Technology Justification. Energy & Fuels 24 (12), 6223–6232. https://pubs.acs.org/doi/full/10.1021/ef101036c.

Zhang, J., Wu, R., Zhang, G., Yu, J., Yao, C., Wang, Y., Gao, S., Xu, G., 2013. Technical Review on Thermochemical Conversion Based on Decoupling for Solid Carbonaceous Fuels. Energy & fuels 27 (mar.-apr), 1951–1966. https://pubs.acs.org/doi/full/10.1021/ef400118b.

Zhang, J., Liu, J., Liu, R., 2015. Effects of pyrolysis temperature and heating time on biochar obtained from the pyrolysis of straw and lignosulfonate. Bioresource Technology 176, 288–291. https://www.sciencedirect.com/science/article/pii/S0960852414016137.

Zhang, P., Bing, X., Jiao, L., Xiao, H., Li, B., Sun, H., 2022. Amelioration effects of coastal saline-alkali soil by ball-milled red phosphorus-loaded biochar. Chemical Engineering Journal 431, 133904. doi:10.1016/j.cej.2021.133904.

Zhang, X.X., Sun, Y.Q., Zhang, Q.Z., Tian, W.J., Khan, E., Tsang, D.C.W., 2024. Leaching characteristics of nutrients in food waste digestate-derived biochar. Bioresource Technology 399, 130634. https://doi.org/ARTN.

Zhang, H., Xiao, R., Huang, H., Xiao, G., 2009. Comparison of non-catalytic and catalytic fast pyrolysis of corncob in a fluidized bed reactor. Bioresour. Technol. 100 (3), 1428–1434. doi:10.1016/j.biortech.2008.08.031.

Zhang, Y.-J., Xing, Z.-J., Duan, Z.-K., Li, M., Wang, Y., 2014. Effects of steam activation on the pore structure and surface chemistry of activated carbon derived from bamboo waste. Appl. Surf. Sci. 315, 279–286. doi:10.1016/j.apsusc.2014.07.126.

Zhang, D., Han, M., Li, Y., Lei, L., Shang, Y., Wang, K., Wang, Y., Zhang, Z., Zhang, X., Feng, H., 2016. Phosphorus and sulfur dual doped hierarchic porous carbons with superior supercapacitance performance. Electrochim. Acta 222, 141–148. doi:10.1016/j.electacta.2016.10.184.

Zhang, H., Chen, C., Gray, E.M., Boyd, S.E., 2017. Effect of feedstock and pyrolysis temperature on properties of biochar governing end use efficacy. Biomass Bioenergy 105, 136–146. doi:10.1016/j.biombioe.2017.06.024.

Zhang, Y., Liu, S., Zheng, X., Wang, X., Xu, Y., Tang, H., Kang, F., Yang, Q.H., Luo, J.J.A.f.m., 2017. Biomass organs control porosity their pyrolyzed carbon. 27(3), 1604687.

Zhang, B., Heidari, M., Regmi, B., Salaudeen, S., Arku, P., Thimmannagari, M., Dutta, A.J.E., 2018. Hydrothermal carbonization fruit wastes: A promising technique for generating hydrochar 11 (8), 2022.

Zhang, C., Zeng, G., Huang, D., Lai, C., Chen, M., Cheng, M., Tang, W., Tang, L., Dong, H., Huang, B., Tan, X., Wang, R., 2019. Biochar for environmental management: mitigating greenhouse gas emissions, contaminant treatment, and potential negative impacts. Chem. Eng. J. 373, 902–922. doi:10.1016/j.cej.2019.05.139.

Zhang, H., Wang, T., Sui, Z., Zhang, Y., Sun, B., Pan, W.-P., 2019. Enhanced mercury removal by transplanting sulfur-containing functional groups to biochar through plasma. Fuel 253, 703–712. doi:10.1016/j.fuel.2019.05.068.

Zhang, J., Hou, D., Shen, Z., Jin, F., O'Connor, D., Pan, S., Ok, Y.S., Tsang, D.C.W., Bolan, N.S., Alessi, D.S., 2020. Effects of excessive impregnation, magnesium content, and pyrolysis temperature on MgO-coated watermelon rind biochar and its lead removal capacity. Environ. Res. 183, 109152. doi:10.1016/j.envres.2020.109152.

Zhang, Y., Liu, N., Yang, Y., Li, J., Wang, S., Lv, J., Tang, R., 2020. Novel carbothermal synthesis of Fe, N co-doped oak wood biochar (Fe/N-OB) for fast and effective Cr(VI) removal. Colloids Surf. A 600, 124926. doi:10.1016/j.colsurfa.2020.124926.

Zhang, Z., Zhao, Y., Wang, T., 2020. Spirulina hydrothermal carbonization: effect on hydrochar properties and sulfur transformation. Bioresour. Technol. 306, 123148. doi:10.1016/j.biortech.2020.123148.

Zhang, B., Jiang, Y., Balasubramanian, R., 2021. Synthesis, formation mechanisms and applications of biomass-derived carbonaceous materials: a critical review. J. Mater. Chem. A 9 (44), 24759–24802. doi:10.1039/D1TA06874A.

Zhang, K., Min, X., Zhang, T., Xie, M., Si, M., Chai, L., Shi, Y., 2021. Selenium and nitrogen co-doped biochar as a new metal-free catalyst for adsorption of phenol and activation of peroxymonosulfate: elucidating the enhanced catalytic performance and stability. J. Hazard. Mater. 413, 125294. doi:10.1016/j.jhazmat.2021.125294.

Zhang, H., Song, X., Zhang, J., Liu, Y., Zhao, H., Hu, J., Zhao, J.J.B.T., 2022. Performance mechanism sycamore flock based biochar in removing oxytetracycline hydrochloride. Bioresour. Technol. 350, 126884.

Zhang, H.Y., Peng, B., Liu, Q.Y., Wu, C.S., Li, Z.W., 2022. Preparation of porous biochar from heavy bio-oil for adsorption of methylene blue in wastewater. Fuel Process. Technol. 238. doi:10.1016/j.fuproc.2022.107485, ARTN 107485.

Zhang, X., Zhao, B., Liu, H., Zhao, Y., Li, L., 2022. Effects of pyrolysis temperature on biochar's characteristics and speciation and environmental risks of heavy metals in sewage sludge biochars. Environ. Technol. Innov. 26, 102288. doi:10.1016/j.eti.2022.102288.

Zhang, Y., Han, M., Si, X., Bai, L., Zhang, C., Quan, X., 2022. Toxicity of biochar influenced by aging time and environmental factors. Chemosphere 298, 134262. doi:10.1016/j.chemosphere.2022.134262.

Zhang, C., Ji, Y., Li, C., Zhang, Y., Sun, S., Xu, Y., Jiang, L., Wu, C., 2023. The application of biochar for CO_2 capture: influence of biochar preparation and CO_2 capture reactors. Ind. Eng. Chem. Res. 62 (42), 17168–17181.
Zhang, F., Wang, J., Tian, Y., Liu, C., Zhang, S., Cao, L., Zhou, Y., Zhang, S., 2023. Effective removal of tetracycline antibiotics from water by magnetic functionalized biochar derived from rice waste. Environ. Pollut. 330, 121681. doi:10.1016/j.envpol.2023.121681.
Zhang, T., Yu, H., Han, Z., Xu, S., Dong, Z., Zhou, K., Zhang, S., Cheng, Z., 2023. Remediation of atrazine in environment by persulfate activation via N/B co-doped Si-rich biochar: performance, mechanisms, degradation pathways and phytotoxicity. Chem. Eng. J. 477, 147131. doi:10.1016/j.cej.2023.147131.
Zhao, Y., Sun, S., Che, H., Guo, Y., Gao, C., 2012. Characteristics of cyclone gasification of rice husk. International Journal of Hydrogen Energy 37 (22), 16962–16966. https://www.sciencedirect.com/science/article/pii/S036031991201943X.
Zhao, Y., Feng, D., Zhang, Z., Sun, S., Wu, J., 2017. Experimental study of cyclone pyrolysis – Suspended combustion air gasification of biomass. Bioresource Technology 243, 1241. https://www.sciencedirect.com/science/article/pii/S0960852417311616.
Zhao, W., Zhou, Q., Tian, Z., Cui, Y., Liang, Y., Wang, H., 2020. Apply biochar to ameliorate soda saline-alkali land, improve soil function and increase corn nutrient availability in the Songnen Plain. Science of The Total Environment 722, 137428. doi:10.1016/j.scitotenv.2020.137428.
Zhao, Y., Song, M., Cao, Q., Sun, P.Z., Chen, Y.H., Meng, F.Y., 2020. The superoxide radicals' production persulfate activated with CuFeO@ Biochar composites to promote the redox pairs cycling for efficient degradation of -nitrochlorobenzene in soil. Journal of Hazardous Materials 400, 122887. https://doi.org/ARTN
Zhao, Y., Zhai, P.F., Li, B., Jin, X., Liang, Z.H., Yang, S.Y., Li, C.Z., Li, C.J., 2022. Banana, pineapple, cassava and sugarcane residue biochars cannot mitigate ammonia volatilization from latosols in tropical farmland. Science of the Total Environment 821, 153427. https://doi.org/ARTN
Zhao, Y., Hu, Z., Lu, Y., Shan, S., Zhuang, H., Gong, C., Cui, X., Zhang, F., Li, P., 2024. Facilitating mitigation of agricultural non-point source pollution and improving soil nutrient conditions: The role of low temperature co-pyrolysis biochar in nitrogen and phosphorus distribution. Bioresource Technology 394, 130179. doi:10.1016/j.biortech.2023.130179.
Zhao, L., Cao, X., Mašek, O., Zimmerman, A., 2013. Heterogeneity of biochar properties as a function of feedstock sources and production temperatures. J. Hazard. Mater. 256-257, 1–9. doi:10.1016/j.jhazmat.2013.04.015.
Zhao, B., O'Connor, D., Zhang, J., Peng, T., Shen, Z., Tsang, D.C.W., Hou, D., 2018. Effect of pyrolysis temperature, heating rate, and residence time on rapeseed stem derived biochar. J. Clean. Prod. 174, 977–987. doi:10.1016/j.jclepro.2017.11.013.
Zhao, B., O'Connor, D., Shen, Z., Tsang, D.C.W., Rinklebe, J., Hou, D., 2020. Sulfur-modified biochar as a soil amendment to stabilize mercury pollution: an accelerated simulation of long-term aging effects. Environ. Pollut. 264, 114687. doi:10.1016/j.envpol.2020.114687.
Zhao, C., Wang, B., Theng, B.K.G., Wu, P., Liu, F., Wang, S., Lee, X., Chen, M., Li, L., Zhang, X., 2021. Formation and mechanisms of nano-metal oxide-biochar composites for pollutants removal: A review. Sci. Total Environ. 767, 145305. doi:10.1016/j.scitotenv.2021.145305.
Zhao, S., Ding, L., Ruan, Y., Bai, B., Qiu, Z., Li, Z., 2021. Experimental and kinetic studies on steam gasification of a biomass char. Energies 14 (21), 7229. doi:10.3390/en14217229.
Zheng, F.-Y., Li, R., Ge, S., Xu, W.-R., Zhang, Y., 2020. Nitrogen and phosphorus co-doped carbon networks derived from shrimp shells as an efficient oxygen reduction catalyst for microbial fuel cells. J. Power. Sources. 446. doi:10.1016/j.jpowsour.2019.227356.
Zheng, X., He, X., Peng, H., Wen, J., Lv, S., 2021. Efficient adsorption of ciprofloxacin using Ga2S3/S-modified biochar via the high-temperature sulfurization. Bioresour. Technol. 334, 125238. doi:10.1016/j.biortech.2021.125238.
Zheng, M., Xu, Z.-N., Fu, M.-L., 2022. Boron-doped activated carbon catalyzed reduction of dilute nitrite acid in oxidative esterification reaction in the coal to ethylene glycol process. J. Environ. Chem. Eng. 10 (3), 107932. doi:10.1016/j.jece.2022.107932.
Zhi, Z.J., Wu, D., Meng, F.Y., Yin, Y., Song, B., Zhao, Y., Song, M., 2022. Facile synthesis of CoFeO@BC activated peroxymonosulfate for p- nitrochlorobenzene degradation: Matrix effect and toxicity evaluation. Science of the Total Environment 828. https://doi.org/ARTN154275
Zhou, Y., Ma, R., Candelaria, S.L., Wang, J., Liu, Q., Uchaker, E., Li, P., Chen, Y., Cao, G., 2016. Phosphorus/sulfur Co-doped porous carbon with enhanced specific capacitance for supercapacitor and improved catalytic activity for oxygen reduction reaction. J. Power. Sources. 314, 39–48. doi:10.1016/j.jpowsour.2016.03.009.
Zhou, S., Liang, H., Han, L., Huang, G., Yang, Z., 2019. The influence of manure feedstock, slow pyrolysis, and hydrothermal temperature on manure thermochemical and combustion properties. Waste Manage.. 88, 85–95. doi:10.1016/j.wasman.2019.03.025.
Zhou, Y., Chen, Z., Gong, H., Wang, X., Yu, H., 2020. A strategy of using recycled char as a co-catalyst in cyclic in-situ catalytic cattle manure pyrolysis for increasing gas production. Waste Manage.. 107, 74–81. doi:10.1016/j.wasman.2020.04.002.
Zhou, X., Zhu, Y., Niu, Q., Zeng, G., Lai, C., Liu, S., Huang, D., Qin, L., Liu, X., Li, B., Yi, H., Fu, Y., Li, L., Zhang, M., Zhou, C., Liu, J., 2021. New notion of biochar: A review on the mechanism of biochar applications in advannced oxidation processes. Chem. Eng. J. 416, 129027. doi:10.1016/j.cej.2021.129027.
Zhou, Y., Qin, S., Verma, S., Sar, T., Sarsaiya, S., Ravindran, B., Liu, T., Sindhu, R., Patel, A.K., Binod, P., Varjani, S., Rani Singhnia, R., Zhang, Z., Awasthi, M.K., 2021. Production and beneficial impact of biochar for environmental application: A comprehensive review. Bioresour. Technol. 337, 125451. doi:10.1016/j.biortech.2021.125451.
Zhou, Y., Qin, S., Verma, S., Sar, T., Sarsaiya, S., Ravindran, B., Liu, T., Sindhu, R., Patel, A.K., Binod, P., Varjani, S., Rani Singhnia, R., Zhang, Z., Awasthi, M.K., 2021. Production and beneficial impact of biochar for environmental application: A comprehensive review. Bioresour. Technol. 337, 125451. doi:10.1016/j.biortech.2021.125451.
Zhou, M., Xu, Y., Luo, G., Zhang, Q., Du, L., Cui, X., Li, Z., 2022. Facile synthesis of phosphorus-doped porous biochars for efficient removal of elemental mercury from coal combustion flue gas. Chem. Eng. J. 432, 134440. doi:10.1016/j.cej.2021.134440.
Zhou, X., Liu, X., Qi, F., Shi, H., Zhang, Y., Ma, P., 2022. Efficient preparation of P-doped carbon with ultra-high mesoporous ratio from furfural residue for dye removal. Sep. Purif. Technol. 292, 120954. doi:10.1016/j.seppur.2022.120954.
Zhou, T., Deng, J., Zeng, Y., Liu, X., Song, B., Ye, S., Li, M., Yang, Y., Wang, Z., Zhou, C., 2024. Biochar meets single-atom: A catalyst for efficient utilization in environmental protection applications and energy conversion. Small. 20 (44), 2404254.
Zhou, X., Guo, Z., Tang, X., Wang, W., Wu, M., Song, B., Xiang, Y., Li, Y., Xiong, W., Huang, D., 2024. Sulfate radical-based advanced oxidation processes for simultaneous removal of antibiotic-resistant bacteria and antibiotic resistance genes and the affecting factors. Chem. Eng. J., 155149.
Zhu, L., Zhao, N., Tong, L., Lv, Y., 2018. Structural and adsorption characteristics of potassium carbonate activated biochar. RSC. Adv. 8 (37), 21012–21019. doi:10.1039/C8RA03335H.
Zhu, X., Li, K., Zhang, L., Wu, X., Zhu, X., 2018. Comparative study on the evolution of physicochemical characteristics of biochar produced from bio-oil distillation residue under different induction atmosphere. Energy Convers. Manage.. 157, 288–293. doi:10.1016/j.enconman.2017.12.010.
Zhu, Y., Yi, B., Hu, H., Zong, Z., Chen, M., Yuan, Q., 2020. The relationship of structure and organic matter adsorption characteristics by magnetic cattle manure biochar prepared at different pyrolysis temperatures. J. Environ. Chem. Eng. 8 (5), 104112. doi:10.1016/j.jece.2020.104112.
Zhu, X., Luo, Z., Zhu, X., 2021. Novel insights into the enrichment of phenols from walnut shell pyrolysis loop: torrefaction coupled fractional condensation. Waste Manage.. 131, 462–470. doi:10.1016/j.wasman.2021.07.007.
Zhu, J., Song, Y., Wang, L., Zhang, Z., Gao, J., Tsang, D.C.W., Ok, Y.S., Hou, D., 2022. Green remediation of benzene contaminated groundwater using persulfate activated by biochar composite loaded with iron sulfide minerals. Chem. Eng. J. 429. doi:10.1016/j.cej.2021.132292.
Zhu, Q., Gao, H., Sun, Y., Xiang, Y., Liang, X., Ivanets, A., Li, X., Su, X., Lin, Z., 2022. Highly efficient adsorption of chromium on N, S-codoped porous carbon materials derived from paper sludge. Sci. Total Environ. 834, 155312. doi:10.1016/j.scitotenv.2022.155312.
Zhu, X., Labianca, C., He, M., Luo, Z., Wu, C., You, S., Tsang, D.C.W., 2022. Life-cycle assessment of pyrolysis processes for sustainable production of biochar from agroresidues. Bioresour. Technol. 360, 127601. doi:10.1016/j.biortech.2022.127601.
Zhu, Y.W., Li, Z.W., Tao, Y.J., Zhou, J.H., Zhang, H.Y., 2022. Hierarchical porous carbon materials produced from heavy bio-oil for high-performance supercapacitor electrodes. J. Energy Storage 47. doi:10.1016/j.est.2021.103624, ARTN 103624.
Zhu, X., Luo, Z., Zhang, Q., He, M., Tsang, D.C.W., 2023. Valorization of slow pyrolysis vapor from biomass waste: comparative study on pyrolysis characteristics, evolved gas evaluation, and adsorption effects. Bioresour. Technol., 129543 doi:10.1016/j.biortech.2023.129543.
Zhu, X., Luo, Z., Zhang, Q., He, M., Tsang, D.C.W., 2023. Valorization of slow pyrolysis vapor from biomass waste: comparative study on pyrolysis characteristics, evolved gas evaluation, and adsorption effects. Bioresour. Technol. 386, 129543. doi:10.1016/j.biortech.2023.129543.
Zhuang, M., Wang, H., Qi, L., Cui, L., Quan, G., Yan, J., 2021. Production of activated biochar via a self-blowing strategy-supported sulfidated nanoscale zerovalent iron with enhanced reactivity and stability for Cr(VI) reduction. J. Clean. Prod. 315, 128108. doi:10.1016/j.jclepro.2021.128108.
Zhuo, S.N., Dai, T.C., Ren, H.Y., Liu, B.F., 2022. Simultaneous adsorption of phosphate and tetracycline by calcium modified corn stover biochar: Performance and mechanism. Bioresource Technology 359, 127477. https://doi.org/ARTN
Zielińska, A., Oleszczuk, P., Charmas, B., Skubiszewska-Zięba, J., Pasieczna-Patkowska, S., 2015. Effect of sewage sludge properties on the biochar characteristic. J. Anal. Appl. Pyrolysis. 112, 201–213. doi:10.1016/j.jaap.2015.01.025.
Zolin, A., Jensen, A., Jensen, P.A., 2001. The Influence of Inorganic Materials on the Thermal Deactivation of Fuel Chars. Energy & Fuels 15 (5), 1110–1122. https://pubs.acs.org/doi/full/10.1021/ef000288d.
Zong, P., Jiang, Y., Tian, Y., Li, J., Yuan, M., Ji, Y., Chen, M., Li, D., Qiao, Y., 2020. Pyrolysis behavior and product distributions of biomass six group components: starch, cellulose, hemicellulose, lignin, protein and oil. Energy Convers. Manage.. 216, 112777. doi:10.1016/j.enconman.2020.112777.
Zou, R., Qian, M., Wang, C., Mateo, W., Wang, Y., Dai, L., Lin, X., Zhao, Y., Huo, E., Wang, L., Zhang, X., Kong, X., Ruan, R., Lei, H., 2022. Biochar: from by-products of agro-industrial lignocellulosic waste to tailored carbon-based catalysts for biomass thermochemical conversions. Chem. Eng. J. 441, 135972. doi:10.1016/j.cej.2022.135972.
Zuhara, S., Pradhan, S., McKay, G.J.I.J.o.E.S., 2023. Pyrolysis of biosolids with waste cardboard: effect of operating parameters, feedstock size and blending ratio. Technol. (Singap World Sci) 1–14.